STRUCTURAL AND MOLECULAR STUDIES OF GROUP II LEUKOCYTE IMMUNOGLOBULIN-LIKE RECEPTORS

by

LEE IAN GARNER

A thesis submitted to
The University of Birmingham
for the degree of
DOCTOR OF PHILOSOPHY

School of Cancer Sciences
College of Medical and Dental Sciences
The University of Birmingham
September 2010

ABSTRACT

The Leukocyte Immunoglobulin-Like Receptors (LILRs) are a family of immunomodulatory transmembrane receptors with both activatory and inhibitory forms, and are primarily expressed on myelomonocytic cells. Group I LILRs include the well-characterised members LILRB1 and LILRB2, which bind MHC Class I and transduce inhibitory signals. Group II LILRs, by comparison, are poorly understood. Particular interest has arisen in the Group II receptor, LILRB4, and its role in the induction of immune tolerance via its actions upon dendritic cells and T cells. I attempted ligand-identification and structural studies on LILRB4. Staining of human PBMCs with multimeric LILRB4 revealed broad expression of the ligand, and upregulation on activated T cells. Investigations into candidate ligands by surface plasmon resonance excluded binding to known costimulatory receptors of the B7/CD28 families. X-ray crystallographic studies revealed LILRB4 has structural similarities to LILRA5, has novel structural features at the interdomain interface, is electrostatically and chemically unsuited to the recognition of MHC Class I, and identified potential ligand interaction sites. Finally, investigations were conducted into the structure and ligand recognition of other Group II LILRs. These studies define the distribution of the LILRB4 ligand and represent the first structural analysis of this important immunoregulatory receptor.

DEDICATION

To the greatest scientist I have ever known: my father, Ian Roger Garner.

"The road goes ever on and on. Down from the door where it began..." – Bilbo Baggins
'The Lord Of The Rings', by J. R. R. Tolkein.

'There's real poetry in the real world. Science is the poetry of reality' – Richard Dawkins

ACKNOWLEDGEMENTS

Thanks to Dr. Stuart Neil, Prof. Wei Cao and Dr. Rachel Allen, for correspondence, discussion and materials in the form of plasmid constructs.

Thanks to Dr. Neil Barclay and Prof. George Gao for collaborative attempts.

Within the institute, my thanks to Prof. Paul Moss and the members of the Moss group, including Dr. Karen Piper, Dr. Oliver Goodyear, Odette Chagoury and Andy McLarnon for help and advice with tissue culture and flow cytometry. Many thanks to Dr. Timothy Knowles and Dr. Mark Jeeves for help and guidance with the NMR experiments. Within the Willcox group, thanks to Dr. Fiyaz Mohammed for both practical and intellectual assistance with X-ray crystallography, Dr. Carrie Willcox for advice on flow cytometry and western blotting, and many thanks to the group's hard-working technicians, Sarah Nicholls and Mahboob Salim. I would also like to acknowledge the help and support of past and present students in the group – in particular Damien Montemat-Sicotte and Daniel Stones.

My warmest thanks to my supervisor, Dr. Benjamin Willcox, for his excellent tuition, advice and inspiration at all stages of my doctoral training (and no end of patience).

Finally, heartfelt thanks to my family, and my fiancée Laura, for all their love, patience and support, without which this work would have been impossible to complete.

COMMONLY – USED ABBREVIATIONS

APS	ammonium persulphate
bp	base-pair
DMSO	dimethylsulphoxide
DNA	deoxyribonucleic acid
dNTP	deoxynucleotide triphosphate
DC	dendritic cell
DTT	dithiothrietol
EDTA	ethylene diamine tetra-acetic acid
kDa	kiloDaltons
LB	Luria-Burtani broth
MES	methane ethane sulphonic acid
PBS	phosphate buffered saline
PCR	polymerase chain reaction
PMSF	phenyl methyl sulphonyl fluoride
SDM	site-directed mutagenesis
SDS-PAGE	sodium dodecyl sulphate – polyacrylamide gel electrophoresis
SPR	surface plasmon resonance
TEMED	tetramethylethylenediamine
Tris	Tris(hydroxymethyl)aminomethane

LIST OF CONTENTS

LIST OF FIGURES

Chapter 1

Chapter 3

Chapter 4

Chapter 5

LIST OF TABLES

CHAPTER 1 - INTRODUCTION

1.1 Dendritic cells, immunity and tolerance

1.1.1 The vertebrate immune system

The vertebrate immune system has evolved complex mechanisms to enable the recognition and elimination of pathogens. Innate immunity provides a rapid, first line of defence *via* the use of germ-line-encoded receptors specific for pathogen-restricted structures, many of which are evolutionarily ancient. Crucially, innate responses are not enhanced upon antigen re-encounter. In contrast, adaptive immune responses are characterised by clonal selection of lymphocytes expressing genetically rearranged antigen receptors providing a high degree of specificity against a vast range of foreign antigens. Although primary adaptive responses to a pathogen are initiated more slowly than innate responses, a key feature of adaptive immunity is the development of immunological memory *via* generation of memory lymphocyte populations, enabling a faster, augmented response upon re-encounter. In reality, innate and adaptive immunity are intimately interwoven, with strong evidence for instruction of adaptive immunity by innate immune cells, allowing a coordinated response.

Innate immune cells include phagocytes such as macrophages and neutrophils, which are able to surround and engulf microorganisms and can secrete inflammatory cytokines in response to microbial infection, and Natural Killer (NK) lymphocytes, which are able to recognise and destroy virally-infected or tumour cells. Dendritic cells (DCs), which are specialised antigen presenting cells (APCs) that play a key role in initiation of adaptive responses, are also phagocytic in their immature state, as discussed below. Monocytes, which circulate in the blood, are recruited to infection sites in response to inflammatory signals, where they can differentiate into macrophages or DCs, bolstering such responses. Other innate immune cells include granulocytes such as eosinophils and basophils, and tissue-resident mast cells, which

are involved in defence against parasitic infections, and are also implicated in allergic immune responses.

The key cellular components of adaptive immunity are T and B lymphocytes, which recognise pathogens via the evolutionarily related T cell receptor (TCR) and B cell receptor (BCR) expressed on their surface. The genes for TCRs and BCRs are somatically rearranged from a large range of Variable, Diversity and Joining segments, resulting in the generation of diverse clonotypically expressed antigen receptors, permitting exquisite specificity to pathogen-derived antigens, and clonotypic expansion (Krangel et al. Immunol Rev 1998, Jung et al. Ann Rev Immunol 2006). B cells contribute to humoral responses by generating antigen-specific antibodies which help neutralise and eliminate pathogens. αβ T cells use their TCRs to recognise foreign antigen in the form of peptides bound to Major Histocompatibility Complex (MHC) molecules at the surface of APCs, and contribute to cell-mediated immunity. Cytotoxic T lymphocytes (CTL) express the coreceptor CD8, and their functions include recognition and destruction of virally-infected or tumour cells, and cytokine production. Helper T (T_H) cells express the CD4 coreceptor at their surface and have key regulatory functions. Upon activation they secrete cytokines that have potent effects on downstream immune effector cells. T_H1 subsets produce Interferon (IFN)-γ and Tumour Necrosis Factor (TNF)-β, which facilitate the activation of macrophages and CTL and promote cellular immunity in the face of intracellular pathogens such as bacteria and viruses. In contrast T_H2 cells produce IL-4, IL-5, IL-13 and IL-10, and contribute to inflammatory responses and humoral responses via stimulation of B cells. T_H17 cells appear to be a specialised subset of $CD4^+$ T cells that produce IL-17, are developmentally distinct from T_H1 and T_H2 subsets, and are highly pro-inflammatory in nature (Weaver et al. Immunity 2006). Regulatory T cells are discussed in Section 1.1.2.

In order for a protein to induce an antigen-specific T cell response, it must first be processed and presented on the surface of an APC, in the context of Major Histocompatibility Complex (MHC) molecules (Trombetta and Mellman Ann Rev Immunol 2005). MHC Class I, which is expressed on all nucleated cells in the body, presents predominantly intracellular antigens, which are degraded in the cytosol by a multisubunit proteolytic complex termed the proteasome, transported into the Endoplasmic Reticulum by the transporter associated with antigen processing (TAP), and via the actions of chaperone proteins is assembled with appropriated MHC Class I heavy chains and β_2-microglobulin light chain (β_2m) before export to the cell surface via the secretory pathway. In contrast, MHC Class II molecules, which are expressed on a more restricted set of cells (including DCs, B cells, activated macrophages), present peptides derived from predominantly exogenously derived antigens, which are degraded under acidic conditions in endosomal/lysosomal compartments to which nascent MHC Class II molecules are routed. In these compartments, self-peptides bound to MHC Class II molecules (derived from MHC Class II-like invariant chain) are displaced by appropriate antigenic peptides, after which the MHC Class II molecules traffic to the cell surface for antigen presentation.

Robust initiation of T cell responses requires interaction of naïve T cells with professional APCs, typically defined as DCs, macrophages, or B cells. Although almost all cells in the human body are capable of capturing proteins by receptor-mediated endocytosis and presenting them via MHC Class I, most are inefficient at this process and also crucially lack accessory and costimulatory molecules that can promote priming of an immune response. Professional APCs are highly specialized cells, able to rapidly uptake proteins by endocytosis, load the resulting peptides onto MHC Class I or Class II molecules, and then display the peptide-MHC (pMHC) complexes on the cell surface for recognition by antigen receptor, in

addition to providing the appropriate costimulatory signals. Importantly, their ability to "cross-present" endogenously-derived antigen in MHC Class I molecules is a key feature. The antigen presentation abilities of professional APC are linked to their maturation status, which is itself dictated by environmental stimuli. These properties distinguish professional APCs, and in particular the myeloid lineage-derived macrophages and DCs, as being a critical link between innate and adaptive immunity, and as discussed in the next section, instrumental in the regulation of immune tolerance.

1.1.2 Control of the immune response via tolerance

The necessity for tolerance – the failure of the adaptive immune system to respond to certain antigens – arises because of the competing demands of the requirement to generate diverse repertoires of antigen receptors, and of the requirement to regulate the immune response in order to prevent immune pathologies. Tolerance is maintained through central and peripheral mechanisms; both are required, because central mechanisms are not 100 % efficient and do not account for an encounter with self neoantigens (for example, the release of sequestered self-antigens as a consequence of tissue damage) or innocuous non-self antigens (Kamradt and Mitchison N Engl J Med 2001, Walker and Abbas Nat Rev Immunol 2002).

Central tolerance and thymic selection

Central tolerance involves the deletion of potentially self-reactive T cells in the thymus, during T cell development. The development of αβ T cells involves stepwise rearrangement and expression of the two antigen-receptor loci. Rearrangement events occur during several steps of development in the thymic cortex, and this process is followed by cessation of recombination, then positive selection of those T cells bearing TCRs with affinity for MHC. Migration of semi-mature single-positive ($CD4^+$ or $CD8^+$) αβ T cells to the medulla then

occurs, where they are subject to negative selection by clonal deletion; those cells bearing TCRs which are high-affinity ligands for self peptide-MHC (pMHC) undergo cell death by apoptosis. Defects in negative selection lead to the development of autoimmunity (Siggs et al. Curr Opin Immunol 2006, von Boehmer and Melchers Nat Immunol 2010). Central tolerance to tissue-specific antigens (TSAs) is promoted by expression of the transcription factor AIRE in the medullary thymic epithelial cells (mTECs), leading to promiscuous expression of TSAs which drives negative selection of potentially autoreactive T cells (Anderson et al. Immunity 2005, Peterson et al. Nat Rev Immunol 2008, Kyewski and Klein Ann Rev Immunol 2006). Analogous selection processes occur for B lymphocytes in the bone marrow, although there is evidence that a degree of receptor editing at later checkpoints in B cell development can also occur (Nemazee Nat Rev Immunol 2006).

Peripheral tolerance mechanisms

Because central tolerance is not completely efficient, and is reliant upon the deletion of T cells with TCRs of high affinity for self pMHC, it follows that systems exist that keep self-reactive T cells of low affinity for self pMHC, or those that fail to engage TSAs expressed at low levels by mTECs, in check in the periphery. These peripheral tolerance mechanisms operate in at least three ways: by ignorance of self antigens (T cell anergy), by deletion of self-reactive T cells in the periphery, and via an actively regulatory subset of immune cells comprising regulatory T cells (Tregs) and tolerogenic DCs (Mueller Nat Immunol 2010).

Anergy and Deletion

Anergy is the state of hyporesponsiveness induced in T cells upon TCR engagement in the absence of costimulatory and/or inflammatory cytokine signals, or upon chronic antigenic stimulation (Schwartz Ann Rev Immunol 2003, Fathman and Lineberry Nat Rev Immunol

2007). Anergy may also be induced by suboptimal engagement of the TCR by low avidity pMHC ligands (Sadegh-Nasseri et al. Immunology 2010). Anergy has been described as an epigenetically maintained state, with active repression of transcription of genes involved in activation (Wells JI 2009). The decision between anergy or activation is made by a series of intracellular proteins that actively oppose IL-2 induction – critical for T cell proliferation and survival - but are inactivated by signals from CD28 and/or the IL-2 Receptor (IL-2R) (Saibil et al. Curr Opin Immunol 2007). Tregs have been described as being in an anergic state, although gene transcription analysis has demonstrated differences between Tregs and experimentally anergised cells. The same study demonstrated that the signalling block in the anergic state could be reversed, whereas in Treg cells it could not (Knoechel et al. JI 2006).

The role of deletion of autoreactive T cells in the periphery is comparatively poorly understood; however apoptosis driven by the down-regulation of the anti-apoptotic molecule Bcl-2 and the upregulation of the pro-apoptotic Bcl-2 family member, Bim, may be a consequence of low-affinity TCR engagement. In addition, these studies suggest parallels between signalling pathways involved in anergy and deletion (Strasser et al Immunol Cell Biol 2008, Parish et al. Blood 2009).

Regulatory and Suppressor T cells

Although T cells with suppressive properties were described in the 1970's, the field then was highly controversial (for a historical perspective, see Sakaguchi et al. EJI 2007). The identification of the high-affinity IL-2R α-chain, CD25, as a key marker (Sakaguchi et al. JI 1995) in combination with the transcription factor FoxP3 (Hori et al. Science 2003) allowed for more reliable identification of a subset of $CD4^+$ T cells with the ability to suppress immune responses, and these were subsequently named regulatory T cells (Tregs). Another

proposed Treg marker is the negative costimulatory receptor Cytotoxic T-Lymphocyte Antigen-4 (CTLA-4, discussed in Section 1.1.4). Tregs actively inhibit the activation, proliferation and cytokine production of other innate and adaptive immune cells. Neonatal mice thymectomized on day 3 – before Treg exit from the thymus – develop severe autoimmune pathologies, which can be reversed by infusion of $CD4^+$ T cells from syngeneic mice (Sakaguchi et al. JEM 1982). Mutations in FoxP3 cause the autoimmune conditions Scurfy in mice (Brunkow et al. Nat Genet 2001) and IPEX syndrome (Immune dysregulation, Polyendocrinopathy and Enteropathy, X-linked) in humans (Bennet et al. Nat Genet 2001). $CD4^+$ $CD25^+$ $FoxP3^+$ Tregs enriched from normal mice dampen allergic reactions, establish tolerance to organ grafts, prevent graft-versus-host disease after bone marrow transplantation, and promote foetal-maternal tolerance (Sakaguchi Nat Immunol 2005). Inversely, selective depletion of Tregs provokes effective anti-tumour immunity (Wang and Wang Curr Opin Immunol 2007) and augments microbial immunity in otherwise non-responding animals (Belkaid and Rouse Nat Immunol 2005). Thus, Tregs play a crucial role in maintaining tolerance in a variety of contexts – autoimmunity, infection, cancer and transplantation.

Treg subsets

Tregs can be divided into two functionally and phenotypically overlapping subsets, natural Tregs (nTregs) and adaptive or inducible Tregs (iTregs). nTregs develop in the thymus and are 'pre-programmed' for the maintenance of central tolerance mechanisms (Wing and Sakaguchi Nat Immunol 2010). Naive T cells differentiate into iTregs under the influence of tolerogenic signals in the periphery during ongoing immune responses (Horwitz et al. Trends Immunol 2008). They can be subdivided into T regulatory Type 1 (Tr1) cells, which can be generated in the presence of the immunosuppressive cytokine IL-10, express high levels of IL-10 and low levels of T_H1 cytokines, are anergic and functionally suppressive *in vitro* and

prevent the development of experimentally induced T_H1 autoimmune diseases such as colitis when transferred *in vivo* (Groux et al. JEM 1996, Groux et al. Nature 1997, Wakkach et al. JI 2001); and T_H3 cells, first observed in the EAE (Experimental Autoimmune Encephalitis) model of human MS (Multiple Sclerosis), which preferentially secrete TGF-β and also suppress autoimmunity (Chen et al. Science 1994, Weiner et al. Immunol Rev 2001). In addition, a number of 'non-conventional' regulatory cell subsets have been described. These include $CD8^+$ $CD28^-$ T suppressor cells (Liu et al. Int Immunol 1998, Vlad et al. Hum Immunol 2008), $CD8^+$ $CD122^+$ Tregs (Endharti et al. JI 2005, Pomié et al. Hum Immunol 2008), and $CD4^-$ $CD8^-$ 'double negative' Tregs (Thomson et al. Immun Res 2006).

Proposed Treg suppressive mechanisms

Identifying the mechanisms by which Tregs exert their tolerogenic effect is an active field of research. A common theme is the production of IL-10 and TGF-β (Taylor et al. Immunology 2006), a mechanism which underlies the effect known as 'bystander suppression'. Tregs activated through their TCR can suppress immune responses via the release of suppressive cytokines, and therefore Tregs of one antigenic specificity can regulate T cells of other specificities. nTregs also operate directly on effector T cells via contact-dependant mechanisms, possibly via inhibitory receptor engagement. Candidates include CTLA-4 and PD-1 (Habicht et al. JI 2007, Fife and Bluestone Immunol Rev 2008). Tregs may directly kill effector T cells or activated APCs via granzyme and perforin release (Grossman et al. Immunity 2004). Metabolic inhibition is another broad mechanism of Treg suppression, for example by competition for IL-2 (Pandiyan et al. Nat Immunol 2007, Wang et al. Immunol Lett 2010), generation of extracellular adenosine via expression of CD39 and CD73 (Tang and Bluestone Nat Immunol 2008), or tryptophan catabolism (discussed later).

Tregs also mediate suppression through modification of APC function, and in particular DCs, which are critical in initiating responses. Tregs can convert DCs to a tolerogenic phenotype, in which key costimulatory molecules on the APC surface such as B7-1 and B7-2, and MHC Class I and II, are downregulated. This leads to a reinforcement of the tolerogenic state, as such tolerogenic DCs can then induce the generation of additional Tregs from naive T cells, a process known as 'infectious tolerance'. The role of tolerogenic DCs will be discussed further in Section 1.1.5, but in order to illustrate how DCs can contribute to tolerance it is first necessary to discuss how they initiate the immune response.

1.1.3 Dendritic Cells and their contribution to the initiation of the Immune Response

Dendritic cells (DCs) were first isolated and characterized by Ralph Steinman and Zanvil Cohn in the 1970's, on the basis of their necessity for *in vitro* antibody responses to sheep red blood cells (Steinman and Cohn JEM 1973, Steinman and Cohn JEM 1974, Steinman EJI 2007). They described a rare population of cells in the mouse spleen that had a characteristic stellate morphology, were highly motile and rich in mitochondria, and continually probed the surrounding media by extending and retracting branched processes or 'dendrites'. Subsequent studies showed that DCs had high level expression of MHC Class II (Steinman et al. JEM 1979). Using the *in vitro* mixed leukocyte reaction (MLR), which mimics T cell–mediated rejection during transplantation, Steinman showed that DCs could initiate the reaction substantially more potently than bulk spleen cells (Steinman and Witmer PNAS 1978). Subsequent studies using purified cells showed that DCs were needed not only for presentation of MHC products, or immune recognition, but as potent accessories for immune responsiveness (Banchereau and Steinman Nature 1998, Banchereau et al. Ann Rev Immunol 2000).

DC Lineages and Subsets

Heterogeneity and functional plasticity are hallmarks of myelomonocytic cells, and have presented major challenges to their study. There are two main lineages of DCs: plasmacytoid DCs (pDCs), and classical (myeloid) DCs. Both are derived from common DC precursors, which differentiate from macrophage/DC progenitors (which also give rise to monocytes) that in turn have differentiated along a maturation pathway from $CD34^+$ haematopoietic stem-cell (HSC) progenitors in the bone marrow (Liu et al. Immun Rev 2010, Geissman et al. Science 2010). Plasmacytoid DCs are involved in the early antiviral innate immune response, by producing large amounts of Type I Interferons (IFN-α, IFN-β) (Liu et al. Ann Rev Immunol 2005). They are relatively long lived and reside in all peripheral organs and the bone marrow. Classical DCs are migratory, moving from the blood (in humans; circulating DCs are rare in the mouse) to the tissues, and then to the lymphoid tissues via the lymphatic system, where they interact with T and B cells. They can be classed as lymphoid DCs or non-lymphoid-tissue DCs, and further subdivided based on function and surface markers (**Table 1.1**). Moreover, DCs can originate directly from monocytes exposed to inflammatory conditions *in vivo* (Randolph et al. Immunity 1999) and in *in vitro* culture (described later). Evidence suggests that this is not a conventional route for DC generation *in vivo* in the steady state. *Listeria monocytogenes* infection activates monocytes via IFN-γ secreted by NK cells, and these activated monocytes – termed Tip-DCs or Inflammatory DCs due to their production of TNF and inducible nitric oxide synthase (iNOS) – have specialized antigen-presentation capacity and express some, but not all, of the cell-surface markers of DCs (Serbina et al. Immunity 2003). This emphasises that cells of the mononuclear phagocytic system display considerable plasticity in terms of phenotype and function.

Tissue	Organ	DC Subset	Function
Lymphoid	Spleen	$CD8^+$ DC	MHC-I cross-presentation of self and bacterial antigens (immunity and tolerance)
		$CD8^-$ DC	MHC-II presentation
	Lymph Node	Migratory DC	Antigen transport from periphery
		$CD8^+$ resident DC	Cross-presentation of self and viral antigens (immunity and tolerance)
		$CD8^-$ resident DC	Unknown
Non-Lymphoid	Lung Liver Kidney	$CD103^+$ DC	Cross-presentation of viral antigens
		$CD11b^+$ DC	Unknown
	Intestine	PP $CD103^+$ DC	Unknown
		LP $CD103^+$ DC	Unknown
		LP $CD103^-$ DC	Antigen transport from lumen to mesenteric LN
	Skin (dermal)	$CD103^+Langerin^+$	Viral immunity, tolerance
		$CD103^-Langerin^-$	Unknown
Non-classical DCs	Skin (epidermal)	Langerhans cells	Regulatory?
	All/BM	pDCs	Innate antiviral response

Table 1.1 Summary of DC subsets in lymphoid and non-lymphoid tissues.
DC, dendritic cell. BM, bone marrow. pDC, plasmacytoid DC. PP, Peyer's patches. LP, lamina propria. LN, lymph node. MHC-I/II, major histocompatibility complex class I/II. (Adapted from Liu and Nussenzweig Immun Rev 2010)

DC Maturation

DC maturation is the process by which immature DCs, which capture antigens in peripheral tissues, become efficient initiators of immunity in response to environmental stimuli

(Rescigno et al. J Leukoc Biol 1997). DC maturation is a temporally separated two-stage process involving first antigen processing and peptide-MHC formation, and then T cell recognition and responsiveness in the context of costimulation (Schuler and Steinman JEM 1985, Romani et al. JEM 1989). Immature DCs (iDCs) have high endocytic activity, low surface expression of MHC Class I and II and costimulatory molecules, and high migratory capacity, moving from the blood to the tissues, where they patrol for antigens, and then to draining lymph nodes via the lymphatics. In contrast, maturing DCs have reduced endocytic capacity, increased surface MHC Class I and II, adhesion and costimulatory molecules (including B7-1 and B7-2), and rapidly home to lymphoid tissues via the chemokine receptor CCR7, where they can then interact with antigen-specific lymphocytes.

DC maturation has been modelled *in vitro* using isolated human $CD14^+$ monocytes. Key signals that may be involved in initiating DC maturation include GM-CSF and IL-4. Monocytes in culture can be induced to differentiate into cells with properties similar to iDCs by the addition of GM-CSF and IL-4, and furthermore can undergo maturation to a phenotype with lower antigen-presentation capacity but increased ability to stimulate T-cell responses upon addition of the inflammatory cytokine TNF-α or costimulating CD40L (Sallusto and Lanzavecchia JEM 1994). Further studies expanded upon this technique and noted the high expression of MHC Class I and II, the DC marker CD83, and the costimulatory molecules B7-1 and B7-2 on functionally-matured cells (Bender et al. J Immunol Methods 1996, Zhou and Tedder PNAS 1996, Kiertscher and Roth J Leukoc Biol 1996, Conti and Gessani Immunobiology 2008).

The cytokine milieu influencing DC differentiation is an important factor in determining downstream responses, and under appropriate conditions, a wide variety of cytokines display

the capacity to differentiate and/or mature DCs from different precursors (Vieira et al. JI 2000, Zou and Tam Eur Cytokine Netw 2002, Schmid et al. Immunol Rev 2010). In the steady state cytokine production is tightly regulated but can be promptly induced both locally and systemically as a consequence of infection. Importantly, under these conditions novel DC populations arise, which can themselves significantly alter the cytokine environment (e.g. Tip-DCs mentioned earlier, or DCs with regulatory properties – discussed later).

DC Response to the Immune Environment

Effective priming of an adaptive immune response requires DCs to be in an activated state; antigen itself is not sufficient and in the absence of costimulation may lead to tolerance. Myelomonocytic cells (such as DCs) are particularly sensitive to their immune environment, and can respond to both microbial products and products of tissue damage and inflammation. The discovery of germline-encoded receptors on the surface of these cells, which are able to detect not just distinct microbial structures but also endogenous signals e.g. necrotic cell products, led to the 'danger hypothesis' suggested by Matzinger (Matzinger Ann Rev Immunol 1994; Matzinger Science 2002), as an attempt to reconcile findings conflicting with the established 'self-nonself' (SNS) model, proposed by Bretscher and Cohn in 1970, and later expanded to include 'self/nonself/altered self' (Medzhitov and Janeway Science 2002). This hypothesis proposed that initiation of the immune response was not primarily due to recognition of infectious 'non-self' antigen but instead upon the recognition of endogenous 'danger signals', thus accounting for non-infectious immune responses only partially explained by the SNS model (e.g. to tumours or during transplantation).

PRRs and PAMPs

Pattern-Recognition Receptors (PRRs) are innate immune receptors that recognise structurally conserved motifs deriving from microbes, called Pathogen-Associated Molecular Patterns, (PAMPs) (Janeway CSH Symp Quant Biol 1989, Palm and Medzhitov Immunol Rev 2009). The four key characteristics of PRRs are the ability to discriminate between self and non-self, resistance to evolutionary escape through non-redundancy of their targets, the recognition of a large number of microorganisms via a limited number of germline-encoded receptors, and the ability to convey information concerning the type of invading pathogen for an effective response. These characteristics derive from the nature of PAMPs, which represent molecular structures unique to pathogens, are essential for pathogen survival, are shared by classes of pathogens, and represent 'molecular signatures' (for example, lipopolysaccharide (LPS) is produced by bacteria but not by eukaryotes; peptidoglycan is essential for the bacterial cell wall; all bacteria have lipoproteins; and LPS, lipoteichoic acid, and mannans are signatures of gram-negative, gram-positive, and fungal pathogens, respectively).

The archetypal PRRs are the Toll-Like Receptors (TLRs). The evolutionary ancestry of these receptors is highlighted by their homology to the *Drosophila* Toll protein; a homologous immune response system based on the Toll signalling domain is found in plants, insects and vertebrates (Medhzitov et al. Nature 1997). TLRs are type I transmembrane proteins whose extracellular domains bind to PAMPs via leucine-rich repeats. They signal via intracellular Toll–IL-1 Receptor (TIR) domains. TLRs recognise a wide range of PAMPS, both extracellular (TLR1, TLR2, TLR4, TLR5, TLR6 and TLR11, which are surface-expressed and primarily recognise pathogen membrane components) and intracellular (TLR3, TLR7, TLR8 and TLR9, which are present in the ER and endolysosomal system and recognize pathogen nucleic acids). TLRs are capable of co-operative signalling, and downstream signalling pathways can be classified as either MyD88-dependent, which drive the induction

of inflammatory cytokines, or TRIF-dependent, which in addition generate Type I IFNs. TLRs are expressed mainly on APCs and many TLR agonists trigger adaptive immunity via T_H1 and T_H17 responses as well as antibody responses (Ozinsky et al. PNAS 2000, Takeda et al. Ann Rev Immunol 2003, Kawai and Akira Nat Immunol 2010).

Other important classes of PRRs include the C-type Lectin-like Receptors (CLRs) (Geijtenbeek et al. Ann Rev Immunol 2004), which interact with pathogens through recognition of carbohydrate structures and lead to their phagocytosis and antigen presentation by APCs; Scavenger receptors (Greaves and Gordon 2009 J Lipid Res); and cytosolic PRRs such as the Nucleotide-binding Oligomerization Domain-like receptors (NLRs) and Retinoic acid-Inducible Gene-I (RIG-I)-helicase Like Receptors (RLRs) capable of instructing adaptive immune responses to intracellular pathogens (Franchi et al. Immu Rev 2009), Nakhaei et al. Semin Immunol 2009, Ishii et al Nature 2008). Fc receptors, which are involved in phagocytosis of opsonised pathogens, could also be considered to be PRRs.

1.1.4 DC Accessory Signalling to and from the T cell

The classical model for activation of the T cell involves a stepwise progression of signals necessary for activation leading to proliferation, effector functions and memory. In the absence of the full signal repertoire, T cells may become anergic, be deleted, or adopt a tolerogenic phenotype. Historically, this model was described as the '2-signal' model, with Signal 1 being engagement of the TCR (plus stabilising coreceptor – CD4 or CD8) with cognate pMHC complex displayed by APCs, and Signal 2 being costimulation via engagement of T cell CD28 with B7-1/B7-2 (CD80/CD86) on an activated APC surface. An expansion of this model includes Signal 3, the involvement of inflammatory cytokines such as IL-12 that determine downstream T_H commitment (Joffre et al. Immunol Rev 2009), and a

modification of Signal 2 to include negative costimulation (discussed below). The costimulatory receptor repertoire includes newly discovered members of the B7 family (Wang et al. Cell Mol Immunol 2004) and other molecules such as the TNF receptor (TNFR) family members CD40-CD40L, OX-2 (CD200, Jenmalm et al. JI 2006), OX40 (CD134, Croft et al. Immunol Rev 2009) and 4-1BB (CD137, Wang et al. Immunol Rev 2009). For a summary of costimulatory pathways, see **Figure 1.1**. I will discuss selected members of the B7:CD28 family, CD40-CD40L, and other IgSF receptors below.

Negative and positive signalling – ITAMs, ITIMs and ITSMs

Immunoreceptors can be activatory or inhibitory, and display conserved amino acid sequences in their cytoplasmic domains that recruit downstream kinases (for activation through phosphorylation of signalling intermediates) or phosphatases (for inhibition through dephosphorylation). ITAMs (Immunoreceptor Tyrosine-based Activation Motifs) were first identified in the antigen receptors and later in activatory Fc receptors. ITAMs may also be present in adaptor molecules (for example, in the FcR common γ-chain, which associates with activatory receptors lacking a cytoplasmic tail via charged transmembrane residues); their consensus sequence is YxxL/I $x_{(6\text{-}12)}$ YxxL/I, and upon phosphorylation at their key tyrosine residues they recruit tandem Src homology-2 (SH2)-domain containing kinases such as Syk. Their inhibitory counterparts, ITIMs (Immunoreceptor Tyrosine-based Inhibitory Motifs), have the consensus S/I/V/LxYxxI/V/L, and recruit SH2-domain containing phosphatases such as SHP-1. However, some ITIM-containing receptors may be activatory, and conversely some ITAM-containing receptors may mediate inhibition; in addition, the definition of an Immunoreceptor Tyrosine-based Switch Motif (ITSM) that can mediate both outcomes has revealed the complexity of these signalling mechanisms (Barrow and Trowsdale EJI 2006).

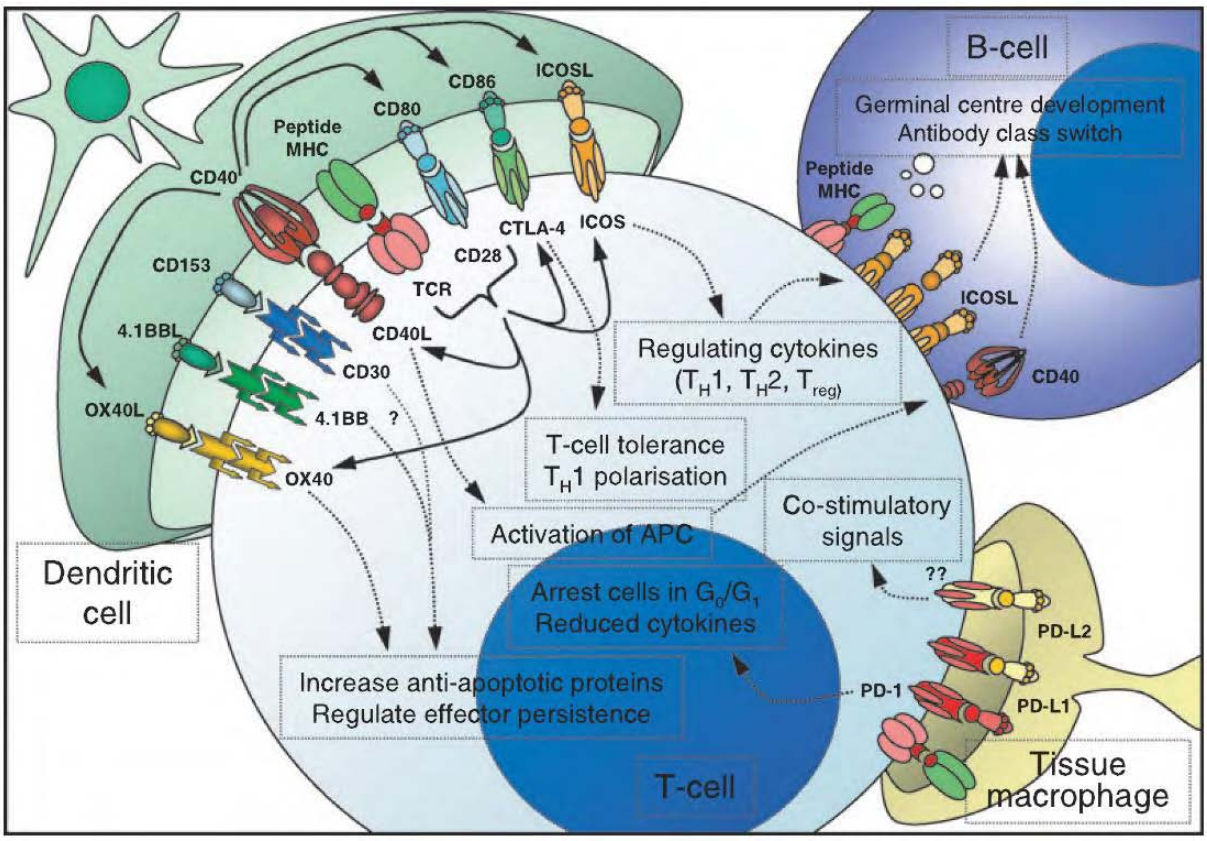

Figure 1.1. Costimulatory molecules of the IgSF and TNFR family. The bidirectional signalling interactions between T cells and DCs, B cells or macrophages mediated by costimulatory molecules of the IgSF (including B7 and CD28 families) and the TNFR family are illustrated, with the downstream consequences for the T and B lymphocyte shown. (Peggs and Allison Br J Haem 2005).

Costimulation of the T cell via B7 family engagement of CD28

Classical costimulation occurs via the interaction of B7-1 or B7-2 on the APC and CD28 on the T cell surface, in conjunction with TCR engagement by pMHC. The CD28 family of transmembrane receptors are characterised by a single extracellular Ig Variable-like (IgV) domain and a short cytoplasmic tail, and homodimerise on the cell surface via an unpaired cysteine residue. CD28 is expressed constitutively on 90 % of resting $CD4^+$ T cells and 50 % of $CD8^+$ T cells. CD28 binds to B7-1 and B7-2 with affinities of 4 and 20 μM, respectively, and expression patterns of B7-1 versus B7-2 are temporally separated; B7-2 is expressed at a low level in resting DCs and can be rapidly upregulated, whereas B7-1 is virtually absent from non-activated DCs and expressed on the cell surface later than the peak of B7-2 expression. However, engagement of either B7-1 or B7-2 is functionally redundant (Borriello et al. Immunity 1997). CD28 engagement in concert with TCR ligation strongly amplifies weak TCR signals, resulting in dependency on Signal 2 when TCR occupancy is low (Viola and Lanzavecchia Science 1996, Diehn et al PNAS 2002; Riley et al. PNAS 2002). Downstream signalling of CD28 involves recruitment of multiple kinases to a phosphorylated YMNM sequence and proline-rich motifs in its cytoplasmic tail. PI3K (Phosphatidyl-Inositol-3-Kinase) activation of the AKT pathway via involvement of src-family kinases lck and fyn then activates multiple pathways linked to protein synthesis, cellular metabolism, and cell survival. Activation of the NF-κB pathway has also been implicated (Raab et al PNAS 1995, Frauwirth et al. Immunity 2002, Takeda et al. Int Immunol 2008).

CD40-CD40L and the DC licensing model

$CD8^+$ T cell immunity has been shown to be dependent on help from $CD4^+$ T_H cells to APCs, a process known as 'DC licensing'. Although initially controversial, due to the dispensable requirement for antigen in some situations, DC licensing via the CD40-CD40L interaction is

now recognised to be necessary for effective CTL memory (Smith et al. Nat Immunol 2004, Ma and Clark Sem Immunol 2009). On the basis of the phenotypes of CD40 -/- mouse models and CD40L-impaired patients with hyper-IgM syndrome, CD40-CD40L interactions were classically thought to be involved in T cell help to B cells (Allen et al. Science 1993, Korthauer et al. Nature 1993, Brown et al. Nat Med 1998). Subsequently, CD40 engagement was shown to modulate APC function through upregulation of B7-1/B7-2 and MHC (Caux et al. JEM 1994, Pinchuk et al. Immunity 1994) and to enhance T cell activation via DC production of IL-12 (Cella et al. JEM 1996). The cytoplasmic tail of CD40 contains sites for the recruitment of TRAFs (TNFR-Associated Factor family of proteins), which mediate downstream signalling pathways leading to cytokine production and upregulation of co-stimulatory molecules (Kobayashi et al. Microbes Infect 2004).

CD40 is widely expressed on many resting subsets, including B cells, monocytes and DCs, and also on activated $CD4^+$ and $CD8^+$ T cells. Its ligand CD40L (CD154) is expressed on activated $CD4^+$ T cells, activated B cells, and is induced on human DCs after CD40 stimulation. Thus, the potential exists for bidirectional CD40-CD40L interactions between APCs and lymphocytes (Mackey et al. JI 1998, Rissoan et al. Science 1999).

Inhibitory costimulation by B7:CD28 family members

CTLA-4

CTLA-4 is the classical negative costimulator, providing an inhibitory 'second-signal' to TCR engagement. CTLA-4 is structurally similar to CD28, being a glycosylated disulphide-linked homodimer, but binds B7-1 with approximately 17-fold higher affinity (van der Merwe et al. JEM 1997). In comparison to CD28, CTLA-4 acts to dampen T cell responses to antigen and is upregulated following T cell activation in order to limit the response. CTLA-4 -/- mice die

from profound multi-organ autoimmunity within 3 weeks of birth (Waterhouse et al. Science 1995). CTLA-4 is primarily expressed intracellularly, in the trans-Golgi network and endolysosomal compartments. Even after optimal T cell activation only a small percentage is redirected to the surface, and is localised at the immunological synapse, with the degree of externalisation dictated by TCR-pMHC affinity (Egen et al. Immunity 2002). CTLA-4 engagement reverses the 'stop signal' induced by TCR ligation and required for stable T cell:APC interaction (Schneider et al. Science 2006), inhibits the formation of lipid rafts which contain adaptor proteins such as LAT (Martin et al. JEM 2001), and disrupts the formation of signalling microclusters necessary for Ca^{2+} influx concomitant to proliferation (Schneider et al. EJI 2008). CTLA-4 may have a role in tolerance; transgenic mice with CTLA-4 deletion targeted specifically to $FoxP3^{+}$ Tregs have reduced suppressive ability of these cells (Wing et al. Science 2008).

PD-1, PD-L1 and PD-L2

PD-1 is expressed on activated T cells, NK T cells, B cells, activated monocytes and myeloid DCs. It negatively regulates signalling through the TCR or BCR; its expression on non-lymphocytes is of unknown functional significance. PD-1 ligation dampens TCR signalling but can be overcome by strong CD28 costimulation. This negative signalling requires proximity of the PD-1 cytoplasmic domain with the TCR and PD-1 has been shown to redistribute to the immunological synapse upon activation. Phosphorylation of the ITIM and ITSM motifs within the cytoplasmic tail of PD-1 by TCR-associated kinases leads to the recruitment of the phosphatases SHP-1 and SHP-2, which then dephosphorylate downstream signalling molecules. PD-1 ligation downregulates IL-2, IFN-γ and TNF-α production, with weaker negative effects upon cell proliferation. Effector cell differentiation and survival are impeded through disruption of signalling via CD28 and IL-2.

PD-1 binds to its ligands, PD-L1 and PD-L2. PD-L1 is more widely expressed than PD-L2, and can be induced on T cells, B cells and myeloid cells as well as being constitutively expressed on a wide range of non-haematopoietic cells. PD-L1 expression can be upregulated upon exposure to IFNs. PD-L2 expression is more restricted to APCs – it is constitutively expressed on peritoneal B1 cells and can be induced on DCs, macrophages and bone marrow-derived mast cells. There is evidence for bidirectional signalling through PD-1:PD-L interactions. Soluble PD-1-Fc inhibits DC activation and leads to a suppressive DC phenotype with increased production of IL-10 (Kuipers et al. EJI 2006). Soluble PD-1 can also induce IL-10 secretion by $CD4^+$ T cells (Dong et al. JCI 2003). PD-L2 blockade of DCs by antibody treatment leads to increased production of proinflammatory IL-6 and TNF-α and increased proliferation of naive T cells (Nguyen et al. JEM 2002).

PD-L1 can also bind to B7-1 and provide negative signals into T cells (Butte et al. Immunity 2007). This explains contradictory observations in the PD-1 field. PD-L1 -/- T cells from PD-L1 deficient mice show increased inflammatory cytokine production (Latchman et al. PNAS 2004). Bidirectional PD-L1/B7-1 interactions are possible between T cells, B cells, DCs and macrophages because both PD-L1 and B7-1 are expressed on these cell types. The presence of B7-1 as well as PD-1 on T cells allows regulation of T cell responses via the interaction with PD-L1 on non-haematopoietic cells. Peripheral tissue expression of PD-1 ligands may thus limit aggressive or self-reactive responses.

ICOS and ICOSL

ICOS, like CD28 and CTLA-4, is a glycosylated disulphide linked homodimer. It is upregulated on $CD4^+$ and $CD8^+$ effector and memory T cells after activation via CD28 and

TCR signalling and contains a cytoplasmic PI3K-binding motif (Coyle et al. Immunity 2000). ICOS is also expressed on activated NK cells. Its ligand, ICOSL, is expressed on a variety of cell types including endothelial and epithelial cells, B cells, DCs, macrophages and a subset of T cells. ICOS/ICOSL interactions are essential for T cell help to B cells; mice lacking ICOS or ICOSL have impaired B cell responses (Hutloff et al. Nature 1999, McAdam et al. Nature 2001, Tafuri et al. Nature 2001). Similarly, homozygous loss of ICOS has been identified as the cause of common variable immunodeficiency disease in a small number of human patients, who display profoundly impaired antibody responses and recurrent bacterial infections (Grimbacher et al. Nat Immunol 2003).

Several studies suggest ICOS-ICOSL interactions are involved in $CD4^+$ T cell suppression by iDCs. This is proposed to be through upregulation of the IL-10R on T cells, which can lead to iTreg generation, thereby highlighting a potential role for ICOS/ICOSL interactions in tolerance induction. (Witsch et al. EJI 2002, Levings et al. Blood 2005, Tuettenberg et al. JI 2009).

Signalling through MHC Class I engagement – KIRs and LILRs

Engagement of MHC Class I by inhibitory receptors has been shown to modulate the functions of a range of immune cells, including DCs, T cells and NK cells. Class I MHC inhibitory receptors underlie 'missing-self' recognition by NK cells, exemplified in humans by their Killer Ig-like Receptors (KIRs). KIRs are polymorphic and exhibit haplotype variability, and engage MHC Class I in a peptide and allele-specific fashion. KIRs have either 2 or 3 extracellular Ig-like domains; inhibitory KIRs have long cytoplasmic tails containing ITIMs, and activatory KIRs have short cytoplasmic tails and associate with the ITAM-containing adaptor, DAP12. Several inhibitory KIRs have well-defined MHC Class I

ligands, but activatory KIRs show either weak or undetectable binding to MHC Class I and their ligands remain unknown (Parham Immunol Lett 2004, Rajagopalan and Long JEM 2005, Khakoo and Carrington Immunol Rev 2006). Of more relevance to modulation of myelomonocytic cell function is a related family of immunoreceptors, the Leukocyte Ig-Like Receptors (LILRs), also encoded within the Leukocyte Receptor Complex (LRC) on human chromosome 19. In contrast to KIRs, the LILRs are more widely expressed, and are found primarily on myelomonocytic cells as well as subsets of B and T cells. This expression pattern has suggested their relevance to APC function and maturation. The LILRs are discussed extensively in Section 1.2.

1.1.5 DCs and their role in Tolerance

Evidence that DCs are instrumental in tolerance arises from several observations. Immature DCs induce anergy of naive T cells or induce the generation of $Foxp3^+$ Tregs (Steinman and Banchereau Nature 2007, Steinman and Nussenzweig PNAS 2002). The phagocytosis of apoptotic cells or self antigens by DCs in the steady state induces a tolerogenic phenotype (Steinman et al. JEM 2000, Hawiger et al. JEM 2001). Disruption of E-cadherin-mediated DC-DC interactions triggers an alternative pathway of maturation and programs DCs to a tolerogenic state (Jiang et al. Immunity 2007). Exposure of DCs to anti-inflammatory and immunosuppressive agents may also promote this effect (Mellor and Munn Nat Rev Immunol 2004, Morelli and Thomson Nat Rev Immunol 2007). Specific DC subsets in mucosal sites (for example, $CD103^+$ DCs in intestinal lamina propria and mesenteric lymph nodes) are programmed to induce Treg cells (Coombes et al. JEM 2007, Denning et al. Nat Immunol 2007). Finally, certain microbial stimuli are also capable of subverting DCs to induce Treg cells (van der Kleij et al. JBC 2002, McGuirk et al. JEM 2002, Manicassamy et al. Nat Med 2009).

Although iDCs were first considered to induce tolerance, due to their low costimulatory molecule expression, it is now accepted that mDCs may also play a role in Treg induction and maintenance (Tan et al. JLB 2005, Hubert et al. JLB 2007). DCs with suppressive properties – tolerogenic DCs – exhibit many of the characteristics of iDCs (low costimulatory and MHC Class II expression, for example). Indeed, the distinctions between iDC, mDC and tolerogenic DC are blurred and may reflect the inherent plasticity of DCs in both their phenotype and responsiveness to the immune microenvironment.

Tolerogenic myeloid cells are likely to exert a powerful influence in the context of tumour immunity. Tolerogenic DCs may present self antigens to $CD4^+$ T cells or cross-present to $CD8^+$ T cells leading to Treg or T_S cell induction (Lutz and Kurts EJI 2009), a process that may be critical to tumour immune evasion. The tumour microenvironment is highly suppressive, with high levels of IL-10 and TGF-β secreted by Myeloid-Derived Suppressor Cells (MDSCs), tumour-associated macrophages, and iDCs. In addition, tumour-antigen cross-presentation by DCs can induce anergy and deletion in T cells, and their conversion to Tregs. Consequently, research to understand tumour-derived tolerance dysregulation is essential to progress new therapies (Peggs et al. Immunol Rev 2008, Melief Immunity 2008, Gallimore and Simon Oncogene 2008).

The mechanisms involved in tolerogenic DC function are an area of active research. Tolerogenic DCs may exert their effects directly upon effector cells, or via the generation of Tregs that then mediate suppression (Cools et al. JLB 2007, Belkaid and Oldenhove Immunity 2008). Established mechanisms for tolerogenic DC activity include the secretion of suppressive cytokines such as IL-10 and TGF-β, which also expand Treg populations; through

surface expression of indoleamine-2,3-deoxygenase (IDO), which metabolises extracellular tryptophan to kynurenines that inhibit T cell proliferation; via the lack of positive costimulation (through downregulation of B7-1, B7-2 and CD40); and finally via inhibitory receptor engagement and negative costimulation (e.g. the expression of CTLA4 or PD-1 ligands) (Coquerelle and Moser Immunol Rev 2010, Pulendran et al. Nat Immunol 2010). This latter mechanism has recently highlighted the involvement of the LILRs, LILRB4 and LILRB2, in tolerance induction (Chang et al. Nat Immunol 2002). In the next section I will discuss functional, structural and clinical aspects of the role of these immunoreceptors in myelomonocytic cell function and maturation.

1.2 The Leukocyte Immunoglobulin-Like Receptor Family

1.2.1 Introduction and initial characterisation

The Leukocyte Immunoglobulin-like Receptors (LILRs) are a family of immunoregulatory receptors located within the Leukocyte Receptor Cluster (LRC) on human chromosome 19. The LILRs share amino acid sequence homology with other immunoglobulin superfamily (IgSF) receptors encoded in the LRC, including the Killer Immunoglobulin-like Receptors (KIRs), the receptor for IgA FcαR, Leukocyte-Associated Immunoglobulin-like Receptors (LAIRs), the NK cell Natural Cytotoxicity Receptor (NCR) NKp46, and the platelet collagen receptor GpVI. The genomic organisation of the LILR locus is shown in **Figure 1.2a**.

LILRs are type I transmembrane proteins and have either two or four extracellular C2-type Ig domains. Inhibitory members of the family have long intracellular tails containing ITIMs, and are designated as LILRB. Activatory members of the family have short intracellular tails and a positively charged arginine residue within the transmembrane region which allows them to associate with the ITAM-containing adaptor protein FcRγ, and are designated LILRA. **Figure 1.2b** outlines the structural elements of each LILR. LILRA3 lacks a transmembrane domain and is expressed solely in soluble form. Although studies had detected soluble forms of LILRA5 and LILRB2 (Borges Blood 2003, Beinhauer EJI 2004), it was only recently that a common splicing mechanism was identified that generates mRNA transcripts for other soluble LILRs, thus providing another level of regulation of LILR function (Jones EJI 2009). Most members of the family have four Ig domains; LILRB4, LILRA5 and a splice variant of LILRA1 have only two. The LILRs were initially identified and characterised in parallel by three different groups. Cosman et al. identified a novel IgSF member that bound to both the human Cytomegalovirus (CMV) MHC Class I homologue, UL18, and to host MHC Class I molecules, and named that protein Leukocyte Immunoglobulin-like Receptor-1, LIR-1

(Cosman et al. Immunity 1997). Samaridis and Colonna isolated novel cDNAs from the LRC with KIR homology and designated them Immunoglobulin-like Transcripts (ILTs) 1 and 2 (Samaridis, Colonna EJI 1997). Another group also identified a member of the family on the basis of its homology with the mouse gp49B1 receptor, which they designated HM18 (Arm et al. JI 1997). The LILRs thus have slightly confusing alternative nomenclatures; in this thesis, the LILR designation will be used. **Table 1.2** summarises the alternative designations of the LILR family, along with their expression patterns.

In contrast to the structurally-similar KIRs, the LILRs exhibit a conserved organization of gene structure, and do not usually display haplotypic variation in gene number. Polymorphisms within the coding sequence of the receptors are relatively rare by comparison with the KIRs, with the exception of LILRB3, which is highly polymorphic (Young et al. Immunogenetics 2001, Volz et al. Immunol Rev 2001). In evolutionary terms, the LILRs may predate the KIRs (Volz et al. Immunol Rev 2001, Martin et al. Trends Immunol 2002, Canavez JI 2001). Mice lack true orthologues of the KIRs, relying instead upon members of the Ly49 family for 'missing-self' recognition by NK cells, but do have receptors with homology to some of the LILRs, the Paired Ig-like Receptors (PIRs), which have been relatively well characterised (Kubagawa et al. PNAS 1997, Pereira et al. JI 2004, Munitz et al. Blood 2008).

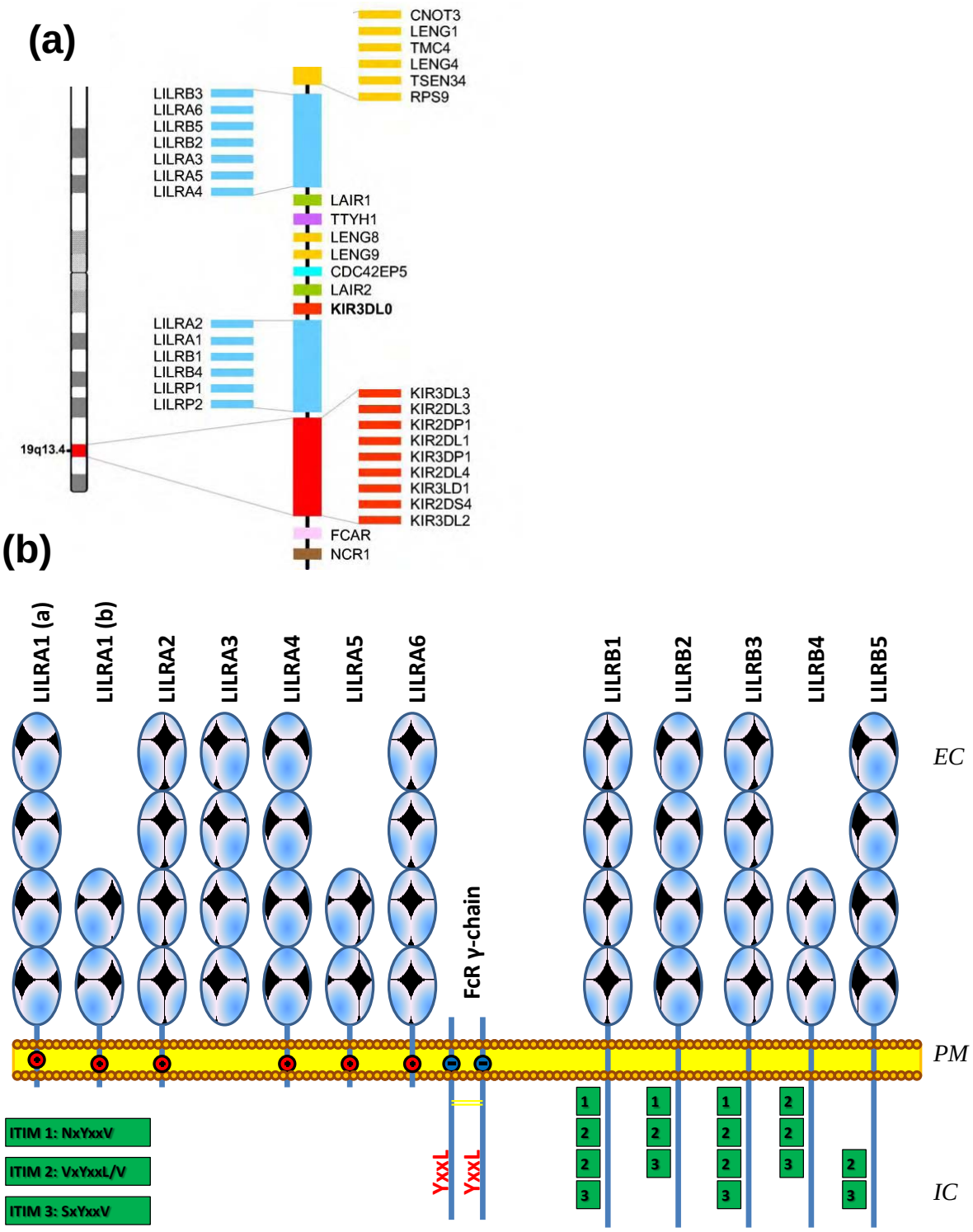

Figure 1.2. Genomic and structural arrangement of the LILRs. (a): Organisation of the LILR clusters within the LRC on human chromosome 19. (Sambrook et al. BMC Genomics 2006). (b): Domain structure of the LILRs, showing extracellular (EC) Ig domains, plasma membrane (PM)-spanning transmembrane domains with Arginine residues for the activatory LILRs, the structure of the FcR γ-chain, and the ITIM sequences in the intracellular cytoplasmic tails for the inhibitory LILRs.

LILR	Alternative Nomenclature	Expression									
		Monocytes	Macrophages	Dendritic Cells	Osteoclasts	Basophils	Eosinophils	NK Cells	T Lymphocytes	B lymphocytes	Other
LILRB1	LIR-1, ILT2, CD85j, MIR7	■	■	■	■		■	□	■	■	1
LILRB2	LIR-2, ILT4, CD85d, MIR10	■	■	■	■	■	■				2
LILRB3	LIR-3, ILT5, CD85a, HL9	■	■	■	■	■	■				
LILRB4	LIR-5, ILT3, CD85k, HM18	■	■	■	■						3
LILRB5	LIR-8, CD85c	?						?			4
LILRA1	LIR-6, CD85i		■								
LILRA2	LIR-7, ILT1, CD85h	■	■	■		■	■	■			
LILRA3	LIR-4, ILT6, CD85e, HM43, HM31	■									
LILRA4	ILT7, CD85g			□							
LILRA5	LIR-9, ILT11, CD85f	■									
LILRA6	ILT8, CD85b	*Unknown*									
LILRP1	ILT9, CD85l	*Pseudogene*									
LILRP2	ILT10, CD85m	*Pseudogene*									

Table 1.2 LILR Family Nomenclature and Expression. Filled squares indicate expression by all or the majority of the named cells, open squares indicate restricted subset expression, question marks for LILRB5 indicate donor variability or mRNA only. Additional expression: 1, placental stromal cells; 2, placental vascular smooth muscle; 3, CLL and some cancers; 4, Mast cell granules. (Adapted from Anderson and Allen Immunology 2009).

1.2.2 Published functional studies of LILR family members

LILRB1

LILRB1 is broadly expressed on T cells, B cells, myeloid cells and subsets of NK cells. The first demonstration of an inhibitory function for LILRB1 was from redirected killing assays involving LILRB1$^+$ NK cell lines (Colonna et al. JEM 1997). Subsequent studies on NK cell clones confirmed HLA-A, HLA-B, HLA-C, and HLA-G molecules all inhibited NK killing in a LILRB1-dependent fashion, and suggested synergism with CD94/NKG2A (Vitale et al. Int Immun 1999).

The inhibitory effects of LILRB1 ligation were also evident in T cells, B cells and myeloid cells. LILRB1 interactions with MHC Class I were able to inhibit superantigen-mediated T cell killing of 721.221 cells (Colonna et al. JEM 1997). Subsequently, LILRB1 was shown to down-regulate antigen-specific cytolytic activity of CD8$^+$ T cells (Saverino JI 2000). Cytolytic CD4+ T cells specific for *Mycobacterium tuberculosis* purifed protein derivative (PPD) could be inhibited from killing by LILRB1 engagement, and also showed reduced IL-2 and IFN-γ secretion (Merlo et al. Inf Immunity 2001). Thus, LILRB1 has functional effects on both cytotoxic CD8$^+$ T cells and helper CD4$^+$ T cell subsets. Engagement of LILRB1 on antigen-activated T cells had a dual effect on cytokine secretion, by upregulation of IL-10 and TGF-β whilst simultaneously downregulating the synergistic cytokines IL-2, IL-13 and IFN-γ. Importantly, the inhibitory effect of LILRB1 engagement could be overcome by the addition of exogenous IL-2. In addition, both naive T cell responses to initial antigenic stimulation, and recall responses of resting/memory T cells were similarly affected (Saverino et al. JI 2002).

In addition to effects on T cells, Ca^{2+} mobilization triggered via BCR engagement in B cells

or HLA-DR triggering in myelomonocytic cells was reduced by co-crosslinking the triggering receptor to LILRB1, via the anti-LILRB1 antibody. Furthermore, co-ligation of FcγRI on monocytes with LILRB1 or LILRB2 led to reduced γ-chain ITAM and downstream Syk phosphorylation and mobilisation of intracellular Ca^{2+}. Therefore, LILRB1 engagement by MHC Class I can negatively regulate the functions of innate and adaptive effector immune cells as well as APCs (Colonna et al. JEM 1997).

LILRB2

LILRB2 is a MHC Class I-binding inhibitory LILR receptor restricted in expression to the myeloid lineage. Like LILRB1, LILRB2 can engage the non-classical MHC Class I molecule HLA-G with a higher affinity than to classical HLA alleles (Shiroishi et al. PNAS 2003). HLA-G is expressed on placental trophoblast cells, thymic epithelial cells and some tumours, suggesting an important *in vivo* role for its interaction with LILRB2 and LILRB1, and possible involvement in maternal-foetal tolerance (Allan et al. JEM 1999). In particular, LILRB2 shows a stronger preference for HLA-G over other HLA alleles. The LILRB2/HLA-G interaction is thus postulated to be important for the function and maturation of myelomonocytic cells. Ristich et al. presented *in vivo* data in support of this notion, using mice transgenic for LILRB2 and HLA-G1. DCs from these mice have a tolerogenic phenotype with reduced expression of MHC Class II, B7-1 and B7-2, and promote skin allograft survival by the induction of Tregs (Ristich et al. Hum Immunol 2007). HLA-G isoforms are capable of multimerisation; HLA-G1 tetramers and HLA-G5 homodimers signal efficiently through LILRB2 leading to the arrest of DC maturation *in vitro* and *in vivo*, through the recruitment of SHP-1 and SHP-2, which exerts its effects via the IL-6/STAT3 pathway (Liang et al. PNAS 2008). A subset of tolerogenic DCs termed DC-10 was recently identified that produces high levels of IL-10 and induces the differentiation of Tr1 cells *via* a

LILRB2/HLA-G dependant mechanism (Gregori et al. Hum Immunol 2009, Gregori et al. Blood 2010). A T cell subset expressing HLA-G and with a regulatory phenotype has also been described (Feger et al. Blood 2007). It is interesting to speculate that these novel suppressive T cells may exert tolerogenic effects via LILRB2 engagement on DCs.

Tolerogenic functions of LILRB4 and LILRB2

LILRB4 has two extracellular Ig-like domains and a long cytoplasmic tail containing three ITIM motifs. Myeloid expression of LILRB4, functional effects of cross-linking and downstream signalling involving SHP-1 were first described by Cella et al. in 1997 (Cella et al. JEM 1997). They also proposed a role for LILRB4 in antigen capture and processing, although that aspect of LILRB4 function has not since been expanded upon. The ligand for LILRB4 has been elusive despite numerous publications on its functional role.

Several functional studies have proposed a role for LILRB2 and LILRB4 in tolerisation of T cell responses, through the action of APCs such as DCs and monocytes that have been given a tolerogenic stimulus (e.g. IL-10, incubation with $CD4^+$ Tregs or $CD8^+$ suppressor T cells, T_S). A key study by Chang *et al*. described the upregulation of LILRB4 and LILRB2 on APCs (monocytes, immature DCs generated from monocytes by treatment with GM-CSF/IL-4, or the myelomonocytic cell line KG1) upon incubation with alloantigen-specific $CD8^+$ $CD28^-$ T_S cells. Such treatment reduced the allostimulatory capacity of these APCs towards $CD4^+$ T_H cells in co-cultures, apparently by reducing the surface expression of B7-1 and B7-2 through inhibition of the CD40-CD40L pathway. Antibody blockade of LILRB4, or LILRB2 plus MHC Class I, reversed the inhibitory effect of $CD8^+$ T_S cells on $CD4^+$ T_H cell proliferation when all three cell types (T_S, T_H and APCs) were cultured together. Overexpression of LILRB4 or LILRB2 by transfection of KG1 cells conferred a tolerogenic capacity, as

evidenced by a reduction in the proliferation of $CD4^+$ T_H cells and an inhibition of the upregulation of B7-1 on the APCs upon co-culture, an effect which could be overcome with exogenous IL-2. The inhibitory effect of LILR over-expression was postulated to be due to disruption of NF-κB signalling. Experiments with the PBMCs from heart allograft transplant patients confirmed a role for LILRB2 and LILRB4 in tolerance induction *in vivo*, as discussed further in Section 1.2.4 (Chang et al. Nat Immunol 2002).

Manavalan *et al*. subsequently demonstrated that $CD4^+$ T_H cells incubated with tolerogenic APCs that have upregulated LILRB4 and LILRB2 expression develop a Treg phenotype. Priming with allogeneic DCs generated $CD4^+$ Tregs that were MHC Class II restricted and induced 'linked suppression' of DCs on which they recognized at least one MHC Class II antigen. Antibody blockade of LILRB4, or LILRB2 plus MHC Class I, reduced this effect, supporting the hypothesis that LILRB4 and LILRB2 play a role in the suppression of immune responses by Tregs and in the phenomenon of 'infectious tolerance'. IL-10 or TGF-β did not mediate the tolerogenic effect of these Tregs; cell-to-cell contact was found to be necessary. Importantly, this work also demonstrated that treatment of DCs with IL-10 plus IFN-α induced a tolerogenic phenotype with upregulation of LILRs in the same fashion as co-incubation with $CD8^+$ T_S or $CD4^+$ Tregs (Manavalan Trans Immun 2003), a result supported by another publication which also lent more credence to the notion that tolerogenic DCs are not simply immature, but have a distinct phenotype and gene signature (Velten et al. EJI 2004). Indeed, DCs stimulated via TLR9 triggering, or a variety of other inflammatory mediators, down-regulate LILRB1 and LILRB4 (Ju et al. Gene 2004) and this suggests that down-regulation of LILR expression may be involved in DC activation, possibly via reduced SHP-1 modulation of the NF-κB pathway. Furthermore, endothelial cells may also be tolerised and up-regulate LILRB4 and LILRB2 in a similar manner, providing further

evidence for their role as accessory APC and for the importance of studying this mechanism of tolerogenesis in the context of organ transplantation (Cortesini et al. Transpl Immunol 2004, Manavalan et al. Int Immunol 2004, Lui et al. Transpl Immunol 2004, Gleissner et al. EJI 2007).

Despite these findings, the molecular mechanism underlying LILRB4 tolerance induction is unclear. Nevertheless, studies utilising APC transfected with recombinant LILRB4 lacking the intracellular ITIMs have demonstrated bidirectional signalling between APC and T cells, rendering the T cells anergic or converting them to Tregs (Kim-Schulze et al. JI 2006, Vlad et al. Int Immunol 2006). This provides some clues to the nature of the LILRB4 ligand, which to date is unknown. Such a ligand would have to be present on T cells and/or DCs and capable of signalling in an inhibitory fashion into those cells. LILRB4-Fc staining experiments have shown the LILRB4 ligand to be up-regulated on $CD4^+$ T cells after 3 days in an allogeneic MLR (Kim-Schulze et al. JI 2006).

LILRA2 and LILRB3

In contrast to the inhibitory LILRs, activatory LILRs remain poorly understood, both on a functional level and in terms of their ligand interactions. Initial characterisation of LILRA2 demonstrated its expression on monocytes, granulocytes, macrophages and DCs, and a small percentage of peripheral blood NK cells. Antibody cross-linking of surface LILRA2 triggered serotonin release from transfected RBL cells, and Ca^{2+} mobilisation from transfected cells or isolated human monocytes. FcεRI γ-chain was shown to co-precipitate with LILRA2 and was necessary for its surface expression (Nakajima et al. JI 1999). LILRA2 was subsequently shown to be expressed on eosinophils and neutrophils, and antibody cross-linking stimulated activation, degranulation and IL-12 release in these cells (Tedla et al. PNAS 2003). A similar

study highlighted LILRA2 expression on basophils and showed LILRA2-mediated activation and release of inflammatory mediators (including IL-4) after cross-linking. Importantly, this study showed that co-engagement of LILRA2 with LILRB3 inhibited activation, and provides the only functional data to date on LILRB3 (Sloane et al. Blood 2004).

LILRA4

LILRA4 is a specific marker for pDCs as opposed to classical DCs, and it is co-expressed with its signalling adaptor protein, FcRγ-chain. Both molecules are rapidly downregulated following activation by CpG-DNA stimulation of TLR9 (Ju et al. Gene 2004). Generation of an anti-LILRA4 antibody allowed confirmation of the restricted cell-surface expression of LILRA4 on pDCs, and investigation of the functional effects of its ligation. Antibody cross-linking of LILRA4 generated Src family kinase and Syk phosphorylation events, via the ITAMs of the adaptor FcRγ chain, leading to intracellular Ca^{2+} mobilisation, an event generally associated with cellular activation. Surprisingly, the effects of LILRA4 ligation upon TLR-mediated IFN-α and TNF-α production were instead inhibitory (Cao et al. JEM 2006). The authors speculated that this may be due to the bi-functional role of the FcεRI γ-chain ITAM, which is capable of recruiting both Syk and SHP-1 (Pasquier et al. Immunity 2005). Alternatively, ligand affinity may determine the functional outcome of LILRA4 engagement (Cho et al. Int Immunology 2007).

Recently, the ligand for LILRA4 was identified as BST2 and shown to negatively regulate the innate immune functions of pDCs via the engagement of LILRA4. Since BST2 is upregulated on a wide variety of cell types upon Type I IFN treatment, the LILRA4/BST2 interaction may constitute a negative feedback mechanism to limit immunopathological

damage resulting from sustained IFN release from pDCs in the face of viral challenge (Cao et al. JEM 2009).

LILRA5

LILRA5 is closely related to LILRB4 in terms of primary sequence, and like LILRB4, it has only two Ig domains. There are four splice variants, LILRA5m1, LILRA5m2, LILRA5s1 and LILRA5s2, where m stands for membrane-bound and s stands for soluble forms, respectively. The difference between the 1 and 2 forms of each receptor resides in the N-terminal amino acids, just after cleavage of the signal peptide, and generates a new N-linked glycosylation site in LILRA5m1 and LILRA5s1. LILRA5m is expressed at the surface of monocytes, and cross-linking of the receptor induces Ca^{2+} mobilisation and the release of the inflammatory cytokines IL-1β, TNF-α and IL-6 (Borges et al. Blood 2003).

LILR Signalling Mechanisms

A small number of studies have investigated the signalling mechanisms downstream of LILRB ligation. LILRB1 co-immunoprecipitates with SHP-1 after sodium pervanadate treatment (Colonna et al. JEM 1997, Cosman et al. Immunity 1997). In addition, Dietrich et al. showed SHP-1 recruitment to the second ITIM, which matches the SHP-1 consensus binding sequence VxYxxV/L, was dependent upon the Src tyrosine kinase $p56^{lck}$ phosphorylating the tyrosine residue. The phosphorylation of key signalling molecules downstream of TCR ligation, namely the TCR ζ-chain and the Linker for the Activation of T cells (LAT), was reduced upon LILRB1 co-engagement, and resulted in reduced recruitment of the downstream kinase ZAP-70. Furthermore, actin polymerization, which is a key event in TCR-mediated signalling, was also markedly inhibited by LILRB1 engagement (Dietrich et al. JI 2001). The cytoskeletal changes downstream of actin polymerization are necessary to

bring signalling molecules into the immune synapse and to polarize the T cell towards the APC (Monks et al. Nature 1998). Thus, TCR engagement of cognate pMHC concomitant with T cell-expressed LILRB1 engagement of MHC Class I on the target cell interferes with a key stage of T cell activation.

Bellon et al. probed the contribution of the four tyrosine residues in the cytoplasmic tail of LILRB1, by transfecting mutant receptors into the rat basophilic leukaemia (RBL) and COS-7 cell lines and analysing the ability of the different mutants to recruit SHP-1 and to inhibit FcεR-induced serotonin secretion. These experiments revealed that the LILRB1 C-terminal tyrosines 614 and 644 are crucial sites for binding to SHP-1. Mutation of residue Y562 had no effect, whereas residue Y533 seemed to be involved in the regulation of receptor tyrosine phosphorylation (Bellon et al. JI 2002). A collaborating group showed that the C-terminal Src kinase (Csk) binds LILRB1 Y562 and hypothesised that Csk regulates the function of LILRB1 (Sayos et al. BBRC 2004).

Data on the signalling cascades downstream of other LILR receptors is sparse. Liang et al. published data showing that LILRB2/HLA-G engagement *in vitro* and *in vivo* recruits SHP-1 and SHP-2 to the phosphorylated receptor, which activates the IL-6–STAT3 pathway leading to up-regulation of IL-6 expression and down-regulation of DC differentiation (Liang et al. PNAS 2008). LILRB4 has been shown to be a potent inhibitor of monocyte activation, as discussed with reference to its tolerogenic effects earlier in this section. Co-ligation of LILRB4 with FcγRI selectively inhibits the phosphorylation of the signalling molecules Lck, Syk, LAT, Erk, and c-Cbl but not the cytoskeletal protein α-actinin-4. Treatment of cells with the broad-spectrum phosphatase inhibitor, sodium pervanadate, significantly reversed this

effect, but treatment with an SHP-1 specific inhibitor did not, suggesting the involvement of other phosphatases (Lu et al. JBC 2009).

1.2.3 Ligand recognition and structural studies of the LILRs

LILRB1

LILRB1 was initially identified on the basis of immunoprecipitation with a UL18-Fc fusion protein. Expression cloning and transfection of the resulting cDNA into COS cells generated a UL18-Fc-binding protein identical in mass to that previously detected. LILRB1-Fc also stained UL18 transfectants, confirming an interaction between the extracellular regions of LILRB1 and UL18. Subsequent to this discovery, an attempt was made to identify the endogenous cellular ligand corresponding to UL18 that was bound by LILRB1, the obvious candidate being host MHC Class I. This proved to be the case, as LILRB1-Fc was shown to stain a wide panel of cell lines and primary cells, and an expression library from a T lymphoblastic leukaemia cell line was probed for LILRB1-Fc binding, yielding two cDNAs encoding HLA-A2 and HLA-B44, respectively. Binding of LILRB1-Fc to primary cells or cell lines could be blocked by pre-incubation with W6/32, a monoclonal antibody that binds all classical (HLA-A, -B, -C) MHC Class I alleles (Cosman et al. Immunity 1997).

In similar experiments, the Cosman group used flow cytometry to test the ability of various LILR-Fc fusion proteins to bind peripheral blood T cells that had been activated non-specifically with PHA and PMA, and showed that LILRB2-Fc, like LILRB1-Fc, could also bind MHC Class I, as this staining could be abrogated by pre-incubation with W6/32. No other LILR-Fc stained these cells, and only LILRB1-Fc stained UL18-transfected cells (Borges et al. JI 1997). Independently, Colonna et al. carried out analogous experiments, using soluble LILRB1-Fc to stain MHC Class I transfected 721.221 cells and analysed them

by flow cytometry, detecting binding to HLA-A, HLA-B, and HLA-G transfectants, but not to HLA-Cw3 (Colonna et al. JEM 1997). LILRB1-Fc and LILRB2-Fc were used in further flow cytometry analyses for binding to a panel of HLA-allele transfected 721.221 cells, and were shown to bind to a broad range of 'classical' MHC Class I alleles including one HLA-C allele (Fanger et al. EJI 1998). This result was consistent with subsequent functional studies of LILRB1^{+} NK cells (Vitale et al. Int Immunol 1999, Navarro et al. EJI 1999).

The mode of ligand recognition used by LILRB1 was first addressed by Chapman et al (Chapman et al. Immunity 1999). Soluble LILRB1 containing truncations of the extracellular domains were produced and LILRB1 – ligand binding was analysed by SPR. The LILRB1 ectodomain bound to UL18 with an equilibrium dissociation constant, K_d, in the nM range, with no demonstrable effect of varying the peptide loaded or glycosylation status of the UL18. A range of classical (HLA-B, HLA-C) and non-classical (HLA-G, HLA-E) MHC Class I alleles were also tested for binding, and shown to have K_d values in the range of 15-100 μM; thus, LILRB1 displays approximately 1000-fold lower affinity for MHC Class I than for UL18. Three other MHC Class I homologues, HFE, FcRn, and ZAG, showed no binding to LILRB1.

Comparative analysis of binding of fragments of LILRB1 containing domains D1, D1D2 or D3D4 allowed localization of the UL18 and MHC Class I binding site to the distal D1 domain, with a minor contribution from D2. Pre-equilibration of UL18 with D1D2 blocks binding of D1D2 to immobilized MHC Class I, thus both ligands for LILRB1 share the same binding site. Domain-swap experiments from HFE into UL18 or MHC Class I and analysis of monomeric LILRB1 D1-D4 or LILRB1-Fc binding to the resulting chimeric proteins showed that the α3 domain of either UL18 or MHC Class I was necessary for binding to the molecule

by LILRB1. This result explained the broad binding specificity of LILRB1 for MHC Class I alleles, since the α3 domain is relatively non-polymorphic, and provides a contrast with the recognition of MHC Class I alleles by KIRs, which are allele-specific and bind at the polymorphic α1-α2 peptide-binding platform of the MHC. Based on the fact that isolated LILRB1 domains fold stably, and data from far UV circular dichroism experiments, it was proposed that LILRB1 would form an extended structure, with the distal D1 domain interacting *in trans* with the α3 domain of a MHC on an opposing cell membrane.

Structural studies on LILRB1

Crystallographic data for LILRB1 became available in 2000, when the structure of the D1D2 construct was obtained to a resolution of 2.1 Å (Chapman et al. Immunity 2000). Similar to KIRs, the two domains are arranged into a bent structure with an acute interdomain angle and each LILRB1 Ig domain is composed of two anti-parallel β-sheets. LILRB1 D1D2 also has extensive helical structure not seen in other IgSF receptors, including a region of 3_{10} helix in the C' strand of D1, and a polyproline type II helix in the strand F-G loop. The interdomain interface between D1 and D2 is composed mainly of hydrophobic/aromatic residues that serve to stabilise the acute domain angle.

Comparison of the interdomain residues across the LILR family showed considerable conservation, suggesting a common arrangement of D1 relative to D2 for the other LILR members. Within LILRB1, similar analysis suggested that D2D3 domains might also form a similar interaction, whereas corresponding residues in D4 were non-conservatively substituted, implying that the D3D4 interaction would take a different form. Based upon this analysis, three models for LILRB1 D1-D4 structure were proposed; a 'bent rod' structure of

~110 Å length, an intermediate form of ~125 Å, or a fully extended form of ~140 Å in which all the domains are nearly parallel.

In parallel with crystallographic analyses, Chapman et al. also used a site-directed mutagenesis approach to probe the UL18 binding site of LILRB1. Alanine scanning mutagenesis implicated residues clustered at the distal tip of D1 of LILRB1, in direct comparison to the residues in KIRs which bind MHC Class I, which are located at the D1D2 interface. As further evidence for the location of D1 as the UL18 binding site, this region was involved in crystal contacts, thus suggesting its suitability for protein-protein interactions.

Co-crystallisation of LILRB1 with HLA-A2 allowed analysis of the mode of binding of LILRB1 with MHC Class I ligands and provided a model for the interaction with UL18 (Willcox et al. Nat Immunol 2003). LILRB1 D1D2 recognized the side of the MHC complex at two sites, the relatively non-polymorphic membrane-proximal α3 domain, and the conserved β_2-microglobulin (β_2m) domain. This recognition event involved residues at the D1 tip interacting with the α3 domain and residues in the D1D2 hinge region interacting with β_2m. The LILRB1-HLA-A2 interface was approximately comparable in size to that of KIR-MHC Class I and also TCR-MHC Class I interfaces; however, unlike these interfaces it involved a predominantly non-polymorphic surface on the MHC Class I molecule, thereby rationalising the broad binding specificity of LILRB1.

Consistent with interactions across the HLA family, both classical and non-classical alleles exhibit high conservation of residues in the α3 domain shown in the crystal structure to interact with LILRB1. The most diverse molecule within this grouping is HLA-G, consistent with a substantially enhanced affinity of HLA-G for LILRB1/B2. In contrast, the MHC Class

I-like molecules FcRn, HFE and ZAG have non-conservative substitutions that are likely to ablate LILRB1 binding. Comparison of the primary sequence of UL18 with the corresponding region of HLA-A2 α3 that contacts LILRB1 reveals the conservation of residues critical for the interaction of MHC Class I with LILRB1. The structural basis of the high affinity interaction between LILRB1 and UL18 has been extensively studied (Wagner et al. JMB 2007, Oochino et al. JI 2008) and the crystal structure for the LILRB1-UL18 complex has subsequently been generated (Yang and Bjorkman PNAS 2008).

An important feature of the LILRB1/HLA-A2 crystal structure was that the LILR family could be separated into two groups based upon the sequence identity with LILRB1 at the HLA-A2 α3 and β2m contact sites. Group I LILRs – LILRB1, LILRB2, LILRA3, LILRA1 and LILRA2 – showed high sequence conservation as compared to LILRB1 in these regions, and thus were postulated to bind to MHC Class I or MHC Class I-like molecules. In contrast, Group II LILRs – LILRB3, LILRB4, LILRB5, LILRA4 and LILRA5 – have several non-conservative substitutions in these regions, and thus are unlikely to bind MHC Class I (Willcox et al. Nat Immunol 2003).

Consistent with these structural data, SPR studies showed that LILRB1 or LILRB2 binding to MHC Class I could interfere with CD8 binding (Shiroishi et al. PNAS 2003). Conceivably this could provide another functional inhibitory effect of LILRB1 ligation on T cells, by blocking T cell co-receptor binding. The kinetics of binding of LILRB1 and LILRB2 to MHC Class I reached equilibrium and dissociated rapidly, typical of cell-cell recognition events. LILRB1 and LILRB2 showed slightly higher affinities for HLA-G in comparison with other alleles; thus, LILRB1 might be important for regulating NK recognition of the

developing foetal trophoblast cells, or for thymocyte development upon interaction with thymic epithelial cells, both of which express HLA-G.

LILRB2

SPR analyses demonstrated binding of LILRB2 to UL18 and to MHC Class I in the μM range (Chapman et al. Immunity 2000, Shiroishi et al. PNAS 2003). The crystal structure of the D1D2 domains of LILRB2 was solved to 1.8A resolution by Willcox et al. in 2002. In comparison with LILRB1, LILRB2 D1D2 contained significantly less helical structure. In particular, a single turn of 3_{10} helix was observed in LILRB2 D1 whereas the corresponding region in LILRB1 D1 contained a much longer helix, resulting in a relative shift in the LILRB2 backbone. The structure also highlighted alterations at the UL18 binding site that could account for the difference in affinity. In LILRB2, the 76-84 residue loop was shifted by approximately 11 Å away from the molecular interface with the MHC Class I molecule relative to LILRB1, which would disrupt interaction with UL18 α3 residues, and may also account for the 3-to-4-fold difference in binding affinity for MHC Class I (Willcox et al. BMC Struc Bio 2002, Willcox et al. Nat Immunol 2003).

One distinguishing feature of LILRB2 is a reduced requirement for β_2m interaction. LILRB2 can bind to free heavy chains (fHC) of HLA-B27 (Allen et al. JI 2001). These lack β_2m and are expressed as monomers and disulphide-linked homodimers at the cell surface. Tetrameric complexes of HLA-B27 fHC were shown to bind to LILRB2, but not LILRB1 transfected cells (Allen et al. JI 2001). More recently, the crystallographic structure of LILRB2 in complex with HLA-G, which can also form fHC and homodimerise at the cell surface, was solved (Shiroishi et al. PNAS 2006). This revealed important differences between the mode of binding of LILRB1 and LILRB2 to MHC Class I. Like LILRB1 binding to HLA-A2,

LILRB2 binds to the α3 and β_2m domains of HLA-G; however, LILRB2 uses a larger interface to interact with α3, involving the cleft in D1, whereas the interface with β_2m is substantially smaller. This suggests the interaction with β_2m is considerably less important than for LILRB1. The crystallographic data also provided structural rationalisation for the increased affinity of LILRB1 and LILRB2 for HLA-G over other MHC Class I members, in particular the hydrophobic interactions formed by F195 with LILRB1 and Y197 with LILRB2. In addition, HLA-G dimerisation would increase receptor avidity, as reflected in the functional studies described earlier.

LILRB2 has recently been described as binding to the MHC Class I-like lipid-presenting molecule, CD1d. This interaction is reported to involve the distal two domains of LILRB2 recognising the α1-α2 domains which comprise the lipid binding groove, and would therefore be distinct from the recognition of MHC Class I as described above (Li et al. JI 2009). It is interesting to speculate that LILRB2 may have alternative modes of recognition of MHC Class I, although no direct evidence to support such a hypothesis has yet been described.

LILRA1

No structural data is yet available for LILRA1, although it was initially described as having both 2-domain and 4-domain splice variants (Borges et al. JI 1997). However, fluorescent tetramers of HLA-B27, both conformed and β_2m free, were shown to bind to LILRA1-transfected 293T cells in a subsequent study (Allen et al. JI 2001).

LILRA2

The structure of LILRA2 D1D2 was recently solved by X-ray crystallography, after first overcoming problems with the intransigent refolding and crystallisation of the receptor by the

introduction of an artificial disulphide bond in the D2 domain of the receptor. Initial SEC analysis of the mutated receptor unexpectedly demonstrated its ability to dimerise, as evidenced by a higher molecular weight peak. Tetramerisation of LILRA2 and staining of transfected cells demonstrated a lack of binding to MHC Class I alleles (Chen et al. Prot Exp Pur 2007).

Subsequently, X-ray data quality crystals were generated and the LILRA2 structure was solved to a resolution of 2.6 Å. This demonstrated that the receptor formed a "domain-swapped" dimer through the exchange of identical β-strands in the D2 domain. Overall structural topology in D1 was similar to the other solved Group I LILR structures, with the exception that the C-C' loop containing 3_{10} helical regions in LILRB1 and LILRB2 instead consisted of a β-strand. Analysis of residues corresponding to the HLA-A2 α3 domain binding sites of LILRB1 demonstrated the unsuitability of LILRA2 for MHC Class I binding; however, conservation of the LILRB1-corresponding β_2m-binding residues suggested that LILRA2 might be able to bind β_2m, possibly in the context of specific alleles of MHC Class I (Chen et al. JMB 2009).

LILRA4

The ligand for LILRA4 was identified by expression cloning as the BST2 antigen. SPR studies demonstrated recombinant LILRA4-Fc binding to immobilised BST2 with estimated micromolar affinity, which could be blocked by anti-BST2 antibody (Cao et al. JEM 2009). BST2 is a cell-surface antigen with an unusual topology, having both an N-terminal transmembrane domain and a C-terminal GPI-linked anchor. Its extracellular domain contains two putative N-linked glycosylation sites, and three cysteine residues which allow it

to dimerise via disulphide bond formation at the cell surface (Ohtomo et al. BBRC 1999, Kupzig et al. Traffic 2003).

LILRA5

To date, the only Group II LILR to be structurally elucidated is LILRA5 (Shiroishi et al. JBC 2006). The overall structure of the receptor was similar to other LRC receptors, including LILRB1 and LILRB2, with an acute interdomain angle between D1 and D2. The topology of the domains was similar but distinct from that of LILRB1 and LILRB2, and bore more resemblance to that of NKp46 or KIR2DL receptor subtypes, with substantially less helical regions in D1 as compared to LILRB1 and LILRB2. The 3_{10} helix in D1 of LILRB1 and LILRB2 that is directly involved in contacting α3 residues of MHC Class I was missing and replaced instead with a β-strand, lacking the hydrophobic core residues present in LILRB1. Residues critical for stabilising this β-strand are well-conserved across the Group II LILRs; thus, Group II LILRs are likely to have a similar motif and are unlikely to bind MHC Class I.

Similarly, differences in the surface charge composition around the D-E strands in the D2 domain of LILRA5 (a region that in KIRs and LILRB1/B2 is involved in interactions with the peptide-binding groove and β2m, respectively) suggested this region in LILRA5 was unlikely to be compatible with MHC Class I recognition. In addition, the overall surface charge distribution of LILRA5 differs considerably from the other receptors. Whereas LILRB1 has a positively charged region that interacts with α3, and KIRs have a large negatively-charged area crucial for contacting the peptide-binding groove, LILRA5 has a more dispersed distribution of small positive and negative patches of electrostatic potential, with some hydrophobic regions also present.

Consistent with these structural observations, LILRA5 shows no binding to MHC Class I alleles by SPR analysis and LILRA5 tetramers do not stain HLA-Cw4 transfected 721.221 cells. Since LILRB4 binds a cellular counter-structure on T cells after allogeneic stimulation, it could be postulated that LILRA5 may bind a similar ligand, due to sequence conservation between the two proteins. In addition, non-self ligands for the Group II LILRs cannot be excluded, since LILRB3 and LILRB5 have been shown to be upregulated in lepromatous leprosy patients with *Mycobacterium leprae* infection (Bleharski et al. Science 2003). It is possible that Group II LILRs may have evolved to recognise bacterial or viral counter-structures, in a similar manner to PRRs, although this is purely conjecture.

Cis interactions of the LILRs

A novel aspect of the mode of binding of the LILRs has been highlighted by recent findings that LILRB1 and LILRB2, and the mouse homologue PIR-B, are capable of binding in *cis* to MHC Class I on the same cell membrane. Confocal microscopy and Fluorescence Resonance Energy Transfer (FRET) studies have demonstrated that this interaction can occur in mast cells and osteoclasts (Masuda et al. JEM 2007, Mori et al. JI 2008), in a similar manner to that described for the murine Ly49 receptors (Doucey et al. Nat Immunol 2004, Scarpellino et al. JI 2007). The functional implications of these findings are unclear, however they may provide another level of regulation of the maturation and activation state of LILR-expressing cells based upon their MHC Class I expression, through constitutive inhibitory signalling via the LILRs.

1.2.4 LILR disease associations, polymorphisms and clinical relevance

LILRs and viral infection

The fact that CMV, a prevalent herpesvirus that is normally asymptomatic but can cause disease in immune-compromised individuals or neonates, encodes an MHC homologue (UL18) that binds to LILRB1 suggests a possible role for this interaction in viral immune evasion. Consistent with this, CMV has evolved numerous immune evasion strategies to enable viral persistence in immunocompetent hosts. One involves downregulation of host MHC Class I molecules, a strategy likely to inhibit priming of CMV-antigen-specific T cells. Such a strategy could potentially leave virus-infected cells to attack by NK cells, on the basis of 'missing self' recognition by non-engagement of inhibitory KIR receptors in combination with activatory receptor recognition of viral proteins or stress induced ligands on the infected cell surface. Conceivably one role of the UL18/LILRB1 interaction may be to inhibit NK cells, potentially potent effectors in the anti-CMV response. Indeed, LILRB1 has approximately 1000-fold higher affinity for UL18 than for MHC Class I (Chapman et al. Immunity 1999) potentially compensating for the low levels of UL18 expressed on CMV-infected cells (Leong et al. JEM 1998).

LILRB1 engagement by UL18 has indeed been shown to inhibit NK cell functions (Reyburn et al. Nature 1997, Kim et al. BBRC 2004) although some conflicting data has been published (Leong et al. JEM 1998, Odeberg et al. Scand J Immun 2002). These conflicts have led to the hypotheses that NK cells may have an activating receptor that recognises UL18, and also that the differential distribution of LILRB1 in NK cell subsets may affect polyclonal responses to CMV infection (Prod'homme et al. JI 2007). In a similar fashion, despite the weight of evidence for an inhibitory role for LILRB1 engagement in T cells (discussed in Section 1.2.2), UL18 has been shown to induce $CD8^+$ T cell activation in a LILRB1-dependent (Saverino et

al. JI 2004) or LILRB1-independent fashion (Wagner et al. JI 2007). Similar hypotheses may explain these observations. Importantly however, UL18 has also been shown to interfere with DC maturation and migration through engagement of LILRB1 (Wagner et al. JLB 2008).

LILRB2 has been implicated in the pathogenesis of HIV-1. Lichterfeld et al. showed that a variant of an immunodominant HIV-1 peptide epitope with a single amino-acid mutation exhibited stronger binding to LILRB2, leading to a tolerogenic phenotype of monocytes and DCs. This result challenges the established notion that LILRB2 recognition of MHC Class I is peptide-independent and the authors suggest that the peptide presented may alter the conformation of the LILRB2 binding site in the α3 domain of the MHC molecule, or that an alternative mode of ligand recognition by LILRB2 may be operating (Lichterfeld et al. JEM 2007). In another study, an association between HLA-B*35-Px alleles and accelerated HIV-1 disease progression was shown to be due to an increased affinity of those HLA-B molecules for LILRB2. Monocyte-derived DCs from these individuals showed reduced allostimulatory capacity attributed to the reduced expression of B7-2 and HLA-DR and decreased expression of IL-6 and IL-12 (Huang et al. JEM 2009).

In summary, these findings demonstrate that viruses can use the immunomodulatory properties of MHC Class I interactions with LILRs as a means to decrease overall antiviral immune activities. Indeed, a recent paper showed that H1N1 influenza virus infection causes increased redistribution of MHC Class I molecules to the cell surface and their accumulation into lipid rafts, leading to enhanced inhibitory signalling via LILRB1 and KIR2DL1 on the surface of NK cells (Achdout et al. J Virol 2008). Viral immune escape strategies may be counteracted by concomitant strategies in the human immune system, such as the evolution of activatory isoforms of innate inhibitory receptors, the so-called ‘counterbalance theory’

(Barclay and Hatherley, Immunity 2008), or the release of soluble decoy forms of the targeted inhibitory receptor, as is the case for LILRB1 and LILRB2 (Beinhauer et al. EJI 2004, Jones et al. EJI 2009). The identification of BST2/Tetherin as the restrictive element preventing retroviral budding and release from infected cells (Neil et al. Nature 2008) and the confirmation of the role that the LILRA4/BST2 interaction plays in the control of innate antiviral immunity via pDCs (Cao et al. JEM 2009) further highlight the importance of studying LILRs in the context of viral infection.

LILRs and bacterial infection

Recent reports have suggested that some LILRs may recognise bacterial pathogens. LILRB3 and LILRB5 have been shown to be upregulated in lepromatous leprosy patients with *Mycobacterium leprae* infection (Bleharski et al. Science 2003). LILRA2 protein expression was also found to be upregulated on monocytes and macrophages from lepromatous leprosy patients, but contrary to its expected activatory role instead impaired monocyte differentiation into immature DCs and antigen presentation to *M. leprae* specific T cells, somewhat reminiscent of the unexpected inhibitory effect of LILRA4 engagement (Lee et al. JI 2007).

The mouse LILR orthologue PIR-B and the activatory PIR-A1 on macrophages bind to *Staphylococcus aureus* and in concert with TLR signalling direct inflammatory responses to the pathogen. LILRB1 and LILRB3 were also reported to bind the bacterium. The authors also suggest a potential link with septic arthritis, which supports a role for LILRs in RA, as discussed later (Nakayama et al. JI 2007). Infection with *Salmonella typhimurium* has been shown to upregulate LILRB2 and LILRB4 (Brown et al. BMC Immunology 2009). Interestingly, the authors showed that continuous LILRB4 ligation during *in vitro* culture of DCs did not reduce costimulatory molecule expression as might be expected. However,

ligation of LILRB4 led to increased secretion of IL-10 and decreased secretion of IL-8, an innate immune cell chemotactic cytokine, by *in vitro* cultured macrophages, in keeping with the inhibitory role of LILRB4 previously described (Brown et al. BMC Immunology 2009).

LILRs and autoimmunity

The LILRs have been implicated in a range of autoimmune diseases. An early study determined the expression of activatory and inhibitory LILRs in rheumatoid arthritis (RA) samples (Tedla et al. Am J Pathol 2002). Polymorphism in the promoter region of the LILRB1 gene was shown to be associated with RA in HLA-DRB1 shared epitope-negative patients (Kuroki et al. Hum Mol Gen 2005). LILRB2, LILRB3 and LILRA2 were shown to be upregulated in synovial biopsies from RA patients, but reduced upon treatment (Huynh et al. Rheumatology 2007). The association between HLA-B27 allele and the ankylosing spondyloarthropathies could be due to the engagement of HLA-B27 by the activatory LILRA1. In addition, LILRB2 is able to bind to HLA-B27 fHCs (Allen et al. JI 2001) and fHC homodimers (Kollnberger et al. Arthritis and Rheumatism 2002), although the functional significance of this is unclear.

LILRs have also been implicated in systemic lupus erythematosus (SLE), an autoimmune disease characterised by the polyclonal activation of B lymphocytes, the production of many different auto-antibodies and defective T cell function, possibly caused by impaired Treg and Ts cells (Miyara et al. JI 2005). One study detected lower levels of LILRB1 on B cells and impaired inhibitory activity of LILRB1 in $CD4^+$ and $CD8^+$ T cell subsets from SLE patients (Monsivais-Urenda et al. J Autoimmunity 2007). Polymorphism in the splice site for LILRA2 has also been linked with SLE (Mamegano et al. Genes Immun 2008).

The activatory receptor LILRA3 has been linked with MS, a degenerative neurological condition arising from demyelination of the CNS. LILRA3 exhibits presence/absence variability more commonly ascribed to the KIRs and displays sequence variability in the putative ligand-binding domain (Torkar et al. EJI 2000, Moodie et al. EJ Immunogenetics 2002, Norman et al. Immunogenetics 2003). A study of German MS patients found evidence for a link between disease and the deletion of the LILRA3 locus (Koch et al. Genes and Immunity 2005). However, this finding as at odds with a functional study showing that recombinant LILRA3 is able to stimulate T cell proliferation in a mixed lymphocyte reaction (Kabalak et al. Ann NY Acad Sci 2007).

LILRs and cancer

Subversion of LILR tolerogenic signalling would be a strong candidate for tumour immune evasion strategies. Indeed, ectopic HLA-G expression in tumours has been noted (Paul et al. PNAS 1998, Maki et al. Leukaemia 2008) and may have just such an effect via the efficient engagement of LILRB2 (Urosevic et al. Blood 2004, LeMaoult et al. FASEB J 2005, Sun et al. Chest 2008). Analogously ectopic B cell expression of LILRB2 and LILRB4 has been described in PBMCs from CLL patients (Colovai et al. CBCC 2007). The presence of soluble LILRB4 with tolerogenic properties in the blood of certain cancer patients suggests the crucial function of this receptor in tolerance induction. In addition, the demonstrated *in vitro* and *in vivo* inhibitory activity of soluble LILRB4 on T cell alloreactivity suggests the usefulness of this reagent for immunosuppressive treatment of allograft recipients or patients with autoimmune diseases, and a potentially important novel therapeutic avenue for the disruption of tumour immune evasion (Suciu-Foca et al. JI 2007, Cortesini JOP 2007). Finally, a recent study addressed autoantibody and tumour-specific responses to LILRB3, which displays much more polymorphism than the other LILRs as well as presence/absence variation like

KIR receptors, in HSCT patients. Polymorphism in LILRB3 was shown to be the underlying cause behind generation of autoantibodies in some HSCT patients, and LILRB3 was also shown to be expressed on myeloid leukaemic cells from these patients, thus eliciting the strong immune response to the polymorphic form of the receptor (Pfistershammer et al. Blood 2009).

1.3 Aims and scope of the work conducted in contribution to this thesis

In light of the potential functional roles of LILRs in tolerance and the regulation of myelomonocytic cells discussed above, it was decided they would be worthy of investigation. Due to the paucity of information with regards to Group II receptors both structurally and in terms of their ligand-binding interactions, the Group II receptors were made the focus of this investigation. In particular, the suggestion in previous publications of the important role of LILRB4 in the control of tolerance induction mediated by DCs and Tregs, and in addition the recent optimisation of methods for recombinant LILRB4 expression and refolding, highlighted this as an interesting and potentially fruitful avenue for progression. I had previously established methods for the generation of recombinant LILRB4 at high yields and purity (Garner et al. Prot Exp Pur 2006), which suggested X-ray crystallography as a strategy for successful structural determination of LILRB4 (an approach that had yielded considerable functional insight into the Group I LILRs, LILRB1 and LILRB2). In addition, these methods would enable cell staining experiments using multimeric LILRB4 reagents, which might define a cellular distribution pattern for the unknown LILRB4 ligand, potentially contributing to its elucidation. These studies would also enable the study of candidate ligand interactions utilising surface plasmon resonance techniques.

CHAPTER 2 - MATERIALS AND METHODS

2.1 Molecular biology techniques

2.1.1 Plasmids

For high-level inducible expression of proteins as *E. coli* inclusion bodies, I utilised the pET23a vector (Novagen). LILRB1, LILRB2, LILRB3, LILRB4, LILRB5 and LILRA5-encoding pET23a plasmids had previously been generated in the laboratory prior to commencement of my PhD. Constructs encoding biotinylated versions of the LILR proteins were also available, having been cloned into the biotinylation construct JMB002 (generated by Jonathan M. Boulter and based on the pGMT7 vector). For investigation of LILRA4 structure and ligand-binding, LILRA4-pCMV-Flag was provided by Dr. Rachel Allen and used as a template for subcloning into pET23a and the *Drosophila* expression vector pMT/BiP/V5-His-A (Novagen). The hygromycin-encoding co-transfection plasmid, pCoHygro, was from Novagen. The BST2-Fc construct, consisting of the BST2 gene in a modified CDM8 expression vector that contained a mouse CD150 leader segment at the N terminus and the Fc segment of human IgG1 at the C terminus (Arase et al. Science 2002), was provided by Prof. Wei Cao (Cao et al. JEM 2009).

2.1.2 Primers, Polymerase Chain Reaction and Site-Directed Mutagenesis

All custom primers were ordered from Invitrogen. Primers were reconstituted in PCR-clean dH_20 at 20 pmole/µl and stored at -20 ºC. Primer sequences are listed in the relevant results chapters.

For full-length cloning, PCRs were conducted using the following reaction mixture: 1 µl of each primer (20 pmoles), 1 µl of plasmid template DNA (approximately 200 ng), 1 µl of 10 mM dNTP solution, 5 µl of *PfuTurbo* reaction buffer, 1 µl of cloned *PfuTurbo* DNA

polymerase enzyme (2.5 U) (Stratagene), in total 50 µl reaction volume made up with PCR-clean dH_20. PCR conditions were as follows: Initial denaturation at 95 ºC for 2', then denaturation at 95 ºC for 30", annealing at 55 ºC for 30", extension at 72 ºC for 1' 30", 25 cycles followed by final extension step at 72 ºC for 10'.

Site-Directed Mutagenesis (SDM) was conducted using the Quikchange SDM kit (Stratagene), according to the manufacturer's instructions. In brief, a PCR was conducted utilising the reaction mixture described above, using custom-designed SDM primers and the appropriate template plasmid, and the following PCR steps: denaturation at 95 ºC for 30", annealing at 55 ºC for 1', extension at 68 ºC for 4' 30", 16 cycles. Following dpnI digestion (2 h at 37 ºC), the reaction mixture was used to transform chemically-competent *E. coli* DH5α, as described below, and transformed bacteria were plated onto LB-ampicillin agar plates for overnight selection and growth of colonies, prior to plasmid miniprep (described in 2.2.1).

2.1.3 Restriction enzyme DNA digestion and DNA ligation

Restriction enzymes (NdeI, HinDIII, BglII, AgeI) and the appropriate buffers were from Roche. Restriction digestion was conducted for 2 h at 37 ºC. Cut vectors were treated with 1 µl alkaline phosphatase (NEB) for 1 h at 37 ºC to prevent re-circularisation. DNA ligation was conducted overnight using T4 DNA ligase plus ligation buffer, as per manufacturer's instructions (NEB).

2.1.4 Agarose gel electrophoresis and gel purification

DNA samples were diluted in 5x DNA loading buffer consisting of 0.25 % bromophenol blue, 0.25 % xylene cyanol FF, 15 % Ficoll in water, prior to gel loading. Agarose gel

electrophoresis was conducted using 1.2 % agarose gels in TBE buffer (89 mM Tris base 89 mM boric acid 2 mM EDTA), at 80 V. Visualisation of DNA was by the addition of Ethidium Bromide after gel melting (0.5 µg/ml final concentration), DNA sizing was with 100 bp ladder (Roche) and digital pictures were recorded under UV illumination using a Syngene Image Capture system. Gel purification of digested vectors and PCR product inserts was by QIAquick Gel Extraction Kit (QIAGEN).

2.1.5 Mini and Maxi plasmid preparation

Miniprep of plasmid DNA was conducted after overnight growth from a single colony of freshly-transformed E. Coli DH5α, selected the previous night by growth on an LB-ampicillin agar plate. Overnight culture was in ~4 ml of LB with 100 µg/ml ampicillin in an orbital rotating shaker at 37 ºC, 200 RPM. Miniprep was conducted using the QIAprep Spin Miniprep kit, following the manufacturer's protocol (QIAGEN). Elution was in PCR-clean dH_20. Maxiprep was by QIAGEN Plasmid Maxi Kit. Purity and yield were verified by agarose gel electrophoresis; successful cloning was verified by test digestion and electrophoresis followed by DNA sequencing. All DNA samples were stored at -20 ºC to prevent nuclease degradation.

2.1.6 DNA sequencing

DNA sequencing was conducted by the Functional Genomics service, University of Birmingham, utilising the ABI BigDye Terminator v3.0 reaction and an ABI 3730 Sequencer.

2.2 Recombinant protein expression

2.2.1 Bacterial transformation and general culture methods

50 µl of chemically-competent *E. coli* strain BL21 (DE3) cells (for protein expression) or strain DH5α (for cloning work) were thawed on ice from storage at -80 ºC and incubated with ~200 ng of plasmid DNA (typically 1 µl of a plasmid DNA miniprep elution) in a 1.5 ml eppendorf tube on ice for 30', then subjected to 90" heat shock at 42 ºC in a waterbath. 150 µl of pre-warmed SOC medium was then added followed by outgrowth at 37 ºC, 200 RPM in an orbital shaker for 1 h. 100 µl of the final transformation mix was then plated out onto pre-warmed LB-ampicillin agar plates, and incubated overnight at 37 ºC.

LB medium recipe: 10 g bactotryptone, 5 g yeast extract, 10 g Na Cl, make to 1 L with dH_20 and autoclave. LB-agar was made using 7.5 g agar / 500 ml LB, followed by autoclaving. To pour LB-ampicillin plates, solid LB-agar was melted in a microwave oven prior to cooling to 55 ºC in a waterbath for addition of 100 µg/ml ampicillin.

All plasmid preparations and protein expression experiments were conducted using fresh transformants, to minimise the risk of loss of plasmid from the bacterial colony.

2.2.2 Insoluble inclusion body expression in *E. coli*

Protein expression in *E. coli* was conducted as previously published. Biotinylated recombinant LILRB4 D1D2-bt was previously generated in the laboratory (Garner et al. Prot Exp Pur 2006). LILR D1 proteins were generated using similar techniques; in brief: For test expression, single colonies of LILR D1-pET23a transformed *E. coli* BL21 (DE3) cells were inoculated into ~4 ml of LB plus 100 µg/ml ampicillin and grown in an orbital shaker at 37 ºC, 200 RPM to OD_{600} of 0.4-0.6 units. A pre-induction sample was taken at this point. Induction was by the addition of 500 µM isopropyl β-D-1-thiogalactopyranoside (IPTG).

Post-induction samples were taken after 4 h. Samples were centrifuged briefly at 13,000 g and resuspended in SDS-PAGE sample buffer for analysis by gel electrophoresis (see below).

For bulk expression, single colonies of LILR D1-pET23a transformed *E. coli* BL21 (DE3) cells were inoculated into ~4 ml of LB plus 100 µg/ml ampicillin for starter growth for ~2-3 h in an orbital shaker at 37 ºC, 200 RPM until the culture became cloudy, then this culture was used to inoculate 4 L of autoclaved LB medium in 4x 2 L conical flasks with the addition of 100 µg/ml ampicillin to maintain selection. Cultures were grown in an orbital shaker at 37 ºC, 200 RPM to OD_{600} of 0.4-0.6 units, induced by the addition of 500 µM IPTG, and grown for a further 4 h. Cells were then pelleted by centrifugation at 4500 rpm for 20 min in a Sorvall RC26Plus centrifuge, supernatant was discarded and the pellet resuspended in 50 ml of PBS. Cells were then lysed by sonication on ice with 8 bursts of 45" maximal power using a Misonix sonicator equipped with a flat-head probe, and inclusion bodies were harvested by centrifugation at 15,000 g for 30'.

Inclusion bodies were then subjected to three rounds of homogenisation in 25 ml of Triton Wash Buffer (500 mM Tris-HCl, 0.5 % Triton X-100, 200 mM Na Cl, 10 mM EDTA, 0.1 % (w/v) Na azide, 2 mM DTT, pH 8.0) followed by centrifugation at 15,000 g for 15' at the end of each wash step, to remove cellular membranes and soluble proteins, and then homogenised in 25 ml of Resuspension Wash Buffer (50 mM Tris-HCl, 100 mM Na Cl, 1 mM EDTA, 1 mM DTT, pH 8.0) followed by centrifugation at 15,000 g for 15' to pellet insoluble, purified inclusion bodies. A small sample was removed at this point for overnight solubilisation in Urea Solubilisation Buffer (8 M Urea, 50 mM MES pH 6.5, 10 mM EDTA, 2 mM DTT) to allow analysis of purity by SDS-PAGE. The remaining sample was solubilised overnight at 4 ºC in ~20 ml of Guanidine Solubilisation Buffer (6 M Guanidine HCl, 50 mM MES pH 6.5,

0.1 mM EDTA, 0.1 mM DTT). Protein concentration was determined by Bradford assay (BioRad).

2.2.3 Chemical refolding from inclusion bodies

In vitro refolding of inclusion bodies was conducted by the standard Garboczi method (Garboczi et al. PNAS 1992), utilising 30 mg of each protein in 500 ml of Refold Buffer (100 mM Tris pH 8.0, 400 mM L-arginine, 2 mM EDTA, 5 mM reduced glutathione, 0.5 mM oxidized glutathione and 0.1 mM PMSF) overnight at 4 ºC with stirring. The refolds were then concentrated to approximately 10 ml volume using N_2 pressurised stir cells (Amicon), filtered with 0.2 μM syringe filters and loaded into the superloop of the Akta FPLC machine for purification by size-exclusion chromatography (SEC).

2.2.4 Size Exclusion Chromatography and general protein handling

SEC was conducted using a Sephadex S200 column connected to an Akta FPLC machine (consisting of a Pump P-920 unit, a Monitor UPC-900 unit and a Frac-950 collector unit under the control of a PC running UNICORN software, GE Healthcare). Pre-equilibration was conducted prior to each protein run using the appropriate final protein buffer. All buffers and protein samples were sterile-filtered prior to use. A standardisation run eluted markers of the following weights and elution volumes: 669 kDa, 112.5 ml; 232 kDa, 145 ml; 67 kDa, 195 ml; 45 kDa, 215 ml; 12 kDa, 260 ml.

Proteins were kept on ice as far as possible during manipulations, and stored at -20 ºC or -80 ºC to prevent aggregation. Concentration of proteins for volumes up to 15 ml or up to 0.5 ml was conducted using Amicon or Microcon centrifugal filtration devices, respectively. Quantification of refolded, purified proteins was conducted by A_{280} spectrophotometry using

calculated absorbance coefficients. Buffer optimisation was conducted by thermal shift screening using Sypro Orange dye and a Thermofluor thermal cycler. Buffer exchange was by PD-10 column (GE Healthcare).

2.2.5 SDS-PAGE

5x Non-Reducing SDS-PAGE Sample Buffer was prepared (1 M Tris pH 6.8, 3 g SDS, 1 g bromophenol blue, to 25 ml with dH_2O). 5x Reducing SDS-PAGE Sample Buffer was prepared by adding 100 µL of 2 M DTT to 300 µl of non-reducing buffer. A 15 % acrylamide resolving gel was prepared (2.3 ml dH_2O, 5 ml 30 % acrylamide, 2.5 ml Tris pH 8.8, 100 µL SDS 10 %, 100 µL APS) and then the stacking gel (2.7 ml dH_2O, 0.67 ml 30 % acrylamide, 0.5 ml 1 M Tris ph 6.8, 40 µl 10 % SDS, 40 µl APS). Both gels were polymerised by adding 4 µl of TEMED. Approximately 10 µg of protein was loaded per lane, in addition to molecular weight standards (BioRad, low molecular weight range). Electrophoresis was carried out using the Mini-PROTEAN 3 system (BioRad), at 120 V for the stacking gel and 180 V for the resolving gel. Gels were then stained with Coomassie Stain (1.25 g Coomassie Brilliant Blue, 250 ml dH_2O, 50 ml acetic acid) for 30', and destained with Destain Solution (300 ml dH_2O, 150 ml of methanol and 50 ml of acetic acid) for 30' or until protein bands were clearly visible.

2.2.6 Recombinant protein expression in *Drosophila* S2 cells

Drosophila Schneider 2 (S2) cells and reagents for protein expression in the *Drosophila* system were obtained from Invitrogen. S2 cells were cultured in Schneider's Medium supplemented with 10 % heat-inactivated FBS (foetal bovine serum) in a tissue-culture incubator maintained at 28 ºC with ambient CO_2 levels. Cells were split approximately 1:5 every 3-4 days by dilution. For freezing, cells were resuspended in Schneider's medium

supplemented with 10 % DMSO and 10 % FBS, frozen at -80 ºC overnight and then stored in liquid nitrogen.

Transfection was by calcium phosphate kit (Invitrogen) using the manufacturer's recommended protocol (Invitrogen Schneider S2 Cell Manual) and 10 µg of expression vector plasmid DNA. For transient transfection, cells were grown for 24 h post-transfection then induced with 500 µM $CuSO_4$. Protein expression was assayed at 3 days and 4 days post-induction by SDS-PAGE and western blotting. For stable transfection, calcium phosphate transfection was conducted as described above with the addition of 1 µg of *pCoHygro* selection vector plasmid DNA, and followed by 2-3 weeks of selection with 300 µg/ml hygromycin-B (Invitrogen), until resistant cells began to grow out. Frozen stocks were then generated and stored as described previously.

For bulk expression, cells were inoculated into 1 L of Schneider medium in 4x 500 ml flasks and grown for 3-4 days in an orbital shaker at RT to log phase density (~2-4 x 10^6/ml) then induced with 500 µM CuSO4 and grown for a further 3 days. Supernatant was harvested by 15' gentle centrifugation at 1000 g to prevent cell lysis and stored at 4 ºC with the addition of 0.01 % Na azide to prevent microbial growth.

For purification of His-tagged proteins, 1 L of supernatant was dialysed overnight in 10 L of dialysis buffer (150 mM Na Cl 20 mM HEPES pH 7.0), 500 ml of dialysed supernatant was applied to a Ni-NTA column overnight at 4 ºC, and then the column was moved to RT and washed with 10 mM Imidazole to remove unbound proteins. Elution was carried out with 250 mM Imidazole. To prevent precipitation of the eluted protein, the protein fractions were stored on ice.

2.2.7 Western blotting

Western blotting was conducted by wet transfer electroblotting of proteins (including prestained protein markers, NEB) from 15 % SDS-PAGE gels to PVDF (Polyvinylidene Fluoride) membranes in the presence of Transfer Buffer (25 mM Tris pH 8.0, 192 mM glycine, 10 % methanol), followed by a wash in TBS-T (100 mM Tris pH 7.5, 150 mM Na Cl, 0.1 % Tween-20) and overnight blocking at 4 Cº in TBS-T plus 5 % powdered milk. Anti-His antibody (Invitrogen) staining (1:1000 in TBS-T plus 5 % milk) was then conducted for 2 h at RT with agitation, followed by three 10' washes with TBS-T and then incubation with goat anti-mouse-HRP-conjugated secondary antibody (1:10,000 in TBS-T) for 1 h followed by three washes in TBS-T. Enhanced Chemilumniscence detection was conducted using the Amersham ECL Kit. Exposure of Kodak Scientific Imaging film (Kodak) was conducted in a darkroom using an intensifier cassette and a developer machine.

2.3 Flow cytometry

Anti-CD3-FITC, CD8-PEcy5, CD4-PE, CD4-PEcy5, CD19-PEcy5, CD14-FITC, CD56-FITC, CD3-PEcy5 and CD69-PEcy5 monoclonal antibodies were from Becton Dickinson. Streptavidin-PE was from BD Pharmingen. Cell lines were kindly donated by various in-house collaborators and Dr. Alison Leese (Cancer Sciences, University of Birmingham). Tetramerisation of LILRB4 was by gradual addition of Streptavidin-PE to biotinylated LILRB4 (100 µg/ml) at a molar ratio of 1:4 over 6 h. Blood was collected from healthy donors by venupuncture, into heparinised syringes. PBMC separation was by density gradient centrifugation in Lymphoprep^{TM} (AXIS-SHIELD UK Limited, Huntingdon, UK).

For antibody and tetramer staining, PBMCs were washed in ice-cold MACS buffer (0.5 % BSA, 2 mM EDTA in PBS), resuspended in 500 µl aliquots (approximately 1 x10^6 cells/tube),

and stained with 5 µl of antibodies, or 10 µl tetramer or Streptavidin-PE (diluted in MACS buffer to the same concentration as that used to make tetramer) for 30' on ice in the dark, washed again with MACS buffer then resuspended in 500 µl MACS buffer plus propidium iodide (1 µg/ml final concentration). Flow Cytometry was conducted using a Beckman-Coulter EPICS XL FACS machine. Flow cytometry data files were analysed using WinMDI 2.9 software (http://facs.scripps.edu/software.html). Statistical analyses were conducted using Graphpad Prism 4 (Graphpad Software, Inc.).

2.4 Surface Plasmon Resonance

SPR binding studies were performed at 25° C using a BIAcore^{TM} 3000 (BIAcore AB St. Albans, UK) using HBS-EP as a running buffer (10 mM HEPES pH 7.4, 150 mM Na Cl, 3.4 mM EDTA, 0.005% surfactant P20. Streptavidin (Sigma) was covalently coupled to Research Grade CM5 sensor chips (BIAcore AB) via primary amines using the Amine Coupling Kit (BIAcore AB). Streptavidin was dissolved in 10 mM sodium acetate pH 5.5 and injected over the sensor chips at 0.5 mg/ml during coupling. R10z8e9 antibody was a kind gift from Dr. Margaret Goodall. Analytes were kept on ice and centrifuged at 13,000 rpm prior to use to remove aggregated proteins. Analytes were injected serially over all four flow cells at a flow rate of 10 µl/min. For test injections, 10 µl was injected (60 s contact time). Data were collected at 10 Hz. Data analysis was conducted using BIAeval software (BIAcore AB) and OriginPro 8 graphing and statistical analysis software (OriginLab Corporation).

2.5 X-ray crystallography

2.5.1 Introduction to the theory and process of X-ray crystallography

X-ray crystallography is a technique used to determine the 3-dimensional structure of molecules, by determining the position of atoms within a crystal of a molecule on the basis of the ability of electrons to diffract X-ray radiation. Crystallisation of macromolecules such as proteins involves their production at high concentrations and subjection to conditions in which water molecules are encouraged to diffuse from the protein in solution, causing the protein molecules to interact and form a crystal lattice. In practice, the hanging-drop method is commonly used and involves sealing a small drop of the protein solution, mixed with a crystallisation condition (typically containing a salt, a buffer, and a precipitant such as polyethylene glycol (PEG)), in an enclosed chamber with a well containing the crystallisation condition. Due to the difference in osmolarity between the drop and the well solution, water molecules leave the drop via vapour diffusion, gradually increasing protein and precipitant concentration towards a supersaturated state. Screening of crystallisation conditions is necessary to identify those conditions that promote intermolecular interactions leading to crystal nucleation and growth, and is an empirical process. The purity of the protein solution is critical since impurities will disrupt the crystal lattice leading to early cessation of growth or amorphous (poorly-ordered) crystals, which are unsuitable for data collection by X-ray diffraction. Once a crystal of a suitable size and morphology has been grown, it can be flash-cooled and then subjected to a focussed X-ray beam, generating a diffraction pattern.

In order to solve the three dimensional structure of a protein the diffraction pattern data is processed which involves calculating three variables (frequency, amplitude and phase) for each reflection. The frequency can be obtained from the wavelength of the X-ray beam used in the X-ray diffraction experiment. The amplitude is directly derived from the intensities of

each reflection. The phase angles of the reflections cannot be experimentally determined (the 'phase problem') but can instead be calculated by comparison with a previously-determined homologous structure (a process known as molecular replacement). By combining amplitudes with estimated phase information an electron density map is calculated which can be interpreted, allowing a molecular model to be built. The molecular model is then improved by a process called refinement, in which the atomic model is adjusted to improve the agreement with the measured diffraction data. The progress of refinement and model building is assessed by monitoring the reduction of two statistics, R_{work} and R_{free}.

2.5.2 Crystallisation screens and protocols used

Commercially-available crystal screens were obtained from Hampton Research, Molecular Dimensions Ltd. and Emerald Biosystems. Small-scale screens were set up in 96-well plates using a Mosquito nanolitre crystallisation robot (TTP Labtech). Scale-up screens were set up in Linbro plates, using vacuum grease to seal glass coverslips over the wells. Except where noted, screens were incubated in a crystallisation incubator at 23 ºC and checked for microcrystal formation at 3 days and weekly thereafter for up to three months using a Leica light microscope.

2.5.3 Data collection and processing

For LILRB4 D1 data collection, ethylene glycol was screened as a cryoprotectant, before flash cooling at 100 K in N_2 (Oxford Cryosystems). X-ray data were collected on an in-house MicroMax 007HF rotating anode X-ray generator (Rigaku) using a Saturn CCD detector (University of Birmingham Macromolecular X-ray Facility). LILRB4 D1 diffraction data sets were integrated, scaled and merged using the XDS suite. Molecular replacement was

conducted using the Crystallography and NMR System suite (CNS), model refinement with CNS and REFMAC5, and model manipulation with COOT.

2.5.4 Data analysis and presentation

Analysis was conducted with the CCP4 and Uppsala software suites, using LSQMAN, PROCHECK, and CONTACT. Electrostatic surfaces were calculated using GRASP. Protein-protein interaction sites were predicted with the SPPIDER web server. Molecular graphic figures were generated with MOLSCRIPT and rendered using POVRAY, or using Swiss-PDB Viewer (for SPPIDER output).

2.6 Nuclear Magnetic Resonance spectroscopy

2.6.1 Basic introduction to NMR theory

Nuclear magnetic resonance spectroscopy derives from two fundamental properties of atomic nuclei. The first is a quantum theoretical property, called spin, which in a highly abstract form can be considered as a rotation of the nucleus about an axis and has an angular momentum, and can be positive or negative. NMR spectroscopy is usually limited to those nuclei which have odd mass numbers and a nuclear spin quantum number, I, of ½; for the study of biomolecules, the most important nuclei with I = ½ are ^{1}H, ^{13}C, and ^{15}N.

The second property is magnetism; those nuclei with nonzero spin also possess a magnetic moment. When an external magnetic field is applied, the spin of the nuclei begin to precess about the axis of the magnetic field and the nuclear spins all align either parallel, or anti-parallel to the field. The frequency of this precession is termed the Larmor frequency. At high magnetic field strengths, introduction of a radiofrequency (RF) pulse – a second oscillating magnetic field perpendicular to the static magnetic field – causes disturbance in the magnetic field which fluctuates as the RF pulse is removed (a process called relaxation). The resulting electrical signal generated in a metal coil surrounding the sample – the free induction decay (FID) – can be analysed by Fourier transform and used to graph a one-dimensional proton spectrum

The electron density around each nucleus varies according to the types of nuclei and bonds in the molecule. Shielding of the nucleus from the magnetic field by the electron cloud alters the Larmor frequency; this is called the chemical shift phenomenon. The FID will be composed of a mixture of many different frequencies, which when Fourier transformed will reveal a spectrum of chemical shifts containing peaks for each chemical environment in which each

atom finds itself. The scale is described in parts per million (ppm) due to the fact that the Larmor frequency of a particular nucleus is proportional to the applied magnetic field.

Heteronuclear Single Quantum Coherence spectroscopy (HSQC) is a two dimensional method that allows correlation between protons and directly attached heteroatoms (in this case ^{15}N). When the protein is doubly-labelled (^{13}C and ^{15}N), it is possible to record a three dimensional experiment consisting of an HSQC plane expanded with a carbon dimension. Six experiments are conducted, HNCO, HNCACO, HNCA, HNCOCA, HNCACB and CBCACONH, which refers to the 'through-bond' resonance transfer across the atoms in the peptide backbone (Amide proton H, amide nitrogen N, alpha carbon - Cα, beta carbon – Cβ, and the carbonyl carbon, C_O).

Analysis of this 3D spectrum allows 'assignment' of peaks in the spectrum to particular atoms within particular residues. In the HNCACO the spectrum contains peaks at the chemical shifts of the C_O in the residue of the HSQC peak and the previous one in the sequence. The HNCO only contains the peak from the previous residue, and it is thus possible to assign the C_O shifts that correspond to each HSQC peak and the one previous to that one. Sequential assignment can then be undertaken by matching the shifts of each spin system's own and previous carbons. The HNCA and HNCOCA allow assignment of the Cα, and the HNCACB and the CBCACONH allow assignment of the Cβ. Computational methods then allow for movement of fragments of the primary sequence assignment to regions of the spectrum, and the assigned chemical shifts can then be finalised and used to elucidate structural information.

2.6.2 Protein expression and optimisation for NMR

LILRA4-pET23a was used to transform *E. coli* BL21(DE3) cells, and colonies from overnight transformants selected on LB-ampicillin agar plates were grown in 2 L of M9 minimal medium with the addition of 2 g/L uniform ^{13}C glucose, 1 g/L ^{15}N NH_4Cl as the sole carbon and nitrogen sources. Growth, induction, harvesting of inclusion bodies and chemical refolding were essentially as previously described. Thermal shift screening was used to identify optimal buffer composition as previously described.

2.6.3 NMR experiments conducted

Backbone assignment spectra were recorded using a Varian Inova 800 MHz spectrometer equipped with an HCN 5 mm z-PFG cryogenic probe with enhanced ^{13}C and ^{1}H sensitivity. Absolute spectrometer frequencies were as follows: ^{1}H, 799.762564; ^{15}N, 81.0392352; ^{13}C, 201.0999208 and were used to calibrate the spectrometer to 0 ppm. Initially, unlabelled LILRA4 was use to generate a 1D proton NMR spectrum (using the Watergate protocol) to show that the protein was folded and suitable for further analysis. 3D NMR was then conducted on doubly-labelled protein, using the experiments ghnca, ghn_co_ca, ghn_cacb, ghn_co, ghn_ca_co and gCBCA(CO)NH provided by Varian Ltd.

2.6.4 Data processing and analysis packages used

Data processing was conducted using the NMRPipe program. Protein backbone assignments were conducted using the program SPARKY 3. Secondary structure prediction was conducted using the TALOS web server.

CHAPTER 3 – LILRB4 LIGAND IDENTIFICATION STUDIES

3.1 Introduction

The physiological function of LILRB4 remains to date unknown, however several studies have suggested this receptor is crucially involved in tolerance induction mechanisms, as discussed in the introduction to this thesis (Section 1.2.2). In particular the reader's attention is drawn to the work of Chang et al. (Nat Immunol 2002) which established the central role of LILRB4 in the generation of tolerogenic DCs. Subsequent studies probed the expression of a potential ligand for LILRB4 on human T cell subsets utilising a recombinant LILRB4-Fc fusion protein and showed that this ligand is upregulated upon T cell activation in an allogeneic antigen-specific model, specifically, mixed-lymphocyte reaction (Kim-Schulze et al. JI 2006). Although identification of this potential ligand was not attempted in that or subsequent studies, these experiments were important in suggesting clues as to the identity of the LILRB4 counterstructure based upon its expression and upregulation upon stimulation. Identification of the LILRB4 ligand would be fundamentally important in suggesting potential ligands for the other receptors within this group, which with the exception of LILRA4 are currently all orphan receptors of unknown physiological function.

Chang et al. (Nat Immunol 2002) utilised a mixed-lymphocyte reaction model, in which the only cell types present were DCs and $CD4^+$ T cells. A logical suggestion arising from these studies is that blocking of the tolerogenic effect utilising anti-LILRB4 antibodies disrupts the interaction between LILRB4 and its ligand on target cells i.e. the LILRB4 counterstructure is present on either DCs or $CD4^+$ T cells (or possibly both). A subsequent paper from members of this group using LILRB4-Fc staining showed the expression of the ligand on $CD4^+$ T cells at low levels (5% of $CD4^+$ T cells staining positive) but significant upregulation upon stimulation (to approximately 25 % of $CD4^+$ T cells staining positive) (Kim-Schulze et al. JI

2006). A homotypic interaction of LILRB4 with itself could thus be ruled out as the sole interaction since LILRB4 is only expressed in cells of the myeloid lineage and not in T lymphocytes. This paper also showed that the LILRB4 ligand is capable of inhibitory signalling, since the tolerogenic effects of membrane-bound LILRB4 (e.g. LILRB4 transfected KG1 APCs) could be equally replicated with soluble recombinant LILRB4-Fc, or expression of a truncated form of the receptor which lacks any cytoplasmic ITIM signalling motif. Bidirectional signalling through the LILRB4 ligand was therefore suggested. Thus, this paper provided further information which might assist in identifying the LILRB4 ligand.

The mode and type of ligand recognized by the Group II LILRs remains unclear, although the recent identification of BST2 as the ligand for LILRA4 has provided some data (Cao et al. JEM 2009). Indeed the very definition of Group I vs. Group II LILRs hinges on the amino acid conservation at those sites in LILRB1 and LILRB2 which have been shown to contact MHC Class I (Willcox et al. Nat Immunol 2003). It is entirely possible that Group II LILRs might bind distinct and diverse ligands even within this group, so subsequent studies might feasibly delineate the group further into Group III, Group IV etc. Nevertheless, identification of the ligand for LILRB4 would be of major interest and potentially therapeutically important for the modulation of tolerance, either to enhance it in the context of autoimmunity or impair it in the presence of infection or tumourigenesis. In this chapter of my thesis I will discuss work conducted with the aim of identifying the LILRB4 ligand.

3.2 Defining the distribution of LILRB4 ligand using multimeric receptor

Defining the distribution of the LILRB4 ligand or ligands on primary cells would be a significant step forwards in the process of identifying any potential ligands. However, many cell surface immune receptor-ligand pairs that have previously been characterised have low affinity constants, and for the LILRs these are generally in the micromolar range (Chapman et al. Immunity 2000, Shiroishi et al. JMB 2006), which render monomeric forms of these receptors unsuitable for cell-staining-based ligand identification studies, as such low-affinity interactions may not be detectable by flow cytometry. However, numerous studies have used multimeric forms of immune receptors as reagents to identify distribution of target ligands, and in some cases as a direct tool to ligand identification (Braud et al. Nature 1998, Allan et al. JEM 1999, Voulgaraki et al. Immunology 2005). In particular, the use of MHC Class I tetramers to define TCR-MHC specificities by flow cytometry is now widespread (Altman et al. Science 1996). The only published study on LILRB4 in this regard involved the use of LILRB4-Fc proteins to suggest the presence of LILRB4 ligands on the surface of T cells (Kim-Schulze et al. JI 2006), but did not examine other cell types.

I had previously developed and optimised methods for recombinant production of soluble LILRB4 using an *E. coli* system. These methods involved overexpression of the two extracellular Ig-like domains (D1D2) by cloning the LILRB4 gene into the pET23a expression vector, purification of the protein from insoluble inclusion bodies, solubilisation of inclusion bodies in 6M Guanidine HCl buffer, *in vitro* dilution refolding using the well-established methods of Garboczi et al (PNAS 1992) and purification by Size Exclusion Chromatography (SEC). SDS-PAGE analysis indicated the resulting protein was both monomeric and suggested correct folding, which was supported by antibody reactivity as shown by surface plasmon resonance (SPR). I had also produced a biotinylation sequence-

tagged protein - LILRB4bt - by the same methods, allowing generation of soluble LILRB4 D1D2 tetramers by conjugation with Streptavidin-PE, for use as a staining reagent to identify the distribution of LILRB4 ligands on target cells by flow cytometry (Garner et al. Prot Exp Pur 2006).

3.2.1 Detection of LILRB4 Tetramer Staining Using Flow Cytometry

LILRB4 tetramers were generated using protocols developed for generation of MHC Class I tetramers (Altman et al. Science 1996, and see Chapter 2), and used to stain PBMCs from a cohort of eight healthy lab donors. Staining was carried out in combination with anti-CD3, anti-CD4 and anti-CD8 antibodies to analyse T cell subsets, anti-CD19 antibody to analyse B cells, and anti-CD14 antibody to analyse monocytes. Unconjugated Streptavidin-PE was used as a control for LILRB4 tetramer staining. T cell subsets were also analysed for LILRB4 tetramer binding after a 3 h period of activation by the mitogen, phytohaemagglutinin (PHA) at 10 µg/ml final concentration to assess whether cellular activation had any effect on expression of LILRB4 ligands. PBMCs were analysed using a Beckman-Coulter EPICS XL flow cytometer. Flow cytometry data files were analysed using WinMDI 2.9 software (http://facs.scripps.edu/software.html). Statistical analyses were conducted using Graphpad Prism 4 (Graphpad Software, Inc.) to carry out Wilcoxon Signed-Rank statistical tests.

Forward Scatter (FS, related to size of detected particles) and Side Scatter (SS, on a logarithmic scale, related to particle granularity) profiles were used to exclude debris. Staining with the DNA intercalating agent Propidium Iodide (PI) was used to exclude necrotic and late apoptotic cells from analysis, as PI is able to enter cells that have lost plasma membrane integrity but is unable to permeate viable cells. The signal from PI was detected in fluorescence channel 3 (FL3). This process of gating on live cells is depicted in **Figure 3.1**.

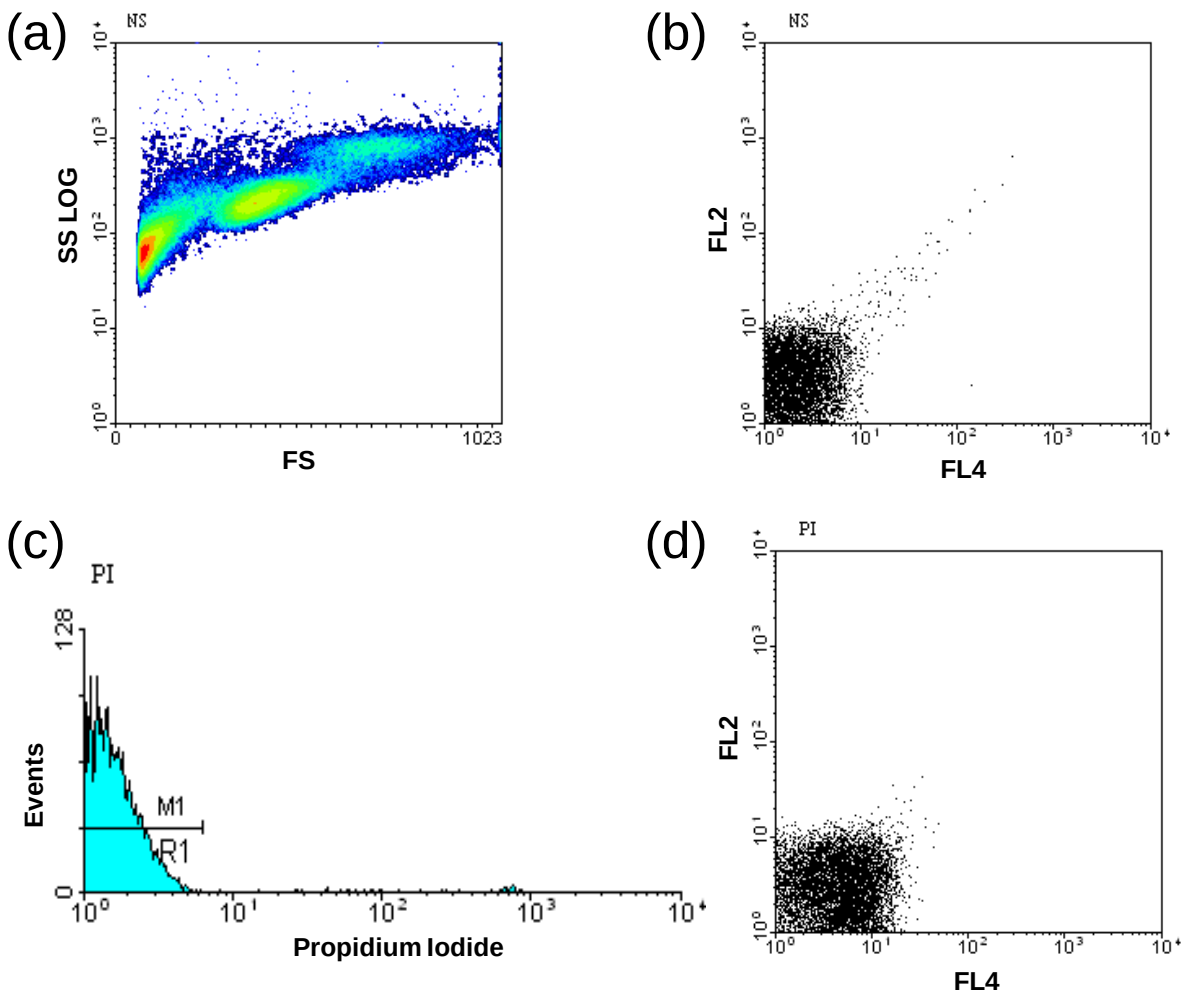

Figure 3.1. Flow cytometry gating on live cells. (a): FS/SS contour plot of unstained cells. (b): Dot plot of FL2 channel against FL4 channel signals showing characteristic non-specific fluorescence from debris. (c): Histogram of data from the FL3 channel showing PI staining of cell debris (necrotic/ late apoptotic cells). R1 is a region set to exclude this signal (d) Dot plot of FL2 channel against FL4 channel gated on region R1 showing cleanup of non-specific signal.

Compensations were set using CD3-FITC for fluorescence channel 1 (FL1), CD4-PE for fluorescence channel 2 (FL2) and CD19-PEcy5 for fluorescence channel 4 (FL4).

3.2.2 Tetramer Staining of Resting PBMC Subsets

FS/SS profiles, in addition to back-gating using the subset markers, were used to set gates for lymphocyte populations. Examples from one donor are shown in **Figure 3.2**. In **Figure 3.2a** and **Figure 3.2b**, CD3-FITC staining is used to define a region within the FL1/FL4 dot plot and that region is used as a gate on the FS/SS contour plot. This allows definition of a region within the FS/SS plot that is then used to gate for lymphocytes. **Figure 3.2c** and **Figure 3.2d** show that the majority of $CD3^+$ and $CD4^+$ T cells fall within this gate, as do the majority of $CD19^+$ B cells (**Figure 3.2e** and **Figure 3.2f**). All subsequent analysis of lymphocytes was conducted with this gate.

For analysis of resting $CD4^+$ T cells, PBMCs from eight healthy normal lab donors were stained with a combination of CD3-FITC, CD4-PEcy5 and either LILRB4 tetramer-PE or Streptavidin-PE as a control. Donors were in two groups of four, and the same gates and regions were applied to donors in each group. **Figure 3.3** shows representative data from one donor.

A dot plot of CD3-FITC against CD4-PEcy5 staining was used to define quadrants for analysis. As shown in **Figure 3.3b**, 55 % of cells within the FS/SS-defined lymphocyte gate were $CD3^+$ T cells and 32 % of cells within the lymphocyte gate were $CD3^+CD4^+$ T cells.

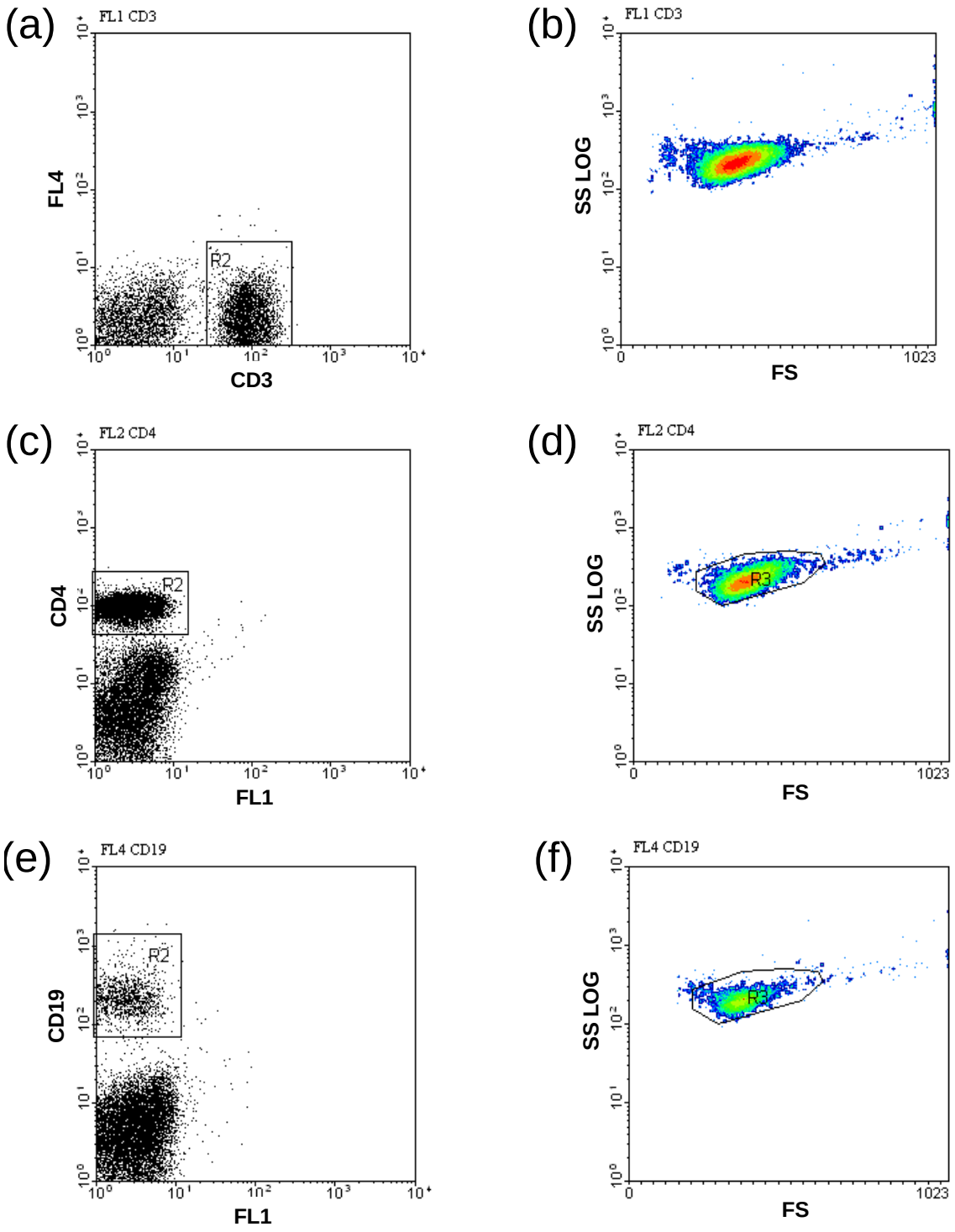

Figure 3.2. Establishing a gate for flow cytometric analysis of lymphocyte populations. (a), (c), (e): Dot plots of CD3-FITC (FL1), CD4-PE (FL2) and CD19-PEcy5 (FL4) staining, respectively, against an unstained fluorescence channel. These plots were used to set compensations during data collection and regions for back-gating during data analysis. (b): Back-gating of $CD3^+$ cell region, R2, onto FS/SS contour plot showing definition of lymphocyte gate. This plot was used to draw a region, R3, around the lymphocyte population as shown in panels (d) and (f).

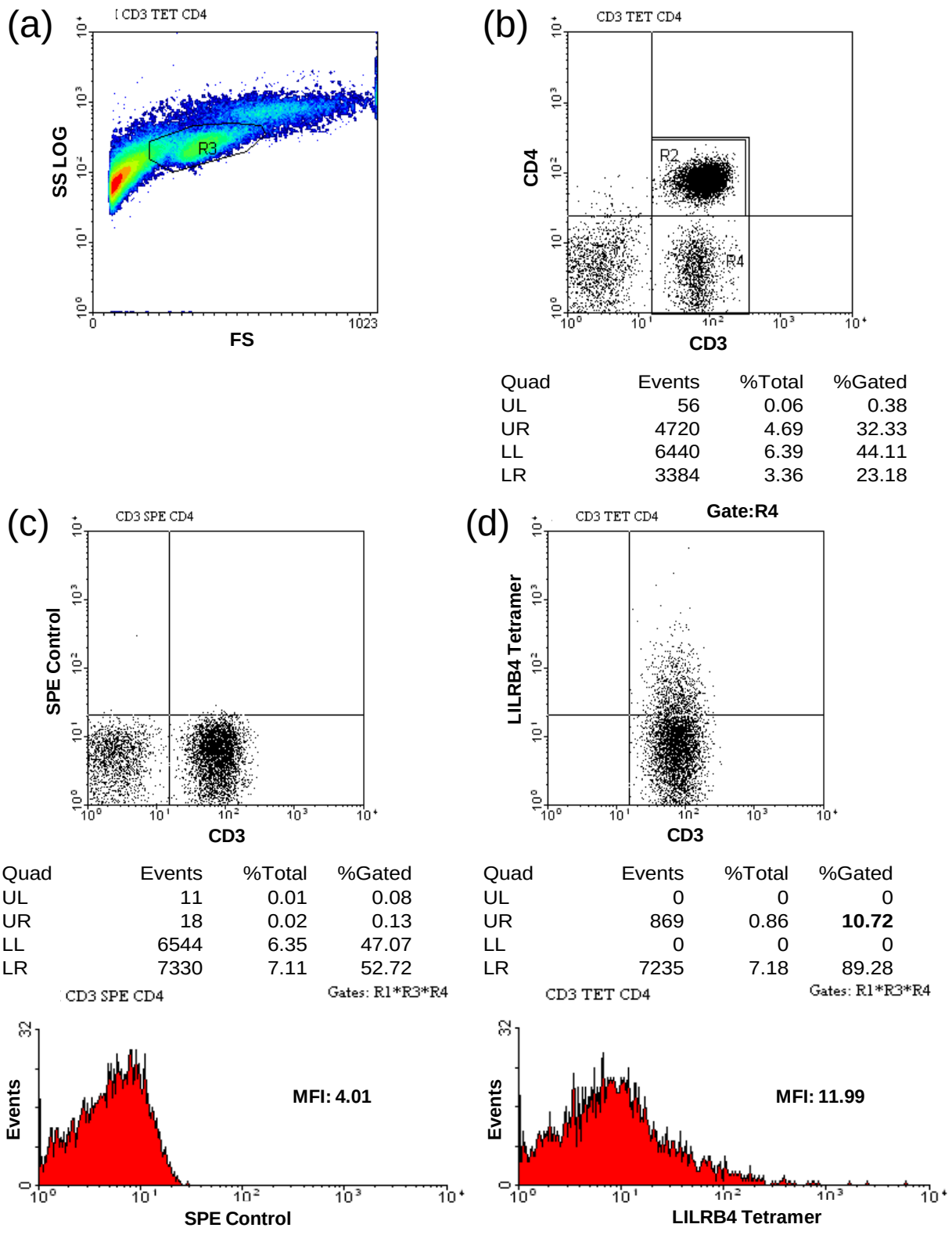

Quad	Events	%Total	%Gated
UL	56	0.06	0.38
UR	4720	4.69	32.33
LL	6440	6.39	44.11
LR	3384	3.36	23.18

Quad	Events	%Total	%Gated
UL	11	0.01	0.08
UR	18	0.02	0.13
LL	6544	6.35	47.07
LR	7330	7.11	52.72

Quad	Events	%Total	%Gated
UL	0	0	0
UR	869	0.86	**10.72**
LL	0	0	0
LR	7235	7.18	89.28

Figure 3.3 *(continued and legend overleaf)*

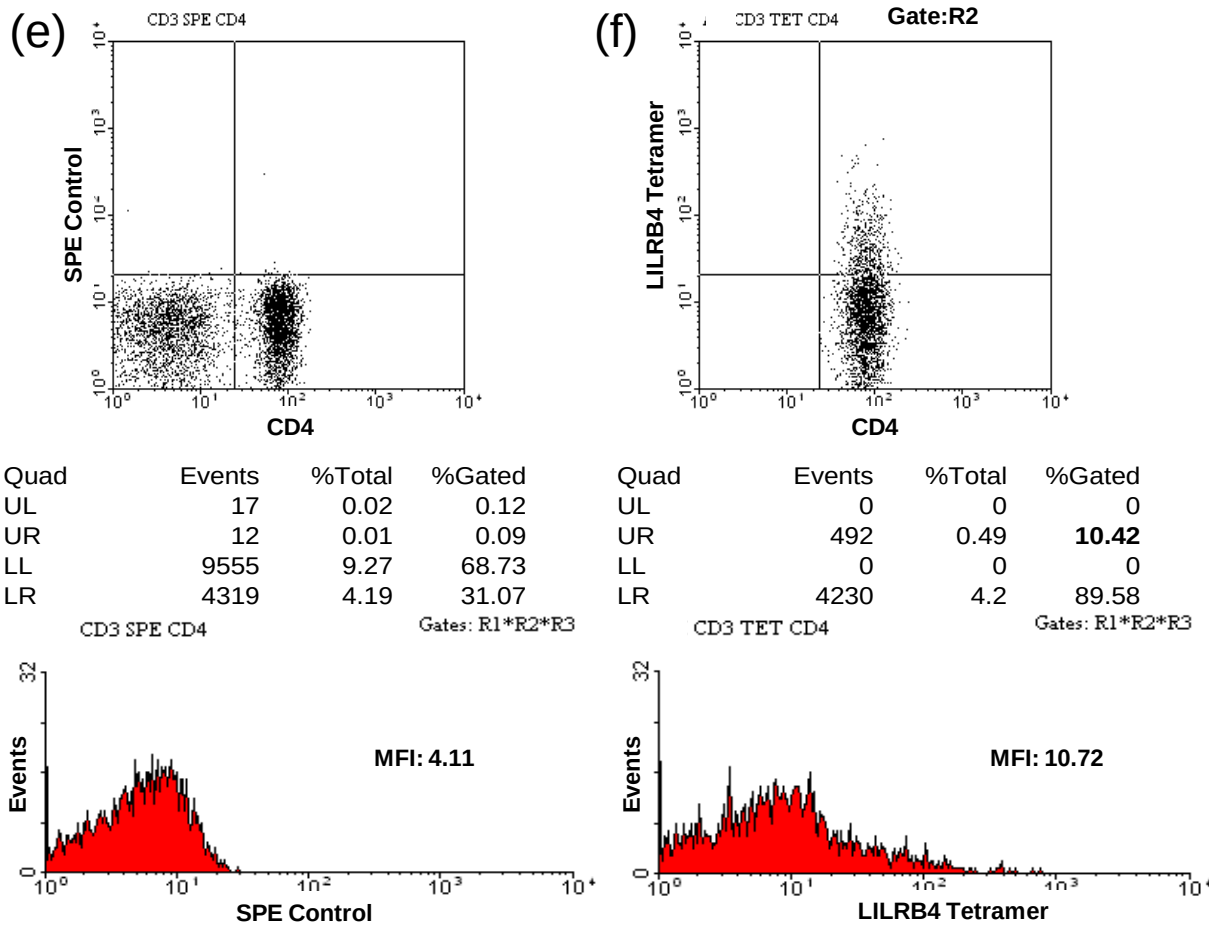

Quad	Events	%Total	%Gated
UL	17	0.02	0.12
UR	12	0.01	0.09
LL	9555	9.27	68.73
LR	4319	4.19	31.07

Quad	Events	%Total	%Gated
UL	0	0	0
UR	492	0.49	**10.42**
LL	0	0	0
LR	4230	4.2	89.58

Figure 3.3. Staining of resting CD3$^+$CD4$^+$ T cells with LILRB4 tetramer. (a) FS/SS contour plot for one donor, showing the position of the lymphocyte gate (defined here as region R3). (b) Dot plot of CD3-FITC against CD4-PEcy5 antibody staining showing T cell subsets. R4 includes all CD3+ T cells and R2 includes CD3+CD4+ cells. (c) and (e): Control staining with Streptavidin-PE for total CD3$^+$ and CD3$^+$CD4$^+$ gates, respectively. (d) and (f): corresponding staining with LILRB4 tetramer.

This plot was also used to define two regions, R4 which encompassed all $CD3^+$ cells and R2 which contained only $CD3^+CD4^+$ double-stained cells.

In **Figure 3.3c** and **Figure 3.3e**, the signal from CD3-FITC or CD4-PEcy5 was plotted against the signal from Streptavidin-PE to illustrate the low background staining using this control reagent. Quadrants were set to define cells staining positive with the LILRB4 tetramer on the basis of this control reagent staining across each group of four donors. Histograms of the fluorescence signal in the second channel (FL2, labelled as SPE Control) are also shown along with the corresponding Mean Fluorescence Intensity (MFI) values.

In **Figure 3.3d** and **Figure 3.3f**, data were gated on total $CD3^+$ T cells or $CD3^+$ $CD4^+$ T cells respectively and staining with the LILRB4 tetramer is shown. For this donor, approximately 11 % of the total $CD3^+$ T cells and a similar value for $CD3^+$ $CD4^+$ T cells stained positively with the LILRB4 tetramer. Corresponding histograms are shown below the dot plots. MFI for LILRB4 tetramer staining for this donor was 12.0 for total $CD3^+$ T cells (SPE control: 4.0) and 10.7 for the $CD3^+$ $CD4^+$ T cell subset (SPE control: 4.1).

Tetramer staining of resting $CD8^+$ T cells was conducted in a similar fashion, using CD3-FITC and CD8-PEcy5 antibodies. **Figure 3.4** shows representative data from a different healthy donor. **Figure 3.4a** shows that approximately 25 % of cells within the lymphocyte gate were $CD3^+$ $CD8^+$ T cells. **Figure 3.4b** shows control staining with Streptavidin-PE and **Figure 3.4c** shows that a low percentage (approximately 4 %) of $CD3^+$ $CD8^+$ T cells stain positive with the LILRB4 tetramer.

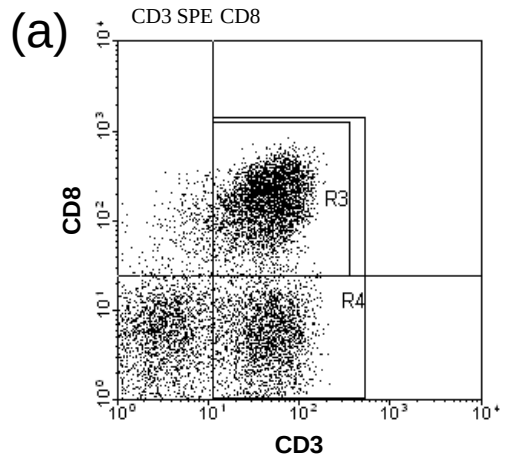

Quad	Events	%Total	%Gated
UL	360	0.36	2.54
UR	3476	3.47	24.54
LL	5802	5.79	40.96
LR	4527	4.52	31.96

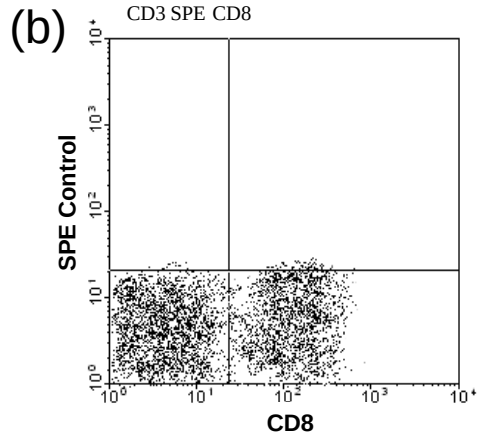

Quad	Events	%Total	%Gated
UL	33	0.03	0.20
UR	42	0.03	0.06
LL	10294	10.01	72.67
LR	3797	3.56	26.80

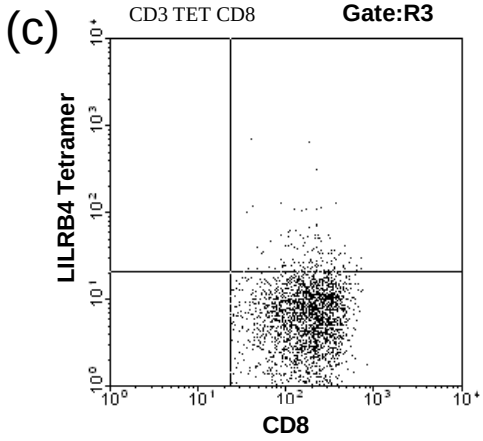

Quad	Events	%Total	%Gated
UL	0	0	0
UR	118	0.12	3.37
LL	0	0	0
LR	3384	3.38	96.63

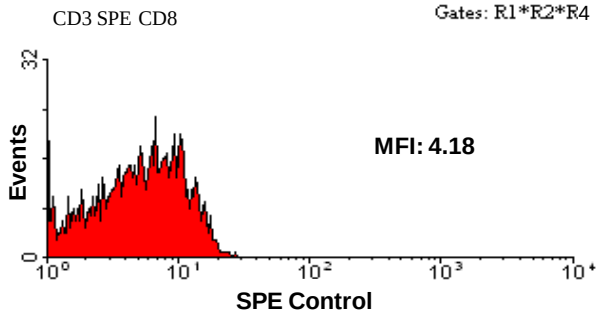

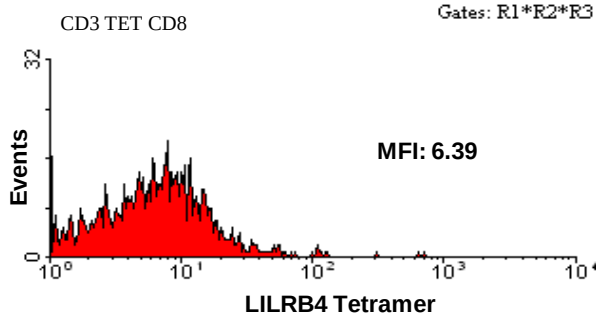

Figure 3.4. Staining of resting CD3$^+$ CD8$^+$ T cells with LILRB4 tetramer. (a) Dot plot of CD3-FITC against CD8-PEcy5 antibody staining showing CD3$^+$CD8$^+$ T cell subset, defined as a region, R3. (b) Control staining with streptavidin-PE of total CD3$^+$ cells (c) Staining of CD3$^+$CD8$^+$ T cells with the LILRB4 tetramer. This dot plot has been gated on Region R3.

These results confirmed that multimeric LILRB4 stained *ex vivo* freshly isolated populations of T cells. Similar results were obtained for other donors. Pooled data for $CD4^+$ and $CD8^+$ T cells for all eight donors are collated and discussed in Section 3.2.5.

For analysis of resting $CD14^+$ monocytes and $CD19^+$ B cells, PBMCs from the same eight healthy normal lab donors were stained with a combination of CD14-FITC, CD19-PEcy5 and either LILRB4 tetramer-PE or Streptavidin-PE as a control. As for T cell analysis, donors were in two groups of four, and the same gates and regions were applied to donors in each group. A dot plot of CD14-FITC against CD19-PEcy5 staining (**Figure 3.5a**) was used to back-gate on FS/SS to define a region, R5, containing both cell populations (**Figure 3.5b-d**). Subsequent analyses of the $CD14^+$ monocyte and $CD19^+$ B cell populations were conducted with this gate in place.

Representative data from one donor are shown in **Figure 3.6**. **Figure 3.6a** shows a contour plot of FS/SS, illustrating the position of the gate for analysis of the two populations as defined by region R5. **Figure 3.6b** shows a dot plot of CD14-FITC (detected in channel FL1) against CD19-PEcy5 (detected in channel FL4) antibody staining for that donor, which was used to define a region containing $CD14^+$ monocytes (R4) and a region containing $CD19^+$ B cells (R2).

In **Figure 3.6c** and **Figure 3.6e**, CD14-FITC or CD19-PEcy5 were plotted against the signal from Streptavidin-PE to indicate control staining. Quadrants were set to define cells staining positive with the LILRB4 tetramer on the basis of this control staining pattern across each group of four donors. Histograms of the fluorescence signal in the second channel

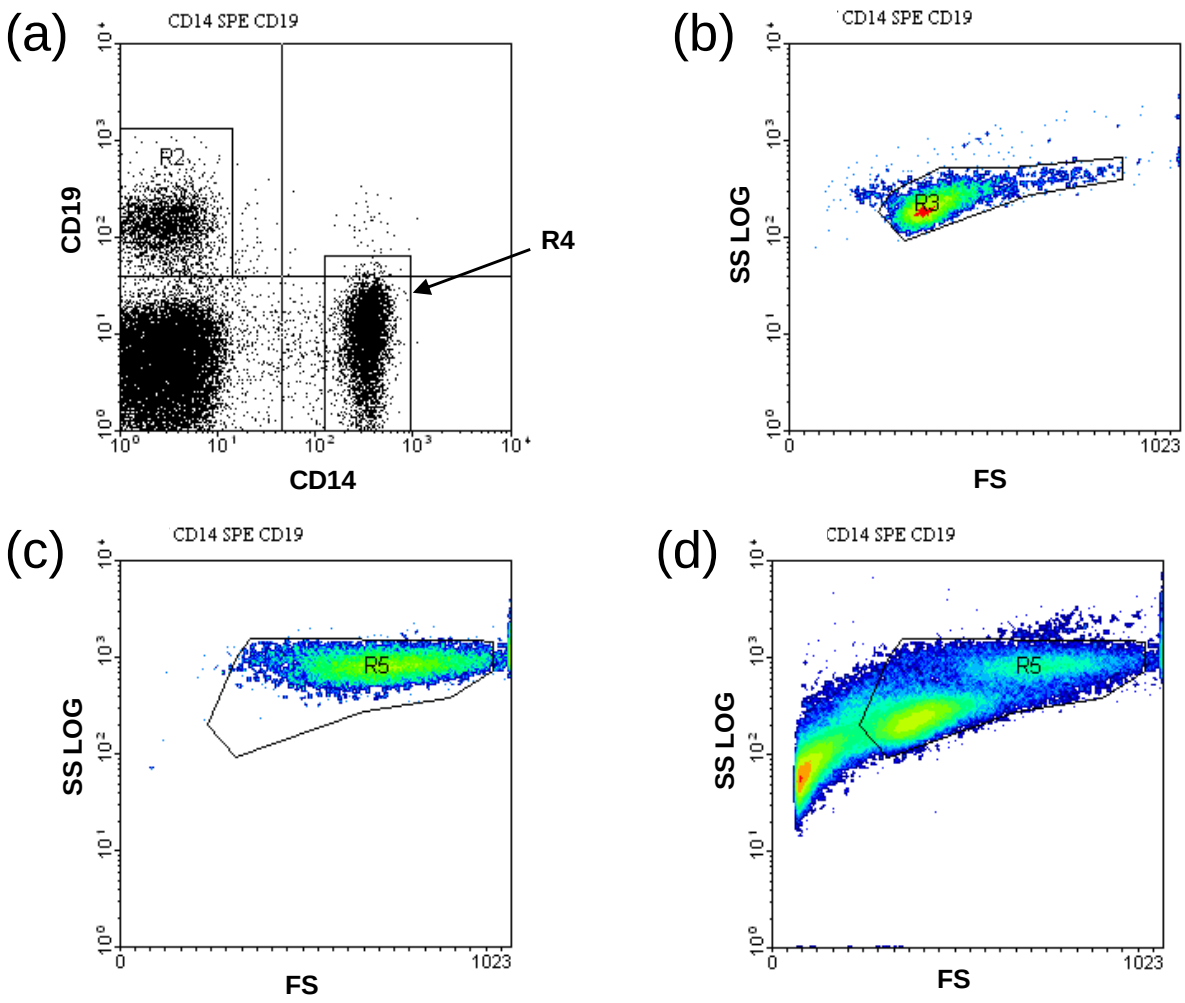

Figure 3.5. Establishing a gate for flow cytometric analysis of resting CD19$^+$ B cells and CD14$^+$ monocytes. (a): Dot plot of CD14-FITC against CD19-PEcy5 antibody staining showing region definitions used to gate on monocytes (region R4) and B cells (region R2), respectively. (b) – (d): Back-gating strategy used to define regions of the FS/SS contour plot containing B cells (region R3) and both B cells and monocytes (region R5).

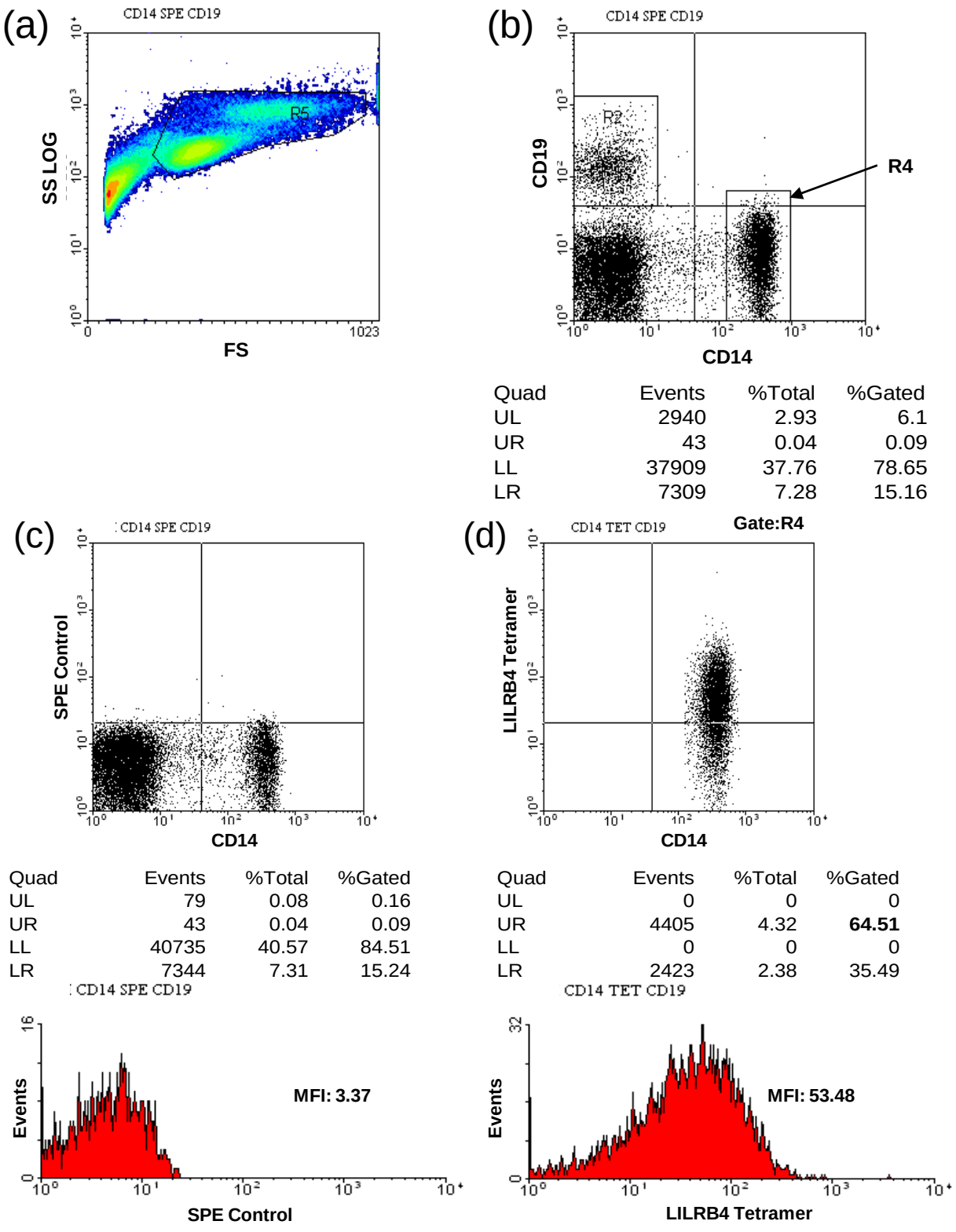

Quad	Events	%Total	%Gated
UL	2940	2.93	6.1
UR	43	0.04	0.09
LL	37909	37.76	78.65
LR	7309	7.28	15.16

Quad	Events	%Total	%Gated
UL	79	0.08	0.16
UR	43	0.04	0.09
LL	40735	40.57	84.51
LR	7344	7.31	15.24

Quad	Events	%Total	%Gated
UL	0	0	0
UR	4405	4.32	**64.51**
LL	0	0	0
LR	2423	2.38	35.49

Figure 3.6 *(continued and legend overleaf)*

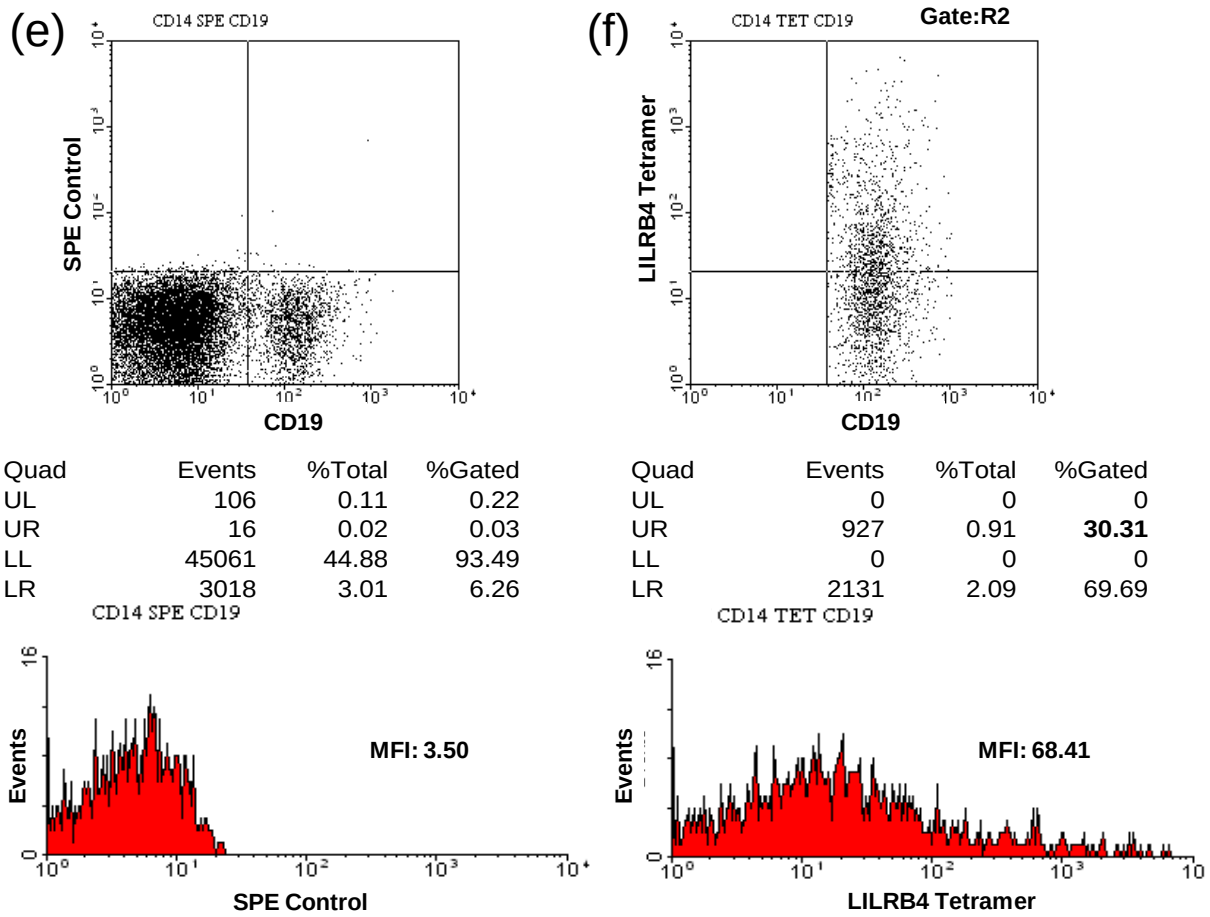

Figure 3.6. LILRB4 tetramer staining of resting CD14$^+$ monocytes and CD19$^+$ B cells. (a): FS/SS plot for one representative donor. (b): Dot plot of CD14-FITC antibody staining against CD19-PEcy5 antibody staining showing definition of gates for CD19$^+$ B cells and CD14$^+$ monocytes. (c): Control staining with Streptavidin-PE for CD14$^+$ monocytes. (d): Corresponding staining with LILRB4 tetramer for CD14$^+$ monocytes. (e): Control staining with Streptavidin-PE for CD19$^+$ B cells (f): Corresponding staining with LILRB4 tetramer for CD19$^+$ B cells.

(corresponding to signal from Streptavidin-PE) are also shown along with the corresponding MFI values.

In **Figure 3.6d**, data were gated on $CD14^+$ monocytes using region R4 and staining with the LILRB4 tetramer is shown. For this donor, it can be seen that a high proportion of the $CD14^+$ monocytes (approximately 65 %) stained positive with the LILRB4 tetramer. Corresponding histograms are shown below the dot plots. MFI for LILRB4 tetramer staining for this donor was 53.5 for $CD14^+$ monocytes (SPE control: 3.4).

In **Figure 3.6f**, data were gated on $CD19^+$ B cells using region R2 and staining with the LILRB4 tetramer is shown. Approximately 30 % of the $CD19^+$ B cells stained positive with the LILRB4 tetramer for this donor and this staining pattern has a higher range of tetramer positive cells, with some brightly staining cells apparent. Corresponding histograms are shown below the dot plots. MFI for LILRB4 tetramer staining for this donor was 68.4 for $CD19^+$ B cells (SPE control: 3.5).

These results present a new finding, which is that freshly-isolated human monocytes and B cells stain brightly with multimeric LILRB4, suggesting that the ligand for LILRB4 is highly expressed upon these PBMC subsets. Pooled data for $CD14^+$ monocytes and $CD19^+$ B cells for all eight donors are collated and discussed in Section 3.2.5.

For analysis of resting $CD3^-$ $CD56^+$ NK cells, PBMCs from one group of four healthy normal lab donors were stained with a combination of CD56-FITC, CD3-PEcy5 and either LILRB4 tetramer-PE or Streptavidin-PE as a control. The same gates and regions were applied for each donor. Representative data from one donor is shown in **Figure 3.7**.

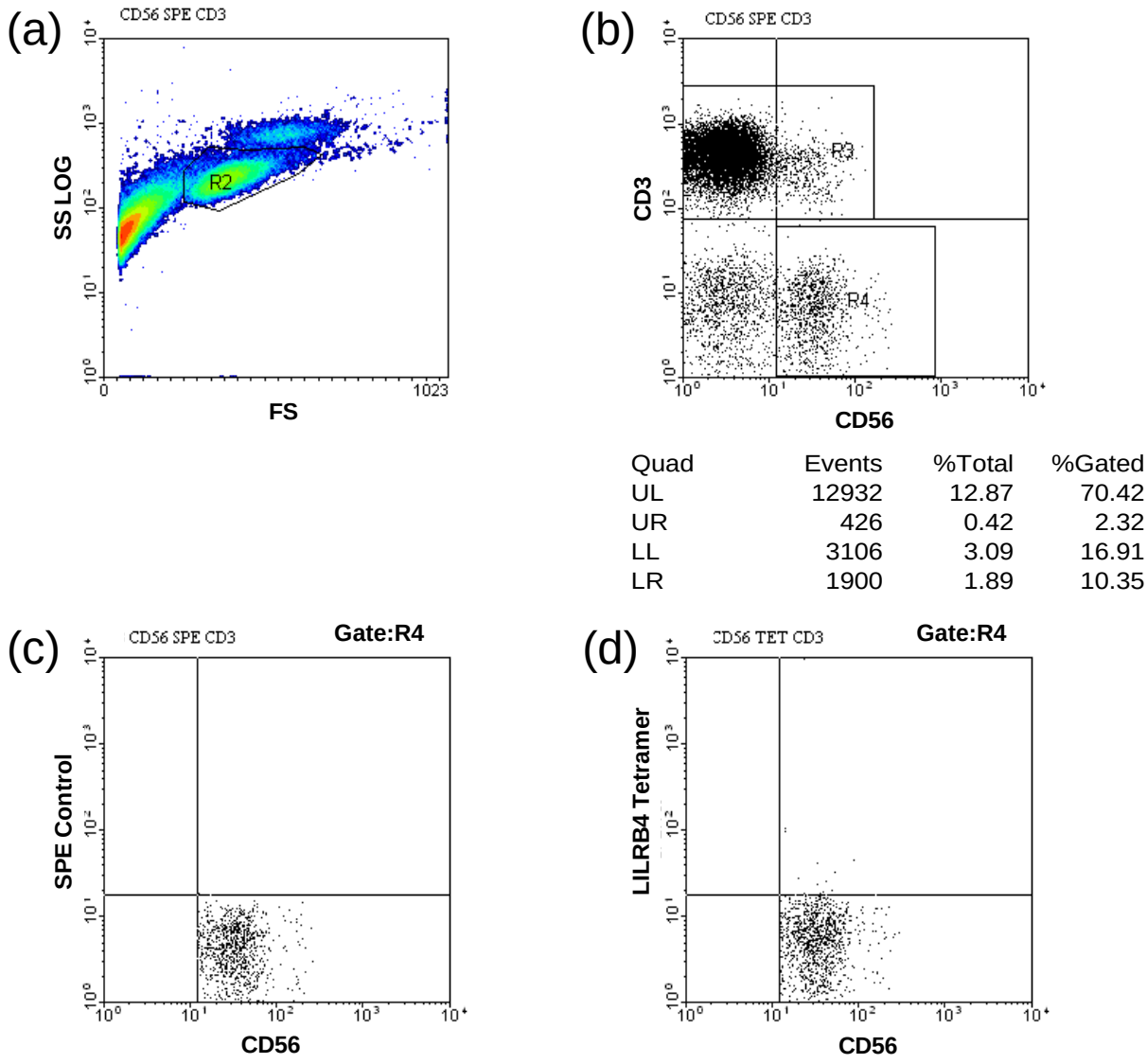

Quad	Events	%Total	%Gated
UL	12932	12.87	70.42
UR	426	0.42	2.32
LL	3106	3.09	16.91
LR	1900	1.89	10.35

Quad	Events	%Total	%Gated
UL	0	0	0
UR	2	0	0.11
LL	0	0	0
LR	1895	1.89	99.89

Quad	Events	%Total	%Gated
UL	0	0	0
UR	18	0.02	0.92
LL	0	0	0
LR	1938	1.91	99.08

Figure 3.7. LILRB4 tetramer staining of resting CD3$^-$ CD56$^+$ NK cells. (a): FS/SS contour plot for one representative donor. (b): Dot plot of CD56-FITC against CD3-PEcy5 staining used to define a region for analysis of NK cells, R4. (c): Control staining with Streptavidin-PE against CD56, gated on region R4. (d): Corresponding staining of CD3$^-$ CD56$^+$ NK cells with the LILRB4 tetramer.

A dot plot of CD56-FITC against CD3-PEcy5 staining (**Figure 3.7b**) was used to define a region, R4, which was $CD3^-$ and $CD56^+$. This region was then used to back-gate on a FS/SS contour plot to generate a lymphocyte gate, R3 (**Figure 3.7a**). Subsequent analysis of the NK cell population was conducted with this gate in place. In **Figure 3.7c**, the signal from CD56-FITC antibody staining has been plotted against the signal from Streptavidin-PE to indicate control staining. This staining pattern was used to set quadrants to define cells staining positive with the LILRB4 tetramer as previously described. These data were gated on $CD3^-$ $CD56^+$ NK cells using region R4 (**Figure 3.7b**).

In **Figure 3.7d**, data were gated on $CD3^-$ $CD56^+$ NK cells using region R4 and staining with the LILRB4 tetramer is shown. For this donor, it can be seen that a small number (less than 1 %) of the $CD3^-$ $CD56^+$ NK cells stained positive with the LILRB4 tetramer.

In summary, these data show that NK cells are essentially negative for surface expression of the LILRB4 ligand and this could be evidence against non-specific binding of the LILRB4 tetramer to PBMCs.

3.2.3 LILRB4 Tetramer Staining of Activated T Cells

To study the expression of the LILRB4 ligand upon T cell activation, flow cytometry analysis was conducted as previously described for total $CD3^+$, $CD3^+$ $CD4^+$ and $CD3^+$ $CD8^+$ T cells after a 3 h incubation with the mitogen, PHA, at a concentration of 10 μg/ml. Gates were redefined to allow for changes in FS/SS profile of activated T cell blasts. The same eight donors were used in two groups of four donors as in the previous experiments.

Figure 3.8 shows representative data from one of the donors. A dot plot of CD3-FITC against CD4-PEcy5 antibody staining (**Figure 3.8a**) was used to define a region containing total $CD3^+$ T cells (R4) which was then back-gated onto the FS/SS contour plot shown in **Figure 3.8b** to define the lymphocyte gate (region R3). Subsequent analysis was conducted with this gate in place. Analysis of CD3-FITC against CD4-PEcy5 antibody staining was simplified with this gate, allowing better discrimination between cellular subtypes as can be seen from the dot-plot shown in **Figure 3.8c**. Region R2 defines the $CD3^+$ $CD4^+$ T cell population.

Representative data from another donor are shown in **Figure 3.9**, to illustrate the LILRB4 tetramer staining pattern for activated $CD3^+$ $CD4^+$ T cells. **Figure 3.9a** shows a contour plot of FS against log SS and shows the lymphocyte gate as defined by region R3 which is discussed above. Regions for analysis of $CD3^+$ cells and $CD3^+$ $CD4^+$ T cells were defined using a dot plot of CD3-FITC against CD4-PEcy5 staining (**Figure 3.9b**).

In **Figure 3.9c** and **Figure 3.9e**, the signal from Streptavidin-PE was plotted against CD3-FITC or CD4-PEcy5, respectively, to illustrate background staining patterns. As before, staining with this control reagent is defined as negative. Quadrants were set to define cells staining positive with the LILRB4 tetramer for each group of four donors, based on the Streptavidin-PE control. Histograms of the fluorescence signal in the second channel are shown along with the corresponding MFI values.

In **Figure 3.9d** and **Figure 3.9f**, staining with the LILRB4 tetramer is shown with data gated on total activated $CD3^+$ T cells or activated $CD3^+$ $CD4^+$ T cells respectively. For this donor, approximately 27 % of the total $CD3^+$ T cells and 33 % of the $CD3^+$ $CD4^+$ T cells stain positive with the LILRB4 tetramer after activation. Corresponding histograms are shown

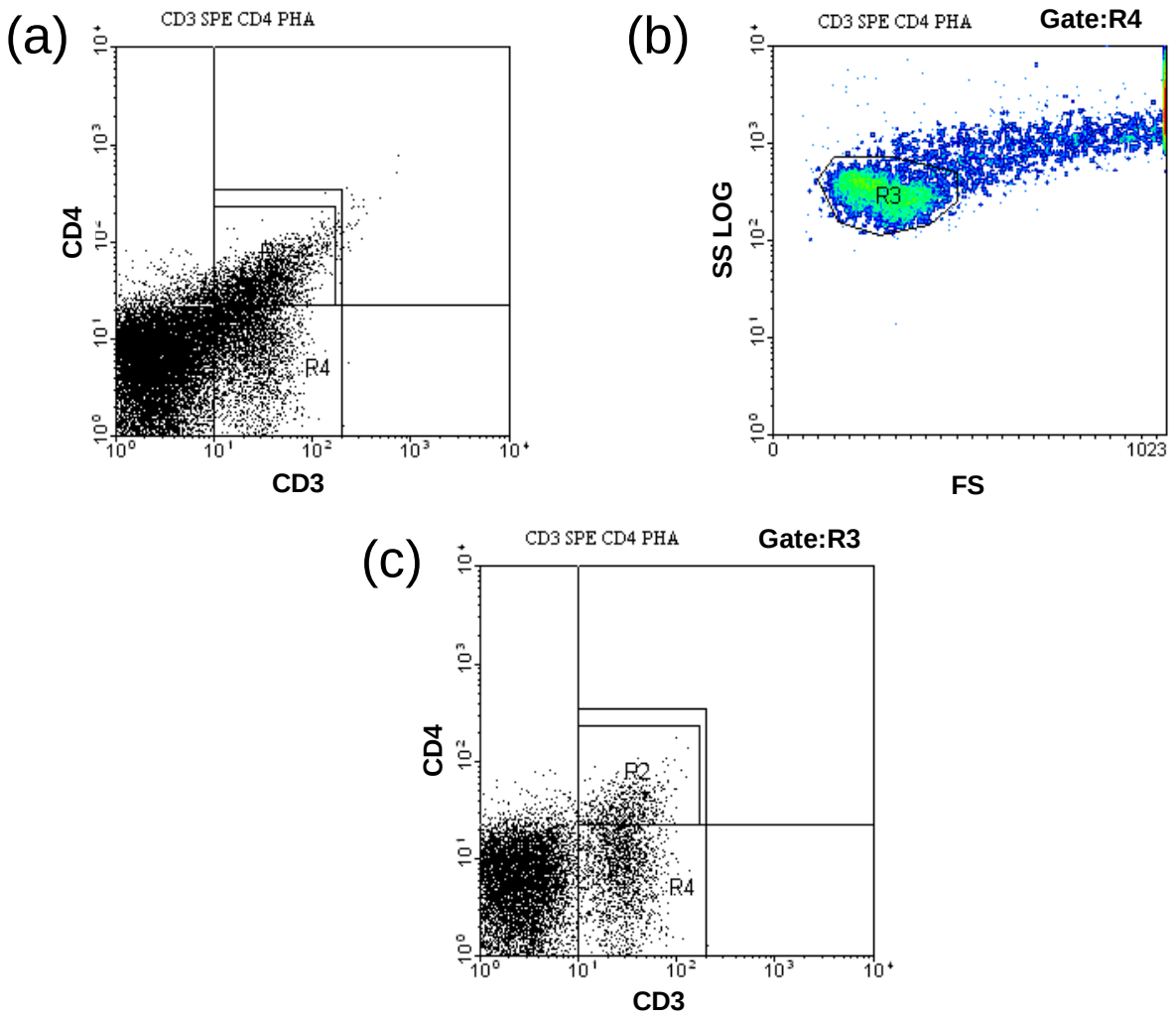

Figure 3.8. Establishing a gate setup for flow cytometric analysis of PHA-activated T cells. (a): Dot plot of CD3-FITC staining against CD4-PEcy5 staining for PBMCs activated with PHA for 3h. A region, R4 has been defined to include the majority of $CD3^+$ T cells for back-gating on FS/SS. (b): Back-gating of R4 on FS/SS contour plot. Another region, R3 has been defined to isolate the lymphocyte population. (c): Gating of R3 on the CD3-FITC staining against CD4-PEcy5 staining dot plot 'cleans up' the plot allowing better visualisation of each T cell subset. Region R2 defines $CD3^+CD4^+$ T cells.

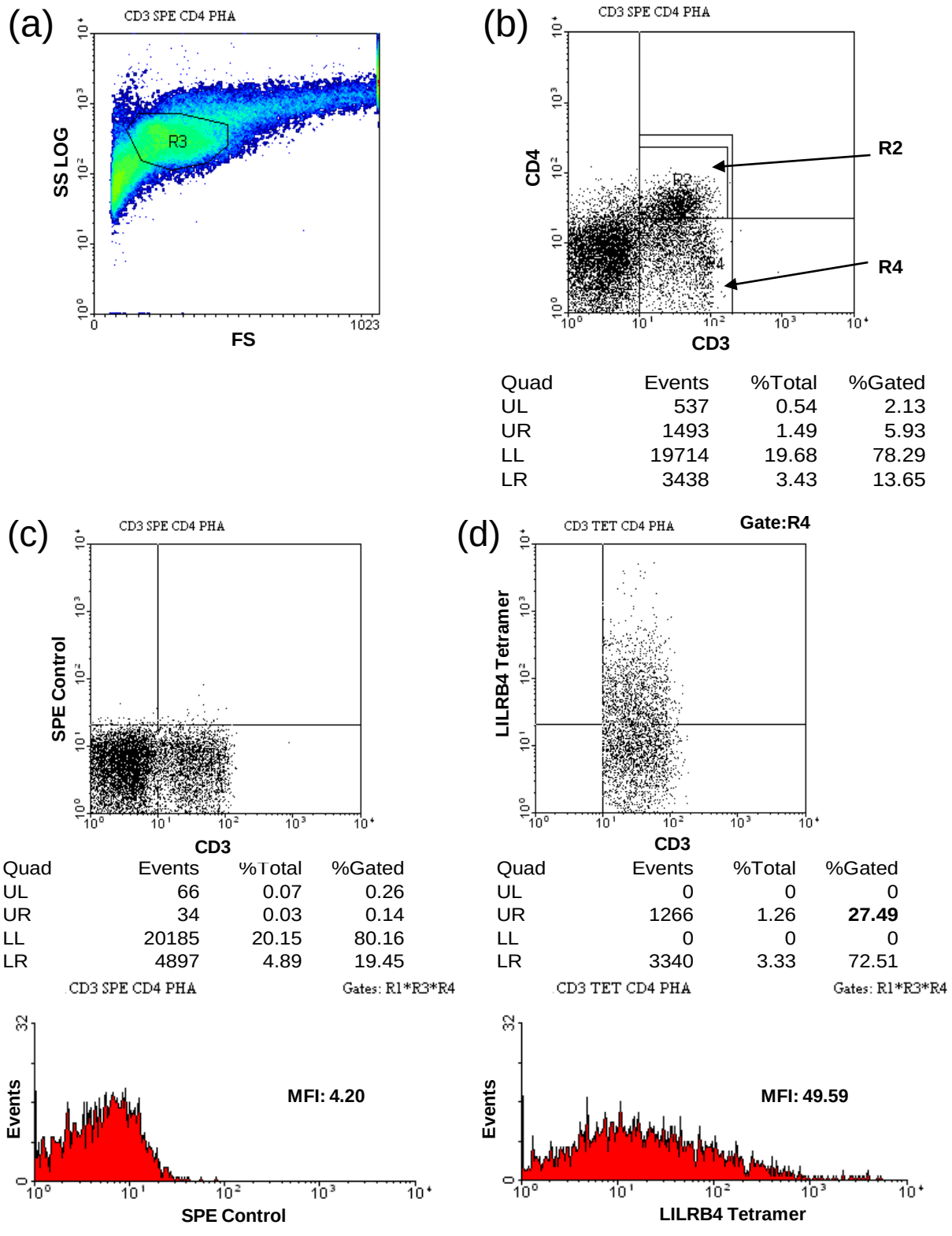

Quad	Events	%Total	%Gated
UL	537	0.54	2.13
UR	1493	1.49	5.93
LL	19714	19.68	78.29
LR	3438	3.43	13.65

Quad	Events	%Total	%Gated
UL	66	0.07	0.26
UR	34	0.03	0.14
LL	20185	20.15	80.16
LR	4897	4.89	19.45

Quad	Events	%Total	%Gated
UL	0	0	0
UR	1266	1.26	**27.49**
LL	0	0	0
LR	3340	3.33	72.51

Figure 3.9 *(continued and legend overleaf)*

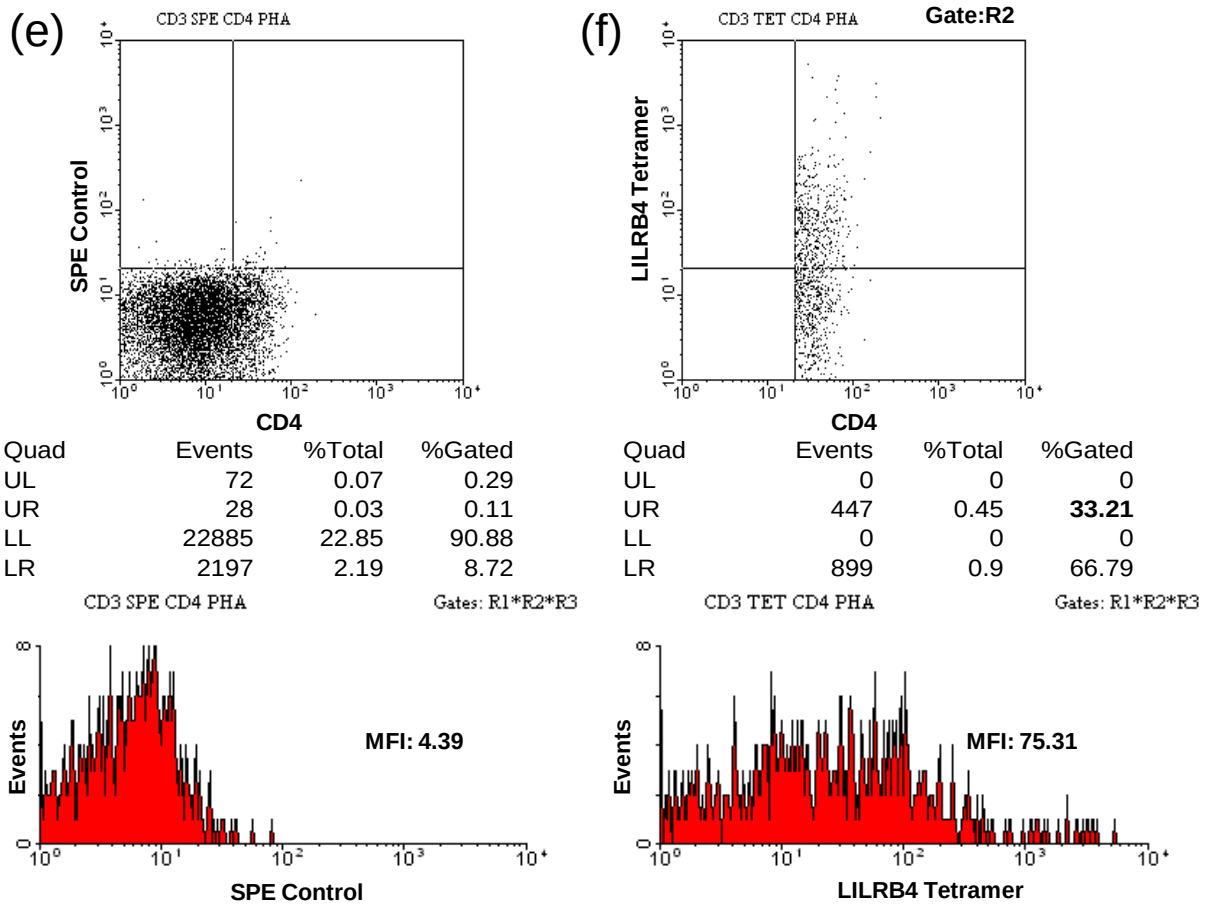

Figure 3.9. LILRB4 tetramer staining of activated CD3$^+$ and CD3$^+$ CD4$^+$ T cells. (a) FS/SS contour plot for one donor showing altered profile after activation. (b) CD3-FITC against CD4-PEcy5 antibody staining showing T cell subsets after activation with PHA. (c): Control staining with Streptavidin-PE for total CD3$^+$ T cells. (d): Corresponding staining with LILRB4 tetramer for total CD3$^+$ T cells. (e): Control staining with Streptavidin-PE for CD3$^+$CD4$^+$ T cells. (f): Corresponding staining with LILRB4 tetramer for CD3$^+$CD4$^+$ T cells.

below the dot plots. MFI for LILRB4 tetramer staining for this donor was 49.6 for total $CD3^+$ T cell (SPE control: 4.2) and 75.3 for $CD3^+$ $CD4^+$ T cells (SPE control: 4.4).

For comparison, the percentages of $CD3^+$ and $CD3^+$ $CD4^+$ T cells staining positive with the LILRB4 tetramer under resting conditions for this donor were 9 % for both respectively, indicating a substantial upregulation in surface expression of the LILRB4 ligand by these lymphocyte subsets upon polyclonal stimulation.

Figure 3.10 shows representative data from one donor, demonstrating the LILRB4 tetramer staining pattern for activated $CD3^+$ $CD8^+$ T cells. Quadrants for analysis were defined using a dot plot of CD3-FITC against CD8-PEcy5 staining (**Figure 3.10b**).

Quadrants were set to define cells staining positive with the LILRB4 tetramer for each group of four donors. In **Figure 3.10c**, control staining with Streptavidin-PE is shown as a dot plot against CD8-PEcy5 antibody staining. Gating on $CD3^+$ $CD8^+$ T cells using region R4 shows approximately 20 % staining with the LILRB4 tetramer after activation with PHA (**Figure 3.10d**).

Under resting conditions the percentage of $CD3^+$ $CD8^+$ T cells that stained positive with the LILRB4 tetramer for this donor was 6 % indicating upregulation in LILRB4 ligand surface expression upon treatment with PHA in a similar fashion to that for $CD4^+$ T cells.

To summarise these data for the expression of the LILRB4 ligand on T cell subsets after 3 h activation with PHA, in accordance with previously published data $CD4^+$ T cells upregulate their expression of the LILRB4 ligand upon activation (Kim-Schulze et al. JI 2006). In

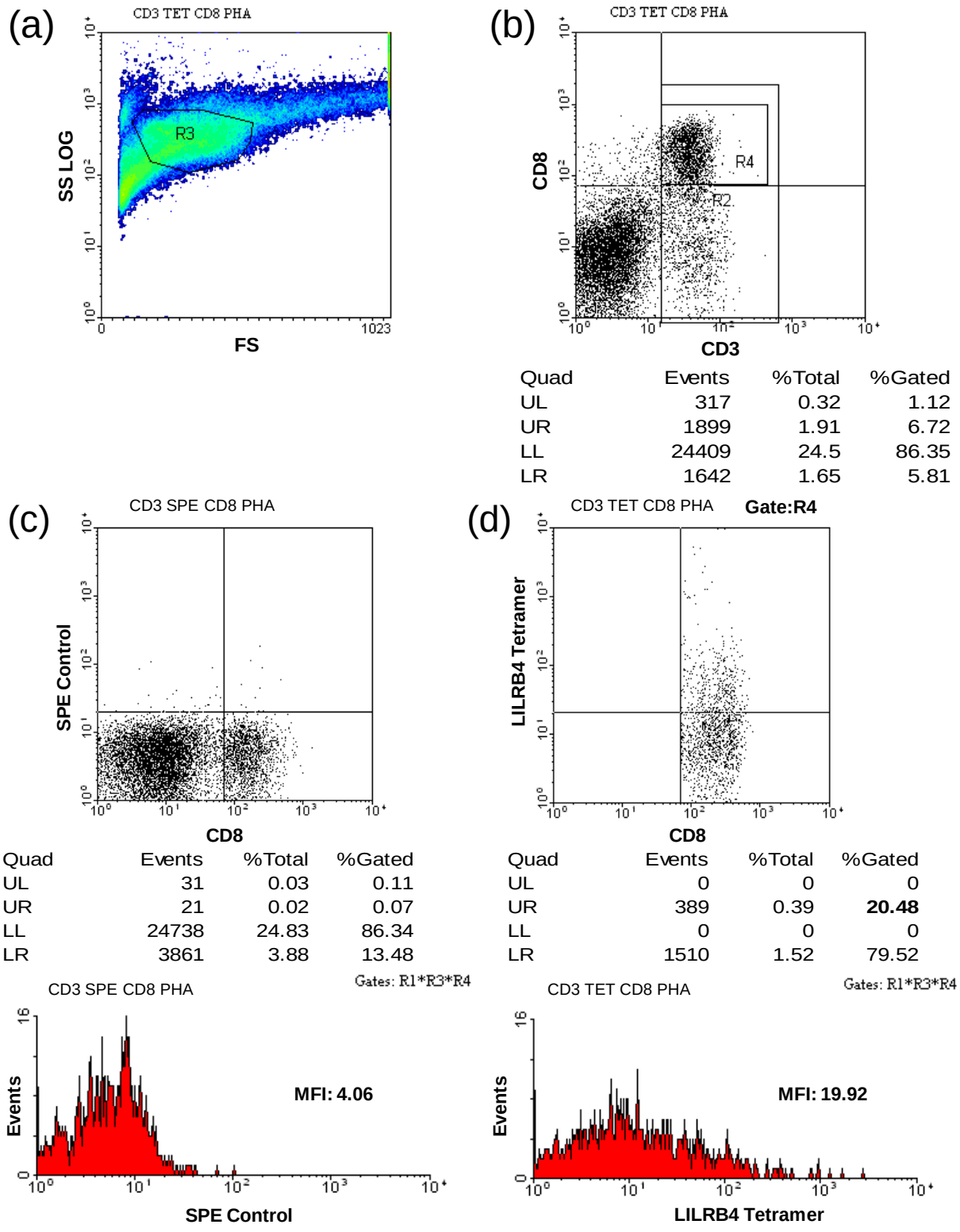

Figure 3.10. LILRB4 tetramer staining of activated CD3$^+$ CD8$^+$ T cells. (a): FS/SS contour plot for one donor showing altered profile after activation. (b): CD3-FITC against CD8-PEcy5 antibody staining showing T cell subsets after activation with PHA. (c): Control staining with Streptavidin-PE for total CD3$^+$ T cells. (d): Corresponding staining with LILRB4 tetramer for CD3$^+$ CD8$^+$ T cells.

addition, a novel finding of this work is that $CD8^+$ T cells also upregulate LILRB4 ligand surface expression to a comparable degree. It is worth noting that my work utilises a strong non-specific polyclonal activation stimulus (i.e. PHA treatment) and analysis is conducted at an early time point (3 h) as compared to seven days in a mixed lymphocyte reaction used in the aforementioned publication.

The data for all eight donors are summarised and compared alongside the data for resting PBMC subsets in Section 3.2.5.

3.2.4 CD69 and LILRB4 Tetramer Staining

In a separate experiment, surface expression of the T cell early activation marker CD69 was analysed to confirm activation of the lymphocytes upon PHA stimulation. PBMCs were harvested from four donors from the original pool of eight and stained with Streptavidin-PE or LILRB4 tetramer-PE plus CD3-FITC and CD69-PEcy5 antibody.

Representative data from one donor is shown in **Figure 3.11**. These data show that a small number (approximately 1 %) of $CD3^+$ T cells are activated and express the CD69 early activation marker in resting PBMCs (**Figure 3.11a**). A dot plot of CD69 staining against LILRB4 tetramer staining, gated on $CD3^+$ T cells, shows no apparent correlation between CD69 expression and LILRB4 ligand expression for resting T cells (**Figure 3.11b**). From **Figure 3.11c** it can be seen that CD69 is rapidly upregulated on $CD3^+$ T cells upon stimulation for 3 h with PHA, with approximately 22 % of T cells staining positively for CD69. **Figure 3.11d** shows that LILRB4 tetramer staining of PHA-activated $CD3^+$ T cells appears to correlate to some degree with the level of CD69 surface expression in this PBMC

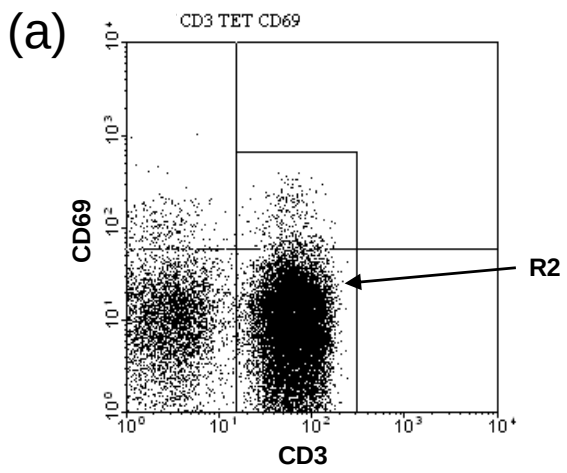

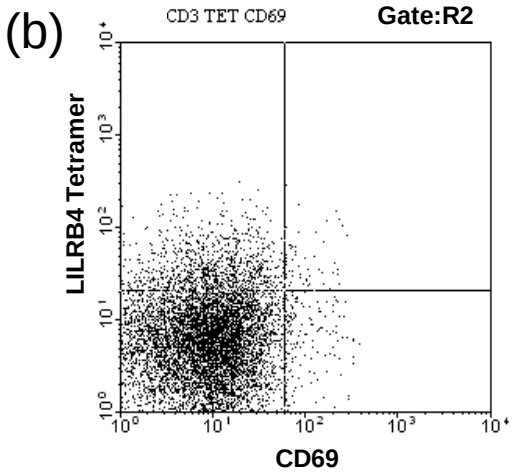

Quad	Events	%Total	%Gated
UL	548	0.54	1.34
UR	336	0.33	0.82
LL	10644	10.57	26.06
LR	29322	29.11	71.78

Quad	Events	%Total	%Gated
UL	1579	1.57	5.32
UR	55	0.05	**0.19**
LL	27743	27.54	93.54
LR	281	0.28	0.95

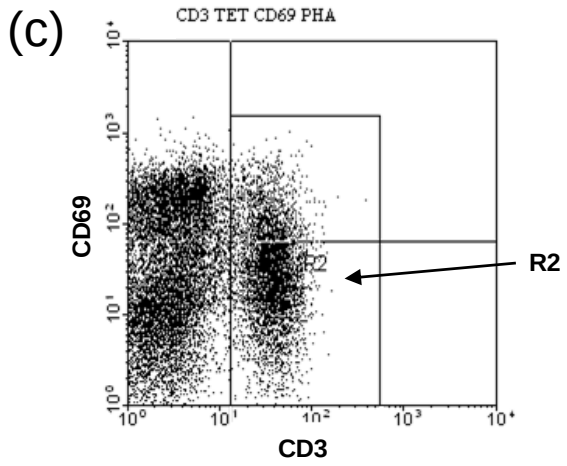

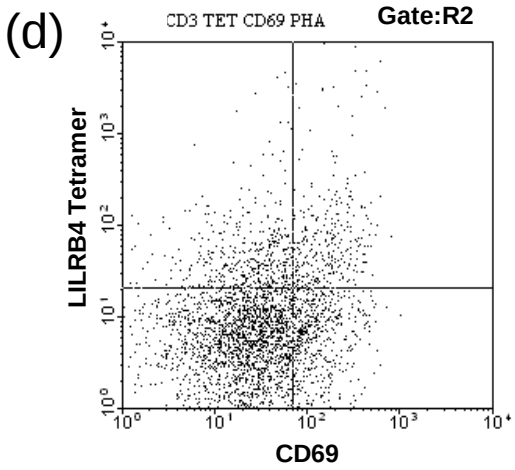

Quad	Events	%Total	%Gated
UL	6918	6.9	19.16
UR	1233	1.23	3.42
LL	23645	23.59	65.5
LR	4304	4.29	11.92

Quad	Events	%Total	%Gated
UL	489	0.49	8.83
UR	300	0.3	**5.42**
LL	3897	3.89	70.38
LR	851	0.85	15.37

Figure 3.11. CD69 staining of resting and activated T cells. (a): Dot plot of CD3-FITC against CD69-PEcy5 antibody staining for resting PBMCs. Region R2 has been defined to include all $CD3^+$ T cells. (b): Dot plot of CD69-PEcy5 antibody staining against LILRB4 tetramer staining for resting PBMCs, gated on $CD3^+$ cells using region R2. (c): Dot plot of CD3-FITC against CD69-PEcy5 antibody staining for PHA-activated PBMCs. Region R2 has been defined to include all $CD3^+$ T cells. (d): Dot plot of CD69-PEcy5 antibody staining against LILRB4 tetramer staining for PHA-activated PBMCs, gated on $CD3^+$ cells using region R2.

subset, and therefore with the activation status of these lymphocytes, with the cells staining brightest for LILRB4 tetramer also staining brightly for CD69 expression.

3.2.5 Summary and Analysis of LILRB4 Tetramer Staining of PBMCs

Pooled data for all eight donors is shown in **Table 3.1** and also as a scatter plot in **Figure 3.12**. Each donor is plotted as a data point for each subset and the horizontal bars show the mean percentage of cells staining positive with the LILRB4 tetramer for each subset. Mean percentages of cells staining positive for the LILRB4 ligand were approximately 12 % for total $CD3^+$ T cells (23 % after PHA activation), 12 % for $CD3^+$ $CD4^+$ T cells (27 % after PHA activation), 5 % for $CD3^+$ $CD8^+$ T cells (17 % after PHA activation), 64 % for $CD14^+$ monocytes and 28 % for $CD19^+$ B cells. For each subset of T cells Wilcoxon Signed-Rank statistical analysis was conducted and showed that the upregulation of LILRB4 tetramer staining on the T lymphocyte subsets upon PHA stimulation is statistically significant ($P < 0.05$).

Donor	CD3		CD4		CD8		CD14	CD19
	Resting	+PHA	Resting	+PHA	Resting	+PHA	Resting	Resting
1	10.72	27.36	10.42	29.30	3.23	21.00	82.76	29.54
2	13.75	23.07	13.60	23.82	3.37	6.91	52.10	23.82
3	12.07	19.69	12.27	22.57	3.61	13.55	40.54	30.50
4	16.31	18.67	16.68	19.60	4.57	16.49	29.22	28.19
5	11.67	23.66	11.40	30.05	7.25	19.68	90.25	31.01
6	8.73	15.77	8.45	23.27	5.45	19.24	70.29	20.65
7	12.20	25.58	11.82	34.76	6.37	20.48	64.51	30.31
8	9.31	27.49	9.31	33.21	9.85	18.81	79.98	26.06
Mean	**11.85**	**22.66**	**11.74**	**27.07**	**5.46**	**17.02**	**63.71**	**27.51**
P-value		*0.0078*		*0.0078*		*0.0078*		

Table 3.1. Collated LILRB4 tetramer staining data. Tabulated data showing the percentage of cells staining with the LILRB4 tetramer for PBMC subsets for all eight donors. Values are listed for resting and PHA-activated $CD3^+$, $CD3^+$ $CD4^+$ and $CD3^+$ $CD8^+$ T cells and for resting $CD14^+$ monocytes and $CD19^+$ B cells. Mean values are listed as well as calculated P-values for Wilcoxon Signed-Rank statistical tests between resting and PHA-activated cells for each subset of T cells.

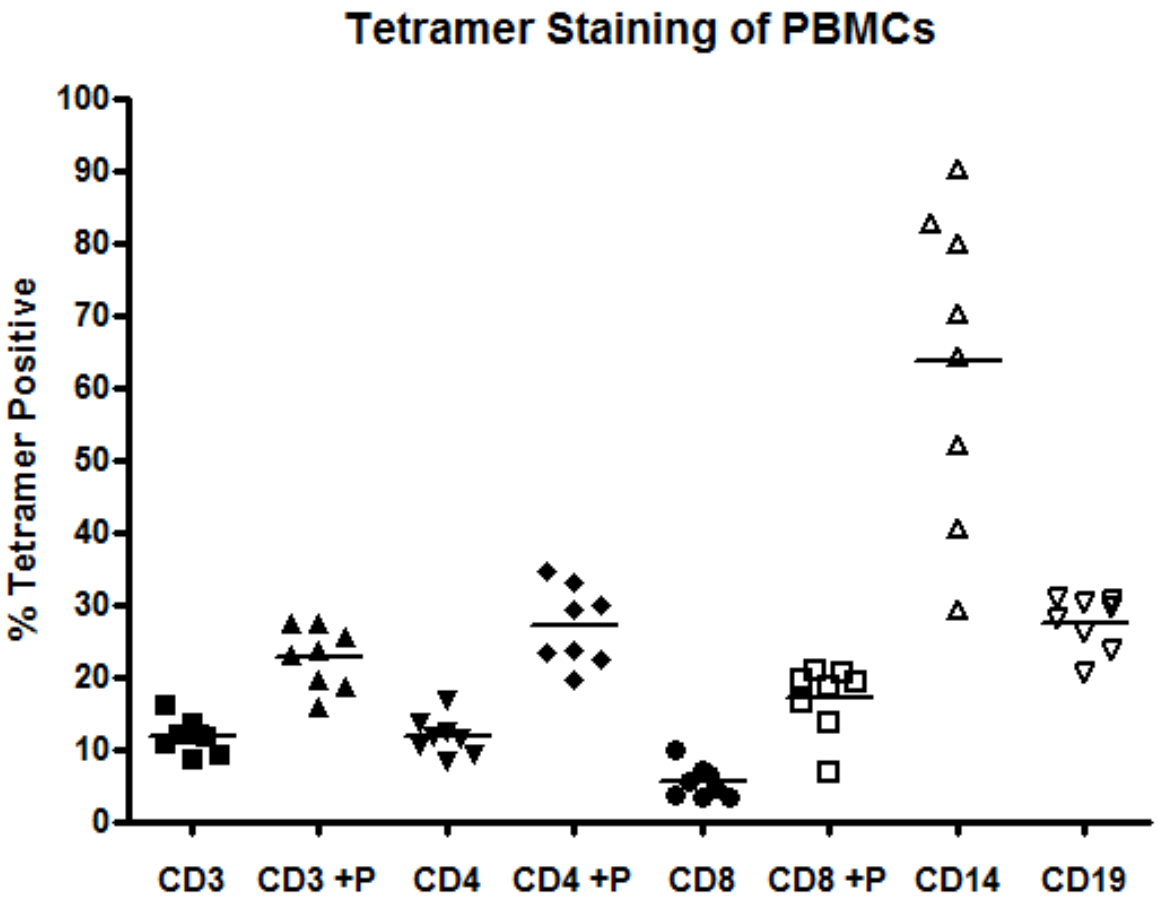

Figure 3.12. Summary of LILRB4 Tetramer Staining of PBMCs. Scatter plot summarising LILRB4 tetramer staining data for all eight donors. Each data point within each category is a single donor, with PBMC subsets as categories on the y-axis and the percentage of cells staining positive with the LILRB4 tetramer on the x-axis. Horizontal bars indicate the mean percentage for each subset. '+P' indicates the addition of PHA.

3.2.6 LILRB4 Tetramer Staining of Human Cell Lines

In order to identify a cellular population that was uniformly positive for LILRB4 ligand and that therefore might be a useful tool in downstream ligand identification approaches the LILRB4 tetramer was used to stain a panel of immortalised human cell lines. These included T cell lines (Jurkat), B cell lines (K422 and REC-1), and a monocyte cell line (THP-1) as well as EBV-positive and EBV-negative immortalised B cell lines derived from lab donors (generated and kindly provided by Alison Leese), plus the adherent melanoma and sarcoma cell lines, LB373 and LB23. The monkey fibroblast cell line COS was also used. The percentage of cells staining positive for the LILRB4 ligand or for Streptavidin-PE as a control are shown in **Table 3.2**.

Cell Line	Origin	Strept-PE	Tetramer-PE
AH LCL	*B LCL*	0.3	2.0
LM LCL	*B LCL*	0.6	5.3
NB4	*Promyelocyte, APL*	0.1	5.1
HL60	*Promyeloblast, APL*	0.1	1.7
BL-2	*Burkitts – low PN*	0.4	5.8
BL-37	*Burkitts – high PN*	0.6	5.2
BL-40	*Burkitts – high PN*	0.1	2.4
Jurkat 1	*T cell ALL*	0.1	1.4
Jurkat 2	*T cell ALL*	0.1	1.6
K422	*B cell NHL*	0.1	2.2
REC-1	*B cell NHL*	0.2	2.9
THP-1	*AMoL*	0.1	2.4
COS	*Monkey fibroblast*	0.1	0.8
LB373mel	*Melanoma, adherent*	0.8	1.5
LB23sarc	*Sarcoma, adherent*	0.2	1.0

Table 3.2. Cell line staining data. Tabulated data showing the percentage of LILRB4 tetramer or Streptavidin-PE staining of cell lines. LCL, lymphoblastoid cell line; APL, Acute Promyelocytic Leukaemia; ALL – Acute Lymphoblastic Leukaemia; NHL – Non-Hodgkins Lymphoma; AMoL – Acute Monocytic Leukaemia. PN = passage number.

Unfortunately, none of the cell lines stained gave a convincingly positive staining pattern with the LILRB4 tetramer. Although the percentage of cells staining with LILRB4 tetramer was higher than that obtained with Streptavidin-PE control, the absolute levels of staining were low (< 6 %).

3.2.7 Summary and Discussion of Flow Cytometry Data

In summary, these data show that multimeric LILRB4 is capable of staining freshly isolated human PBMC. Similarly to previous studies, they show staining to $CD4^+$ T cells which is increased upon activation with PHA. As LILRB4 is not expressed by resting or activated T cells, this staining pattern cannot be due solely to homotypic interactions.

However, my dataset extends previous studies considerably, by showing staining of tetramerised LILRB4 on $CD8^+$ subset T cells in addition to $CD4^+$ T cells, and this staining was increased by activation with PHA. Previous studies used mixed lymphocyte reaction over several days to show this increase upon activation by comparison with 3 h treatment with PHA used in this study, which is a strong and non-specific stimulus to T cells. However, the levels of expression on $CD4^+$ T cells and the degree of upregulation of expression of the proposed LILRB4 ligand are comparable to these studies. In this study I used CD69 expression as a read-out of T cell activation and found a trend for LILRB4 and CD69 co-expression, suggesting that LILRB4 ligand expression may be linked to the activation status of lymphocytes.

Furthermore, I have demonstrated staining of multimeric LILRB4 on other subsets of PBMCs, specifically monocytes, which stain at a high frequency and with high levels, and B

cells, which stain at an intermediate frequency and level between that of monocytes and T cells. The wide span of MFI values is indicative of a wide variation in the level of LILRB4 ligand expression both within and between subsets of PBMCs, and is an observation also seen with LILRB4-Fc staining of PBMC subsets reported in earlier studies (Kim-Schulze et al. JI 2006).

The novel nature of these data may be due to the progression from an Fc-fusion protein with a dimeric avidity used in previous studies to the LILRB4 tetrameric protein with a tetrameric affinity as used in this study. In addition, the use of Fc-fusion proteins is complicated by the presence of Fc receptors on monocytes and B cells. These receptors can be blocked with human or mouse serum, but the presence of these receptors may have given concern to authors of previous studies as to the validity of their findings, if they detected staining of the aforementioned PBMC subsets with the LILRB4-Fc reagent. My data suggests that the expression of the LILRB4 ligand or ligands may be considerably more widespread than previously thought.

Although these results should be interpreted with a degree of caution, several factors suggest that these staining patterns are not likely to be due to non-specific interactions. Firstly, the NK cell PBMC subset does not stain positive with the LILRB4 tetramer and may be a true negative population. Secondly, many of the cell lines tested also did not stain positively. Immortalised cell lines tend to undergo high levels of cell death due to apoptosis which can often lead to binding in a non-specific fashion, but this was not observed. Thirdly, initial experiments conducted with recombinant monomeric LILRB4 showed very weak staining to PBMCs and suggested the need for multimerisation of the receptor to achieve an avidity sufficient for detection of the LILRB4 ligand (Garner et al. Prot Exp Pur 2006). Finally,

control experiments showed that LILRB4bt was antibody reactive, monomeric and pure suggesting it was likely to retain biological reactivity (Garner et al. Prot Pur Exp 2006). These factors lend credence to the notion that the results shown in this section are valid and a true indicator of expression of the LILRB4 ligand.

Transformed immortalised cell lines were used to attempt to identify positively and negatively staining cells which could then have provided reagents for LILRB4 ligand identification – either via the generation of cDNA libraries and expression cloning or through a proteomics and mass spectrometry approach. However, these cell lines did not stain substantially with LILRB4 tetramer to a degree which would have given me confidence in attempting these methods (which are both time consuming and far from technically trivial to conduct successfully).

Why did these cell lines not stain positive for the LILRB4 ligand? One possibility is that the expression of the LILRB4 ligand is selected against in long-term culture of immortalised cell lines. This suggestion is consistent with the finding that LILRB4 binding to unidentified ligands on T cells inhibits target cell proliferation, suggestive of an inhibitory function for the LILRB4 counterstructure. Furthermore, transformed cell line culture systems are unlikely to be the most physiologically relevant biological scenario in which to observe LILRB4 ligand expression and investigate LILRB4 function.

LILRB4 is not expressed in the mouse and the closest homologous receptors – the PIR family – do not have a corresponding member of the family (being similar instead to Group I LILRs which bind to MHC Class I molecules) thus ruling out the use of wild-type mice to study LILRB4 and its ligand in an *in vivo* setting. Instead, *ex vivo* clinical studies of patients with

cancer or autoimmune diseases could be more revealing of LILRB4 ligand expression and function, against the background of the inhibitory tumour microenvironment or dysregulated tolerogenic systems. Indeed a small number of studies have recently been published investigating LILRB4 expression and function in such settings (Cortesini J Pancreas 2007, Suciu-Foca JI 2007).

Despite the failure of the LILRB4 tetramer to stain transformed cell lines, these studies, which focussed on freshly isolated *ex vivo* human PBMC populations, suggested testable hypotheses regarding the identity of the LILRB4 ligand. In particular, the broad expression of LILRB4 ligand or ligands on different cellular subsets, combined with the well-established role of LILRB4 in tolerance induction and the upregulation of the putative ligand upon cellular activation, suggested that members of the B7 and CD28 families of immune costimulatory proteins were worthy of investigation as candidate ligands, a concept addressed in subsequent sections of this chapter.

3.3 Surface Plasmon Resonance Studies of Potential LILRB4 Ligands

3.3.1 Introduction

As discussed in my Introduction (Chapter 1 Section 1.2.2), LILRB4 has a well-documented role in the induction of tolerance to self-antigens, particularly in the induction of T cell tolerance and has been shown to be crucial for the generation of $CD4^+$ $CD25^+$ $FoxP3^+$ T regulatory cells upon its upregulation on the surface of tolerogenic DCs or transfection into model APCs *in vitro*. The paper of Kim-Schulze et al. (Kim-Schulze et al. JI 2006) showed that recombinant LILRB4-Fc or KG1 cells transfected with a cytoplasmic domain-truncated LILRB4 expression construct could also mediate the induction of tolerance in T cells despite the absence of the LILRB4 ITIM signalling motifs, suggesting that the ligand for LILRB4 is capable of bidirectional signalling both into the T cell and – through LILRB4 engagement – into the APC.

In this study I replicated previous findings which established that the ligand for LILRB4 is upregulated upon T cell activation but also presented new evidence that the ligand is more widely expressed than was previously thought. These cell staining experiments in addition to the work of Chang et al. and Kim-Schulze et al. suggested potential ligands for further investigation. CTLA-4 is one such candidate ligand, being an inhibitory receptor which is upregulated upon T cell activation and having a known role in tolerance induction and also T regulatory cell effector mechanisms (for a more complete discussion see Chapter 1 and **Figure 1.1**). However, CTLA-4 expression is restricted to T cells and thus does not fit the staining pattern described in the previous section.

CTLA-4 is a member of the CD28 family of costimulatory immunoreceptors, whose counter-structures belong to the B7 family. The canonical interaction between these families is the

positive costimulatory 'second signal' to TCR-pMHC engagement that occurs between CD28 on T cells and B7.1 or B7.2 on APCs. As well as having signalling motifs of its own that signal directly into the T cell, CTLA-4 acts to downregulate T cell responses by disrupting the CD28-B7 interaction as it has a higher affinity for B7 than CD28 thus sterically blocking binding. Members of the CD28 and B7 family are discussed in detail in Section 1.1.4, however for reference see **Table 3.3** and **Table 3.4** (adapted from Greenwald et al. Ann Rev Immunol 2005).

Receptor	Identity	Ligands	Expression *Haematopoietic*	Expression *Other*
B7-1 (CD80)	100%	CD28, CTLA-4, PD-L1	T, DC, B, Mφ	Rare
B7-2 (CD86)	27%	CD28, CTLA-4	T, DC, B, Mφ	Rare
ICOSL (B7-H2)	27%	ICOS	T, DC, B, Mφ	Fibroblast, Endothelial, Epithelial
PD-L1 (B7-H1)	25%	PD-1, B7-1	T, DC, B, Mφ	Endothelial, Tissues, Tumours
PD-L2 (B7-DC)	23%	PD-1	DC, Mφ	Some B cell lymphomas
B7-H3	29%	Unknown	T, DC, B, Mφ, NK	Bone Marrow
B7-H4 (B7x, B7S1)	21%	Unknown	T, DC, B, Mφ	Lung and ovarian Tumours

Table 3.3. B7 family members. Table listing percentage amino acid identity, known ligands, and haematopoietic and other tissue distributions of members of the B7 family of counterstructures for CD28 family receptors. T = T cell, NK = natural killer cell, B = B cell, Mφ = macrophage.

Collectively the CD28 and B7 family members are widely expressed both on haematopoietic and non-haematopoietic cells and are involved in positive and negative costimulation of immune responses. This role in addition to the broad expression pattern of these receptors suggested one possibility for LILRB4 ligand recognition, namely that LILRB4 might bind to

more than one receptor within a family of structurally related receptors. This would fit with the broad staining pattern of the LILRB4 tetramer utilised in this study. I chose to address this idea by directly testing LILRB4 interaction with CD28 and B7 family members using SPR, focussing particularly on those involved in T cell tolerance mechanisms.

Receptor	Identity	Ligands	Signal Motifs	Expression	Function
CD28	100%	B7-1, B7-2	PI3K, PP2A	T	Naive T cell activation, proliferation, IL-2 production, survival
CTLA-4	30%	B7-1, B7-2	PI3K, PP2A, SHP2	T	Inhibition of T cell responses
ICOS	27%	ICOS-L	PI3K	T, NK	Effector T cell function; proliferation; Ig class switching; IL-10, IFN-γ, IL-4 production
PD-1	23%	PD-L1, PD-L2	ITIM, ITSM	T, B, Mφ	Effector T cell functions, proliferation; IL-10, IFN-γ production; CTL apoptosis Inhibition of T cell responses
BTLA	23%	Unknown	2x ITIM	T, B	Inhibition of T and B cell responses

Table 3.4. CD28 family members. Table listing percentage amino acid identity, known signalling motifs in the cytoplasmic domain, cellular subset expression and proposed function of the members of the CD28 family of costimulatory receptors. PI3K = phosphatidyl inositol-3-kinase, PP2A = protein phosphatase 2A, SHP2 = SH2 domain–containing protein tyrosine phosphatase–2, ITIM = immunoreceptor tyrosine-based inhibitory motif, ITSM = immunoreceptor tyrosine-based switch motif.

3.3.2 CD28-Fc and B7-Fc Fusion Proteins as Potential LILRB4 Ligands

SPR was used to detect LILRB4 - ligand interactions and conduct affinity analysis utilising a BIAcore 3000 SPR machine. Two main methods were used to immobilise proteins of interest to CM5 sensor chips, either immobilisation to streptavidin-coated chips or to chips coated with the anti-human-IgG antibody, R10z8e9, for biotinylated or Fc-fusion proteins respectively. Notably, both methods provided orientation of the immobilised ligand, and each has been used extensively to study immune receptor/ligand interactions. For details of the SPR methodology used, see Chapter 2: Materials and Methods.

Recombinant biotinylated LILRB4 ectodomain was produced as previously described (Garner et al. Prot Pur Exp 2006). Recombinant biotinylated LILRA5 ectodomain was produced by S. Nicholls and used as an additional control. Recombinant biotinylated HLA-A2 complex, containing β2m and a peptide derived from Wilms Tumour antigen 1 (WT1, peptide sequence: CYTWNQMNL) had been previously produced in the laboratory and was used as a negative control. In addition one flow cell was left blank (streptavidin only). After activation of the CM5 chip with EDC/NHS and immobilisation of streptavidin to all four flow cell surfaces, recombinant proteins were injected and immobilisation levels matched as closely as possible.

B7 and CD28 family proteins, in the form of commercially available Fc-fusion proteins – CTLA4, PD-1 and its ligands PD-L1 and PD-L2, and ICOS and its ligand ICOS-L – were then injected serially over all four flow cells to test for binding. Fc-fusion proteins were all injected at 100 µg/ml in HBS-EP. Results for the six test injections are shown in **Figures 3.13 – 3.15**.

(a)

FC	Streptavidin	Ligand	Level	Total
1	7835	Blank	N/A	**7835**
2	7719	LILRB4 D1D2	2264	**9983**
3	7308	LILRA5 D1D2	2399	**9707**
4	7074	HLA-A2-WT1	2652	**9726**

(b)

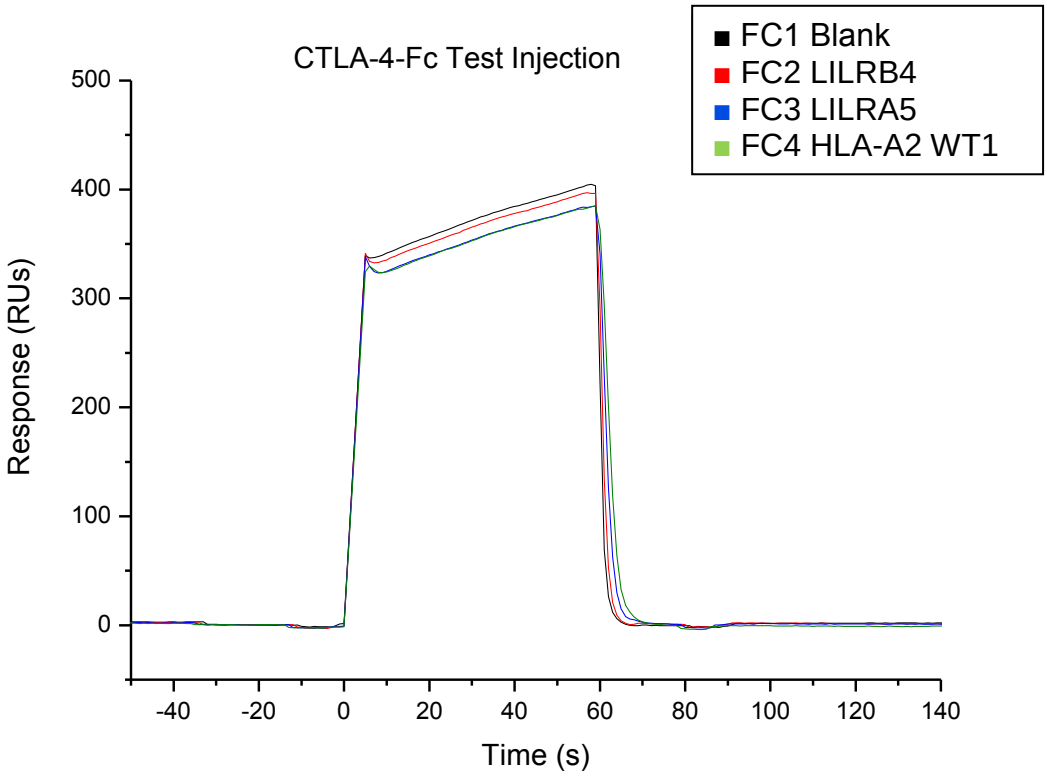

Figure 3.13. Testing interaction of CTLA4-Fc fusion protein with LILRB4 by SPR. (a): Immobilisation levels in Resonance Units (RUs) for streptavidin and proteins under test. Total levels are also shown for each flow cell (FC). (b): CTLA4-Fc fusion protein (100 µg/ml) was injected over flow cells coated with LILRB4 (FC2, red line), LILRA5 (FC3, blue), HLA-A2 (FC4, green), and a blank flow cell (FC1, black).

In **Figure 3.13a**, levels of immobilised streptavidin and proteins are listed for each flow cell and apply to **Figures 3.13 – 3.15**. In **Figure 3.13b**, a SPR sensorgram trace is shown for the test injection of CTLA-4-Fc fusion protein over the LILRB4-coated flow cell (FC2) and over the control flow cells. Time is plotted on the x-axis, where t= 0 is the start of the injection of the analyte. The response (in arbitrary resonance units, RUs) is plotted on the y-axis. Although an increase in signal is seen after the initial spike post-injection, this increase is across all four flow cells. If an interaction of a reasonable affinity was occurring between CTLA-4-Fc and immobilised LILRB4, one would expect to see a higher signal over FC2 than over the control surfaces.

In a similar fashion to the data shown in **Figure 3.13**, **Figure 3.14** shows sensorgram traces for the injection of PD-1 and its ligands over LILRB4 and control surfaces, and **Figure 3.15** shows sensorgram traces for the injection of ICOS and its ligand ICOS-L over the same sensor chip surface. As is the case with CTLA-4-Fc, these proteins showed no evidence of an interaction with LILRB4.

These Fc-fusion reagents are dimeric and would therefore be expected to have an avidity which would allow the detection of binding as visualised by an increase in the response over surface coated with LILRB4 relative to the control surfaces. Assuming a monomeric affinity one could also expect a slow off rate as both molecules in the dimer would need to disengage from the ligand for the dimer to unbind. The total molecular mass of the Fc reagent is considerable, and the immobilisation level for LILRB4 is relatively high and also orientated with the LILRB4 molecule projecting from the streptavidin surface, therefore I would expect to observe a sizeable response and a slow off rate if any of the Fc reagents were a genuine ligand for LILRB4.

(a)

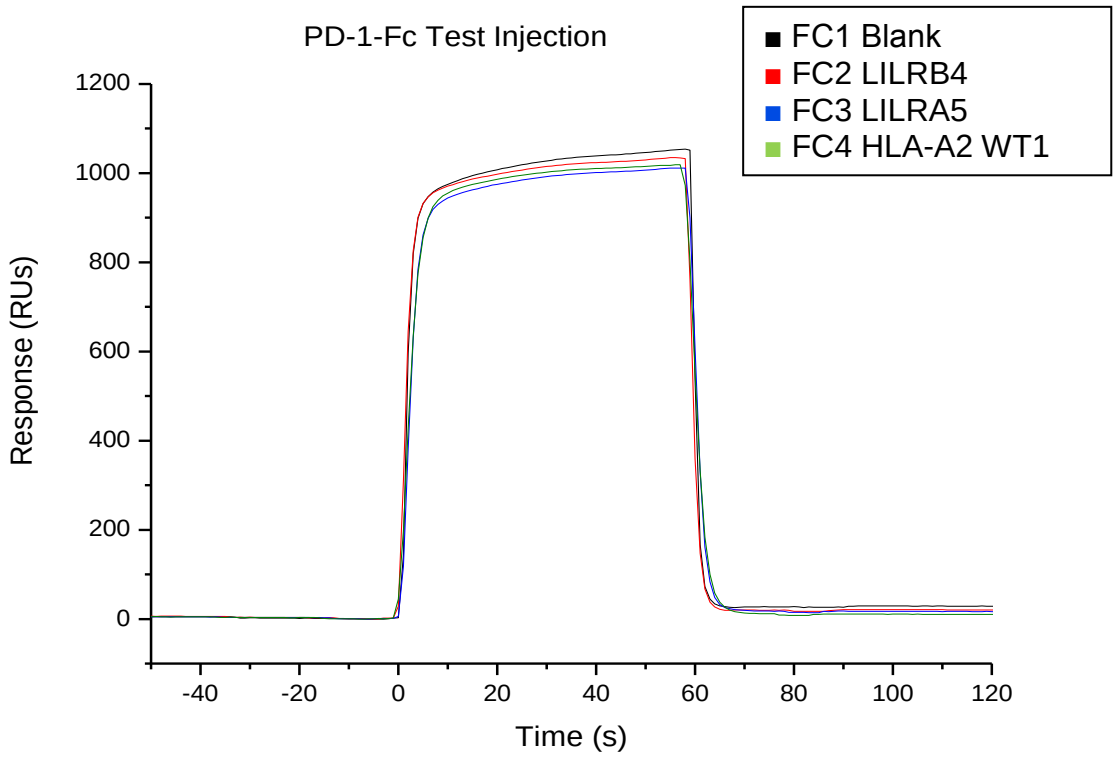

(b)

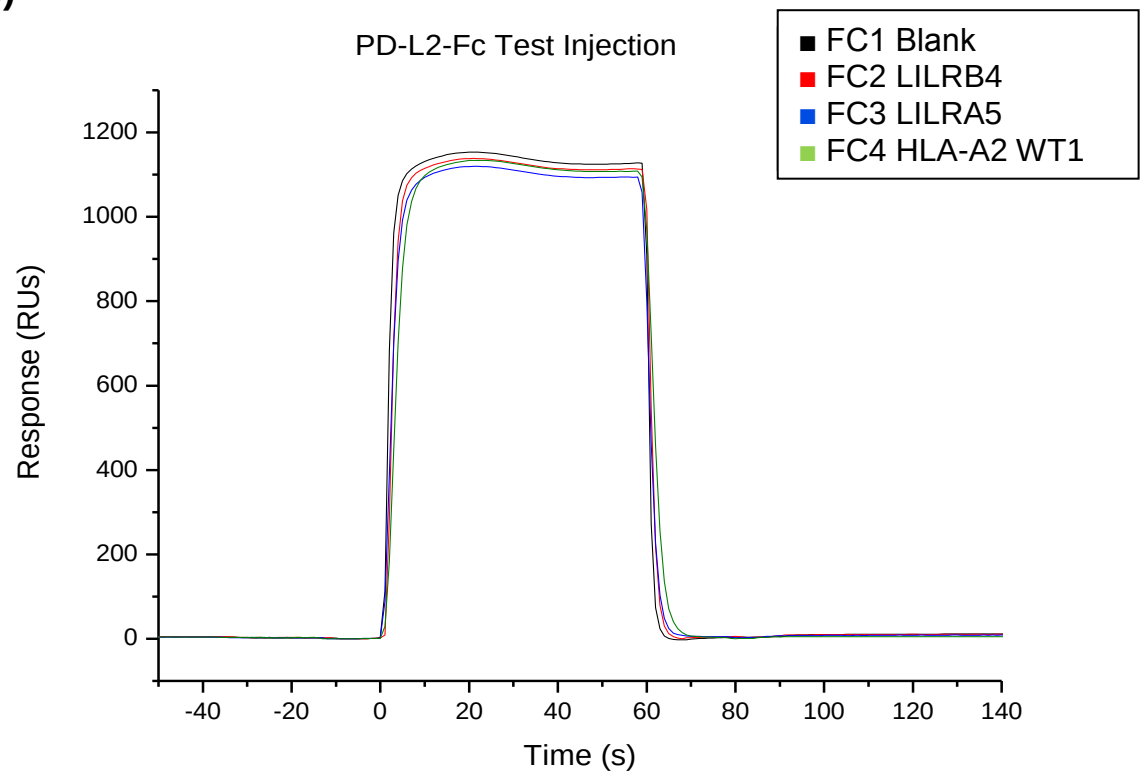

Figure 3.14 *(continued and legend overleaf)*

(c)

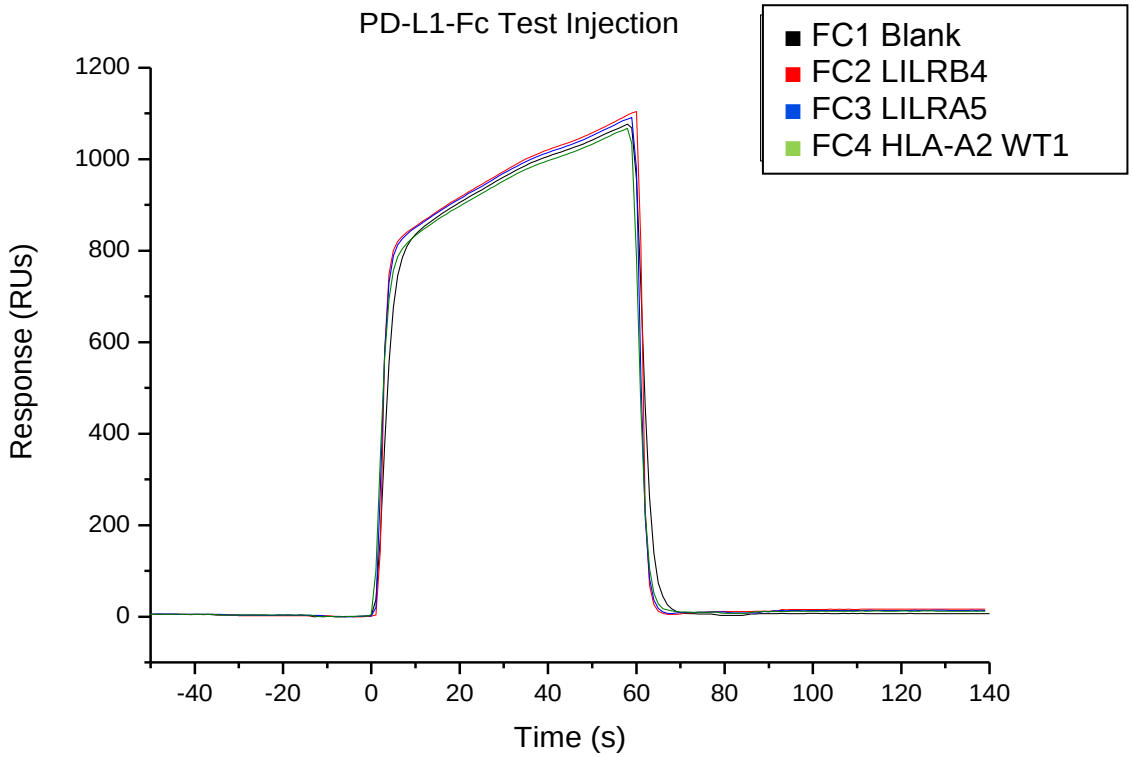

Figure 3.14. Testing interaction of PD-1 and ligands with LILRB4 by SPR. (a): PD1-Fc fusion protein was injected over flow cells coated with LILRB4 (FC2, red line), LILRA5 (FC3, blue), HLA-A2 (FC4, green), and a blank flow cell (FC1, black). (b): PD-L1-Fc test injection. (c): PD-L2-Fc test injection. Immobilisation levels were the same as in Figure 3.13a. All Fc fusion proteins were at a concentration of 100 µg/ml.

(a)

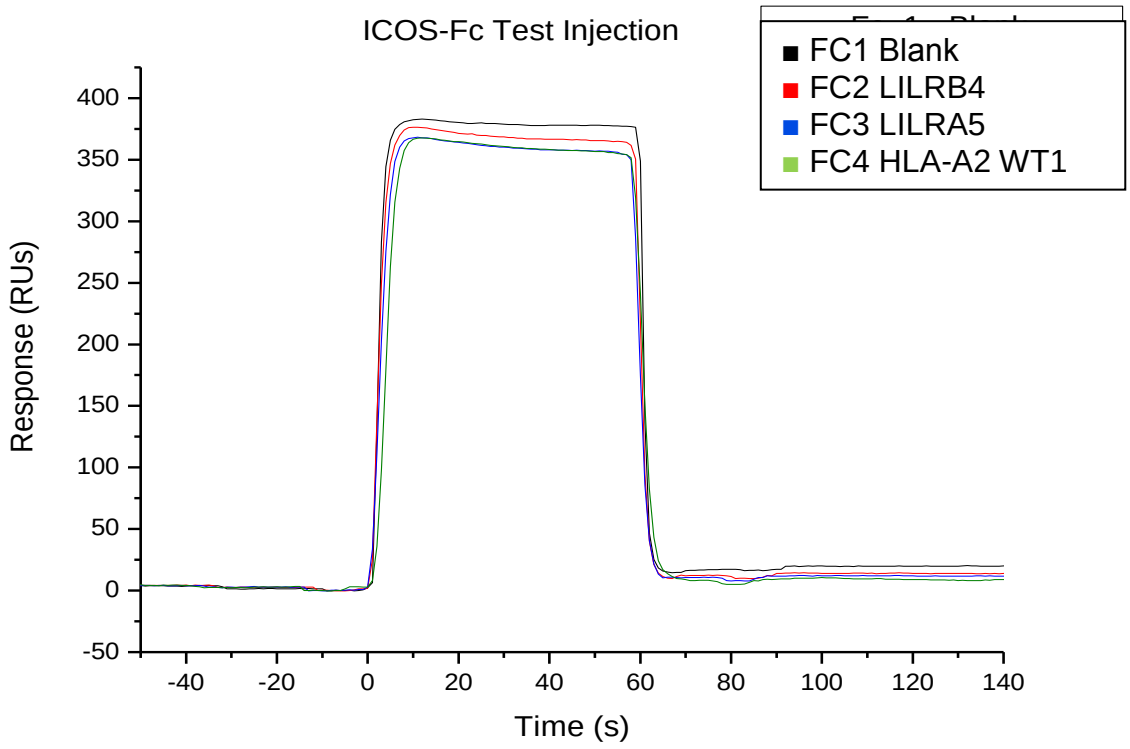

(b)

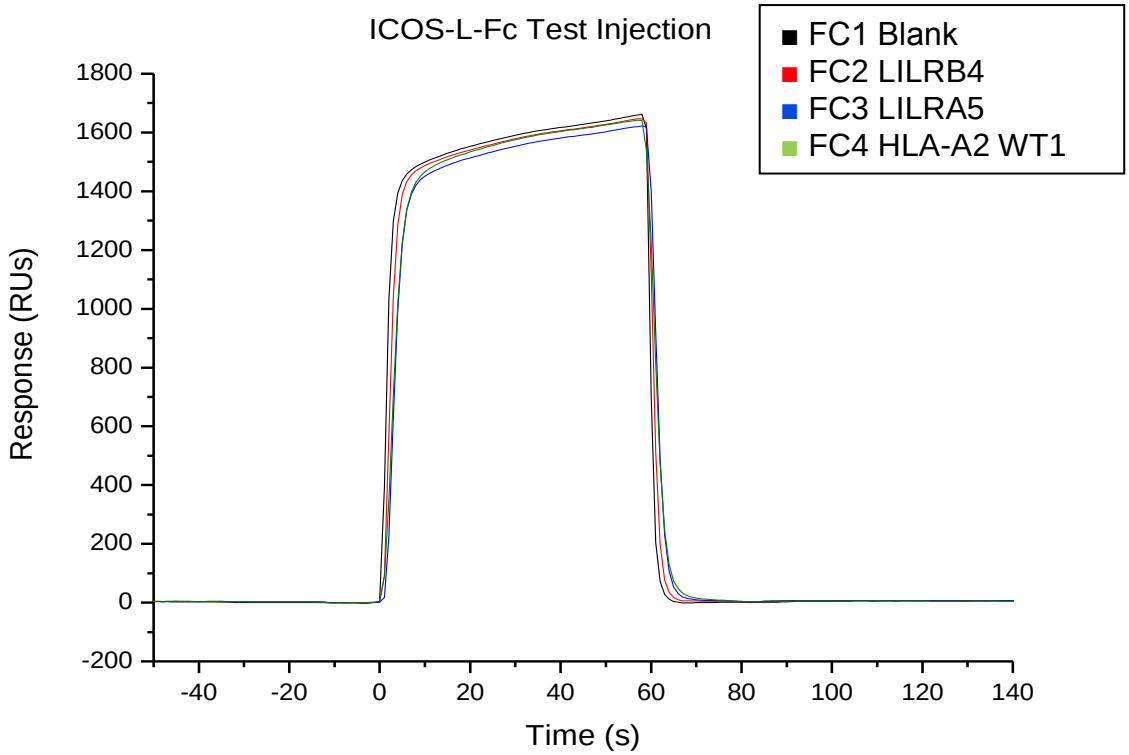

Figure 3.15. Testing interaction of ICOS and ICOS-L with LILRB4 by SPR. (a): ICOS-Fc test injection. (b): ICOS-L-Fc test injection. Flow cells were coated with LILRB4 (FC2, red line), LILRA5 (FC3, blue), HLA-A2 (FC4, green), and one flow cell was left blank (FC1, black). Immobilisation levels were the same as in Figure 3.13a. The Fc fusion proteins were at a concentration of 100 µg/ml.

None of the B7/CD28 family member potential ligands tested bound to the LILRB4 coated flow cell with any convincing signals over the background. Control surfaces (Blank, HLA-A2 and LILRA5) gave practically equivalent signals. PD-1-Fc, PD-L1-Fc and ICOS-Fc showed some degree of non-specific sticking across all flow cells, as evidenced by a failure of the signal to return to pre-injection levels at the end of the injection, but in each case the effects were minimal (< 20 RUs). This sticking could be due to the presence of a low concentration of aggregated protein (although all samples were centrifuged for ten minutes at 13,000 RPM in a bench top centrifuge prior to use). CTLA-4-Fc injection also resulted in a small artefactual buffer signal at the start of the injection. Regardless of these experimental issues, there was no evidence for binding to LILRB4 (or indeed LILRA5) by any of the B7 family members tested.

3.3.3 Investigation of LAIR-1 as a Potential LILRB4 Ligand

An alternative to the hypothesis that the staining pattern of LILRB4 tetramer represented a composite pattern resulting from interactions with multiple ligands was the possibility that it represented interactions with a single, widely expressed ligand. One such candidate ligand was Leukocyte-Associated Ig-like Receptor-1, LAIR-1. LAIR-1 is a widely expressed inhibitory receptor that is known to bind collagen on the surface of target cells (Meyaard et al. Immunity 1997, Meyaard et al. JI 1999, Lebbink et al. JEM 2006). This possibility was highlighted to me by Professor Neil Barclay and Dr Lei Jiang (based at the Sir William Dunn School of Pathology, University of Oxford), who proposed a direct interaction between LILRB4 and LAIR-1. However, analysis of their preliminary results did not provide particularly strong evidence for the interaction, as the response was very low (tens of RUs)

and immobilisation levels were not adequately controlled, with differing levels of protein immobilised on each flow cell (data not shown).

To test the possibility that LILRB4 did recognise LAIR-1, I was provided (by Professor Barclay and Dr. Jiang) with recombinant human LAIR-1 fusion protein (hLAIR-1 ectodomain fused to Rat CD4 domains 3 and 4 as a linker, incorporating a C-terminal biotinylation tag) either biotinylated for streptavidin immobilisation, or non-biotinylated for antibody-mediated coupling to the sensor chip via OX68 (mouse anti-Rat-CD4-domains 3 and 4 antibody). The aim was to attempt to reproduce the initial results but instead utilising our recombinant soluble LILRB4 ectodomain (the Oxford group used LILRB4 - Rat CD4d3d4 chimeric protein) at higher concentrations and with adequately controlled immobilisation levels for controls (P. Anton van der Merwe, 'Protein-ligand Interactions: Hydrodynamics and Calorimetry. Practical Approach series'. Chapter 6: Surface Plasmon Resonance. Oxford University Press, 2001).

The results for this experiment are shown in **Figure 3.16**. Streptavidin immobilisation was conducted by standard amine-coupling as previously described and then test proteins – HLA-A2-WT11 and hLAIR-1-CD4d3d4 at two immobilisation levels – were injected into separate flow cells. Immobilisation levels for this experiment are listed in **Figure 3.16a**. LILRB4 (either D1D2 or D1 domain) was injected over the four flow cells to assess binding.

As can be seen from the sensorgrams in **Figures 3.16b-d**, injection of LILRB4 over immobilised LAIR-1 provided no evidence for specific binding, even at the high concentration of LILRB4 attainable in Na citrate buffer. As expected buffer signals from this analyte were higher and there was some evidence for sticking of analyte aggregates to

(a)

FC	Streptavidin	Ligand	Level	Total
1	3574	Blank	N/A	**3574**
2	3423	HLA-A2-WT1	1771	**5194**
3	3326	hLAIR1-CD4d3d4	1878	**5204**
4	3303	hLAIR1-CD4d3d4	4125	**7428**

(b)

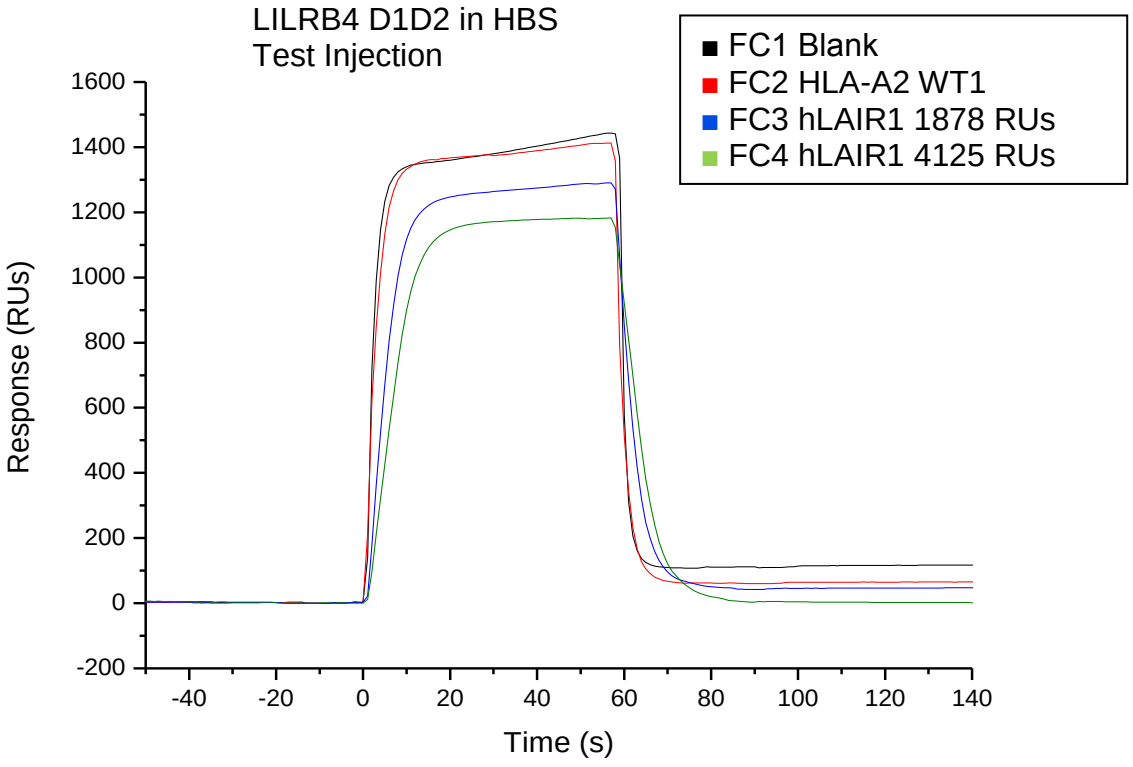

Figure 3.16 *(continued and legend overleaf)*

(c)

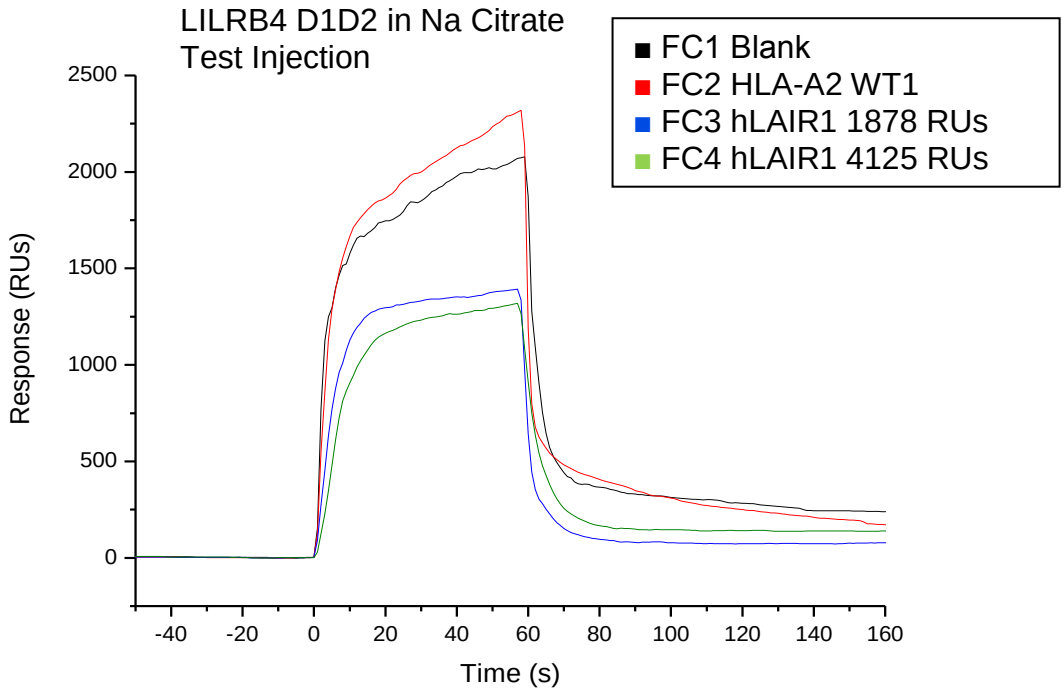

(d)

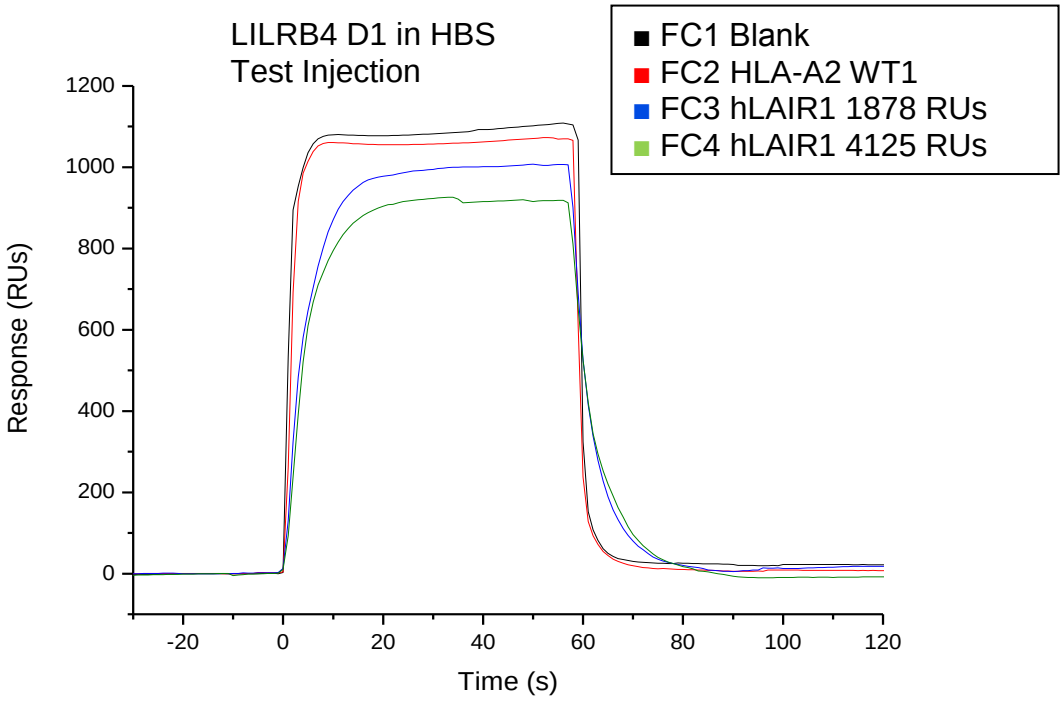

Figure 3.16. Testing interaction of human LAIR-1 with LILRB4 by SPR. (a): Immobilisation levels in Resonance units (RUs) for streptavidin and proteins under test. Flow cells were coated with HLA-A2 (FC2, red line), two different levels of hLAIR-1 (FC3, blue and FC4, green), and one flow cell was left blank (FC1, black). (b): Test injection of LILRB4 D1D2 at 307 μM in HBS-EP buffer. (c): Test injection of LILRB4 D1D2 at 506 μM in Na citrate buffer. (d): Test injection of LILRB4 D1 at 746 μM in Na citrate buffer.

surfaces as evidenced by the slow return to pre-injection levels of response at the end of the injection. The single distal domain of LILRB4 (LILRB4 D1, produced as described in Chapter 4) also gave no specific binding to hLAIR-1 (Figure **3.16d**). In each case, signals across the hLAIR-1-coated flow cells were actually lower than across control flow cells (Streptavidin-coated alone and also streptavidin-coupled HLA-A2). Although I cannot exclude the possibility of an extremely weak interaction with LAIR-1, these data provide no evidence of interaction. One noticeable feature of all three experiments was that LILRB4 injection led to a somewhat greater response over FC3 than FC4, even though FC4 had substantially more LAIR-1 immobilised. However, it is possible to rationalise the difference in signal between FC3 and FC4 in terms of the total level of protein immobilised on each flow cell, as, in the absence of differential binding of the analyte, analyte injections over flow cells with greater levels of immobilised protein are known to yield marginally lower response signals than over those with less protein immobilised, due to greater proximity of analyte to the sensor surface (P. Anton van der Merwe, 'Protein-ligand Interactions: Hydrodynamics and Calorimetry. Practical Approach series'. Chapter 6: Surface Plasmon Resonance. Oxford University Press, 2001). Such differences would be expected to be overcome in the presence of a *bone fide* interaction, with FC4 yielding substantially higher responses. The fact this was not observed provided further indication that no interaction is evident. Furthermore, the control flow cell (FC2, HLA-A2) is very well controlled in terms of total protein immobilisation level when compared to the test flow cell (FC3, hLAIR-1) – 5194 RUs cf. 5204 RUs, however in each case, signals over FC2 are marginally higher than FC3, again indicative of lack of interaction at these concentrations of LILRB4.

To exclude the possibility that streptavidin-biotin immobilisation of LAIR-1 prevented interaction with LILRB4, I repeated this experiment using an alternative immobilisation

method. For this alternative method, the mouse anti-Rat-CD4-domains 3 and 4-antibody, OX68, was amine-coupled to a fresh sensor chip and used to coat a single flow cell (FC2) with hLAIR-1-CD4d3d4. As a negative control, OX68 antibody alone was coupled to FC1. The rationale for this experiment was that the increased distance provided by the OX68 antibody between the surface and the hLAIR-1 domain might reduce any steric hindrance that could occur by direct streptavidin coupling of biotinylated hLAIR-1-CD4d3d4 to the surface. SPR sensorgram traces for the three test injections are shown in **Figure 3.17**, with immobilisation levels for these experiments listed in **Figure 3.17a**. As for the previous experiment, the analytes tested were LILRB4 D1D2 in HBS-EP buffer, LILRB4 D1D2 at higher concentration in Na Citrate buffer, and LILRB4 D1 in Na Citrate buffer.

Signals across the hLAIR-1-OX68 coated surface were slightly but consistently lower than across the control surface (OX68 antibody alone), consistent with the higher level of immobilised protein. Although test and control surfaces would ideally have been matched for total protein, this experiment provides no evidence for LILRB4/LAIR-1 interaction, confirming the results of previous experiments using biotinylated hLAIR-1 immobilised via streptavidin.

3.3.4 Investigating Potential Homotypic Interaction of LILRB4

Additional communications from Dr. Jiang suggested a weak homotypic interaction between LILRB4 in solution and immobilised LILRB4 (albeit chimeric LILRB4-CD4d3d4). To test this a third experiment was conducted, involving immobilisation of biotinylated LILRB4 D1D2 and control HLA-A2 WT1 onto separate streptavidin-coated flow cells. In addition, one flow cell was left blank as an extra negative control, and a final flow cell was coated with hLAIR-1, providing an additional opportunity to confirm previous results that failed to detect

(a)

FC	OX68 Ab.	Ligand	Level	Total
1	6846	Blank	N/A	**6846**
2	6799	hLAIR1-CD4d3d4	1360	**8159**

(b)

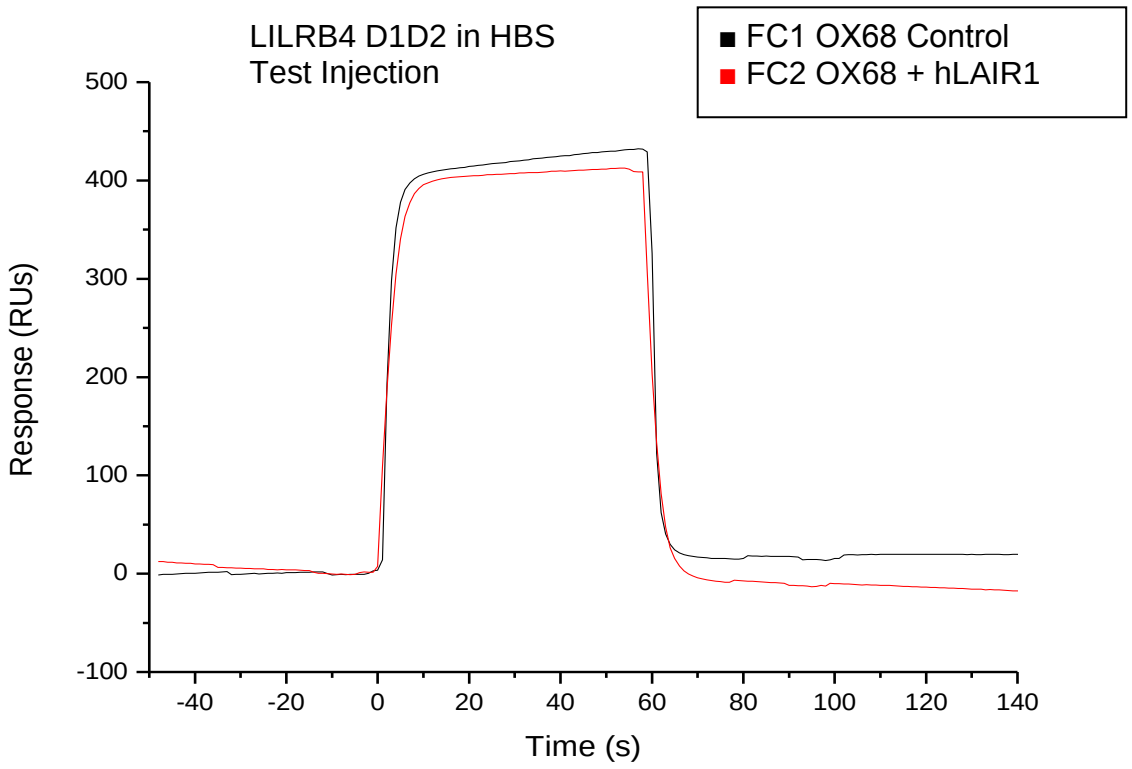

Figure 3.17 *(continued and legend overleaf)*

(c)

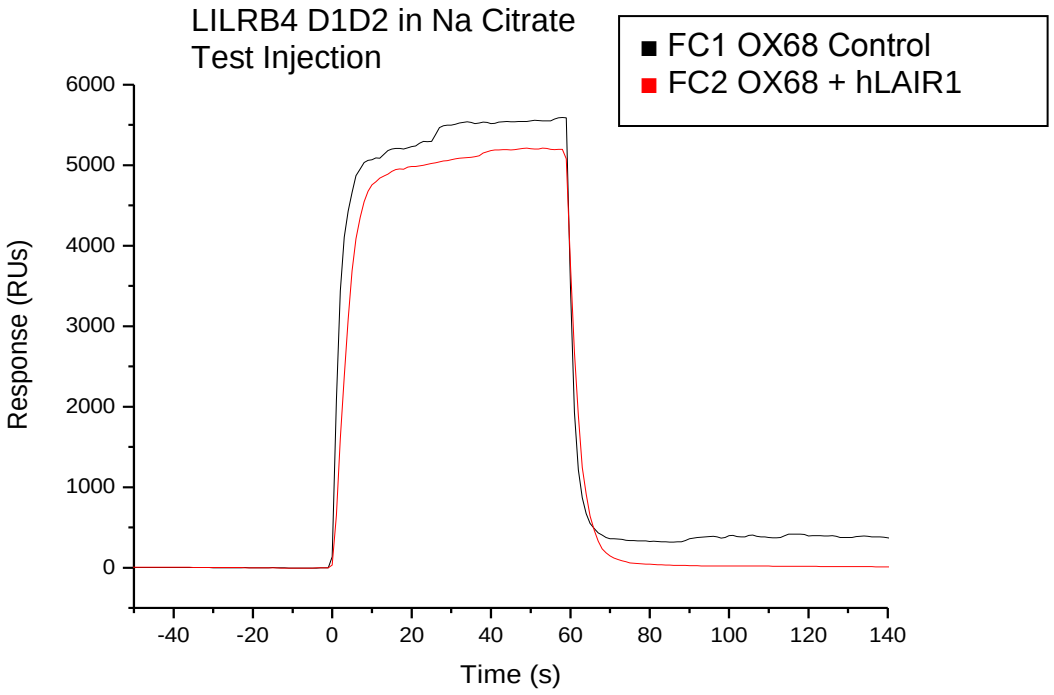

(d)

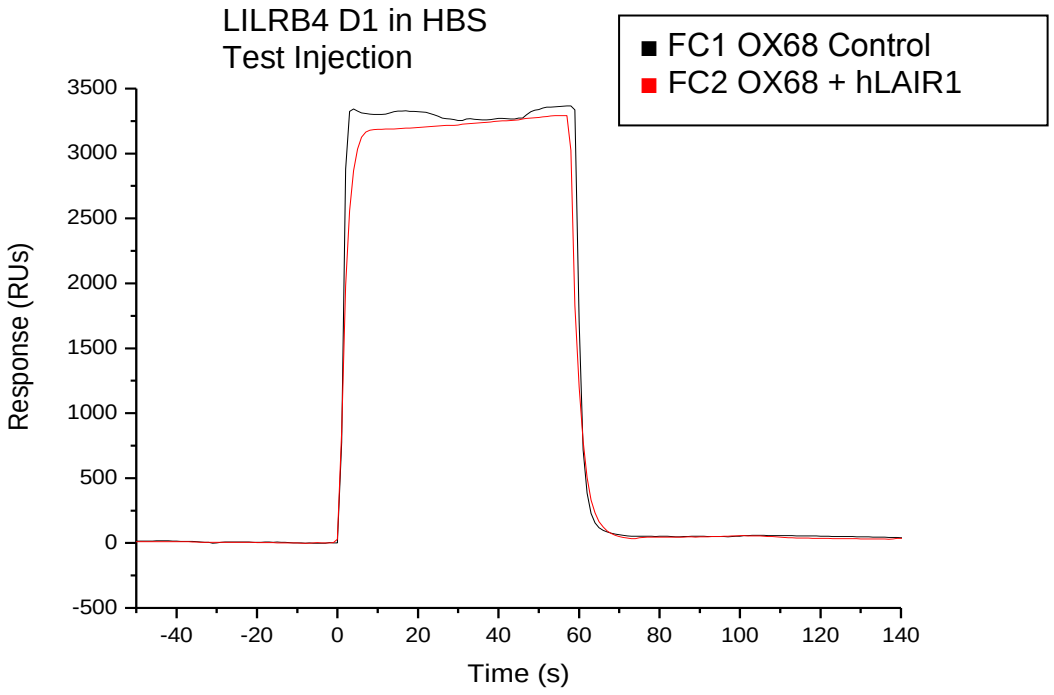

Figure 3.17. Testing interaction of LILRB4 with hLAIR-1 immobilised via OX68 antibody. (a): Immobilisation levels in Resonance units (RUs) for OX68 and hLAIR-1. Flow cells were coated with OX68 alone as a control (FC1, black line) or OX68 plus hLAIR-1 (FC2, red line). (b): Test injection of LILRB4 D1D2 at 307 μM in HBS-EP buffer. (c): Test injection of LILRB4 D1D2 at 506 μM in Na citrate buffer. (d): Test injection of LILRB4 D1 at 746 μM in HBS-EP buffer.

LILRB4/LAIR-1 interaction. The results are shown in **Figure 3.18**. LILRB4 D1D2 at a concentration of 179 μM in HBS-EP buffer was injected over all four flow cells at a flow rate of 10 μl/min. The injection was curtailed to 5 μl (30 s contact time) to minimise aggregation. As a positive control for binding, LILRB1 D1D2 was also injected over all four flow cells at a concentration of 135 μM in HBS-EP buffer.

As in the previous experiments, there was no evidence for LILRB4 D1D2 binding to hLAIR-1. However, there was some evidence for homotypic adhesion between soluble LILRB4 and immobilised LILRB4, with a specific binding response approximately 400 RUs above the streptavidin blank control (**Figure 3.18b**). However, these results should be interpreted cautiously since there were two indications of non-specific binding. Firstly there was a weak signal across the HLA-A2 control surface (FC2), and secondly, the relatively slow association and dissociation phases were suggestive of aggregate binding. Consistent with this, LILRB4 shows a high propensity to aggregate in solution, particularly in a non-optimised buffer system (Garner et al. Prot Exp Pur 2006 and unpublished observations). In comparison, injection of LILRB1 D1D2 resulted in a very clear specific binding response of approximately 600 RUs across the HLA-A2 coated flow cell, and a relatively fast association and dissociation phase (**Figure 3.18c**).

Although it was uncertain if this interaction was physiologically relevant, the experimental system theoretically allowed an affinity of the postulated LILRB4/LILRB4 homotypic interaction to be determined by equilibrium affinity analysis. Assuming that the LILRB4/LILRB4 interaction obeyed simple Michaelis-Menten kinetics and the Langmuir (1:1 stoichiometry) binding model, the dissociation constant, K_d, could be calculated by non linear curve fitting to the saturation binding plot. The Michaelis-Menten equation is used to

(a)

FC	Streptavidin	Ligand	Level	Total
1	2083	Blank	N/A	**2083**
2	1872	HLA-A2-WT1	1688	**3560**
3	1660	LILRB4 D1D2	1795	**3455**
4	1524	hLAIR1-CD4d3d4	1957	**3481**

(b)

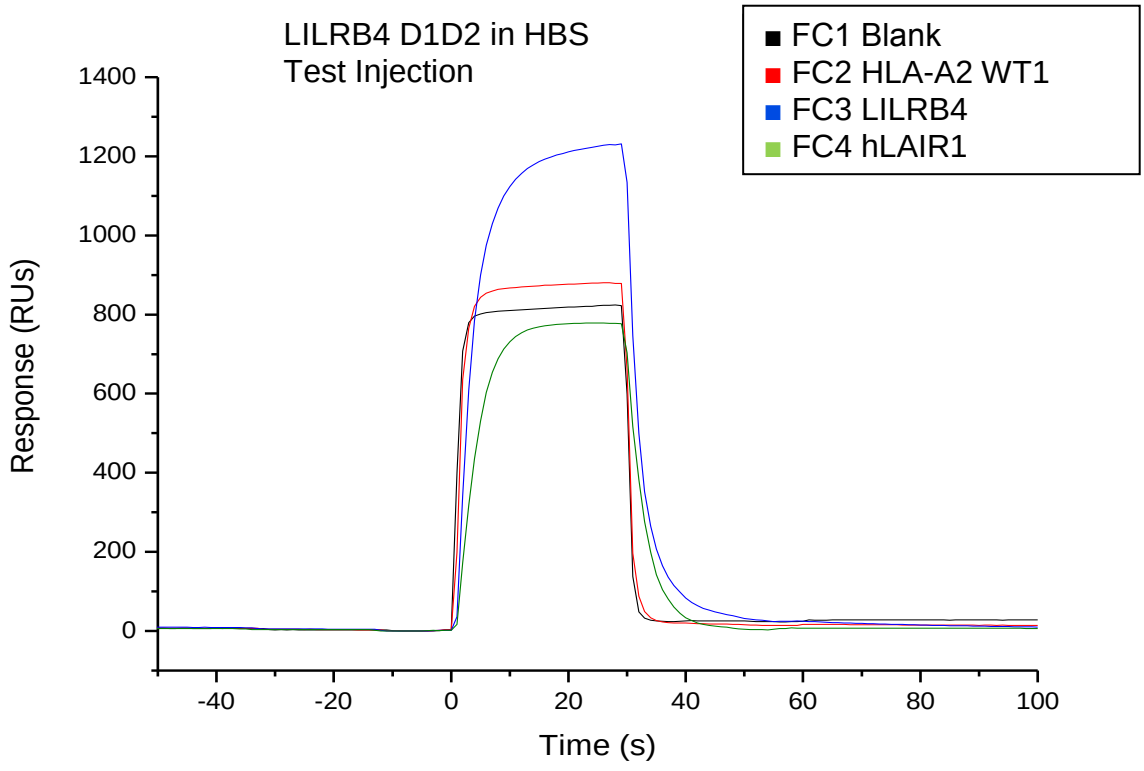

Figure 3.18 *(continued and legend overleaf)*

(c)

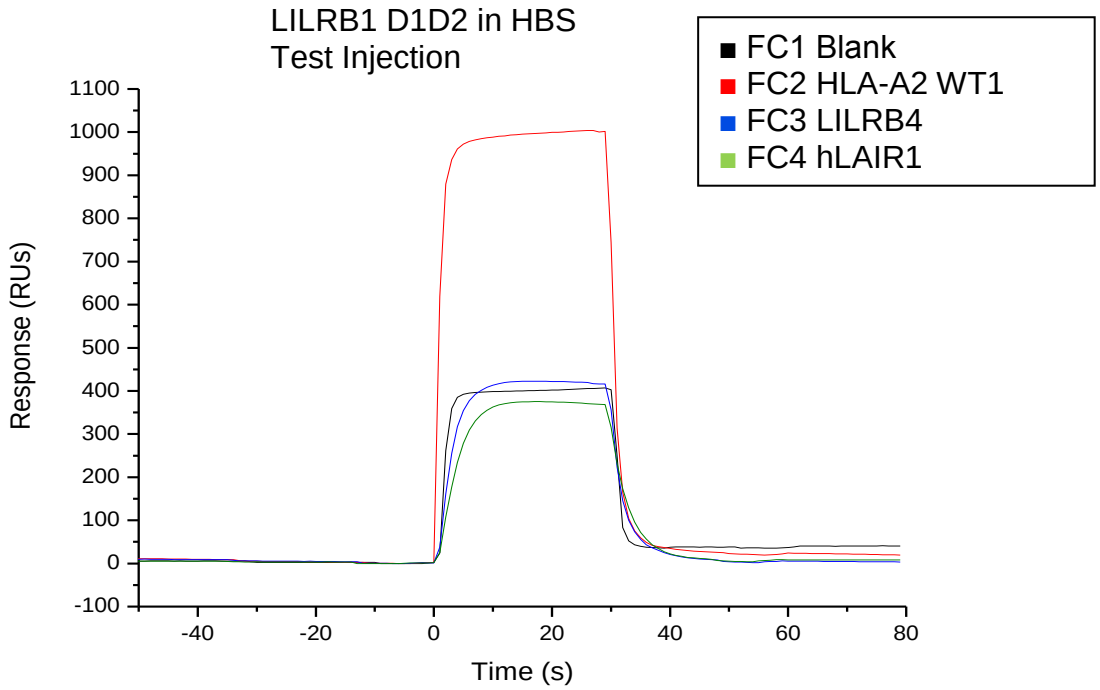

Figure 3.18. Investigating potential LILRB4 homotypic interaction by SPR. (a): Immobilisation levels in Resonance units (RUs) for streptavidin plus flow cells coated with HLA-A2 (FC2, red line), LILRB4 (FC3, blue), hLAIR1-CD4d3d4 (FC4, green), and a blank flow cell (FC1, black). (b) Test injection of LILRB4 D1D2 at 179 μM in HBS-EP buffer. (c): Test injection of LILRB1 D1D2 at 135 μM in HBS-EP buffer showing positive control binding to HLA-A2.

define a hyperbola which predicts the maximum binding response (P1) and the affinity of the interaction (P2, equivalent to the concentration of analyte at half maximal binding). In principle, Scatchard analysis could also be carried out; a plot of Bound *vs.* Bound/Free allows calculation of a line of best fit, the negative reciprocal of the slope of which is equal to the dissociation constant of the interaction (slope = $-1/K_d$).

An experiment was conducted to measure the K_d for LILRB4/LILRB4 binding. Amine-coupled streptavidin was used to coat flow cells with biotinylated HLA-A2 WT1, LILRB4 D1D2, or hLAIR-1, and LILRB4 was subsequently injected over all four surfaces. The results are shown in **Figure 3.19**; **Figure 3.19a** tabulates the immobilisation levels and the serial injections of LILRB4 are shown in **Figure 3.19b**. The equilibrium binding response curve is shown in **Figure 3.19c**. From this curve it can be seen that there is a failure to reach saturation of binding as the concentration of LILRB4 is increased. Scatchard analysis of the results, as shown in **Figure 3.19d**, also proved impossible due to the high number of data points that would have to be discarded in order to draw a line of best fit. I was therefore unable to calculate an affinity for the proposed LILRB4/LILRB4 homotypic interaction.

This failure may be due to the assumption of an incorrect binding model. The proposed analysis discussed above assumes that the Langmuir 1:1 binding model is obeyed for the molecule analysed in solution binding to the immobilised ligand; however, as the hypothesis tested here is that LILRB4 interacts with itself, it follows that some of the LILRB4 in solution will interact with other LILRB4 molecules in solution, preventing binding to surface-immobilised LILRB4. This effect would lead to a relative decrease in the propensity for LILRB4 in solution to interact with immobilised LILRB4 as the concentration of LILRB4 in solution increases, which could conceivably prevent saturation of the response as a function

of increasing LILRB4 concentration, a hypothesis supported by the result shown in **Figure 3.19c**.

(a)

FC	Streptavidin	Ligand	Level	Total
1	2587	Blank	N/A	**2587**
2	2248	HLA-A2-WT1	2764	**5012**
3	2020	LILRB4 D1D2	3053	**5073**
4	1874	hLAIR1-CD4d3d4	2861	**4735**

(b)

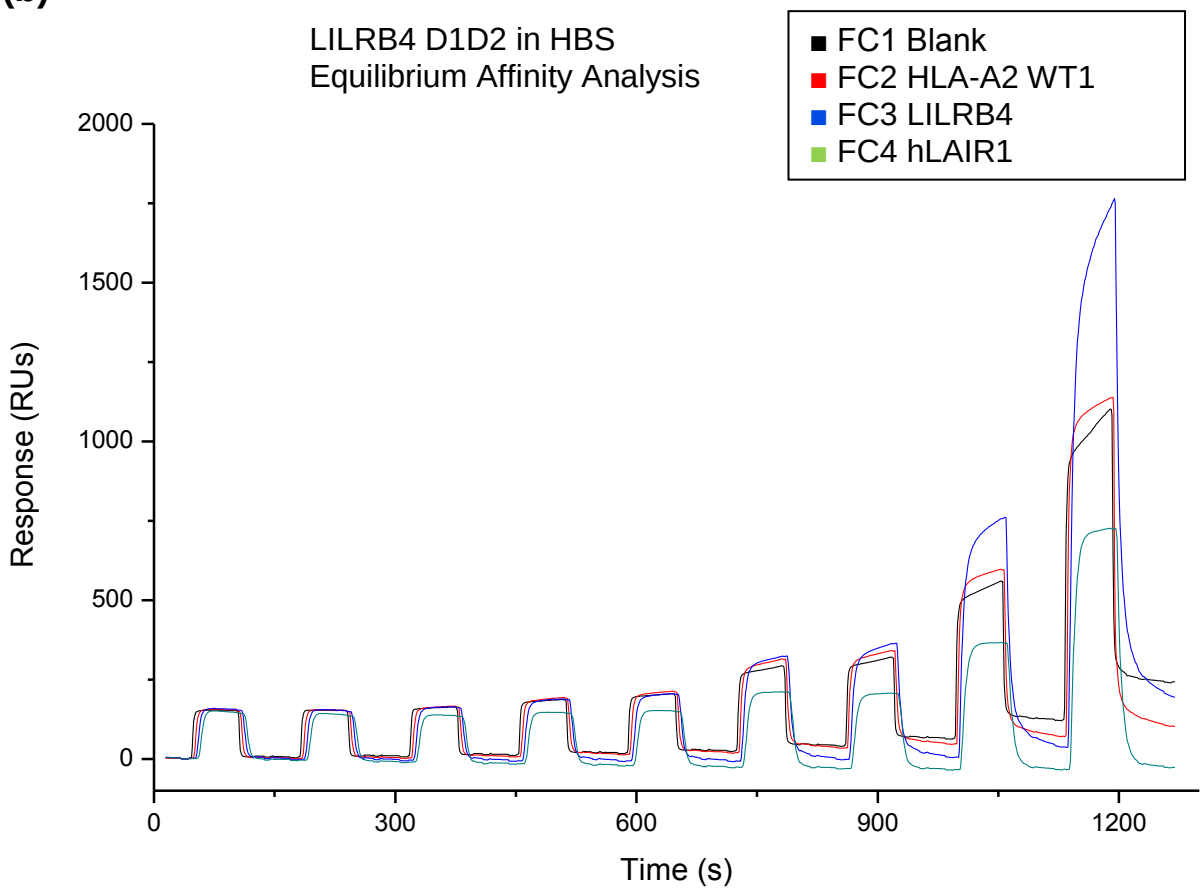

Figure 3.19 *(continued and legend overleaf)*

(c)

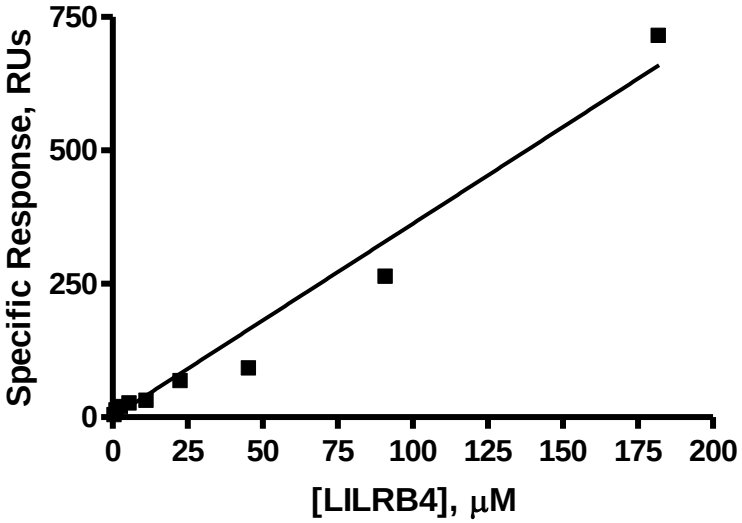

(d)

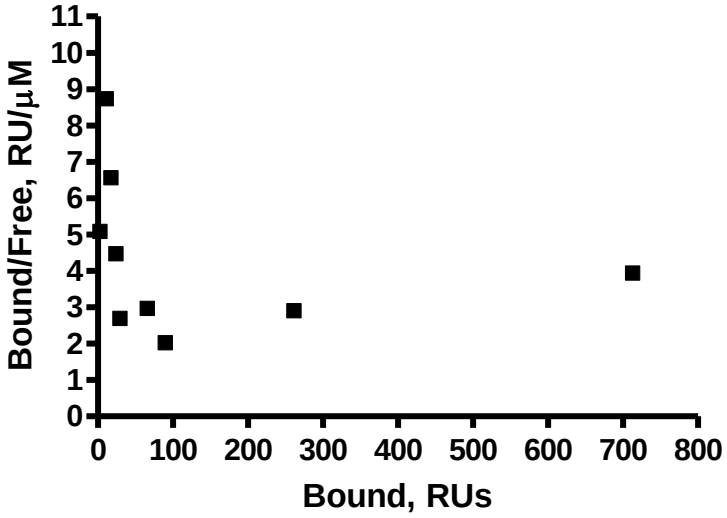

Figure 3.19. Equilibrium affinity analysis of LILRB4 homotypic interaction. (a): Immobilisation levels in Resonance units (RUs) for each flow cell (FC). (b): Equilibrium affinity analysis. LILRB4 D1D2 was injected serially over all four flow cells in HBS-EP at a concentration of 364 μM and nine 2-fold serial dilutions thereof. For each injection, once the association phase was complete, equilibrium responses were recorded. (c): Saturation binding plot of the soluble LILRB4 analyte concentration plotted against the specific response (i.e. with the response from the control blank flow cell subtracted) from the LILRB4 coated flow cell. A non-linear curve fit is shown. (d): Attempted Scatchard analysis of LILRB4 - LILRB4 affinity data.

3.4 Chapter Summary and Discussion

In this chapter, I have presented data to show the cell surface expression pattern of the LILRB4 ligand in freshly isolated human PBMCs. The expression pattern of the putative ligand(s) appears to be relatively broad, as it is present on a variety of cell types, including T cells, B cells and monocytes, with low expression on T cells, intermediate expression on B cells and high expression on monocytes. Expression on both $CD4^+$ and $CD8^+$ T cells can be upregulated upon polyclonal activation with the mitogen, PHA. This potentially composite staining pattern led me to investigate members of the B7 and CD28 family of costimulatory receptors as potential ligands for LILRB4, utilising recombinant LILRB4 and commercially available B7 and CD28 family Fc fusion proteins in a SPR based assay. I focussed upon those members of the B7:CD28 family that are postulated to have critical roles in tolerance and negative regulation of immune response, namely CTLA-4, PD-1 and its ligands PD-L1 and PD-L2, and the inducible costimulator ICOS and its ligand ICOS-L.

CTLA-4 provides inhibitory signals to T cells, curtailing immune responses and limiting autoimmune damage (Brunet et al. Nature 1987, Waterhouse et al. Science 1995). CTLA-4 is thought to function in tolerance induction by Tregs (Wing et al. Science 2008), and thus might be proposed to be a candidate for engagement by LILRB4 and subsequent delivery of the bidirectional inhibitory signal as described earlier (Kim-Schulze et al. JI 2006). CTLA-4 is primarily expressed intracellularly and its surface expression is weak and restricted to the immunological synapse upon T cell activation (Egen et al. Immunity 2002), which is compatible with the upregulation of LILRB4 tetramer staining to T cells upon activation by PHA, as described here in Section 3.2.3. However, CTLA-4 expression is restricted to T cells, which does not fit with the LILRB4 tetramer staining of monocytes and B cells described in Section 3.2.2, unless LILRB4 is capable of recognising more than one ligand.

This hypothesis would explain the widespread distribution of staining to multiple PBMC subsets i.e. a composite staining pattern based upon binding to multiple proteins that interact with LILRB4.

PD-1 is more broadly expressed than CTLA-4. It is upregulated upon B and T cell activation and acts to inhibit signalling downstream of antigen receptor ligation, and its expression on monocytes and DCs could be postulated to contribute to tolerance through the regulation of myelomonocytic maturation and/or antigen presentation function (Agata et al. Int Immun 1996, and for review see Keir Ann Rev Immun 2008).

PD-1 binds to its ligands, PD-L1 and PD-L2. PD-L1 is expressed on non-haematopoietic cells and can be upregulated on T cells, B cells and myeloid cells by interferon treatment. PD-L2 expression can be induced on APCs such as mast cells, macrophages and DCs. There is evidence for bidirectional signalling through PD-1/PD-L interactions, with potentially tolerogenic outcomes (Kuipers et al. EJI 2006, Dong et al. JCI 2003, Nguyen et al. JEM 2002), which is suggestive of the functional effects of LILRB4 engagement (Chang et al. Nat Immunol 2002, Kim-Schulze et al. JI 2006), and the extensive expression of the PD-1 family members on multiple PBMC subsets is in keeping with the pattern of LILRB4 tetramer staining (see Section 3.2.2), although it is worth noting that the hypothesis that PD-L1 is a ligand for LILRB4 was not supported by my cell-line staining data, which included some non-haematopoietic cells (Section 3.2.6 and see **Table 3.2**).

ICOS, in a similar fashion to CTLA-4 and PD-1, is upregulated on T cells after activation (Coyle et al. Immunity 2000). ICOS is also expressed on activated NK cells. ICOSL is

expressed in many tissues and cell types (endothelial/ epithelial cells, B cells, DCs, macrophages, some T cells) and ICOSL engagement has been proposed to be involved in tolerance induction through IL-10 mediated mechanisms (Tuettenberg et al. JI 2009). These reported findings are compatible with ICOSL being a potential ligand for LILRB4 and are also supported by my cell staining experiments.

The expression patterns and functional roles of these receptors suggested them as potential LILRB4 ligands i.e. widely expressed, upregulated upon activation and involved in the generation of T cells with suppressive phenotype upon interaction with tolerogenic DCs or regulatory T cells. However, there was no evidence from my SPR binding studies for any interaction of these receptors with LILRB4, utilising commercially available Fc-fusion proteins. It is possible that there could be an interaction of low affinity below the threshold detectable using this methodology, however I consider it unlikely that such an interaction would be functionally relevant unless the avidity of the interaction is substantially increased by multimerisation of either LILRB4 or the target ligand (possibly by sequestration within lipid microdomains or within the immunological synapse, thus increasing the local concentrations of the receptors). Nevertheless these data are useful in provisionally eliminating LILRB4 binding partners. Although I did not test any such interactions, it could be possible that LILRB4 might provide tolerogenic signals to T cells by disrupting binding to a positively costimulatory ligand or receptor (e.g. CD28, B7-1, B7-2).

I also attempted to generate data in support of a hypothesis that LAIR-1 binds to LILRB4, as proposed by Neil Barclay's group. LAIR-1 was first identified by Meyaard et al. in 1997 as a cell-surface Ig-family receptor with two cytoplasmic ITIM motifs widely expressed on PBMCs, including T cells, B cells, monocytes and NK cells. The LAIR-1 gene is present

within the LRC and shows close homology with the LILRs (32 %). Using a redirected killing assay, this group showed that LAIR-1 cross-linking on human NK cells inhibits target cell lysis by resting and activated NK cells and also subsequently showed inhibitory effects upon cytotoxic T cells and B cells (Meyaard et al. Immunity 1997, Meyaard et al. JI 1999, van der Vuurst de Vries EJI 1999). LAIR-1 is thought to have a constitutive negative signalling role through association with SHP-1 (Sathish et al. JI 2001). There is evidence that surface expression of LAIR-1 is upregulated upon TCR ligation (Maasho et al. Mol Immun 2005).

My data shows no evidence of an interaction between LILRB4 and LAIR-1 by SPR analysis, even at high concentrations of LILRB4 and utilising soluble LILRB4 ectodomain rather than a LILRB4-Rat CD4 fusion protein, and also utilising two different immobilisation methods (antibody coupling and streptavidin-biotin immobilisation). The initial data from the Barclay group were unconvincing and also poorly controlled in terms of protein immobilisation levels between control and experimental flow cells, and during my experiments I ensured protein immobilisation levels were more closely matched to avoid experimental artefacts. Despite this there was no suggestion from my data that LILRB4 binds to LAIR-1.

Although LAIR-1 could be considered to be a good candidate ligand on the basis of its functional role in dampening immune responses and also its widespread expression pattern, it is worth noting that flow cytometric analysis of the level of expression on PBMCs first presented by the Meyaard group (Meyaard et al. Immunity 1997) does not match with the pattern of staining evidenced by the LILRB4 tetramer as used in my flow cytometry studies. In particular, this group showed much higher expression levels across various PBMC subsets with a distinct population staining positive by flow cytometry analysis as opposed to the more diffuse staining patterns that I detected (although it is worth considering that they detected

LAIR-1 expression using a monoclonal antibody, which would be expected to have a much higher binding affinity than a tetrameric ligand). In addition, LAIR-1 is highly expressed upon NK cells, whereas I found no evidence for LILRB4 tetramer binding to NK cells.

At the time of my experimentation the LILRB4/LAIR-1 data provided by Barclay et al., was unpublished but they have since published that LILRB4 interacts with both collagen and LAIR-1, albeit with a very low affinity (Jiang and Barclay, EJI 2009). I would dispute the veracity of this conclusion based upon a number of points. Firstly, the authors suggest that the mouse genome contains a homologue to LILRB4, mLilrb4, which they use in a number of their assays. Katz has published a review specifying mLilrb4 (also known as Gp49B1) as being the orthologous receptor to human LILRB4 (LILRB4 to use the alternative nomenclature). However, the amino acid identity between Gp49B1 and LILRB4 is relatively low (~30 %) and this publication fails to cite a single functional paper discussing human LILRB4, suggesting that this assumption may be controversial (Katz Immun Rev 2007).

Jiang and Barclay detect an interaction between collagen or the collagen related peptide, $(GPO)_{10}$ and soluble monomeric mLilrb4 fused to rat CD4 domains 3 and 4, with a K_d of 39 or 33 μM respectively. This affinity is low but not outside the range common for Group I LILRs for MHC Class I. Full sensorgram traces for this experiment are not shown and so non-specific effects cannot be ruled out. Further experiments utilising multivalent mLilrb4-coated beads were used as evidence for an interaction between LAIR-1 and LILRB4, and an experiment utilising monomeric soluble LAIR-1-rCD4d3d4 flowing over immobilised LILRB4-rCD4d3d4 detected only a very weak interaction with a calculated K_d of >200 μM. The authors specify in the publication that this interaction is at the limits of detection for this methodology. I would suggest that the use of multivalent beads in these assays might lead to

spurious results due to an innate property of the beads, a possibility that the authors themselves discuss. Artefacts during SPR assays are a common problem and not easily controlled for (van der Merwe and Barclay Curr Opin Immun 1996, Karlsson and Fält J Immun Methods 1997, P. Anton van der Merwe, 'Protein-ligand Interactions: Hydrodynamics and Calorimetry. Practical Approach series'. Chapter 6: Surface Plasmon Resonance. Oxford University Press, 2001).

LAIR-1 engagement as conducted in the previously-mentioned functional studies (see Meyaard et al. Immunity 1997), whilst being inhibitory for T cell activation, does not seem to recapitulate the generation of regulatory T cells as shown by Manavalan et al. (Manavalan et al. Trans Immun 2003), although the *in vitro* stimulations used are different so an argument could be made that these results are not directly comparable. On the basis of the above points – the different expression patterns, kinetics and functional outcomes of LAIR-1 engagement, plus the lack of evidence for direct binding between LILRB4 and LAIR-1 – I think it unlikely that LAIR-1 is a true ligand for LILRB4. Collagen also seems unlikely as a ligand, although its widespread expression in the tissues would fit with a general role for tolerance to self, particularly upon tissue damage during wounding or infection. It is hard to envisage how engagement of collagen would lead to tolerogenic signalling into activated T cells and thus I find it highly unlikely that collagen is the counterstructure for LILRB4 which is upregulated upon T cell activation.

The paper of Jiang and Barclay also suggests that LILRB4 may interact with itself in a homotypic fashion, with an estimated K_d greater than 200 μM (Jiang and Barclay EJI 2009). This value is relatively high compared to many immune receptor/ligand interactions, which typically range between 1-100 μM, and is indicative of a very weak interaction. For

comparison within the LILR family, calculated affinities for LILRB1 and LILRB2 for MHC Class I are of the order of 10 - 30 μM (Chapman et al. Immunity 2000, Shiroishi et al. PNAS 2003); these fall within the 1 – 50 μM range of calculated TCR-pMHC interaction affinities but are significantly weaker than antibody – antigen interactions, which are usually of the order of nM (Davis et al. Nat Immunol 2003).

I investigated the possibility of homotypic LILRB4 interaction by SPR analysis, utilising soluble recombinant LILRB4 ectodomain flowed over streptavidin-immobilized biotinylated LILRB4bt. My data do provide some evidence for a homotypic LILRB4/LILRB4 interaction, although the calculated equilibrium affinity was unfeasibly low and saturation of binding was incomplete even at very high concentrations of LILRB4, suggesting that this interaction might be non-specific and possibly due to aggregation of the receptor rather than true binding (P. Anton van der Merwe, 'Protein-ligand Interactions: Hydrodynamics and Calorimetry. Practical Approach series'. Chapter 6: Surface Plasmon Resonance. Oxford University Press, 2001). Soluble recombinant LILRB4 has a propensity to aggregate at high concentrations, especially under non-optimised buffer conditions (e.g. in HBS-EP) and thus I would dispute whether this interaction is truly physiological. Although this interaction could explain binding of LILRB4 tetramer to monocytes, LILRB4 is not expressed on T cells or B cells but these cell types do stain with the LILRB4 tetramer. This fact is consistent with the hypothesis that LILRB4 could bind more than one ligand but strongly suggests that LILRB4 homotypic interaction is not responsible for the tolerogenic signalling into activated T cells.

While my studies leave the identity of the physiological ligand or ligands of LILRB4 unresolved, they do provide a putative ligand expression pattern on freshly-isolated human PBMC against which any candidate ligand can be compared. They also suggest that the

CD28 and B7 family receptors CTLA-4, PD-1, PD-L1, PD-L2, ICOS and ICOSL, and the IgSF receptor LAIR-1, whilst in principle appear to be attractive candidate ligands for LILRB4, do not seem to interact with the LILRB4 receptor. This evidence suggests that LILRB4 effects on tolerance are likely to be mediated via interaction with other as yet undefined receptor or receptors.

Potential future approaches to ligand identification for LILRB4 are discussed in Chapter 6. In the next chapter, I will discuss investigations into the structure of LILRB4 using X-ray crystallographic methods.

CHAPTER 4 - CRYSTALLOGRAPHIC STUDIES OF LILRB4

4.1 Introduction

As discussed in Chapter 1, Group I LILRs have been extensively studied both functionally and structurally and their initial identification and characterisation suggested their involvement in the modulation of myelomonocytic cell functions through their engagement with MHC Class I. The structures of LILRB1, LILRB2, LILRA5 and LILRA2 have been elucidated by X-ray crystallography and comprehensively analysed (Chapman et al. Immunity 2000, Willcox et al. BMC Struc Bio 2002, Willcox et al. Nat Immunol 2003, Shiroishi et al. JBC 2006, Chen et al. JMB 2009). However, the molecular basis of ligand recognition by Group II LILRs remains poorly understood.

Numerous reports have highlighted the Group II receptor LILRB4, which is expressed on dendritic cells, monocytes and macrophages (Cella et al. JEM 1997), as playing an important role in the regulation of immune tolerance (Chang et al. Nat Immunol 2002, and for reviews see Suciu-Foca and Cortesini Cell Immunol 2007, Vlad et al. Hum Immunol 2009). In particular, T suppressor cells were found to induce the up-regulation of expression of LILRB4 and LILRB2 on APCs rendering them tolerogenic to T cells. In addition, recombinant LILRB4-Fc has also been shown to modulate T cell responses via induction of T helper cell anergy and differentiation of $CD8^+$ T suppressor cells (Kim-Schulze et al. JI 2006), and soluble LILRB4 has been detected in the blood of patients with cancer and can promote tolerance of tumour grafts in a humanized mouse model (Kim-Schulze et al. JI 2006, Suciu-Foca JI 2007). In terms of functional studies LILRB4 is one of the most studied receptors within the LILR family, second only to LILRB1.

Despite numerous publications, the molecular basis of such effects is unclear, since in contrast to LILRB1, both the ligands and structure of LILRB4 have remained elusive. Interestingly, LILRB4 is somewhat unusual since whereas most family members contain four Ig-like domains in their extracellular region (designated D1, D2, D3 and D4), LILRB4 is one of two members that is constitutively expressed as two Ig-like domains (the other one is the closely related activating receptor LILRA5 (Borges et al. Blood 2003)). In addition, a previous study found that LILRB4 behaves as an "outlier" in family phylogenetic analysis (Borges et al. JI 1997, and see below). These findings suggest that structural analysis of LILRB4 could provide some insight into its function and ligand recognition properties.

In order to generate structural data for LILRB4, I carried out recombinant expression of its complete extracellular domain with the aim of conducting X-ray crystallographic analysis of the receptor. Due to the refractory nature of the LILRB4 D1D2 protein in crystallisation trials, I ultimately solved and analysed a partial structure of the D1 membrane distal domain matching the native sequence of LILRB4 in this region. In addition, in a collaboration with the group of Professor George Gao (Institute of Microbiology, Chinese Academy of Sciences, Beijing, China), I carried out detailed structural analyses of a structure of a mutated form of the full LILRB4 ectodomain region that incorporated a non-native disulphide bond to aid in protein stabilisation and crystallisation.

4.2 Bioinformatic Analysis of LILRB4

In order to shed light on the distinct structural features of LILRB4, we compared the sequence of the LILRB4 ectodomain with that of other LILR receptors. Sequence alignments were conducted by using the ClustalW web resource (Larkin et al. Bioinformatics 2007). Phylogenetic trees constructed on the basis of comparison of D1D2 fragment sequences highlighted a delineation between Group I receptors and Group II receptors, consistent with previous structural results which initially proposed the Group I/II classification based on conservation (Group I) or lack of conservation (Group II) of amino acids involved in MHC Class I binding (Willcox et al. Nat Immun 2003). Consistent with its poor conservation of residues involved in MHC Class I binding, comparison of the complete LILRB4 ectodomain sequence placed it close to other Group II receptors in terms of identity (**Figure 4.1a**).

Alignment of the D1 domains of LILRB1 and LILRB2 gave a sequence identity of 75 %, with 24 amino acid substitutions across the domain. In comparison, the LILRB4 to LILRA5 D1 alignment gives a sequence identity of 82 %, with 18 amino acid substitutions. Therefore, since LILRA5 possesses the highest sequence identity for LILRB4 within the LILR family it was considered to be the best available search model for molecular replacement during subsequent structural studies (see below) and suitable for comparative analysis with LILRB4 (**Figure 4.1b**). Comparing the entire LILR family, the D1 domains of Group I LILRs (those LILRs with high sequence identity to LILRB1 residues that contact MHC Class I) are more conserved than the D1 domains of Group II LILRs (those LILRs thought unlikely to bind MHC Class I due to non-conservative substitutions at those amino acid positions, which includes LILRB4 and LILRA5) which might suggest that Group II LILRs could bind a diverse range of ligands.

```
LILRB4          GPLPKPTLWAEPGSVISWGNSVTIWCQGTLEAREYRLDKEESPAPWDRQNPLEPKNKARF 60
LILRB1          GHLPKPTLWAEPGSVITQGSPVTLRCQGGQETQEYRLYREKKTAPWITRIPQELVKKGQF 60
LILRB2          GTIPKPTLWAEPDSVITQGSPVTLSCQGSLEAQEYRLYREKKSASWITRIRPELVKNGQF 60
LILRB3          GPFPKPTLWAEPGSVISWGSPVTIWCQGSLEAQEYQLDKEGSPEPLDRNNPLEPKNKARF 60
LILRB5          GTLPKPTLWAEPASVIARGKPVTLWCQGPLETEEYRLDKEGLPWARKRQNPLEPGAKAKF 60
LILRA1          GTLPKPTLWAEPGSVITQGSPVTLWCQGILETQEYRLYREKKTAPWITRIPQEIVKKGQF 60
LILRA2          GHLPKPTLWAEPGSVIIQGSPVTLRCQGSLQAEEYHLYRENKSASWVRRI-QEPGKNGQF 59
LILRA3          GPLPKPTLWAEPGSVITQGSPVTLRCQGSLETQEYHLYREKKTALWITRIPQELVKKGQF 60
LILRA4          ENLPKPILWAEPGPVITWHNPVTIWCQGTLEAQGYRLDKEGNSMSRHILKTLESENKVKL 60
LILRA5          GNLSKATLWAEPGSVISRGNSVTIRCQGTLEAQEYRLVKEGSPEPWDTQNPLEPKNKARF 60
LILRA6          GPFPKPTLWAEPGSVISWGSPVTIWCQGSLEAQEYRLDKEGSPEPWDRNNPLEPKNKARF 60
                  :.*. ***** .**   ..**: ***  ::. *:* :*  .          *   : ::

LILRB4          SIPSMTEDYAGRYRCYYRS-PVGWSQPSDPLELVMTGAYSKPTLSALPSPLVTSGKSVTL 119
LILRB1          PIPSITWEHAGRYRCYYGSDTAGRSESSDPLELVVTGAYIKPTLSAQPSPVVNSGGNVTL 120
LILRB2          HIPSITWEHTGRYGCQYYS-RARWSELSDPLVLVMTGAYPKPTLSAQPSPVVTSGGRVTL 119
LILRB3          SIPSMTQHHAGRYRCHYYS-SAGWSEPSDPLELVMTGAYSKPTLSALPSPVVASGGNMTL 119
LILRB5          HIPSTVYDSAGRYRCYYET-PAGWSEPSDPLELVATGFYAEPTLLALPSPVVASGGNVTL 119
LILRA1          PIPSITWEHTGRYRCFYGSHTAGWSEPSDPLELVVTGAYIKPTLSALPSPVVTSGGNVTL 120
LILRA2          PIPSITWEHAGRYHCQYYSHNHS-SEYSDPLELVVTGAYSKPTLSALPSPVVTLGGNVTL 118
LILRA3          PILSITWEHAGRYCCIYGSHTAGLSESSDPLELVVTGAYSKPTLSALPSPVVTSGGNVTI 120
LILRA4          SIPSMMWEHAGRYHCYYQS-PAGWSEPSDPLELVVT-AYSRPTLSALPSPVVTSGVNVTL 118
LILRA5          SIPSMTEHHAGRYRCYYYS-PAGWSEPSDPLELVVTGFYNKPTLSALPSPVVTSGENVTL 119
LILRA6          SIPSITEHHAGRYRCHYYS-SAGWSEPSDALELVMTGAYSKPTLSALPSPVVASGGNMTL 119
                 * *   . :*** * * :     *: **.* ** *  * .*** * ***:*  *  :*:

LILRB4          LCQSRSPMDTFLLIKERAAHPLLHLRSEHG-AQQHQAEFPMSPVTSVHGGTYRCFSSHGF 178
LILRB1          QCDSQVAFDGFILCKEGEDEHPQCLNSQPHARGSSRAIFSVGPVSPSRRWWYRCYAYDSN 180
LILRB2          QCESQVAFGGFILCKEGEDEHPQCLNSQPHARGSSRAIFSVGPVSPNRRWSHRCYGYDLN 179
LILRB3          RCGSQKRYHHFVLMKEGEHQLPRTLDSQQLHSGGFQALFPVGPVNPSHRWRFTCYYYYMN 179
LILRB5          QCDTLDGLLTFVLVEE-EQKLPRTLYSQKLPKGPSQALFPVGPVTPSCRWRFRCYYYYRK 178
LILRA1          HCVSQVAFGSFILCKEGEDEHPQCLNSQPRTHGWSRAIFSVGPVSPSRRWSYRCYAYDSN 180
LILRA2          QCVSQVAFDGFILCKEGEDEHPQRLNSHSHARGWSWAIFSVGPVSPSRRWSYRCYAYDSN 178
LILRA3          QCDSQVAFDGFILCKEGEDEHPQCLNSHSHARGSSRAIFSVGPVSPSRRWSYRCYGYDSR 180
LILRA4          RCASRLGLGRFTLIEEGDHRLSWTLNSHQHNHGKFQALFPMGPLTFSNRGTFRCYGYENN 178
LILRA5          QCGSRLRFDRFILTEEGDHKLSWTLDSQLTPSGQFQALFPVGPVTPSHRWMLRCYGSRRH 179
LILRA6          QCGSQKGYHQFVLMKEGEHQLPRTLDSQQLHSGGFQALFPVGPVNPSHRWRFTCYYYYMN 179
                 * :      * * :*   .    * *.         * *.:.*:.        *:

LILRB4          SHYLLSHPSDPLELIVS 195
LILRB1          SPYEWSLPSDLLELLVL 197
LILRB2          SPYVWSSPSDLLELLVP 196
LILRB3          TPRVWSHPSDPLEILP- 195
LILRB5          NPQVWSNPSDLLEILVP 195
LILRA1          SPHVWSLPSDLLELLVL 197
LILRA2          SPYVWSLPSDLLELLVP 195
LILRA3          APYVWSLPSDLLGLLVP 197
LILRA4          TPYVWSEPSDPLQLLVS 195
LILRA5          ILQVWSEPSDLLEIPV- 195
LILRA6          TPRVWSHPSDPLEILP- 195
                     * *** * :
```

LILRA5	LILRA6	LILRB3	LILRA4	LILRB5	LILRB1	LILRA1	LILRA2	LILRA3	LILRB2
64	62	61	56	53	52	52	51	50	48

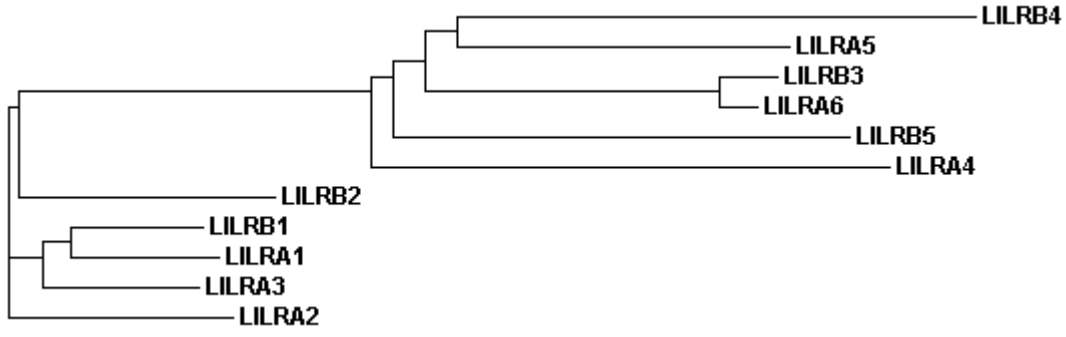

Figure 4.1. Phylogenetic analysis of Group I and Group II LILRs. (a): ClustalW alignment of LILR family member D1D2 domains. Percentage identity of LILR family members with LILRB4 D1D2 is tabulated, and a phylogram of the alignment is depicted. Red: small, hydrophobic, aromatic, not Y. Blue: acidic. Magenta: basic. Green: hydroxyl, amine, amide, basic. Conservation strength is indicated by * > : > .

```
LILRB4          GPLPKPTLWAEPGSVISWGNSVTIWCQGTLEAREYRLDKEESPAPWDRQNPLEPKNKARF 60
LILRA5          GNLSKATLWAEPGSVISRGNSVTIRCQGTLEAQEYRLVKEGSPEPWDTQNPLEPKNKARF 60
LILRB3          GPFPKPTLWAEPGSVISWGSPVTIWCQGSLEAQEYQLDKEGSPEPLDRNNPLEPKNKARF 60
LILRA6          GPFPKPTLWAEPGSVISWGSPVTIWCQGSLEAQEYRLDKEGSPEPWDRNNPLEPKNKARF 60
LILRB5          GTLPKPTLWAEPASVIARGKPVTLWCQGPLETEEYRLDKEGLPWARKRQNPLEPGAKAKF 60
LILRB2          GTIPKPTLWAEPDSVITQGSPVTLSCQGSLEAQEYRLYREKKSASWITRIRPELVKNGQF 60
LILRA2          GHLPKPTLWAEPGSVIIQGSPVTLRCQGSLQAEEYHLYRENKSASWVRRIQ-EPGKNGQF 59
LILRB1          GHLPKPTLWAEPGSVITQGSPVTLRCQGGQETQEYRLYREKKTAPWITRIPQELVKKGQF 60
LILRA3          GPLPKPTLWAEPGSVITQGSPVTLRCQGSLETQEYHLYREKKTALWITRIPQELVKKGQF 60
LILRA1          GTLPKPTLWAEPGSVITQGSPVTLWCQGILETQEYRLYREKKTAPWITRIPQEIVKKGQF 60
LILRA4          ENLPKPILWAEPGPVITWHNPVTIWCQGTLEAQGYRLDKEGNSMSRHILKTLESENKVKL 60
                  :.*. ***** .**   ..**: ***  ::. *:* :*  .         *   : ::

LILRB4          SIPSMTEDYAGRYRCYYRSPVG-WSQPSDPLELVMTGAY 98
LILRA5          SIPSMTEHHAGRYRCYYYSPAG-WSEPSDPLELVVTGFY 98
LILRB3          SIPSMTQHHAGRYRCHYYSSAG-WSEPSDPLELVMTGAY 98
LILRA6          SIPSITEHHAGRYRCHYYSSAG-WSEPSDALELVMTGAY 98
LILRB5          HIPSTVYDSAGRYRCYYETPAG-WSEPSDPLELVATGFY 98
LILRB2          HIPSITWEHTGRYGCQYYSRAR-WSELSDPLVLVMTGAY 98
LILRA2          PIPSITWEHAGRYHCQYYSHNH-SSEYSDPLELVVTGAY 97
LILRB1          PIPSITWEHAGRYRCYYGSDTAGRSESSDPLELVVTGAY 99
LILRA3          PILSITWEHAGRYCCIYGSHTAGLSESSDPLELVVTGAY 99
LILRA1          PIPSITWEHTGRYRCFYGSHTAGWSEPSDPLELVVTGAY 99
LILRA4          SIPSMMWEHAGRYHCYYQSPAG-WSEPSDPLELVVT-AY 97
                 * *   . :*** * * :     *: **.* ** *  *
```

LILRA5	LILRA6	LILRB3	LILRB5	LILRA1	LILRA4	LILRB1	LILRA3	LILRA2	LILRB2
82	82	81	69	63	62	61	58	57	55

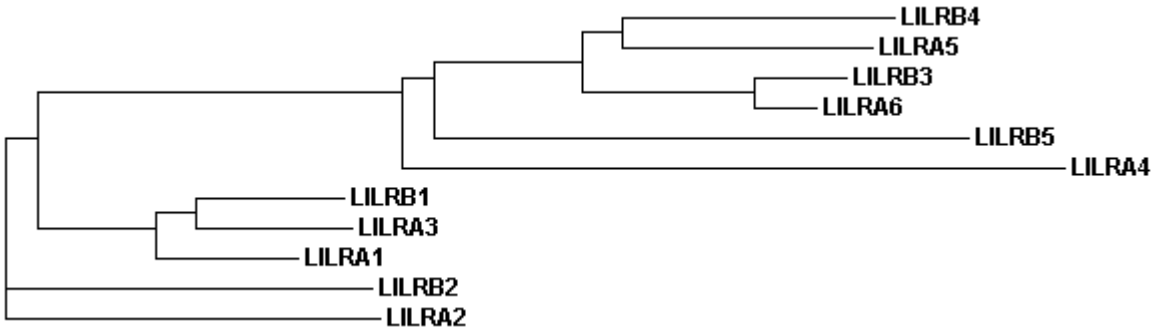

Figure 4.1. Phylogenetic analysis of Group I and Group II LILRs, continued:
(b): ClustalW alignment of LILR family member D1 domains, ordered by alignment output. Percentage identity of LILR family members with LILRB4 D1 is tabulated, and a phylogram of the alignment is depicted. Red: small, hydrophobic, aromatic, not Y. Blue: acidic. Magenta: basic. Green: hydroxyl, amine, amide, basic. Gray: others. Conservation strength is indicated by * > : > .

```
LILRA2          SKPTLSALPSPVVTLGGNVTLQCVSQVAFDGFILCKEGEDEHPQRLNSHSHARGWSWAIF 60
LILRA3          SKPTLSALPSPVVTSGGNVTIQCDSQVAFDGFILCKEGEDEHPQCLNSHSHARGSSRAIF 60
LILRB1          IKPTLSAQPSPVVNSGGNVTLQCDSQVAFDGFILCKEGEDEHPQCLNSQPHARGSSRAIF 60
LILRB2          PKPTLSAQPSPVVTSGGRVTLQCESQVAFGGFILCKEGEDEHPQCLNSQPHARGSSRAIF 60
LILRA1          IKPTLSALPSPVVTSGGNVTLHCVSQVAFGSFILCKEGEDEHPQCLNSQPRTHGWSRAIF 60
LILRB3          SKPTLSALPSPVVASGGNMTLRCGSQKRYHHFVLMKEGEHQLPRTLDSQQLHSGGFQALF 60
LILRA6          SKPTLSALPSPVVASGGNMTLQCGSQKGYHQFVLMKEGEHQLPRTLDSQQLHSGGFQALF 60
LILRB5          AEPTLLALPSPVVASGGNVTLQCDTLDGLLTFVLVEE-EQKLPRTLYSQKLPKGPSQALF 59
LILRA5          NKPTLSALPSPVVTSGENVTLQCGSRLRFDRFILTEEGDHKLSWTLDSQLTPSGQFQALF 60
LILRA4          SRPTLSALPSPVVTSGVNVTLRCASRLGLGRFTLIEEGDHRLSWTLNSHQHNHGKFQALF 60
LILRB4          SKPTLSALPSPLVTSGKSVTLLCQSRSPMDTFLLIKERAAHPLLHLRS-EHGAQQHQAEF 59
                 .*** * ***:*  *  :*: * :      * * :*   .    * *         * *

LILRA2          SVGPVSPSRRWSYRCYAYDSNSPYVWSLPSDLLELLVP 98
LILRA3          SVGPVSPSRRWSYRCYGYDSRAPYVWSLPSDLLGLLVP 98
LILRB1          SVGPVSPSRRWWYRCYAYDSNSPYEWSLPSDLLELLVL 98
LILRB2          SVGPVSPNRRWSHRCYGYDLNSPYVWSSPSDLLELLVP 98
LILRA1          SVGPVSPSRRWSYRCYAYDSNSPHVWSLPSDLLELLVL 98
LILRB3          PVGPVNPSHRWRFTCYYYYMNTPRVWSHPSDPLEILP- 97
LILRA6          PVGPVNPSHRWRFTCYYYYMNTPRVWSHPSDPLEILP- 97
LILRB5          PVGPVTPSCRWRFRCYYYYRKNPQVWSNPSDLLEILVP 97
LILRA5          PVGPVTPSHRWMLRCYGSRRHILQVWSEPSDLLEIPV- 97
LILRA4          PMGPLTFSNRGTFRCYGYENNTPYVWSEPSDPLQLLVS 98
LILRB4          PMSPVTSVHGGTYRCFSSHGFSHYLLSHPSDPLELIVS 97
                .:.*:.        *:          * *** * :
```

LILRA4	LILRA5	LILRA2	LILRB1	LILRA3	LILRB2	LILRA1	LILRB3	LILRA6	LILRB5
49	46	45	43	43	42	42	41	41	37

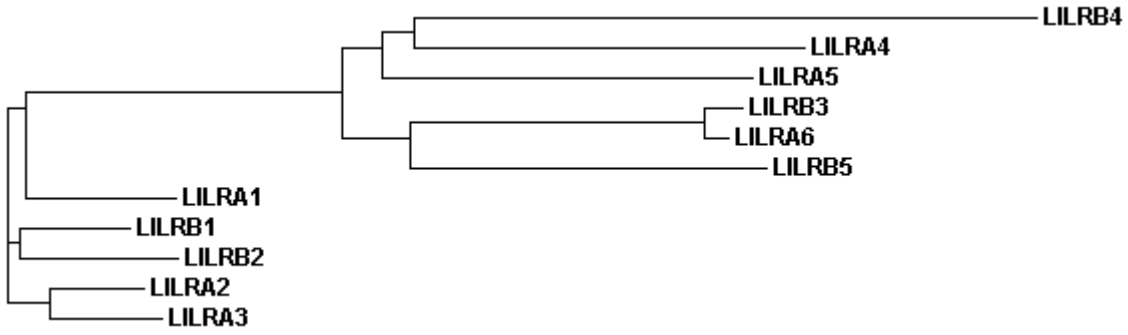

Figure 4.1. Phylogenetic analysis of Group I and Group II LILRs, continued:
(c): ClustalW alignment of LILR family member D2 domains, ordered by alignment output. Note that LILRB4 is bottom of the alignment indicating least conservation across the LILR family. Percentage identity of LILR family members with LILRB4 D2 is tabulated, and a phylogram of the alignment is depicted. Red: small, hydrophobic, aromatic, not Y. Blue: acidic. Magenta: basic. Green: hydroxyl, amine, amide, basic. Gray: others. Conservation strength is indicated by * > : > .

```
LILRB4          MTGAYSKPTLSALPSPLVTSGKSVTLLCQSRSPMDTFLLIKERAAHPLLHLRSEHGAQQH 60
LILRB1          AGQFYDRVSLSVQPGPTVASGENVTLLCQSQGWMQTFLLTKEGAADDPWRLRSTYQSQKY 60
LILRB2          TGQIHGTPFISVQPGPTVASGENVTLLCQSWRQFHTFLLTKAGAADAPLRLRSIHEYPKY 60
LILRB3          AGQIYDTVSLSAQPGPTVASGENVTLLCQSWWQFDTFLLTKEGAAHPPLRLRSMYGAHKY 60
LILRB5          AGLIPDIPALSVQPGPKVASGENVTLLCQSWHQIDTFFLTKEGAAHPPLCLKSKYQSYRH 60
LILRA1          AGQFRGRPFISVHPGPTVASGENVTLLCQSWGPFHTFLLTKAGAADAPLRLRSIHEYPKY 60
LILRA2          TGQFYDRPSLSVQPVPTVAPGKNVTLLCQSRGQFHTFLLTKEGAGHPPLHLRSEHQAQQN 60
LILRA3          TGQIRARPFLSVRPGPTVASGENVTLLCQSQGGMHTFLLTKEGAADSPLRLKSKRQSHKY 60
LILRA4          AGQISDRPSLSVQPGPTVTSGEKVTLLCQSWDPMFTFLLTKEGAAHPPLRLRSMYGAHKY 60
LILRA6          AGQIYDTVSLSAQPGPTVASGENVTLLCQSRGYFDTFLLTKEGAAHPPLRLRSMYGAHKY 60
                          :*. * * *:.*:.*******   : **:* *  *..    *:*     :

LILRB4          QAEFPMSPVTSVHGGTYRCFSSHGFSHYLLSHPSDPLELIVS 102
LILRB1          QAEFPMGPVTSAHAGTYRCYGSQSSKPYLLTHPSDPLELVVS 102
LILRB2          QAEFPMSPVTSAHAGTYRCYGSLNSDPYLLSHPSEPLELVVS 102
LILRB3          QAEFPMSPVTSAHAGTYRCYGSYSSNPHLLSFPSEPLELMVS 102
LILRB5          QAEFSMSPVTSAQGGTYRCYSAIRSYPYLLSSPSYPQELVVS 102
LILRA1          QAEFPMSPVTSAHSGTYRCYGSLSSNPYLLSHPSDSLELMVS 102
LILRA2          QAEFRMGPVTSAHVGTYRCYSSLSSNPYLLSLPSDPLELVVS 102
LILRA3          QAEFPMSPVTSAHAGTYRCYGSLSSNPYLLTHPSDPLELVVS 102
LILRA4          QAEFPMSPVTSAHAGTYRCYGSRSSNPYLLSHPSEPLELVVS 102
LILRA6          QAEFPMSPVTSAHAGTYRCYGSYSSNPHLLSFPSEPLELMVS 102
                **** *.****.: *****:.:     :**: ** . **:**
```

LILRA2	LILRA4	LILRA6	LILRB3	LILRB1	LILRA1	LILRA3	LILRB2	LILRB5
64	63	61	60	56	56	56	55	55

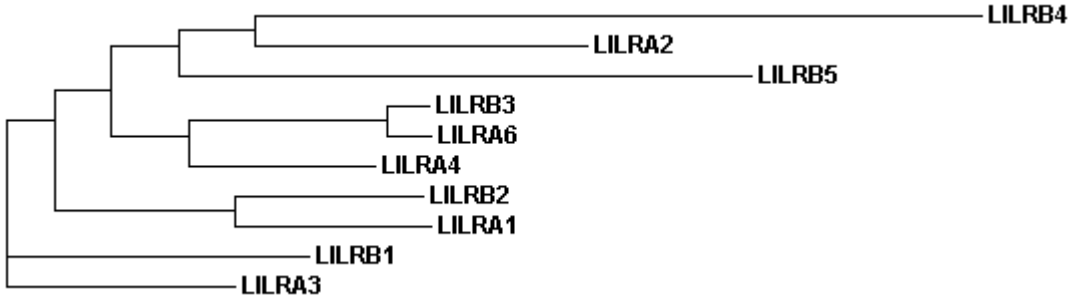

Figure 4.1. Phylogenetic analysis of Group I and Group II LILRs, continued:
(d): ClustalW alignment of LILRB4 D2 domain onto LILR family D4 domains. LILRA5 is excluded from analysis since it is a two-domain LILR. Percentage identity of LILR family D4 domains with LILRB4 D2 is tabulated, and a phylogram of the alignment is depicted. Note that identity is higher than for D2 alignment as shown in Figure 4.1c. Red: small, hydrophobic, aromatic, not Y. Blue: acidic. Magenta: basic. Green: hydroxyl, amine, amide, basic. Gray: others. Conservation strength is indicated by * > : > .

More detailed analysis of the individual domains of the receptor highlighted that although the D1 domain bore similarity to other LILR D1 domains (**Figure 4.1b**), the LILRB4 D2 domain shared highest identity with the D4 domains of other family members, as previously noted (Borges et al. JI 1997) (**Figure 4.1c-d**). Therefore, LILRB4 is distinguished by an unusual domain organization comprising a classical LILR D1 domain, juxtaposed to an Ig domain that is most similar to the membrane-proximal D4 domains of other LILR receptors.

4.3 Previous Attempts to Crystallise the Ectodomain of LILRB4

Attempts to crystallise the two-domain recombinant form of LILRB4, produced as described in Chapter Two (and see Garner et al. Prot Exp Pur 2006) were conducted by myself and the group's protein crystallographer, Dr. Fiyaz Mohammed. Despite considerable effort these attempts were largely unsuccessful. Microcrystals were grown in two conditions – 1.4M Na / K Phosphate pH 6.6 and 1.0M Na / K Phosphate pH 7.2 – with two different crystal morphologies – 'plates' and 'bones' respectively – at a protein concentration of 8.2 mg/ml (**Figure 4.2a**). However, SDS-PAGE analysis of the washed crystals showed an apparent mass of a single Ig domain (~12 kDa) instead of the expected 25 kDa, and seemed to consist of two protein species that formed a close doublet band (**Figure 4.2b**).

N-terminal amino acid sequencing of the excised doublet protein band was carried out by Dr. John Fox (Alta Biosciences, University of Birmingham) and identified both bands as consisting of the N-terminal D1 domain of LILRB4. This result as determined by SDS-PAGE could be reproduced by incubating refolded LILRB4 for 14 days at room temperature (**Figure 4.2c**).

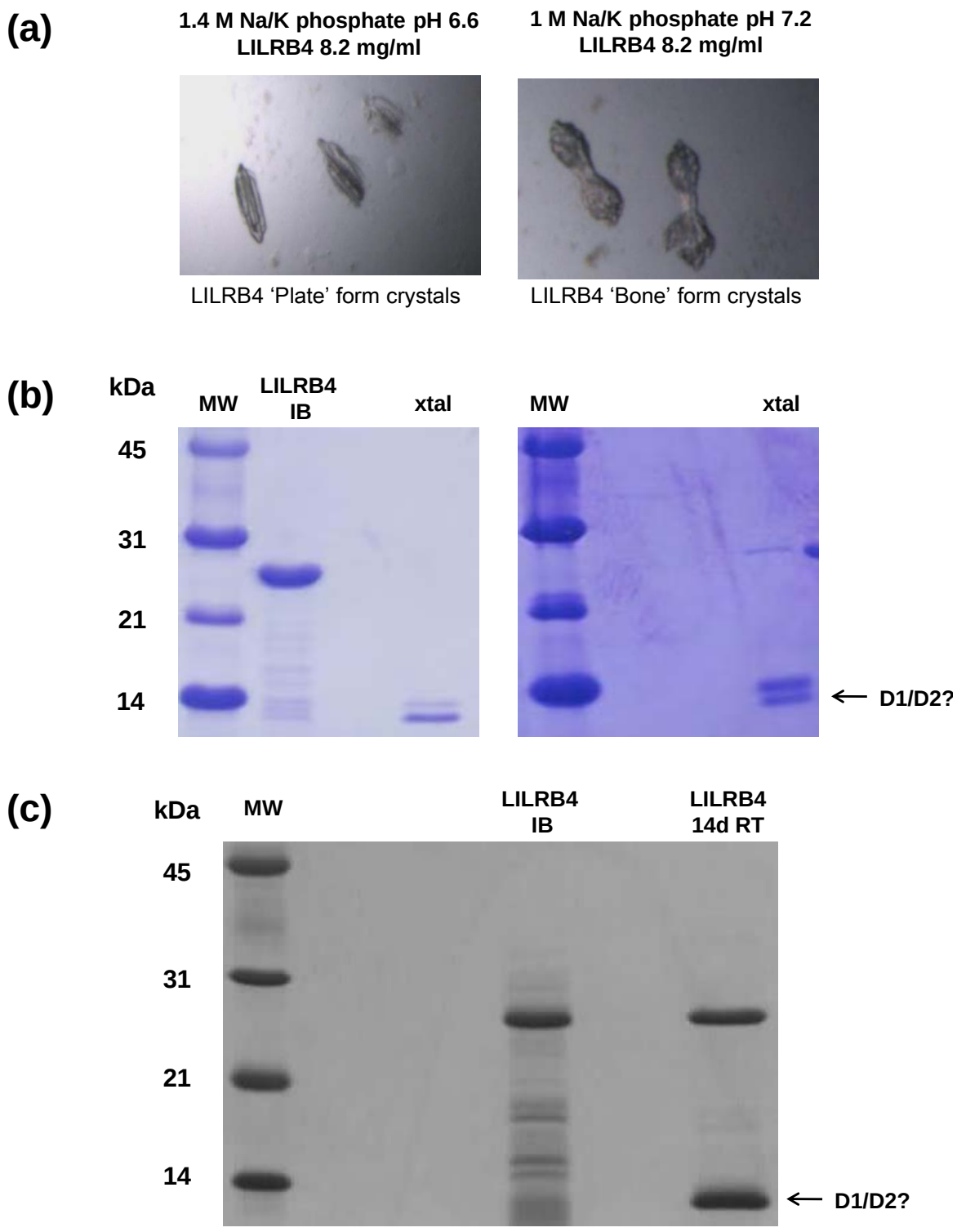

Figure 4.2. Characterisation of LILRB4 D1D2 crystals. (a): Potential LILRB4 D1D2 crystals exhibit two distinct morphologies, plates (left panel) and bones (right panel). (b): SDS-PAGE analysis of the two crystal forms. (c): SDS-PAGE analysis of LILRB4 degradation products after 14 days incubation at RT.

This led us to hypothesise that proteolytic cleavage of the two-domain LILRB4 at the interdomain region was occurring in the crystallisation droplets, followed by preferential crystallisation of the D1 fragment, probably aided by further proteolytic cleavage and/or precipitation of the D2 domain.

This result suggested that, in the absence of successful crystallisation of the complete ectodomain of LILRB4, attempts to crystallise just the N-terminal D1 domain of the receptor might be more promising and could yield useful structural data. It could be hypothesised that, due to the two-domain nature of LILRB4 (rather than the extended four-domain arrangements of LILRB1 or LILRB2), ligand binding regions of the receptor would be more likely to be located at the tip of the D1 domain, with the D2 domain acting merely to provide sufficient length and/or flexibility for ligand engagement in a 'head-to-head' fashion on an opposing cell surface (rather than the 'sideways-on' fashion of ligand engagement between the D1D2 domains of LILRB1 or LILRB2 and the $\alpha 3$ and β_2M domains of MHC Class I, which involves residues at the interdomain interface of the receptor as well as those at the distal D1 tip). Therefore in the absence of crystals of the full LILRB4 ectodomain, attempts to crystallise the D1 domain might yield useful structural information.

4.4 Structure Determination of LILRB4 D1

4.4.1 Production of Recombinant Soluble LILRB4 D1 Domain in *E. coli*

In order to produce soluble LILRB4 D1 domain, a stop codon was introduced into the previously generated LILRB4-pET23a expression vector (Garner et al. Prot Exp Pur 2006) by SDM (Quikchange SDM kit, Stratagene). Selection of the position for the stop codon was

based upon structural analysis of the corresponding interdomain region of LILRB1 (PDB code 1G0X; Chapman et al. Immunity 2000) and LILRB2 (PDB code 2GW5; Willcox et al. BMC Struc Bio 2002) with the crystallographic software package, COOT (Emsley and Cowtan, Acta Cryst D 2004). Two constructs were generated, LILRB4 D1 GAYstop and LILRB4 D1 VMTstop, with stop codons after amino acid positions 99 and 96 respectively. A map of the pET23a expression vector and the DNA sequence for LILRB4 coding for the D1 domain, along with the corresponding SDM primer sequences is shown in **Figure 4.3**.

After the SDM PCR reactions utilising the LILRB4-pET23a vector as template, the restriction enzyme DpnI was used to degrade the template DNA and the remaining, theoretically template-free mutated plasmid solution was transformed into the *E. coli* strain DH5α. Following a miniprep plasmid preparation, DNA sequencing (utilising BigDye Terminator 3.0 reaction and the sequencing service of Functional Genomics, Department of Biosciences, University of Birmingham) confirmed that the expected sequence for each LILRB4 D1 construct was obtained.

Test expression and SDS-PAGE analysis showed clear induction of a protein corresponding in size to LILRB4 D1, indicating successful test expression (**Figure 4.4a**). Subsequently, full-scale expression of both LILRB4 D1 constructs was conducted in *E. coli* BL21 (DE3) cells and inclusion bodies were purified, solubilised in 8M Guanidine buffer **(Figure 4.4b)** and subjected to standard *in vitro* refolding conditions (Garboczi et al. PNAS 1992). Refolds of LILRB4 D1 GAYstop (hereafter referred to as LILRB4 D1) were purified by size exclusion chromatography (into 20 mM Na Citrate buffer, pH 5.5) providing high yield and purity as

(a)

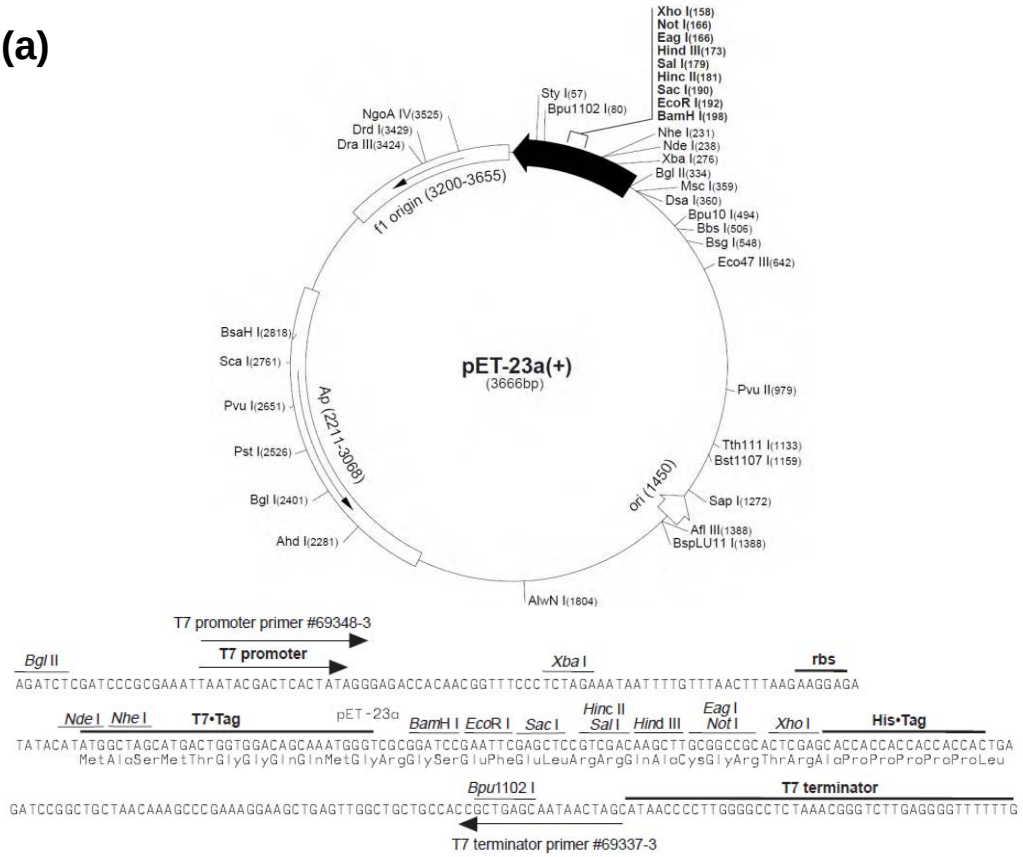

(b)

```
ATGggTccActTccAaaaccAacTctctgggctgagccaggctctgtgatcagctgggggaactctgtgaccatc
M  G  P  L  P  K  P  T  L  W  A  E  P  G  S  V  I  S  W  G  N  S  V  T  I
tggtgtcaggggaccctggaggctcgggagtaccgtctggataaagaggaaagcccagcaccctgggacagacag
W  C  Q  G  T  L  E  A  R  E  Y  R  L  D  K  E  E  S  P  A  P  W  D  R  Q
aacccactggagcccaagaacaaggccagattctccatcccatccatgacagaggactatgcagggagataccgc
N  P  L  E  P  K  N  K  A  R  F  S  I  P  S  M  T  E  D  Y  A  G  R  Y  R
tgttactatcgcagccctgtaggctggtcacagcccagtgacccccttggagctggtgatgacaggagcctacagt
C  Y  Y  R  S  P  V  G  W  S  Q  P  S  D  P  L  E  L  V  M  T  G  A  Y  S
aaacccacccttcagccctg...
K  P  T  L  S  A  L  ...
```

LILRB4 D1 VMT Stop 5' GGAGCTGGTGATGACA**T**GAGCCTACAGTAAACCC
Reverse complement 5' GGGTTTACTGTAGGCTCATGTCATCACCAGCTCC

LILRB4 D1 GAY Stop 5' GGTGATGACAGGAGCCTAC**TGA**AAACCCACCCTTTC
Reverse complement 5' GAAAGGGTGGGTTTTCAGTAGGCTCCTGTCATCACC

Figure 4.3. Generation of LILRB4 D1-pET23a expression vector. (a): Map of the pET23a expression vector and MCS. Reproduced from the Novagen pET23a manual. (b): LILRB4 D1 construct sequence showing SDM sites and SDM primers for generation of the LILRB4 GAYstop and VMTstop vectors. Bases previously mutated from the original LILRB4 sequence for optimal *E. coli* expression (Garner et al. Prot Pur Exp 2006) are in uppercase, and the primer region is underlined.

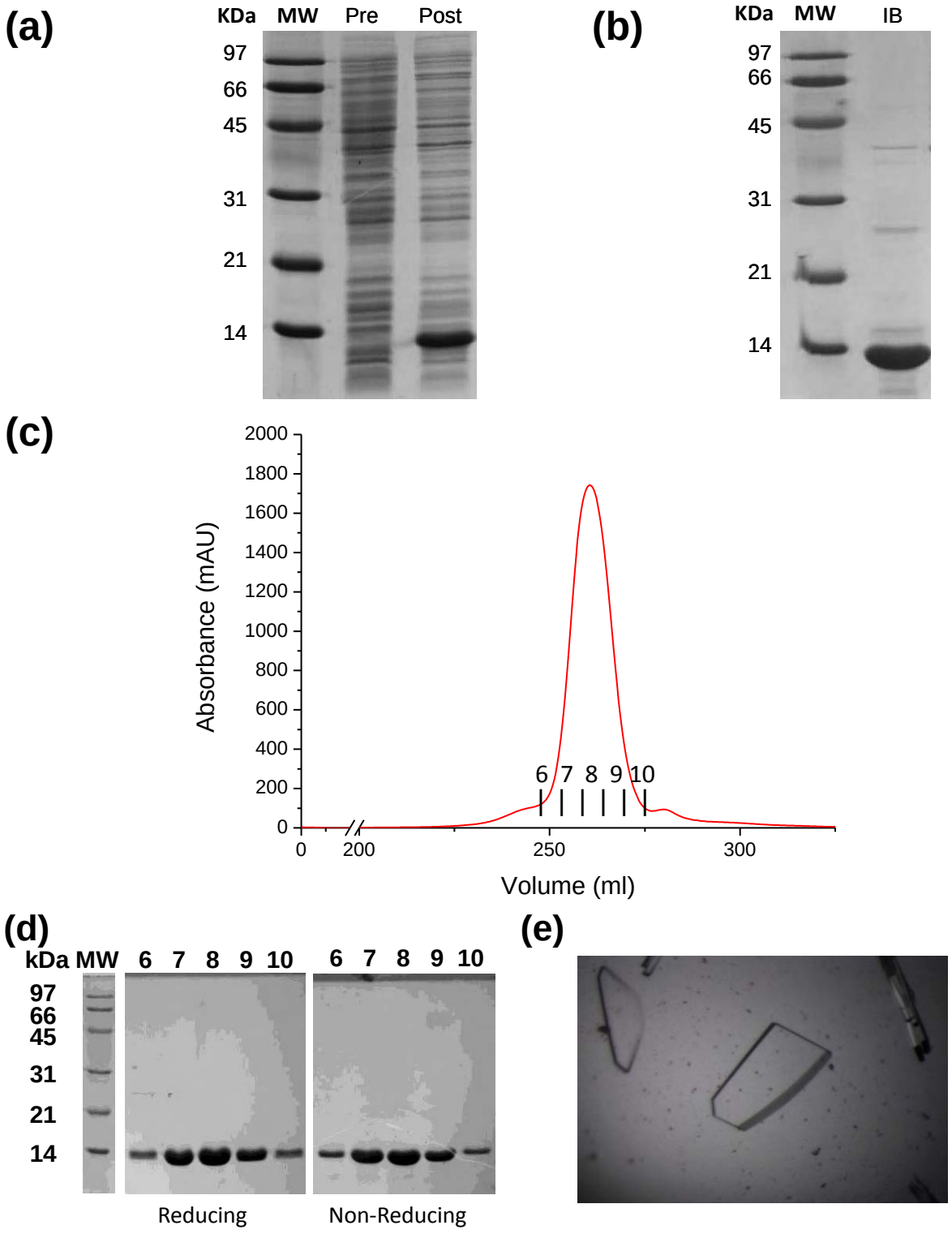

Figure 4.4. Purification and SDS-PAGE analysis of LILRB4 D1. SDS-PAGE analysis of (a): test expression and (b): inclusion body preparation of LILRB4 D1. (c): size exclusion chromatography elution profile for LILRB4 D1 after FPLC using S200 column. Fraction positions are marked. (d): SDS-PAGE analysis of FPLC fractions under reducing (left panel) and non-reducing (right panel) conditions. (e): light microscope image of LILRB4 D1 crystals.

judged by the presence of a single peak on the elution profile (**Figure 4.4c**) and subsequent analysis of peak fractions by SDS-PAGE. As expected, a single protein band of ~12 kDa was visible after concentration of the peak fractions under both reducing and non-reducing conditions, consistent with a single, monomeric correctly folded species. Purity of the protein was judged sufficient enough for subsequent crystallisation trials (**Figure 4.4d**). Attempts to refold LILRB4 D1 VMTstop suffered from much lower yields and were abandoned (data not shown).

4.4.2 Crystallisation of LILRB4 D1

Initial crystallisation trials were set up utilising a Mosquito nanolitre crystallisation robot (TTP LabTech), using a hanging drop vapour diffusion approach. In brief, three 96-well plates each consisting of 96 crystallisation conditions, and each corresponding to one of three commercial screens (JCSG$^+$, Index and PEG/Ion I & II) were set up at 100 µl volume, whereby the robot pipetted 100 nl of protein solution at a concentration of 10 mg/ml to 100 nl of well solution. The drops were then sealed and stored in a 23 ˚C crystallisation incubator for 72 h before inspection under a light microscope for precipitation and microcrystal formation.

Crystallisation was particularly successful in this instance, with 166 of 288 conditions (58 %) yielding microcrystals. Those with the most promising morphologies were selected for scale-up and optimisation, in order to generate crystals large enough for X-ray data collection. In total 24 conditions were selected (8 from each commercial screen) and placed in a 24-well Linbro plate (reservoir volume = 1 ml) and equilibrated against hanging drops consisting of 1

μl of protein solution (10 mg/ml) plus 1 μl of well condition. After a 72 h incubation period, the hanging drops were inspected for crystal formation and the results are tabulated in **Table 4.1**. In particular, two conditions stood out as giving rise to large crystals of good morphology for data collection: Index condition 73 (0.2 M Sodium Chloride, 0.1 M Tris pH 8.5, 25 % w/v PEG 3350) and PEG/Ion Screen I condition 25 (0.2 M Magnesium acetate tetrahydrate pH 7.9, 20 % w/v PEG 3350). Data were collected from crystals grown in Index condition 73 (see **Figure 4.4e**).

4.4.3 Data Collection and Processing

Prior to data collection LILRB4 D1 crystals were soaked in reservoir buffer supplemented with increasing concentrations (5, 10 and 15 %) of ethylene glycol as cryoprotectant, before being flash cooled at 100 K in a nitrogen gas stream (Oxford Cryosystems). X-ray data were collected to 1.6 Å resolution (**Figure 4.5**) under the supervision of Dr Fiyaz Mohammed on an in-house MicroMax 007HF rotating anode X-ray generator (Rigaku) using a Saturn CCD detector (University of Birmingham Macromolecular X-ray Facility). The crystals belonged to the space group $P2_1$ with unit cell parameters (a= 41.1 Å, b= 40.7 Å and c= 55 Å; β=108.5˚). LILRB4 D1 diffraction data set were integrated, scaled and merged using programs of the XDS suite (Kabsch Acta Cryst D 2010). The relevant data processing statistics are listed in **Table 4.2** (overleaf).

Screen	Tube	Salt	Buffer (0.1M)	pH	Precipitant	Crystal Morphology
JCSG$^+$ (1)	5	0.2M Magnesium formate	-	-	20% PEG 3350	plates, stacks
JCSG$^+$ (1)	10	0.2M Potassium formate	-	-	20% PEG 3350	6 L stacks, one v thick
JCSG$^+$ (1)	42	0.2M Magnesium chloride	Tris-HCl	8.5	20% PEG 8000	precipitate, s plate
JCSG$^+$ (2)	10	-	Bicine	9.0	10% PEG 6000	precipitate, light
JCSG$^+$ (2)	29	0.005M Co/Cd/Mg/Ni chloride	Hepes	7.5	12% PEG 3350	precipitate, s plate
JCSG$^+$ (2)	33	0.1M Potassium thiocyanate	-	-	30% PEG 2000 MME	3 L stacks
JCSG$^+$ (2)	39	-	Bis-Tris	5.5	25% PEG 3350	multiple s star stacks
JCSG$^+$ (2)	47	0.2M Magnesium chloride	Bis-Tris	5.5	25% PEG 3350	~ dozen small plates
Index	15	0.5M Mg formate dihydrate	Hepes	7.5	-	3 s plates
Index	42	-	Bis-Tris	5.5	25% PEG 3350	4 L stacks, v thick
Index	43	-	Bis-Tris	6.5	25% PEG 3350	multiple s star stacks
Index	71	0.2M Sodium chloride	Bis-Tris	6.5	25% PEG 3350	multiple m star stacks
Index	**73**	**0.2M Sodium chloride**	**Tris-HCl**	**8.5**	**25% PEG 3350**	**6 L plates, stack**
Index	81	0.2M Ammonium acetate	Tris-HCl	8.5	25% PEG 3350	dispersed L plates
Index	85	0.2M Mg chloride hexahydrate	Tris-HCl	8.5	25% PEG 3350	multiple dispersed s plates
Index	87	0.2M Sodium malonate	-	7.0	20% PEG 3350	stacks, dispersed plates
PEG-Ion-I	1	0.2M sodium fluoride	-	7.3	20% PEG 3350	3 L plate stacks, salt*
PEG-Ion-I	**25**	**0.2M Mg acetate tetrahydrate**	**-**	**7.9**	**20% PEG 3350**	**2 star stacks, L plates**
PEG-Ion-I	37	0.2M K Na tartrate tetrahydrate	-	7.4	20% PEG 3350	multiple dispersed s plates
PEG-Ion-II	2	0.2M Sodium malonate	-	4.0	20% PEG 3350	heavy precipitate + s plates
PEG-Ion-II	20	0.2M Succinic acid	-	7.0	20% PEG 3350	multiple L plates/stacks
PEG-Ion-II	26	0.2M NaAc trihydrate	-	7.0	20% PEG 3350	multiple s star stacks
PEG-Ion-II	30	0.2M NH3 tartrate dibasic	-	7.0	20% PEG 3350	multiple dispersed s plates
PEG-Ion-II	31	2% v/v Tacsimate pH4.0	NaAc pH4.6	4.0 or 4.6	16% PEG 3350	heavy precipitate

Table 4.1: Scale-up of LILRB4 D1 crystallisation conditions. Crystal observation abbreviations: L, large; m, medium; s, small; v, very * indicates salt crystals observed in the control. Tube refers to the tube number in the crystal screen kit.

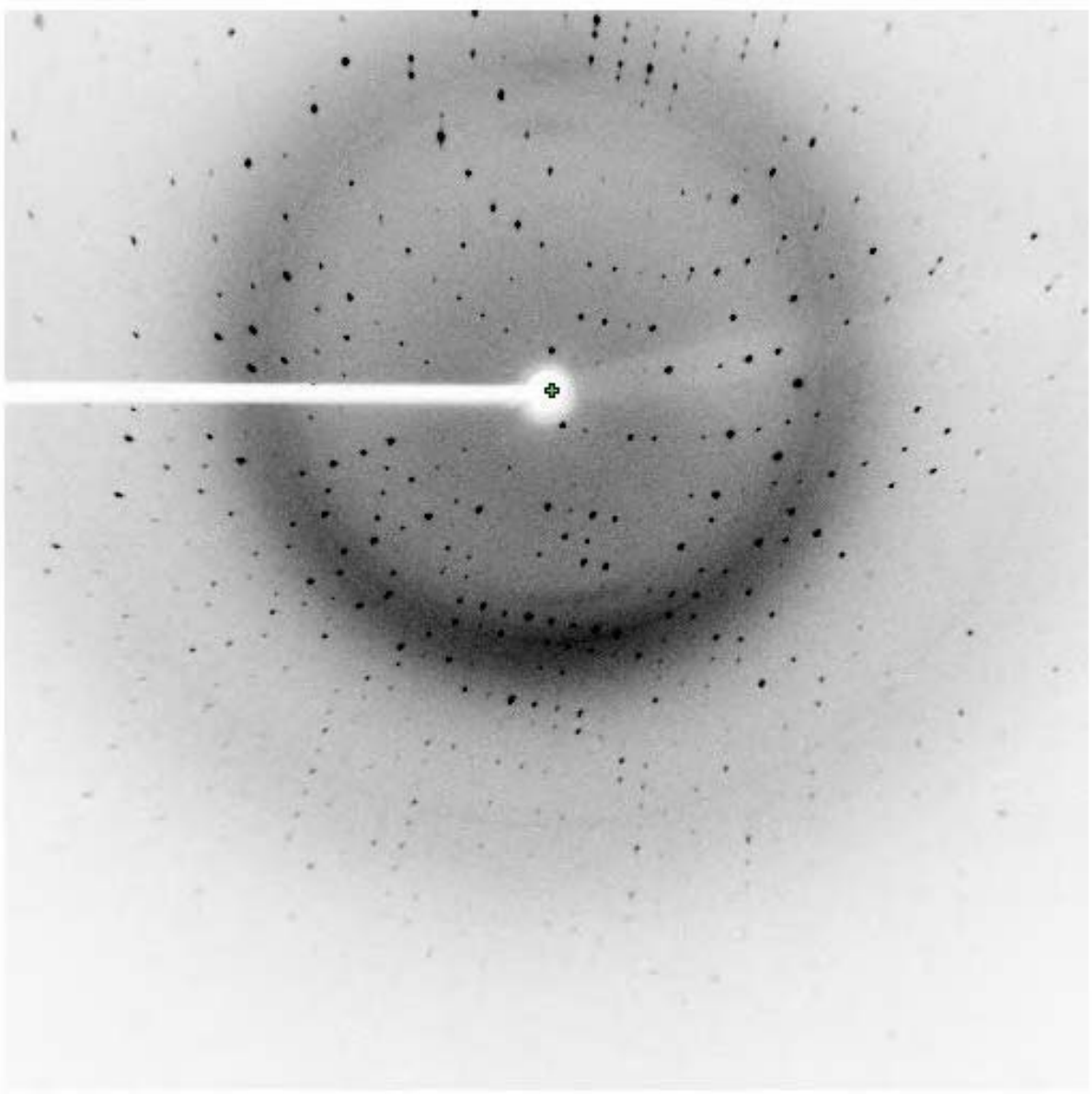

Figure 4.5. Diffraction pattern for LILRB4 D1 X-ray data. A 0.5° oscillation image of LILRB4 D1 crystal collected at 100 K using the University of Birmingham Macromolecular X-ray Facility. The crystal diffracted X-rays to a resolution of 1.6 Å.

Space Group	$P2_1$
Unit Cell Dimensions	a=41.1, b=40.7, c=55 (Å) α=90, β=108.5, γ=90 (°)
Resolution (Á)	20-1.6 (1.7-1.6)
Observed Reflections	138176 (12449)
Unique Reflections	22154 (3203)
Multiplicity	6.2
Completeness (%)	96.4 (84.3)
R_{merge} (%)	4.5 (14.6)
I/σ(I)	25.1 (8.5)

Table 4.2: Data processing statistics for LILRB4 D1. Figures in parentheses apply to data in the highest resolution shell. Completeness = (number of independent reflections/total theoretical number). R_{merge} (I) = ($\Sigma|I(i) - \langle I(h)\rangle|/\Sigma I(i)$), where I(i) is the *i*th observation of the intensity of the hkl reflection and <I> is the mean intensity from multiple measurements of the h,k,l reflection.

4.4.4 LILRB4 D1 Structure Solution

Assuming the LILRB4 D1 crystals possess two LILRB4 D1 molecules within the asymmetric unit, a solvent content of 50 % was calculated. Initial phase information for the structure determination of LILRB4 D1 was obtained by molecular replacement with CNS (Brünger et al. Acta Cryst D Bio Cryst 1998). The search model consisted of the D1 domain from the recently solved LILRA5 D1D2 crystal structure (Shiroishi et al. JBC 2006), with co-ordinates for water molecules omitted. Firstly, a cross-rotation function was performed to determine the orientation of the search model with respect to the target protein (**Table 4.3**). The output from

the cross rotation function is a list of rotation angles (θ_1, θ_2 and θ_3) with their corresponding correlation coefficients (RF-function). The cross rotation function yielded two significant solutions (**Table 4.3**) with RF-functions of 3.2 and 3.0 (with the next peak being at 2.1), respectively. These cross rotation function solutions (θ_1= 79.99°, θ_2= 50.87°, θ_3= 150.24° and θ_1= 112.11°, θ_2= 74.35°, θ_3= 314.21°) corresponded to the orientation of the two LILRB4 D1 molecules within the asymmetric unit and confirmed the solvent content calculations.

Index	θ_1	θ_2	θ_3	RF-function
1	**79.994**	**50.870**	**150.238**	**3.2365**
2	**112.105**	**74.348**	**314.211**	**3.0426**
24	194.150	43.043	29.579	2.1783
25	191.171	54.783	249.776	2.1764
30	47.119	70.435	40.573	2.1299
31	158.970	66.522	228.200	2.1276
32	237.759	23.478	29.338	2.1218
45	344.172	54.783	0.916	2.0214
67	231.313	66.522	72.083	1.9271
68	299.534	62.609	204.024	1.9266

Table 4.3: Cross Rotation Function. The 10 highest peaks following the cross rotation search performed with CNS.

The next stage involved performing a translation function search to determine the position (translation vectors x, y and z) of the search model with respect to the target protein (**Table 4.4**). The translation function was performed in space group $P2_1$ using the orientations determined from the cross-rotation function calculations (**Table 4.3**). Prior to the translation function search the orientations were refined using the PC-refinement feature within CNS. The translation function produced a list of translation vectors (x, y and z) with their

corresponding score function (monitor) and packing value (this being the percentage of the unit cell covered by the molecule). Notably, both cross rotation function solutions (θ_1= 79.96°, θ_2= 52.26°, θ_3= 149.01° and θ_1= 111.98°, θ_2= 76.66°, θ_3= 314.91°) yielded large translation function solutions (x= 6.39, y= 0.63, z= 8.50 and x= 10.39, y= -0.49, z= 3.11) with scores of 0.229 (with next score of 0.090), providing further evidence for the existence of only two LILRB4 D1 molecules per asymmetric unit (**Table 4.4**).

R#	θ_1	θ_2	θ_3	transX	transY	transZ	monitor	packing
1	**79.96**	**52.26**	**149.01**	**6.39**	**0.63**	**8.50**	**0.229**	**0.3119**
2	**111.98**	**76.66**	**314.91**	**10.39**	**-0.49**	**3.11**	**0.229**	**0.3133**
3	196.67	47.12	30.59	15.42	-2.32	11.09	0.090	0.2921
4	189.45	52.78	248.22	8.29	-1.01	3.09	0.078	0.2963
5	47.71	68.97	33.40	-7.10	-2.75	21.34	0.077	0.2750
6	159.02	64.07	228.04	2.79	-0.53	10.29	0.084	0.3118
7	238.57	34.04	38.27	8.11	-3.55	23.05	0.091	0.3004
8	345.24	48.60	3.50	-3.96	-1.11	4.82	0.085	0.3181
9	233.28	63.14	71.92	2.12	-0.17	9.55	0.081	0.3139
10	301.13	60.24	207.13	0.93	0.45	13.16	0.066	0.3158

Table 4.4: Translation Function. The highest translation function peak for each cross-rotation solution (see table 4.3) calculated with CNS.

Finally the position of the first LILRB4 D1 molecule was fixed (θ_1= 111.98°, θ_2= 76.66°, θ_3= 314.91°, x= 10.39, y= -0.49 and z= 3.11) and the translation search was repeated to determine

the position of the second LILRB4 D1 molecule with respect to the same origin (**Table 4.5**). The translation function provided an unambiguous translation function solution for the second LILRB4 D1 molecule (x= 35.51, y= 37.92 and z= -17.85) with a score function of 0.42. In addition, the packing value had increased from the previous translation function calculation indicating minimal overlap for this solution compared to the others.

R#	θ_1	θ_2	θ_3	transX	transY	transZ	monitor	packing
1	**81.03**	**51.38**	**148.21**	**35.51**	**37.92**	**-17.85**	**0.420**	**0.6212**
2	111.94	76.00	314.03	8.32	0.54	7.93	0.218	0.4168
3	195.03	47.43	33.19	16.72	13.80	6.02	0.173	0.4236
4	189.04	53.76	247.68	36.67	9.02	7.21	0.160	0.4168
5	47.69	68.82	35.95	38.45	27.15	-23.59	0.173	0.4501
6	160.99	66.01	227.45	24.90	21.82	5.31	0.190	0.4767
7	239.55	31.73	35.24	8.64	30.75	22.79	0.186	0.4786
8	343.93	50.43	1.87	26.35	0.45	8.07	0.169	0.5972
9	233.37	63.24	70.72	2.67	25.39	9.28	0.185	0.5302
10	301.10	59.79	207.47	40.41	34.76	-23.4	0.191	0.5201

Table 4.5: Translation Function for Second LILRB4 D1 Molecule. The highest translation function peaks for each cross rotation solution after fixing the position of the first LILRB4 D1 molecule (θ_1= 111.98°, θ_2= 76.66°, θ_3= 314.91°, x= 10.39, y= -0.49 and z= 3.11).

4.4.5 LILRB4 D1 Structure Refinement

The molecular model was refined with CNS and REFMAC5 (Murshudov et al. Acta Cryst D 1997). The progress of refinement was verified by monitoring reduction in the R_{free} (Brünger Nature 1992) calculated from an independent set of reflections, which were set aside for

cross-validation purposes. The models were subjected to several rounds of alternating simulated annealing/positional refinement followed by isotropic B factor refinement. Following the initial round of refinement the R_{work} and R_{free} converged to 32.4 % (reduced from 46.4 %) and 33.9 % (reduced from 45.3 %), respectively. Examination of the resulting electron density maps revealed unbiased features in the electron density which corresponded to LILRB4 D1 residues (**Figure 4.6**) and confirmed the validity of the molecular replacement solution.

All model manipulations were performed using COOT. Once the R-factors had dropped below 30 %, water molecules were included in the models if they appeared in *Fo-Fc* maps contoured at > 3σ and were within hydrogen bonding distance to chemically acceptable groups. These water molecules were added in successive steps and were included in the subsequent refinement cycles. After further cycles of refinement interspersed with model building, the R_{work} and R_{free} converged to 20.3 and 23.9 %, respectively for all data between 20 Å and 1.6 Å. The final model consists of two LILRB4 D1 molecules (designated subunit A (residues 3-93) and subunit B (residues 3-95)), 3 ethylene glycol molecules and 130 solvent molecules. The quality of the final refined model was verified using PROCHECK (Laskowski et al. J App Cryst 1993) which demonstrated that non-glycine residues were absent from the disallowed regions of the Ramachandran plot (**Figure 4.7**). The majority of the residues are well defined with the exception of a few solvent exposed side chains, which are likely to be flexible. Hydrogen bonding and van der Waals contacts were analysed using CONTACT (Collaborative Computational Project Number 4, Acta Cryst D 1994). The final refinement statistics are summarised in **Table 4.6** (overleaf).

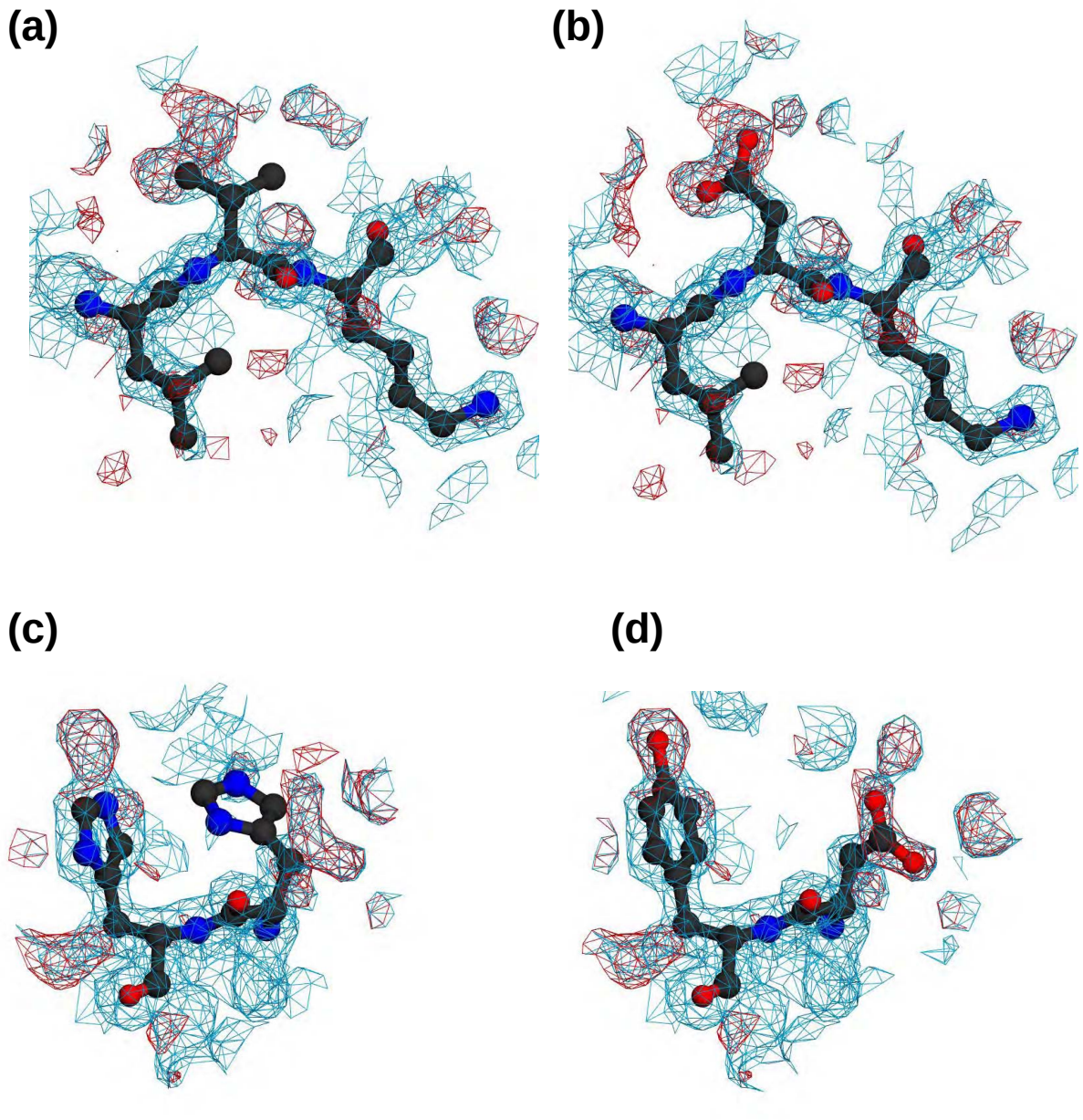

Figure 4.6. Unique electron density features used to validate molecular replacement of LILRB4 D1 structure. (a): Part of the LILRB4 electron density map after first rebuild, showing LILRA5 model residues L37, V38 and K39 in ball-and-stick representation. Note that V38 does not fit the observed electron density. (b): The same region after final structural solution, this time with LILRB4 residues L37, D38 and K39 in ball-and-stick representation. (c): Electron density map after first rebuild for another region, this time showing LILRA5 model residues H68 and H69 in ball-and-stick representation. (d): The same region after final structural solution showing how LILRB4 residues D68 and Y69 fit the observed electron density. The Fo-Fc map (depicted in red) is contoured at the 2σ level, whereas the 2Fo-Fc map (depicted in cyan) is contoured at the 1σ level.

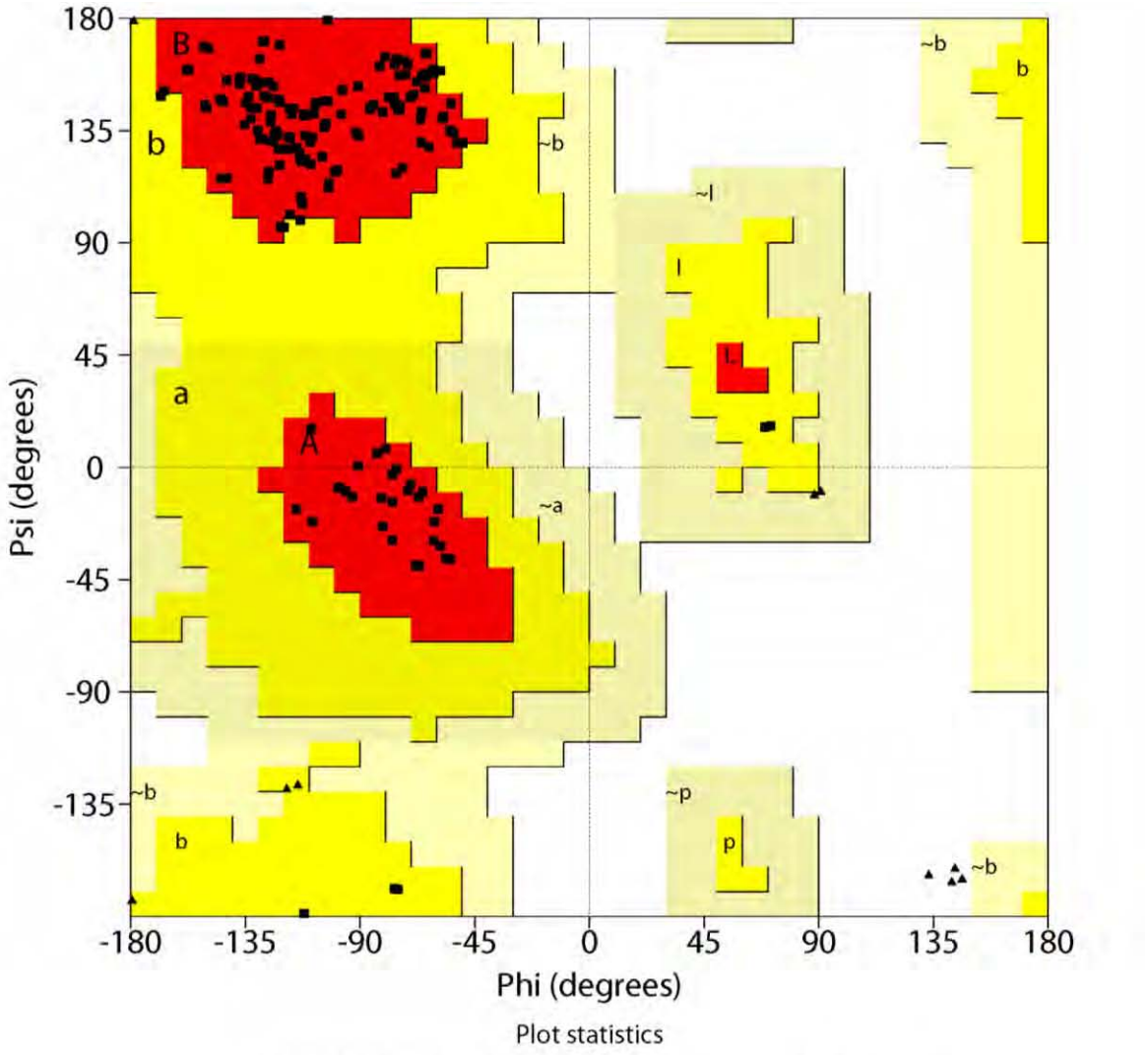

Plot statistics

Residues in most favoured regions [A,B,L]	138	93.2%
Residues in additional allowed regions [a,b,l,p]	10	6.8%
Residues in generously allowed regions [~a,~b,~l,~p]	0	0.0%
Residues in disallowed regions	0	0.0%
Number of non-glycine and non-proline residues	148	100.0%
Number of end-residues (excl. Gly and Pro)	4	
Number of glycine residues (shown as triangles)	10	
Number of proline residues	22	
Total number of residues	184	

Figure 4.7. Ramachandran plot for LILRB4 D1. The Phi and Psi dihedral angles for the peptide bond of each amino acid residue in the LILRB4 D1 structure are plotted as squares. The regions of the Ramachandran plot are categorized as most favoured (red), addionally allowed (yellow), generously allowed (cream) and disallowed (white). Glycine residues exhibit additional flexibility and are depicted as triangles.

Resolution (Å)	19.5-1.6
Reflections in working set	19991
Reflections in test set	1081
R_{work} (%)	20.3
R_{free} (%)	23.9
Number of protein atoms	1510
Average B-factor (Å^2) **Subunit A** **Subunit B**	 9.6 9.5
Number of water molecules	130

Table 4.6: Refinement Statistics for LILRB4 D1 structure.
R_{work} (F) = $\Sigma_h||F_{obs}(h)|$ - $|F_{calc}(h)||/\Sigma_h|F_{obs}(h)|$ and $|F_{calc}(h)|$ are the observed and calculated structure factor amplitudes for the h, k, l reflection. R_{free} is calculated over reflections in a test set not included in atomic refinement.

4.4.6 Overall Structure of LILRB4 D1 Domain

Structural analysis of LILRB4 D1 and comparisons with LILRB1, LILRB2 and LILRA5 D1 structures were performed with COOT and the CCP4 software suite (Collaborative Computational Project Number 4, Acta Cryst D 1994). All main-chain superpositions between the D1 domains of LILRB4 and LILRA5, LILRB1 and LILRB2 were conducted using LSQMAN (Kleywegt Acta Cryst D 1996). All molecular graphic figures were generated with MOLSCRIPT (Kraulis J App Cryst 1991) and rendered using POVRAY (http:// www.povray.org).

The two molecules of LILRB4 D1 in the asymmetric unit were designated A and B. Superposition of LILRB4 D1-A onto LILRB4 D1-B gave a very low Root Mean Square Deviation (RMSD) value of 0.16 Å, indicating that both molecules in the unit cell are essentially identical. Subsequent analysis of LILRB4 D1 was conducted using molecule A.

As expected the superposition of LILRB4 D1 onto LILRA5 D1 shows that the main chains of both proteins are structurally very similar (**Figure 4.8a**) and this is reflected in the low RMSD value of 1 Å. This raises questions as to whether LILRB4 and LILRA5 bind ligands that are structurally related. In contrast, superposition of LILRB4 D1 onto LILRB1 D1 (**Figure 4.8b**) revealed substantial differences in the main chain particularly in the C-C' loop and at the distal D1 tip, with a RMSD value of 3.5 Å, highlighting structural differences between Group I and Group II LILRs. Interestingly, the superposition of LILRB1 D1 onto LILRB2 D1 (**Figure 4.8c**) resulted in a relatively high RMSD value (3.1 Å) demonstrating that as a subset, Group I LILR proteins also exhibit large differences in their backbone topology. One of the most significant differences between LILRB1 D1 and LILRB2 D1 is at the loop at the distal tip of the D1 domain which conceivably contributes to the differences in affinity between LILRB1 and LILRB2 in binding to MHC Class I ligands and UL18 (Willcox et al. BMC Struc Bio 2002, Willcox et al. Nat Immun 2003). However, despite these differences the LILRB1 and LILRB2 membrane distal domains have similar overall secondary structure and bind the same MHC Class I ligands, thus an important caveat is that it is hard to extrapolate the similarity in backbone structure between LILRB4 and LILRA5 into a propensity to bind similar ligands (which are currently unknown).

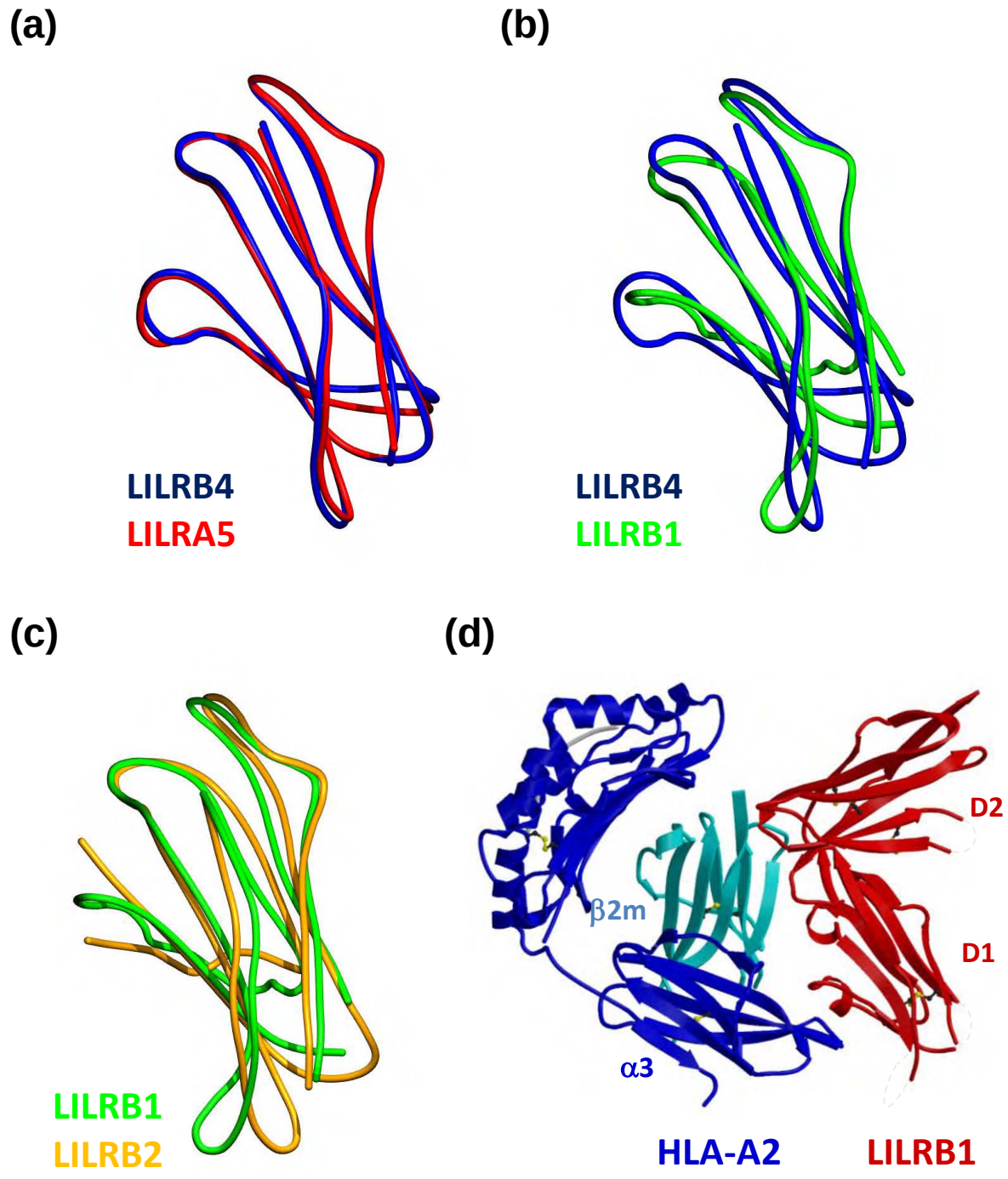

Figure 4.8. Main-chain superposition of LILRB4 D1 domain. LILRB4 superposed onto (a): LILRA5 (b): LILRB1. (c):LILRB1 superposed onto LILRB2 for comparison. (d): For orientation purposes the LILRB1 D1D2/HLA-A2 complex is shown. In panels (a), (b) and (c) the domain is orientated at the same angle as the D1 domain of LILRB1 as shown in (d), in which the MHC Class I binding face is pointing left and the distal tip of the D1 domain is at the bottom of the figure.

4.4.7 Secondary Structure Analysis of D1 Domains of Group I and Group II LILRs

The secondary structure of LILRB4 D1 was analysed using the CCP4 program PROCHECK and compared to LILRB1, LILRB2 and LILRA5 D1 secondary structures. The output from PROCHECK and the overall topology of the LILRB4 D1 domain are shown in graphical form in **Figure 4.9**.

The overall secondary structure topology of LILRB4 D1 is very similar to LILRA5 D1, with the standard C2-Ig type domain as conserved across the LILR family, comprising two anti-parallel β-sheets formed by the ABE and the CFG β-strands respectively, separated by a short 3_{10} helix region and with the G strand interrupted by a Polyproline Type II Helix motif. As in the other LILRs, the C strand is interrupted either by a loop region (LILRA5) or a helix (LILRB1 and LILRB2) resulting in the formation of a C and a C' strand. In LILRB4 D1 the A strand is defined as being much shorter by PROCHECK as the lack of electron density for residues at the C-terminal end of the G strand (due to disorder at the end of the D1 domain) causes some hydrogen bonding with A' to be disrupted, although the appearance of the A' strand on COOT is of that of an extended strand in a similar manner to the other LILRs.

The secondary structures of LILRB1, LILRB2, LILRB4 and LILRA5 D1 are shown in graphical form in **Figure 4.10**. By comparison with the known D1 domain structures of the Group I LILRs LILRB1 and LILRB2, the D1 domains of the Group II LILRs, LILRB4 and LILRA5, have fewer helical regions (lacking helices following the C strand) and have the distal D1 loop orientated in a more similar position to LILRB2 than to LILRB1.

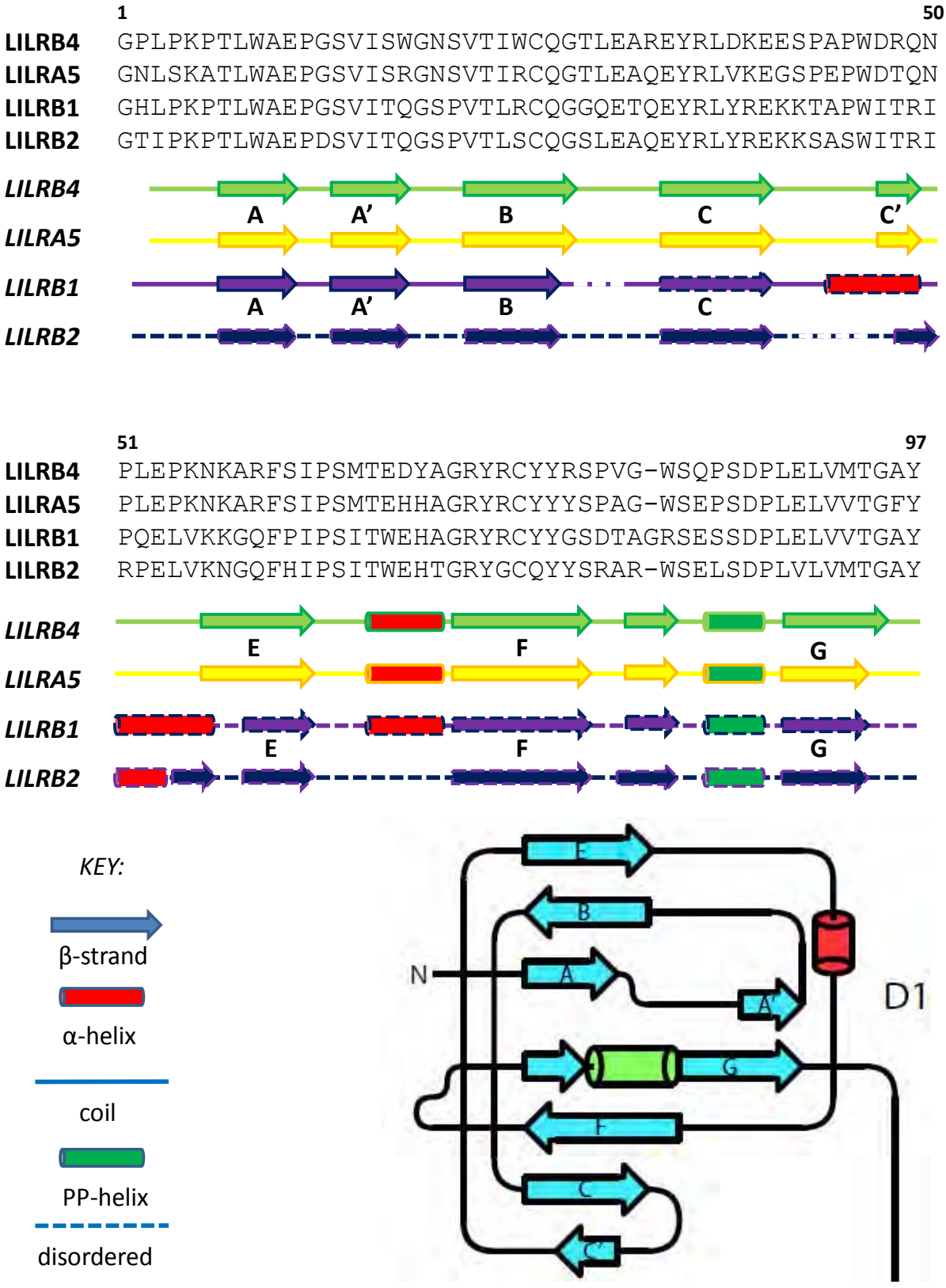

Figure 4.9. PROCHECK secondary structure assignment for LILRB4 D1. The output from PROCHECK is shown in two graphical forms, as an alignment of the primary sequence of LILR D1 structures with secondary structures indicated underneath (top panel) and as a topological map of the LILRB4 D1 domain (bottom panel). Interacting strands are adjacent to each other and helices are shown.

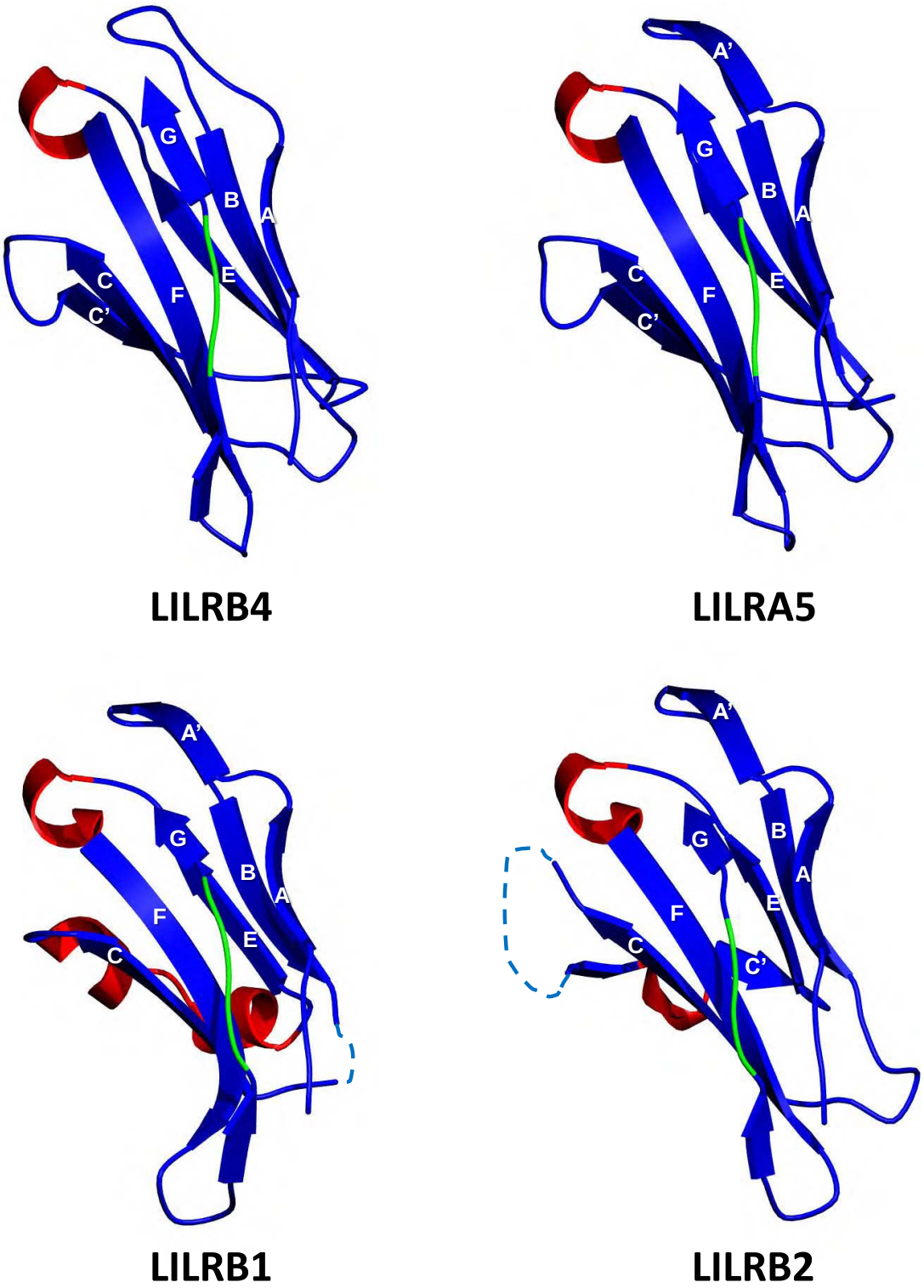

Figure 4.10. Comparison of tertiary structures of LILR D1 domains. LILRB4 D1 is shown alongside LILRA5 D1 (top panels). The D1 domains of the Group I LILRs, LILRB1 and LILRB2, are shown underneath for comparison. Images were generated using MOLSCRIPT and POVray. β-strands are shown as arrows and labelled with their strand designation; α-helices are shown in red and polyproline helices are in green. Disordered loops are shown as dotted lines. Orientation of each molecule is as in Figure 4.8.

4.4.8 Rationalisation for Non-binding of LILRB4 D1 to MHC Class I

Although the LILRB4 D1 structure is just a single domain, as opposed to the known structures of the binding domains of LILRB1 and LILRB2 which are the distal D1D2 domains, comparison of the structure and residue substitutions in this domain allowed the development of hypotheses for why LILRB4 does not bind to MHC Class I. Alignment of the primary amino acid sequences of LILRB1 D1 and LILRB4 D1 identified eight amino acid substitutions (**Figure 4.11**) that are located at the LILRB1/HLA-A2 binding interface (Willcox et al. Nat Immun 2003). Of these, only two are conservative substitutions (E68D and R39K) and the remaining are non-conservative changes that either involve charged (W67E, K41E, K42S and Y38D) or hydrophobic residues (Q18W and T43P). The net change in charge introduced by such substitutions is -5; thus the surface electrostatic potential at the CFG face, a region corresponding to the LILRB1-D1/HLA-A2 binding interface, is substantially more negatively charged. Notably, the substitution of Q18W and W67E may be compensatory, in order to maintain a hydrophobic tryptophan residue at the interdomain interface.

These non-conservative substitutions, which result in predominantly charge-related changes in comparison to LILRB1 D1, may disrupt LILRB4 D1 binding to the α3 and β_2m domains of MHC Class I, particularly as the α3 domain contacted by LILRB1/2 D1 domain is itself negatively charged (see below). In addition, the superposition of LILRB4 D1 onto the LILRB1/HLA-A2 complex structure shows that the conformation of the LILRB4 D1 C-C' loop encompassing residues 41-46 is substantially shifted, such that the A44 side chain could sterically clash with the backbone carbonyl of V194 of the α3 domain of MHC Class I and thus impair binding. Interestingly, the LILRB2 D1 helical region between the C and C'

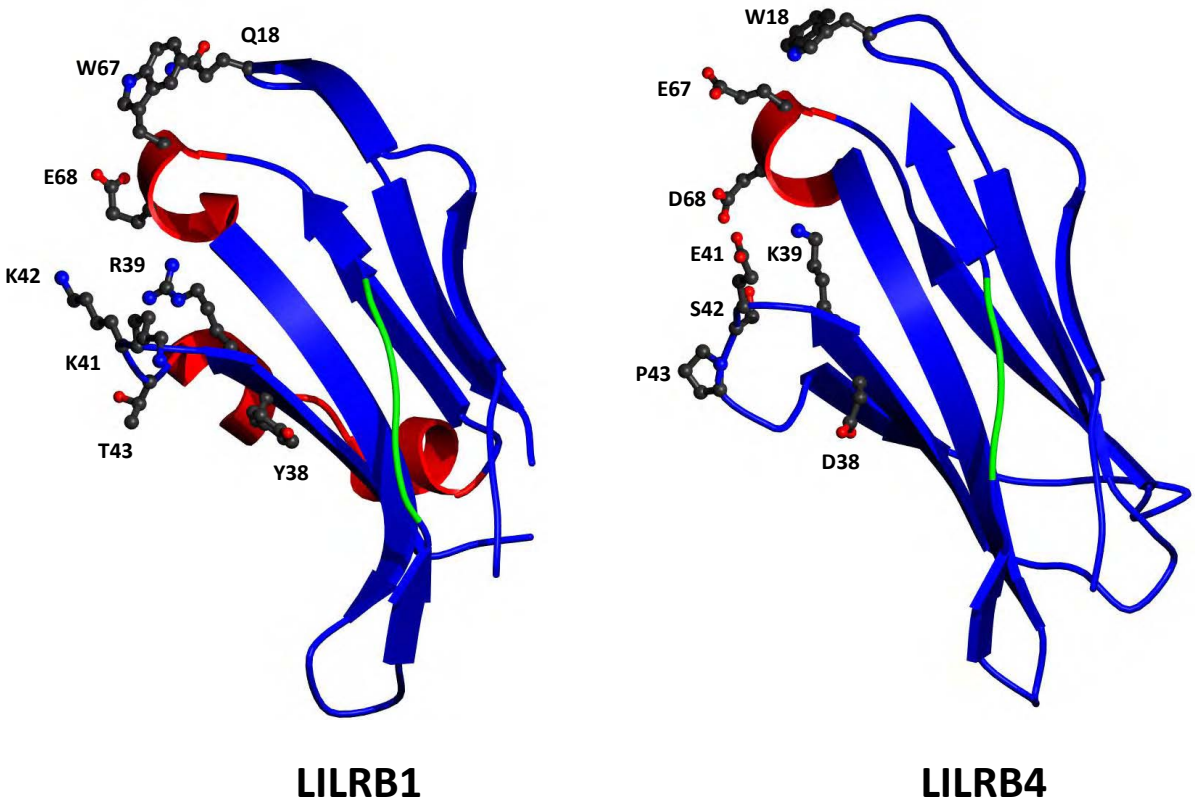

Figure 4.11. Amino acid substitutions between LILRB1 D1 and LILRB4 D1 located at the LILRB1 D1/HLA-A2 binding interface. Images were generated using MOLSCRIPT and POVray. β-strands are shown as arrows; α-helices are shown in red and polyproline helices are in green. Amino acid side-chains for substituted residues are shown in ball-and-stick representation. Orientation of each molecule is as in Figure 4.8.

strands has been implicated in binding to HLA-G (Shiroishi et al. PNAS 2006) and the lack of such a helix in LILRB4 D1 provides further evidence for its failure to bind MHC Class I.

This helix is also absent in LILRA5, which is known not to bind to MHC Class I. Mapping of the LILRA5 substitutions on the LILRB1/HLA-A2 binding interface also suggest that binding to MHC class I would be unlikely (Willcox et al. Nat Immun 2003, Shiroishi et al. JBC 2006). The structural elements of LILRB4 D1D2 which make it unsuited to MHC Class I recognition are discussed extensively in Section 4.5.4.

4.4.9 Comparison of LILRB4 D1 with LILRA5 D1

LILRA5 has the closest primary sequence comparison to LILRB4 across the whole LILR family, with 83 % identity across the D1 domain. Based on sequence alignments of the LILRA5 D1 and LILRB4 D1 domains it has been possible to map the substituted residues onto the corresponding tertiary structures. Of the 18 amino acid substitutions found between LILRA5 D1 and LILRB4 D1, ten substitutions involve charge changes which comprise R18W, R25W, Q33R, V38D, G41E, E44A, T48R, M68D, Y78R, and E85Q. In particular, this analysis has revealed significant changes in charge distribution between LILRA5 and LILRB4 from electronegative to electropositive residues (E44A, T48R, E85Q, Y78R and Q33R), particularly at the CFG face and D1 distal tip (which is important for LILRB1 and LILRB2 binding to MHC Class I). This is illustrated in **Figure 4.12**.

The large difference in surface charges between LILRB4 D1 and LILRA5 D1 across the CFG face is clearly visible when calculating the electrostatic potential for each residue and generating the electrostatic surface for each receptor using GRASP (Nicholls et al. Proteins:

Struc Func Genet 1991), as illustrated in **Figure 4.13**. I would hypothesise that this could have implications for ligand binding between the two Group II receptors. The broad difference in the electrostatic surface between LILRB4 D1 and LILRA5 D1 could suggest that the ligands for LILRB4 and LILRA5 are different, despite the overall structural similarity. Further investigation into the structures of other Group II LILRs is warranted and may indeed delineate the LILR family into additional sub-groups.

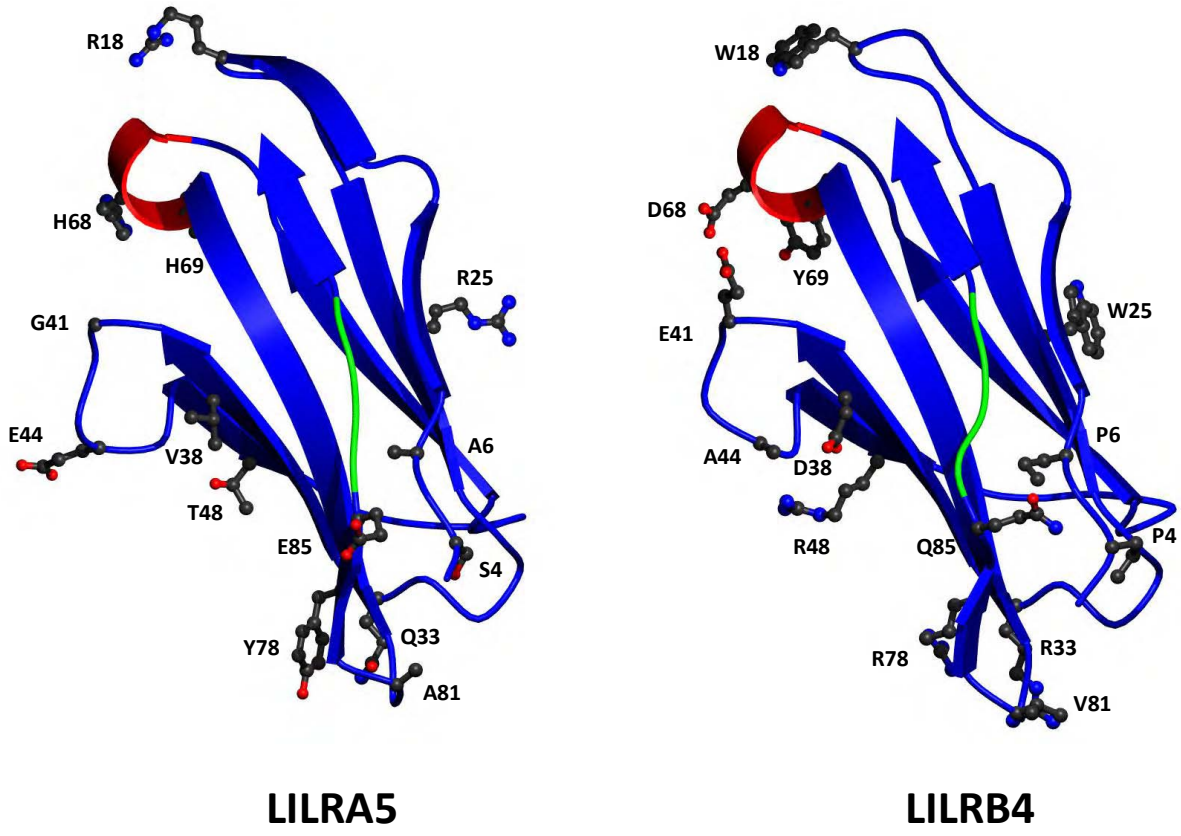

Figure 4.12. Amino acid substitutions between LILRA5 D1 and LILRB4 D1. Images were generated using MOLSCRIPT and POVray. β-strands are shown as arrows; α-helices are shown in red and polyproline helices are in green. Amino acid side-chains for substituted residues are shown in ball-and-stick representation. Orientation of each molecule is as in Figure 4.8.

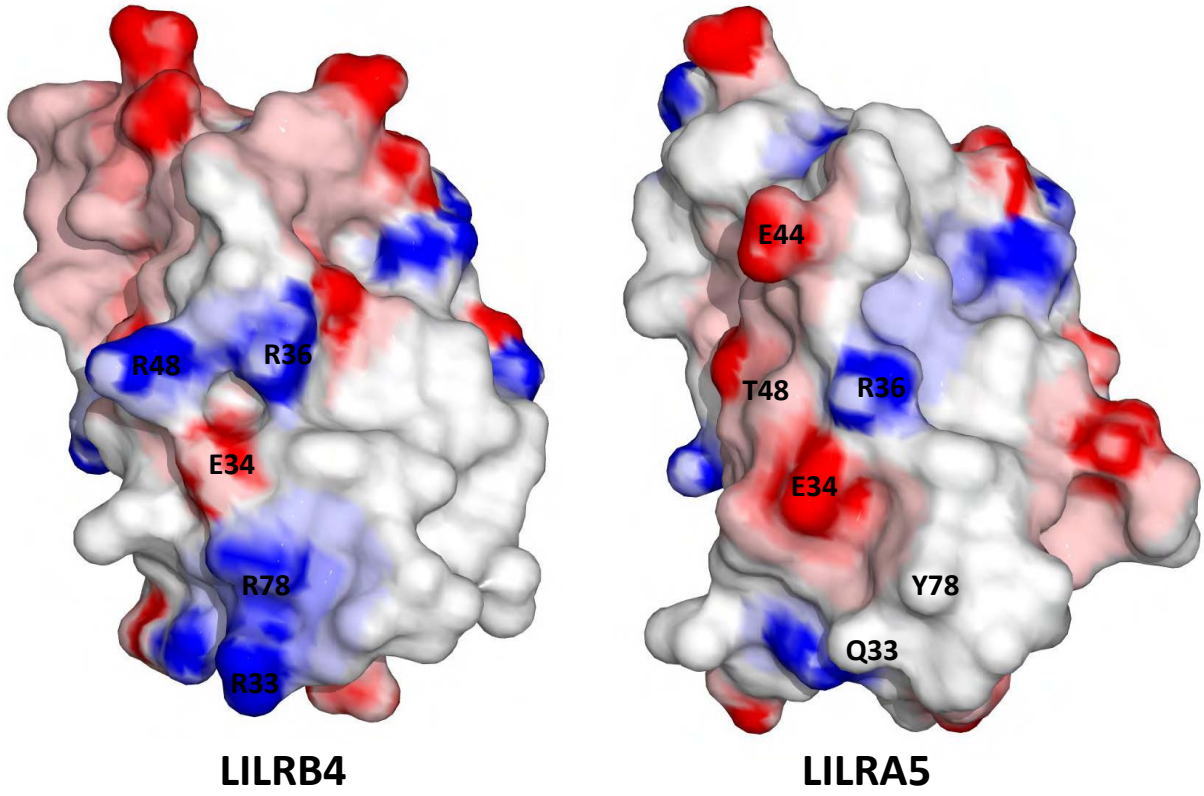

Figure 4.13. Electrostatic surface potential of LILRB4 D1 compared to LILRA5. LILRB4 D1 and LILRA5 D1 molecular surface depicted using GRASP with electropositive residues shown in blue and electronegative residues in red. The molecule is oriented with the CFG face – which corresponds to the MHC Class I binding surface in LILRB1/LILRB2 - towards the observer. Selected residues have been labelled.

4.5 Structural Analysis of LILRB4 D1D2 Incorporating a Non-native Disulphide Bond

Recently, we were approached by Professor George Gao (Chinese Academy of Sciences, Beijing, China) who contacted the Willcox group with the news that his group had successfully determined the crystal structure of the full ectodomain (D1D2) of LILRB4. A collaboration was established whereby my role was to comprehensively analyse the LILRB4 D1D2 structure, compare it with my LILRB4 D1 structure, and determine the implications of each for LILRB4 ligand recognition.

4.5.1 Generation, Crystallisation, and Structure Solution of LILRB4 D1D2

As described above, crystallisation of the wild-type D1D2 ectodomain of LILRB4 had proven problematic, both for myself and for the Gao group. To overcome intransigent crystallisation LILRB4 was engineered to include a non-native disulphide bond, based on the observation that LILRB1 and LILRB2, which both crystallised readily, contained an additional disulphide bond in the D2 domain, close to the C-C' flexible loop region. By introducing mutations to comparable positions in LILRB4 (I133C and H143C), it was hoped to stabilise the D2 C-C' flexible loop region, which was hypothesised to affect protein stability and crystallisation. This strategy had previously been employed to facilitate the structural determination of LILRA2 (Chen et al. JMB 2007). Mutated LILRB4 D1D2 was found to have higher stability and could be concentrated to substantially higher levels than the wild-type protein, displaying considerably less precipitation during concentration steps.

The mutated LILRB4 protein was subsequently successfully refolded by standard Garboczi methods (Garboczi et al. PNAS 1992); analysis of the mutated protein was carried out by the

Gao group by size exclusion chromatography, analytical ultracentrifugation (AUC) and SDS-PAGE and the protein was judged to be correctly folded and pure enough for crystallisation trials. In addition, their AUC data showed a narrower molar mass distribution peak suggesting reduced flexibility of the protein with the engineered disulphide bond as compared to wild-type LILRB4 (data not shown). In contrast to wild type LILRB4, the mutated LILRB4 D1D2 protein was crystallized to data-collection quality at 4 °C in hanging drops equilibrated against a reservoir solution containing 0.2 M sodium sulfate heptahydrate, 20 % w/v PEG 3350. The crystal diffracted X-rays to a resolution of 1.8 Å resolution and belongs to the tetragonal space group $P4_12_12$, (unit cell constants: a= b= 61.92 Å, c= 115.87 Å, α= β= γ= 90°), with one LILRB4 molecule per asymmetric unit.

The LILRB4 D1D2 structure was determined by molecular replacement using LILRA5 D1D2 as the search model with MOLREP (Vagin and Teplyakov Acta Cryst D Bio Cryst 2010) and PHASER (McCoy Acta Cryst D Bio Cryst 2007). Refinement of the molecular model was carried out in CNS and REFMAC5, interspersed with iterative manual rebuilding with the program COOT. Subsequent 2Fo-Fc and annealed omit electron density maps allowed for the placement of all LILRB4 residues. After further cycles of refinement the R_{work} and R_{free} converged to 18.7 % and 22.1 %, respectively for all data between 50 Å and 1.8 Å (Chen et al, manuscript in preparation).

Superposition of my LILRB4 D1 structure onto the LILRB4 ectodomain structure showed a high degree of correlation between the two structures, with RMSD values of 0.71 Å and 0.72 Å for the A and B subunits, respectively, onto the D1 domain of the ectodomain structure,

indicating the D1 conformation of each structure was essentially identical. This lends a high degree of confidence about the validity of both structures.

4.5.2 Overall Structure of LILRB4 D1D2

The LILRB4 D1D2 structure is comprised of two C2-type Ig-like domains arranged at a ~ 90° angle, and defined as D1 (residues 2-95) and D2 (residues 96-195). The disulphide bonds formed between C26 and C75 in D1, C121 and C172 in D2, in addition to the artificial disulphide introduced between C133 and C143, collectively stabilize the arrangement of six β-strands into two anti-parallel β-sheets per domain, as observed in other members of the LILR family. The most notable difference with LILRB1 and LILRB2 include the lack of the helical region following the C strand in D1, which is consistent with the LILRB4 D1 structure (see Section 4.4.6). In addition, LILRB4 displays two novel 3_{10} helical regions not previously observed in other LILR receptors, one located between the C-C' strands, and another between the E-F strands (**Figure 4.14a**). The divergence in the D2 domain of LILRB4 is consistent with the finding that its primary sequence has higher identity with the D4 domains of the other LILR family members and has been noted before in an early LILR publication (Borges et al. JI 1997) and discussed here in Section 4.2. However, arguably the most striking feature of the structure was the interdomain angle. In contrast to previous LILR structures, where the D1-D2 interdomain angles are ~84 - 90° in their ligand-free forms, the LILRB4 structure displayed an obtuse D1-D2 interdomain angle, of 107° (**Figure 4.14b**).

The topology of the LILRB4 domains was similar to that of other LILRs, but with some distinctive features (**Figure 4.14c**). In the D1 domain, LILRB4 displays some topological

differences compared to LILRB1 and LILRB2. In these Group I receptors, the region between the C and E strands, which in many Ig domains forms a strand termed D, instead includes helical secondary structural elements (Chapman et al. Immunity 2000, Willcox et al. BMC Struc Bio 2002). In contrast, in LILRB4 D1, the corresponding region is replaced by a β-strand termed C' that pairs with strand C, as in the KIR receptors (**Figure 4.14c**), and also observed in the LILRB4 single domain D1 structure. Interestingly, recent studies have shown that the 3_{10} helix region between the C-E strands in LILRB2 D1 is directly involved in the recognition of the α3 domain of HLA-G (Shiroishi et al. PNAS 2006), and the corresponding region of LILRB1 also forms interactions with the α3 domain of HLA-A2 (Willcox et al. Nat Immun 2003). Alterations in this region of LILRB4 relative to LILRB1/LILRB2 could therefore affect LILRB4 ligand interactions. Notably, the C' strand observed in LILRB4 has previously been noted in LILRA2 and LILRA5, suggesting this topological feature can be present in both Group I and Group II receptors and in Group II is not restricted to LILRA5. In contrast to the loss of helical elements in the C-E region in LILRB4, the 3_{10} helix observed between E and F strands in LILRB1, LILRB2 and LILRA5 is preserved in LILRB4. These findings were entirely consistent with our previous analysis of the LILRB4 D1 domain structure.

In D2, LILRB4 displays two novel 3_{10} helical regions not previously observed in other LILR receptors, one located between the C-C' strands, and another between the E-F strands (**Figure 4.14c**). For the C-C' helix, the possibility cannot be excluded that introduction of the additional disulphide bond into this region affects that propensity for 3_{10} helix formation. However, notably LILRB1 and LILRB2 contain this additional disulphide in their native form, and do not have a helix in this region, suggesting instead the divergent sequence of

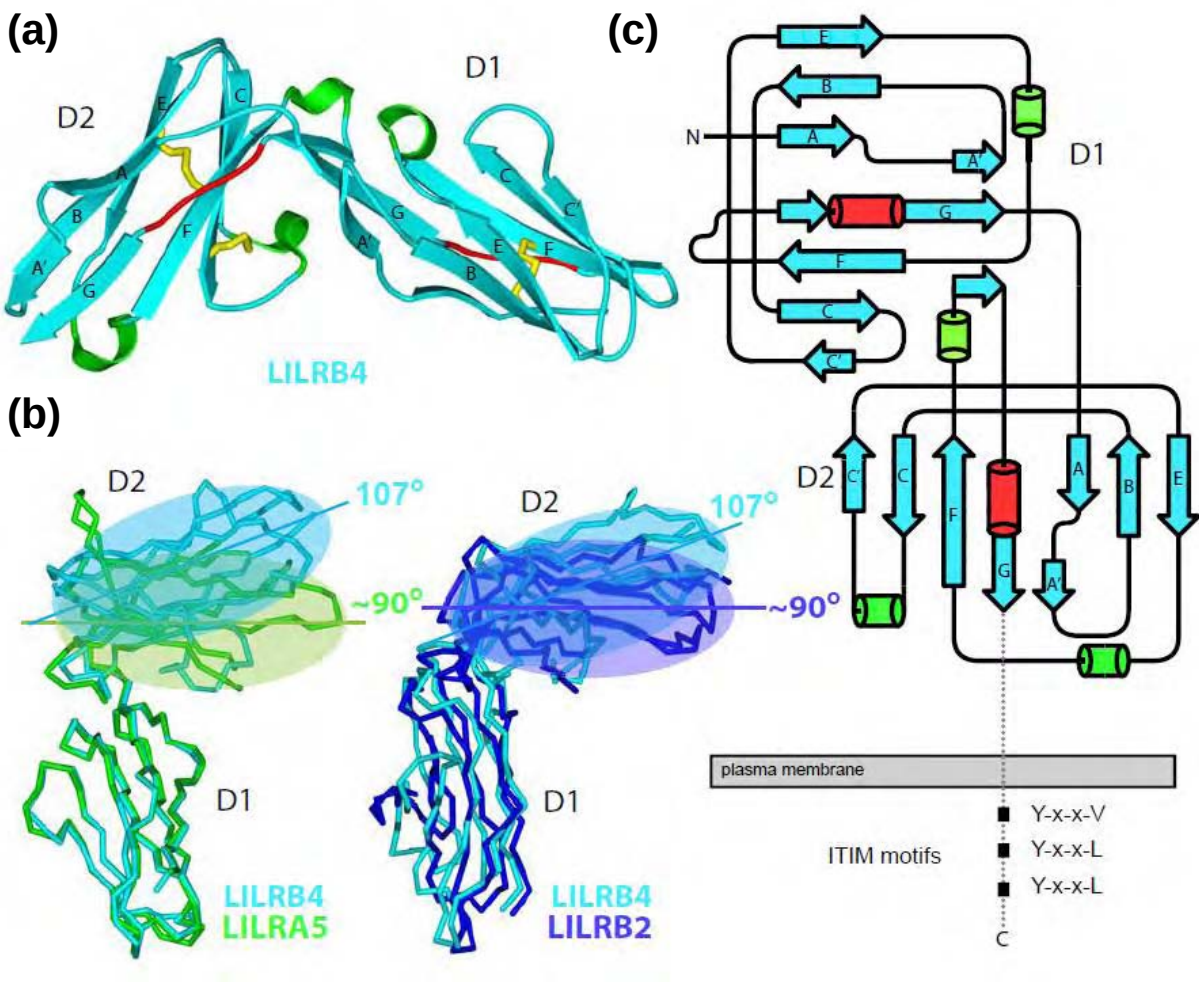

Figure 4.14. Overall LILRB4 D1D2 structure. (a): Tertiary structure of LILRB4 D1D2 generated using MOLSCRIPT and POVray. β-strands are shown as arrows with their strand designation, helices are shown in green for 3_{10} helix and red for polyproline Type II helix, and disulphide bonds are shown in yellow. (b): Comparison of the interdomain angles of LILR family members using DomAngle software. Protein backbones are shown, with LILRB4 in cyan, LILRA5 in green and LILRB2 in blue. The more obtuse angle of LILRB4 is readily apparent. (c): Topological map of the secondary structure of LILRB4 D1D2 as calculated using PROCHECK, showing strands as arrows and helices as cylinders (note 3_{10} helices are in green and polyproline helices are in red). The stalk region, transmembrane domain and cytoplasmic domain are shown as a dotted line.

LILRB4 in this region relative to other LILRs may underlie this novel structural feature. Finally, in addition to 3_{10} helical regions, LILRB4 also contains a region of polyproline II helix in the F-G loop of each domain, and this is also present in LILRB1, LILRB2 and LILRA5 as well as other LRC receptors such as KIRs (Saulquin et al. JEM 2003) and NKp46 (Foster et al. JBC 2003).

4.5.3 Structural Features at the LILRB4 D1D2 Interface

Analysis of the LILRB4 D1-D2 interdomain interface using the program CONTACT indicated a buried surface area of 878 $Å^2$, intermediate between that of LILRB1 (946 $Å^2$) and LILRB2 (776 $Å^2$) and comparable with LILRA5 (843 $Å^2$). Consistent with a broadly similar interdomain interface, some of the hydrogen bonding interactions present at the D1-D2 interface in LILRB1, LILRB2 and LILRA5 were conserved in LILRB4. These interactions are located from the D1 F strand (R72) to the short strand bearing Y183 in LILRB1 (equivalent to Y181 in LILRB4) as shown in **Figure 4.15a**.

However, several other hydrophobic interactions were altered. Firstly, the hydrophobic interactions between W67 and E184 in LILRB1 are lost as the residues are replaced in LILRB4 by E67 and L182 (**Figure 4.15a-b**). This decreases interdomain interactions as E67 loses all contacts to L182. Although LILRA5 also has E67, this mediates compensatory interactions with F97, whereas this is not the case in LILRB4 as the interaction with the side-chain of F97 is replaced with the shorter side-chain of A97.

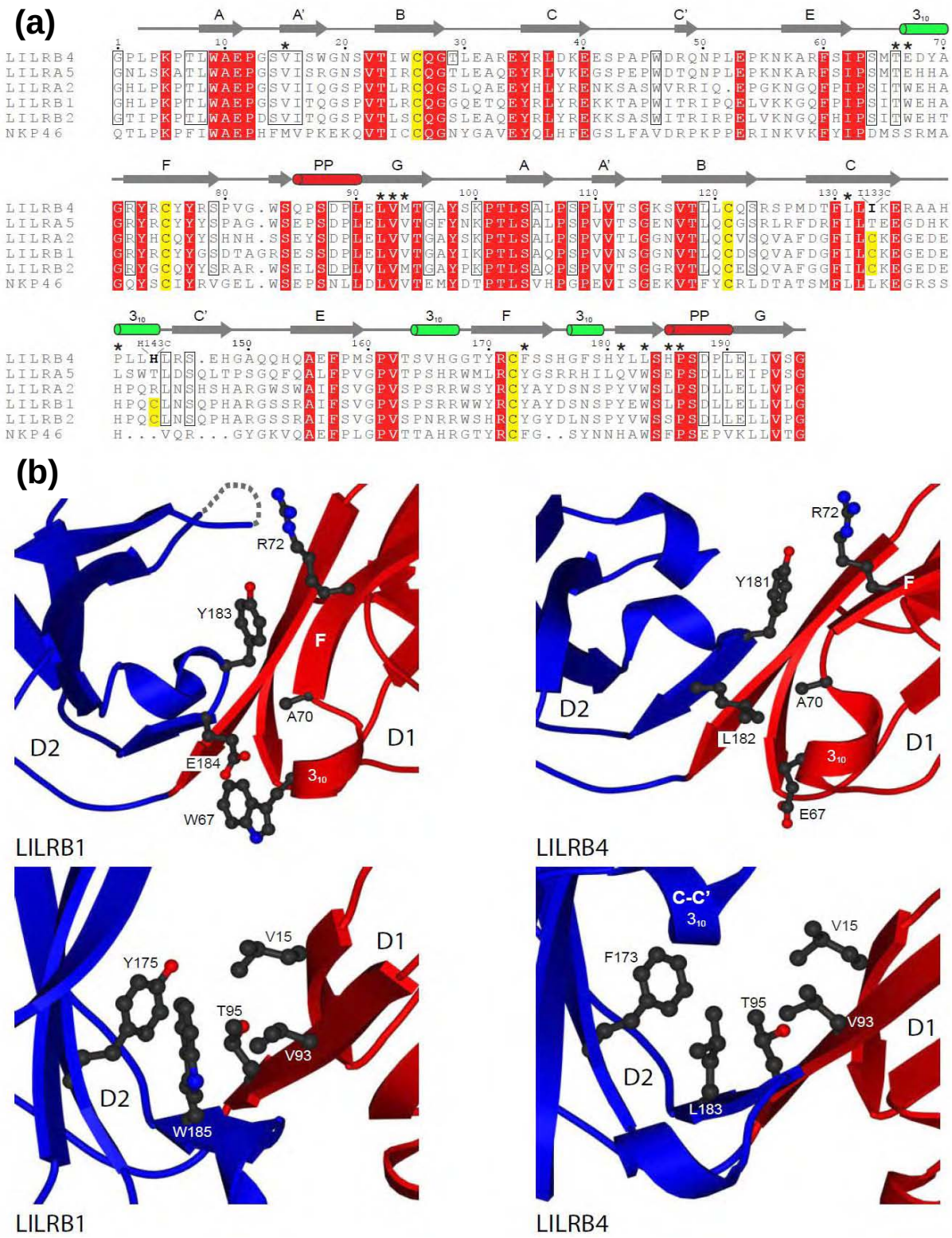

Figure 4.15. Analysis of the LILRB4 interdomain interface. (a): Sequence alignment of known LILR structures and NKp46. * indicates interface stabilizing residues. Conserved residues are boxed/shaded red. Disulfide bond cysteines are shaded yellow. LILRB4 secondary structure is shown with 3_{10} helices in green and polyproline type II helices in red (b): LILRB4 and LILRB1 D1-D2 interfaces compared. Key residues are shown in ball-and-stick representation. Top and bottom panels show slightly different orientations, for clarity.

A second alteration is the substitution of Y175 in LILRB1 (also conserved at the equivalent position in LILRB2 and LILRA5) with a phenylalanine residue at the corresponding position (F173) in LILRB4 (**Figure 4.15b**) which makes substantially fewer contacts. Finally, arguably the most significant alteration at the LILRB4 D1-D2 interface is substitution of W185 (present in LILRB1, LILRB2 and at the equivalent W184 in LILRA5) to the less bulky leucine residue at the equivalent position in LILRB4 (L183) (**Figure 4.15b**). The shorter size of the L183 side-chain in LILRB4 results in reduced contacts to V15 and V93 as compared with the extensive contacts between W185 and these residues in LILRB1, LILRB2 and LILRA5. Strikingly, L183 of LILRB4 only makes 22 contacts to neighbouring atoms (<4.00 Å), whereas the equivalent W184 in LILRA5 forms 44 contacts. These observations indicate that the LILRB4 D1-D2 interface, although of a similar size to that of other LILR family members, involves considerably fewer stabilizing hydrophobic interactions.

4.5.4 LILRB4 D1D2 is Conformationally and Electrostatically Unsuited for Recognition of MHC Class I

The crystal structures of LILRB1/HLA-A2 (Willcox et al. Nat Immunol 2003) and LILRB2/HLA-G complexes (Shiroishi et al. PNAS 2006) showed that the ligand binding portion of LILRB1/2 comprises residues located in two distinct surface patches, firstly a membrane distal portion of the D1 domain that forms contacts to the HLA α3 domain, and secondly in the inter-domain D1-D2 hinge region, which contacts the β_2m domain. These interacting residues are highly conserved among Group I LILRs, but extremely poorly conserved in Group II LILRs including LILRB4 and LILRA5. Determination of the LILRB4 structure allowed the conformation and electrostatic properties of these potential interaction

surfaces to be examined, as well as alterations in the LILRB4 interdomain orientation relative to MHC Class I-bound forms of LILRB1 and LILRB2 to be assessed.

Preliminary analysis of the LILRB4 D1D2 structure particularly in regions analogous to the MHC Class I-binding surfaces of LILRB1 and LILRB2 (i.e. the distal D1 tip and the D1D2 hinge region), did not reveal gross structural changes in these regions, despite the low amino acid conservation at these two sites. However, superposition of the LILRB4 D1 and D2 domains onto the previously determined LILRB1/HLA-A2 complex structure (Willcox et al. Nat Immunol 2003) provided a clear rationale for why this mode of MHC Class I recognition could not be feasible for LILRB4.

In terms of contacts with the α3 domain, in LILRB1, residues within strand C and the loop following strand C (including Y38, K41 and T42) as well as Y76 in the F strand, form hydrophobic and van der Waals contacts to residues V194, S195, D196, T200 and V248 of the α3 domain of HLA-A2. Although no drastic steric clashes are evident in the LILRB4/HLA-A2 superposition at this region, non-conservative amino acid substitutions are prevalent and there are secondary structural rearrangements, with the 3_{10} helix present in LILRB1 replaced by the C' strand in LILRB4. Consequently the potential molecular contacts at the LILRB1/α3 interface are likely to be lost in LILRB4.

With regards to the β_2m domain, the substitution of Q18 (LILRB1) with W18 (LILRB4) creates substantial steric clashes with Q89 of β_2m (**Figure 4.16**) and results in the loss of hydrogen bonding between these two residues. The loss of LILRB1 W67 (replaced with E67 in LILRB4) reduces a significant number of hydrogen bonding, van der Waals and

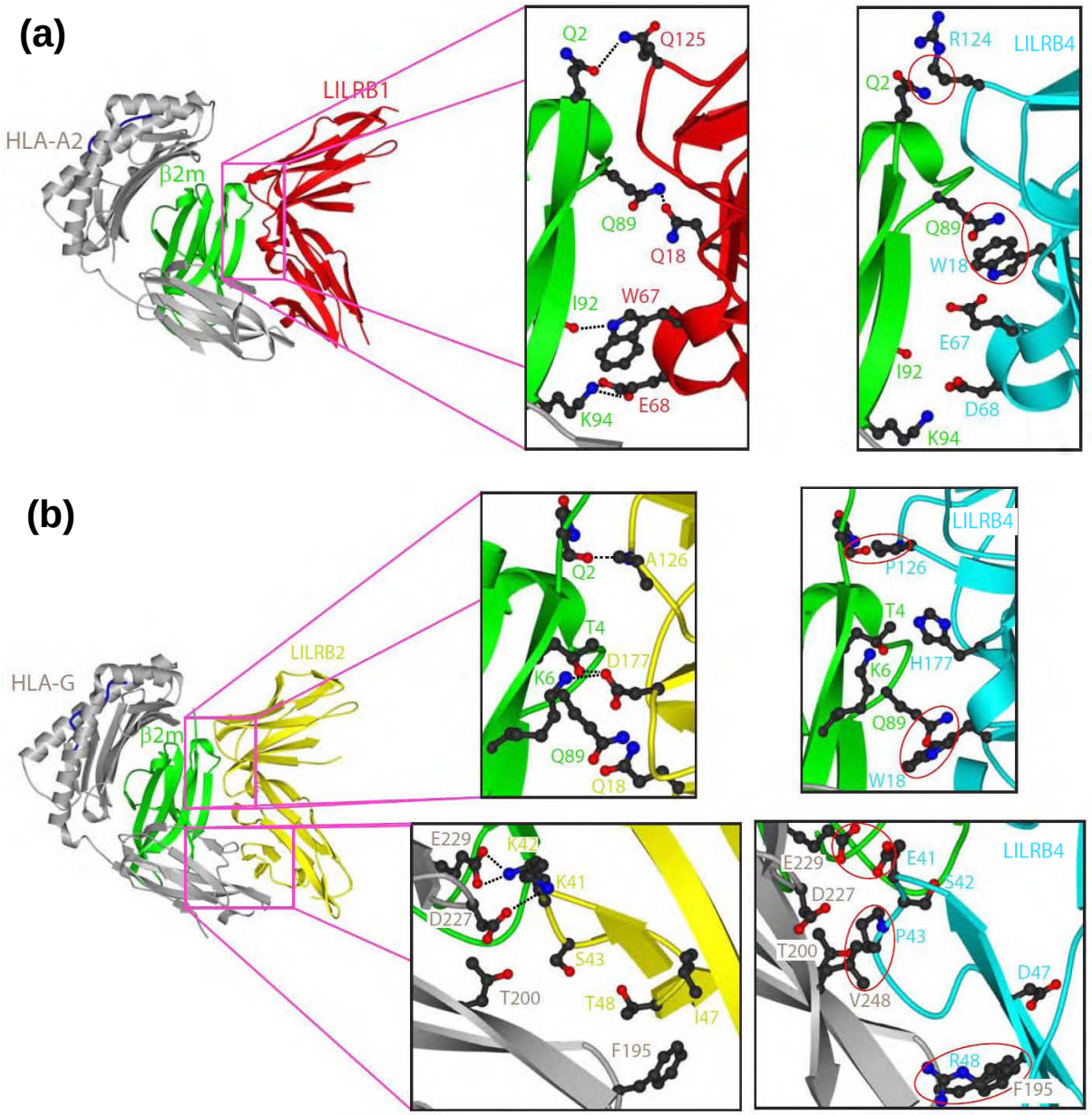

Figure 4.16. Conformational incompatibility at the LILRB4/MHC Class I interface. (a): Analysis of the LILRB1/HLA-A2/β_2m interaction (far left), and expanded views of LILRB1 contacts with the β_2m moiety (centre), and of critical changes at the hypothetical LILRB4/β_2m interface (right, with steric clashes indicated by red circles). The β_2m moiety is shown in green, with LILRB1 in red, and LILRB4 in cyan. (b): Analysis of the LILRB2/HLA-G/β_2m interaction (far left), with expanded views of LILRB2 contacts with the β_2m moiety (top centre), and of critical changes at the LILRB4/β_2m interface (top right) The lower expanded panels show LILRB2 contacts at the HLA-G α3 domain (centre), and relevant alterations at the hypothetical LILRB4/HLA-Gα3 interface (right). The HLA-G heavy chain is shown in grey, β_2m in green, and LILRB2 and LILRB4 in yellow and cyan, respectively. As for (a), likely steric clashes are indicated by red circles.

hydrophobic interactions with K91, I92 and V93 of the HLA-A2 β_2m domain and would thus be energetically unfavourable, in addition to changing the electrostatic properties in this region. Conservation of electrostatic charge via the LILRB1 E68 to LILRB4 D68 is apparent however the shorter D68 side-chain is unable to maintain the bidentate salt bridge to K94 of the β_2m domain which is present in the LILRB1/HLA-A2 complex.

Finally, substitution of Q125 (LILRB1) with R124 (LILRB4) results in the loss of a side-chain hydrogen bond and creates a steric clash with the side-chain of residue Q2 (β_2m), contributing to many of the disallowed contacts between the LILRB4 D2 domain and the β_2m domain of HLA-A2. Furthermore, minor clashes are observed between residue H153 (LILRB4) and residue I1 (β_2m) (**Figure 4.16a**). Therefore, amino acid changes at the LILR/β2m interface would be predicted to result in both steric clashes and loss of individual contacts.

Superposition of the LILRB4 D1 and D2 domains onto the LILRB2/HLA-G complex also highlighted a combination of steric clashes, loss of contacts, and electrostatic repulsion effects at the interaction surfaces, which also strongly suggest that LILRB4/MHC Class I binding is unlikely. In terms of the α3 domain residues of HLA-G, a number of steric clashes occur with the LILRB4 C-C' loop and C' strand (R36, P43, A44, P45 and R48). The salt bridge between K41 (LILRB2) and D227 (HLA-G) is lost by the substitution to E41 in LILRB4 and replaced with electrostatic repulsion of similar charges. In a similar fashion, the bidentate salt bridge between K42 (LILRB2) and E229 (HLA-G) is disrupted by the replacement to the uncharged residue S42 in LILRB4 (**Figure 4.16b**). In addition, secondary structure changes resulting from the substitution of S43 (LILRB2) to P43 (LILRB4) introduces steric clashes with the

side chain of V248 (HLA-G) and loss of interactions with T200 in the α3 domain. The substitution of I47 and T48 (LILRB2) with D47 and R48 (LILRB4) results in the loss of interface stability due to impaired hydrophobic contacts with F195 (HLA-G) and a steric clash with R48 (LILRB4), in addition to greatly changing the electrostatic properties at this interaction surface.

In terms of LILR interaction with the HLA-G β2m domain, hydrogen bonding between A126 (LILRB2) and Q2 of β2m is eliminated by the change to P126 (LILRB4) and furthermore causes a steric clash between these two residues. The Q18 (LILRB2) to W18 (LILRB4) substitution also creates a steric clash with Q89 of β_2m in a similar fashion to the LILRB4/HLA-A2 superposition. Finally, substitution of D177 (LILRB2) to H177 (LILRB4) results in the disruption of a salt bridge to β2m residue K6 and loss of a hydrogen bonding interaction to T4, thereby reducing the favourable interactions necessary for LILR binding to MHC Class I (**Figure 4.16b**).

As well as the specific electrostatic charge changes and loss of salt bridges discussed in detail above, comparison of the electrostatic surfaces of the LILRB1/HLA-A2 complex and LILRB2/HLA-G complex with LILRB4 also suggested LILRB4 was unsuited for the recognition of MHC Class I. **Figure 4.17a** shows an overview of the LILRB1/HLA-A2 complex colored by electrostatic potential. Notably, the α3 region of the MHC Class I heavy chain for both HLA-A2 and HLA-G contacted by the LILRs is predominantly negatively charged and features numerous acidic residues. The α3-interacting surface on both LILRB1 and LILRB2 is relatively positively charged (**Figure 4.17a-b**), and several interacting residues are basic, including R39 and K41 (on LILRB1) and R36, K41 and K42 (on LILRB2), suggesting substantial electrostatic complementarity between the interacting surfaces.

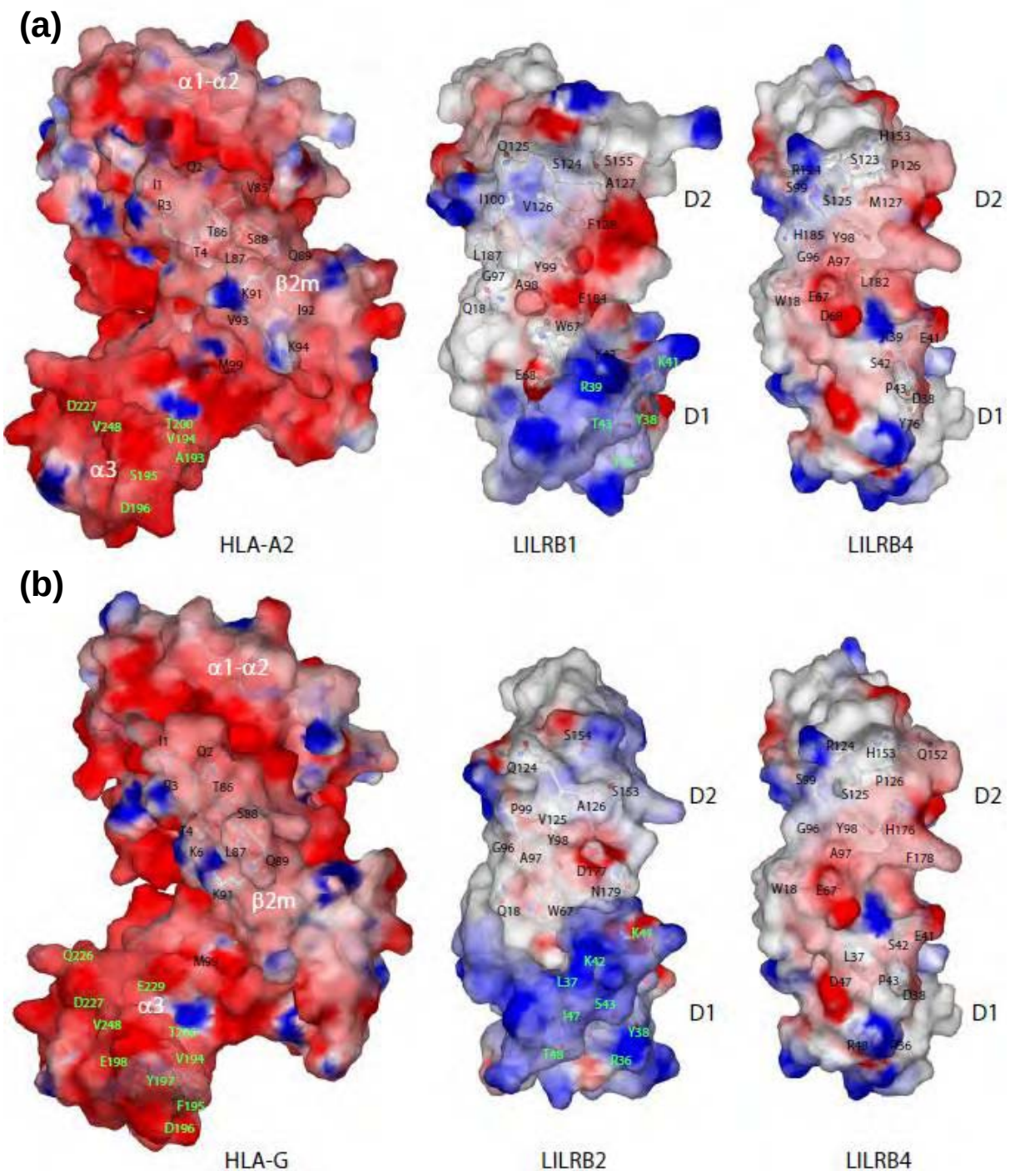

Figure 4.17. Electrostatic incompatibility at the LILRB4/MHC Class I interface. (a): Electrostatic surface representations of HLA-A2 (left), LILRB1 (centre) and LILRB4 (right), with the LILR receptors rotated to show the interaction surface. Residues involved in LILRB1- β_2m interaction are indicated in black, and those involved in LILRB1-α3 interaction in green. Equivalent residues on LILRB4 are all shown in black. (b): Electrostatic surface representations of HLA-G/β_2m (left), LILRB2 (centre) and LILRB4 (right). Interacting residues are colour-coded as in (a).

However, the comparable LILRB4 surface that would contact the α3 domain residues is considerably less positively charged than that of LILRB1 and LILRB2 (**Figure 4.17a-b, right panels**). Furthermore, within this surface, there is a K41E change that reverses charge and would introduce electrostatic repulsion at the interface with MHC Class I. In addition, whereas in the LILRB2/HLA-G interaction hydrophobic interactions with the aromatic residue F195 on HLA-G are mediated by I47 and T48 on LILRB2, in LILRB4 these are changed to D47 and R48, respectively, resulting in a highly charged surface in proximity to the hydrophobic HLA-G residue (**Figure 4.17b**). Furthermore, D177 on LILRB2 forms salt bridges to K6 on HLA-G (β2m), whereas in LILRB4 this residue is altered to H176, eliminating this charged residue and the interactions it mediates. Therefore, the electrostatic properties of LILRB4 are unsuitable for recognition of MHC Class I in comparison to the MHC Class I-recognising receptors LILRB1 and LILRB2.

These findings collectively suggest that the region of LILRB4 equivalent to the ligand binding surface of LILRB1 and LILRB2 is unsuited for MHC class I interaction, both in terms of conformation and also the chemical nature of the surface. Consistent with these differences, neither LILRB4 nor the related Group II receptor LILRA5 have shown any significant binding to MHC Class I molecules (Shiroishi et al. JBC 2006, Garner et al. Prot Exp Pur 2006).

4.6 Implications of LILRB4 D1 and LILRB4 D1D2 Structures for Ligand Recognition

Although the ligands of LILRB4 are unknown, analysis of the LILRB4 structure was conducted to try to identify components of an interaction surface or surfaces for ligand binding. Firstly, manual inspection of the surface of the D1 domain structure using COOT highlighted a group of residues on the ABE face of the domain, consisting of two exposed hydrophobic residues (W9 and W25), with three charged groups in close proximity (E11, K57 and R59). The residues contributing to this putative binding site are conserved across Group II LILRs with the exception of W25 in LILRA5 (substituted by R25) and R59 (it is substituted conservatively to K59 in LILRB5 and LILRA2). The two solvent-exposed tryptophan side-chains would constitute a hydrophobic patch at the ABE face opposing the CFG face which is involved in contacting MHC Class I in LILRB1 and LILRB2 (**Figure 4.18a**). Closely-grouped hydrophobic residues at the surface of a receptor are often indicative of a potential binding site. Intriguingly, in the LILRB4 ectodomain structure this region interacts with a sulphate anion (**Figure 4.18b**). While this observation is suggestive of potential as an interaction surface, it is highly unlikely to reflect physiological ligand interaction.

Secondly, automated analysis of the LILRB4 ectodomain crystal structure was conducted using the SPPIDER web server (**S**olvent accessibility based **P**rotein-**P**rotein **I**nterface i**DE**ntification and **R**ecognition) which utilises an artificial neural network for prediction of protein-protein binding sites. The SPPIDER protein interface recognition server can be used to predict residues to be at the putative protein interface(s) by considering a single protein chain with resolved 3D structure. SPPIDER uses Relative Solvent Accessibility-based methods for prediction of protein-protein binding sites, based on discrepancies between

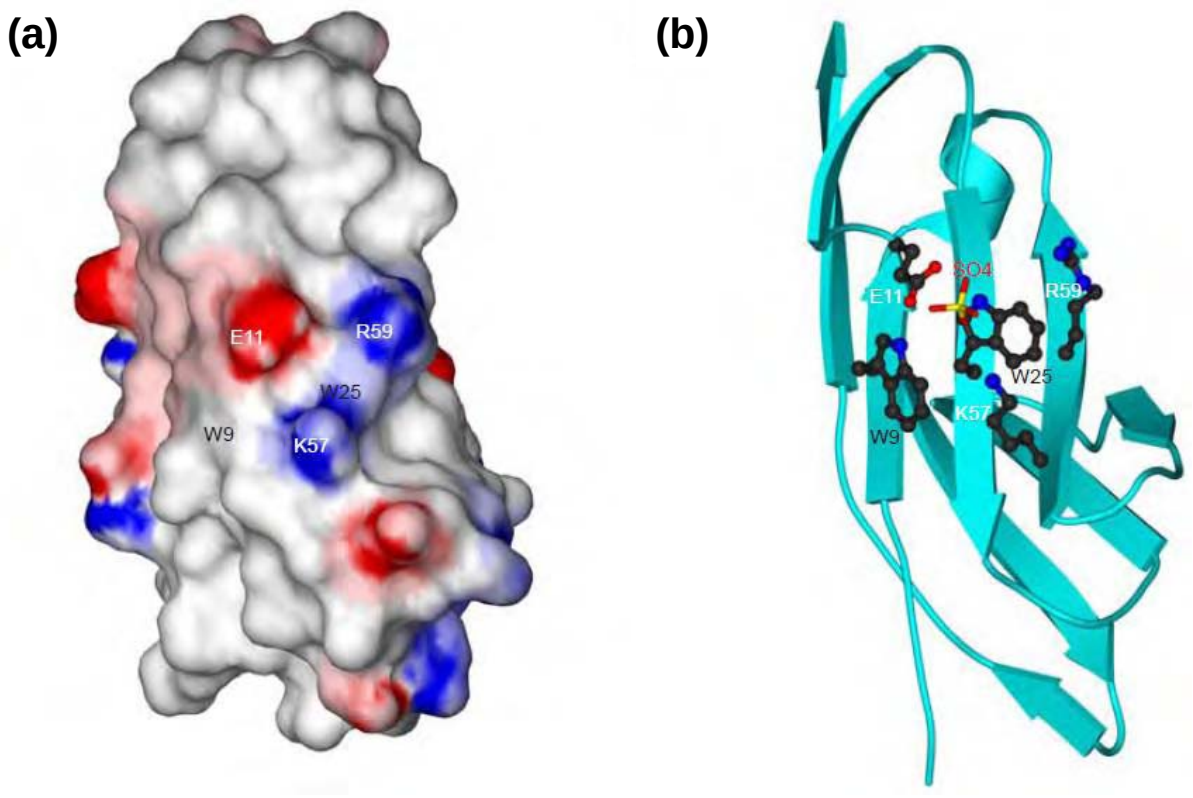

Figure 4.18. Proposed ligand binding site on the LILRB4 D1 structure. (a): The LILRB4 D1 molecular surface is depicted using GRASP with electropositive residues shown in blue and electronegative residues in red. The molecule is oriented with the ABE face – which opposes the MHC Class I binding surface in LILRB1/LILRB2 - towards the observer. Selected conserved residues have been labelled. (b): Position of the sulphate anion in the LILRB4 D1 structure. The secondary structure is depicted as a ribbon diagram with strands shown as arrows, and the conserved residues contributing to the proposed binding site displayed in ball-and-stick representation. The sulphate anion is shown in yellow.

predicted and observed (in an unbound protein structure) surface exposure of amino acid residues (Porollo and Meller, Proteins: Struc Func Bioinformatics 2007).

Output from the SPPIDER web server is in the form of a modified PDB file, with the values for B-factor for each residue replaced by a percentage probability score, reflecting the likelihood that a particular residue is involved in protein-protein interactions. The output for the submitted LILRB4 ectodomain structure is visualised in **Figure 4.19**. From this figure, which shows the molecular surface of the LILRB4 ectodomain colour-coded according to the SPPIDER output, it can be seen that there are three main regions of potential protein-protein interaction site, as predicted by SPPIDER: residues 2-5, 80-82 and 85 at the D1 tip of the receptor (particularly P2, V81 and Q85); residues 11-15 and 138-142 at the D1D2 interface (noting P12 and L142 as having probability greater than 75 %); and a larger number of residues - principally 102-116, 158-165 and 189-195 - with higher probability scores at the D2 tip (noting L110, S113, G114, S160, P161 and S164 as having probability 95 % or higher).

Both the D1 tip of LILRB1/LILRB2 and the D1D2 interface of these two MHC Class I-binding receptors are involved in ligand recognition. This could suggest that the ligand binding surfaces of Group II receptors such as LILRB4 share features with Group I LILRs that recognize MHC Class I. The D2 tip region in LILRB4 may be falsely recognised as a protein-protein interaction site due to its proximity to the plasma membrane, as LILRB4 has only a short stalk region connecting the transmembrane domain to D2.

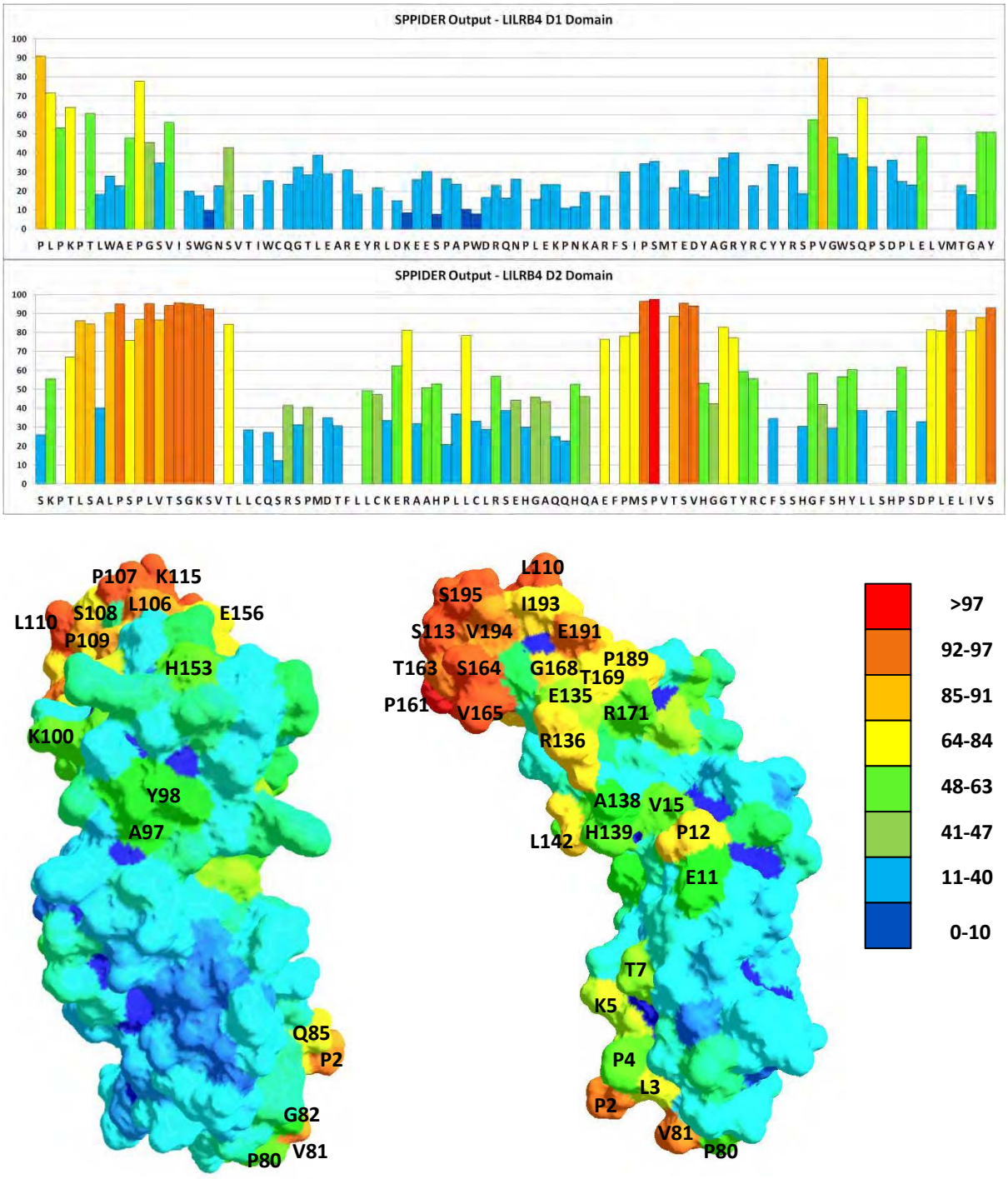

Figure 4.19. SPPIDER prediction of protein-protein interaction sites in LILRB4. The LILRB4 D1D2 PDB file was submitted to the SPPIDER web server and the output is depicted as a bar chart of probability of interaction against amino acid residue (top panel). Each bar is colour coded as per the lower panels. The lower panel shows the molecular surface of LILRB4, generated using Swiss PDB Viewer and colour coded according to probability. Two views are shown, towards the CFG face (lower left panel) or towards the ABE face (lower right panel). Residues of interest above the 50% probability limit are labelled.

Finally, although SPPIDER predictions failed to match the surface highlighted by manual inspection, the D1D2 hinge region site predicted by SPPIDER also included E11, and therefore overlapped minimally with this surface. Nevertheless one could consider the presence of a hydrophobic patch at the ABE face of the receptor to be indicative of a potential ligand binding site and this possibility cannot be easily discounted.

4.7 Chapter Summary and Discussion

In previous work to conduct structural and ligand identification studies on LILRB4, the extracellular domain of wild type LILRB4 D1D2 was produced using *E. coli* expression and *in vitro* refolding methodologies. Although pure, antibody-reactive material was produced to high levels (Garner et al. Prot Exp Pur 2006), its limited *in vitro* stability and propensity for precipitation during concentration steps proved problematic and crystallization trials only produced microcrystals of insufficient quality for X-ray diffraction data collection.

In order to progress LILRB4 structural analyses, I adopted an alternative strategy to obtain diffraction-quality crystals, i.e. production of the single D1 domain form of the receptor, on the basis that partial structural information was better than no information at all, and in concert with the hypothesis that the D1 domain would be more likely to constitute the ligand-binding portion of the receptor, due to the two-domain arrangement of LILRB4 (as opposed to the four-domain composition of most of the other LILR molecules). The phylogenetic analysis of the LILR family provided some support for this hypothesis, as the D2 domain of LILRB4 has more identity with the D4 domains of the other LILRs, which has been shown not to be involved in ligand recognition (for those LILRs where the ligand and binding sites are known).

This approach proved particularly successful, both in terms of solving stability and protein precipitation obstacles and also in terms of crystallisation. The isolated D1 domain of LILRB4 readily crystallised and these crystallisation conditions were rapidly optimised to produce crystals capable of X-ray diffraction to a resolution of 1.6 Å. Use of the previously-

published LILRA5 structure as a model for molecular replacement – again on the basis of phylogenetic analysis of the LILR family – was also highly successful and resulted in high-resolution structural data with publishable refinement statistics (see **Table 4.2** and **Table 4.6**, and also **Figure 4.6** and **Figure 4.7**). This allowed for analysis of structural elements of the LILRB4 D1 domain, namely secondary structure assignment and tertiary structural arrangement, rationalisation for non-binding to MHC Class I on the basis of steric and electrostatic clashes by comparison with LILRB1/HLA-A2 and LILRB2/HLA-G, and comparison with its closest LILR family member, LILRA5. It also allowed me to formulate a hypothesis regarding a potential ligand-binding site on the ABE face of the domain.

Nevertheless, despite these successes more complete structural information was desirable. An alternative strategy to overcome problems with the LILRB4 ectodomain was undertaken by Prof. Gao's group, namely the production of a mutated form of the receptor introducing a non-native disulphide bond into the D2 domain in order to reduce flexibility in the molecule and thus minimize precipitation and promote crystallisation. This approach had previously been utilised and had resulted in the successful crystallisation and structure determination of LILRA2 (Chen et al. JMB 2007).

Analysis of the interdomain interface of the LILRB4 ectodomain revealed that the more obtuse D1-D2 interdomain angle of LILRB4 is shifted out by approximately 20° relative to the other LILR family members. This is accompanied by a marginally reduced buried solvent accessible area at the interdomain region (846 $Å^2$ for LILRB4 compared to 957 $Å^2$ for LILRB1) and the substitution of a key bulky hydrophobic residue resulting in the loss of

contacts to neighboring residues. LILRB4 is therefore unique in terms of its more obtuse interdomain angle, and this may have profound implications for ligand recognition by LILRB4 and supports the hypothesis that LILRB4 may interact with its ligand in a 'head-on' fashion, primarily through the D1 domain, with the D2 domain serving to orientate the ligand-binding D1 domain towards its target or targets. However, one caveat with respect to this issue is that the presence of the engineered disulphide could affect the topology of the LILRB4 D2 C-C' loop such that it artificially contributes to stabilization of this particular interdomain angle, due to the involvement of residues from the unique LILRB4 C-C' 3_{10} helix (**Figure 4.15b**) and in particular P140, which are absent in LILRB1/LILRB2/LILRA5, in interdomain interactions. In the absence of this disulphide bond, it seems highly likely that the native form of LILRB4 would exhibit a high degree of flexibility at the D1D2 hinge region and therefore have the capacity to adopt a range of interdomain angles, which is consistent with the high degree of proteolytic cleavage observed between the D1 and D2 domains of the native receptor.

The introduction of the artificial disulphide into the C-C' loop of LILRB4 D2 may affect the overall structure in two ways; firstly, it may affect the propensity of this region to form a helical structure (residues 139-143) and secondly it may affect the interdomain interface, since the resulting loop lies in close proximity to the first domain and effectively 'blocks' the hinge region. It is therefore possible introduction of the non-native disulphide may account for the more obtuse interdomain angle, which is calculated to be 107˚ (DomAngle software program, Su et al. Science 1998), in contrast to the ~90˚ angle adopted by the other LILR receptors which have been crystallised. **Figure 4.15** illustrates that this arrangement can provide a region of close proximity between D2 C-C' loop residues and D1 residues. The

interdomain interface contacts thus introduced could stabilize this interdomain angle and reduce interdomain flexibility, thereby favouring crystallization of the receptor. It is tempting to speculate that the native disulphide in this region in LILRB1 and LILRB2, which corresponds to the artificial disulphide introduced into LILRA2 and LILRB4 and allowed crystallization of these receptors, contributes to the propensity of LILRB1 and LILRB2 to crystallize by reducing flexibility in this region. However, notably the D2 C-C' loop adjacent to the disulphide is not involved in contacting D1 in either LILRB1 or LILRB2, and an alternative possibility is that the naturally more extensive D1-D2 interdomain interface interactions in LILRB1 and LILRB2 result in less flexibility at the D1-D2 hinge region and instead underlie their greater propensity to crystallise.

Structural analyses of LILRB4 identified strong rationalisation for its non-binding to MHC Class I. Analysis of the D1 structure alone identified key amino-acid substitutions with LILRB1 at the known MHC binding sites. In addition, the LILRB4 D1D2 ectodomain structure was superimposed on the LILRB1/HLA-A2 and LILRB2/HLA-G complex structures and revealed a number of steric clashes, loss of hydrogen bonding networks and disruption of salt bridges which would make LILRB4/MHC Class I binding unlikely (see **Figure 4.16**). Further evidence to support this hypothesis comes from analysis of the electrostatic surface of LILRB4, which shows major changes in electrostatic charge – both in terms of polarity and in loss/gain of charges – in comparison to LILRB1 and LILRB2 at the known MHC Class I binding sites (see **Figure 4.17**).

Analysis of potential non-MHC ligand-binding sites in the LILRB4 D1 structure by visual inspection and also in the LILRB4 D1D2 ectodomain structure by an automated computational method, SPPIDER, suggested a number of possibilities for protein-protein interaction sites at the receptor surface. In addition, the ABE surface of the D1 domain of LILRB4 has a close grouping of residues that are mostly conserved across the Group II LILRs and this includes charged residues and two solvent-exposed hydrophobic tryptophan residues in close proximity. Although SPPIDER failed to detect most of these residues as being highly probable for protein-protein interaction, some additional evidence for this hypothesis is provided by the presence of a sulphate anion bound to this ABE face site in the LILRB4 D1D2 ectodomain structure.

The SPPIDER analysis detected probable ligand interaction sites at the D1 tip, the D1D2 interdomain region, and at the D2 tip of LILRB4. These first two sites are reminiscent of the binding sites for MHC Class I on LILRB1 and LILRB2, although the balance of evidence suggests that MHC Class I is not the ligand for LILRB4. However, the possibility remains that LILRB4 uses regions analogous to those on LILRB1/2 involved in MHC Class I binding, for recognizing different ligand interaction sites. In keeping with this concept, KIRs and FcαR use regions analogous to those used by LILRB1/2 for binding to distinct ligand sites on either MHC Class I (the α1α2 platform, for KIRs) or IgA (for FcαR) (Willcox et al. Nat Immun 2003). Another possibility which is supported by the more obtuse domain angle of LILRB4 and the arrangement of its two domains is that the receptor engages such a ligand in a 'head-on' fashion as discussed earlier.

Further studies of LILRB4 are thus necessary to solve the puzzle of its ligand and the high-resolution structural data presented herein may contribute to the search for this elusive binding partner. In an attempt to glean further information about the Group II LILRs, which could conceivably shed light on the nature of the LILRB4 ligand I attempted structural studies on the other members of this group, and I will present these data in the following chapter.

CHAPTER 5 - STRUCTURAL STUDIES OF OTHER GROUP II LILRS

5.1 Introduction

Following the successful crystallisation and X-ray structural analysis of the D1 domain of LILRB4, I decided to attempt a similar strategy to obtain structural information for other Group II LILRs. Previous attempts at *in vitro* refolding of other LILR family members had been largely unsuccessful, hypothetically as a result of flexibility of the two-domain recombinant proteins and/or incorrect disulphide bond formation leading to instability in solution and concomitant precipitation during the refolding process. Although this strategy would yield structural data for only one of the domains it was reasoned that obtaining limited structural information across the Group II LILRs would still be valuable. The high yield of inclusion bodies from *E. coli* transformed with the LILRB4 D1 pET23a vector and the high yield and purity of correctly refolded LILRB4 D1 obtained gave me confidence that such a strategy would be fruitful for generation of crystals of other Group II LILRs for X-ray data collection. Since the crystal structure of the LILRA5 ectodomain had previously been elucidated by Maenaka et al. in 2006, we focussed on the remaining Group II LILRs, LILRB3, LILRB5 and LILRA4. LILRA6 was ignored as its amino acid sequence is identical to LILRB3 in the D1 domain.

The published literature on LILRB3 and LILRB5 is sparse and relatively little is known about these two receptors functionally or structurally. Both are predicted to have four Ig domains in the extracellular region and ITIM motifs in the cytoplasmic domain (Borges et al. JI 1997). LILRB3 is expressed on cells of the myeloid lineage, with upregulation of its expression on monocytes and granulocytes as the cells undergo maturation (Sloane et al. Blood 2004). LILRB3 is also expressed on human cord-blood derived progenitor mast cells, but not on

mature mast cells, further suggesting a role in maturation and differentiation of myeloid cells (Tedla et al. J Leuk Bio 2008). Abnormal expression of LILRB3 has been detected in rheumatoid arthritis patients, with upregulation of the receptor on synovial fluid mast cells (Tedla et al. Am J Pathol 2002, Huynh et al. Rheumatology 2007). LILRB3 may therefore have involvement in autoimmune pathologies.

The expression levels of both LILRB3 and LILRB5 are elevated in skin samples from patients with lepromatous leprosy (Bleharski et al. Science 2003). LILRB5 expression at the mRNA level was first described in a restricted subset of NK cells only (Borges et al. JI 1997) but protein expression remained undetected until recently, when it was described as being in the granules of mature cord-blood derived mast cells: intracellular LILRB5 colocalizes with tryptases in mast cell granules, is mobilized to the surface and also released as a soluble form upon FcεRI cross-linking, suggesting that the function of the soluble protein is as a decoy receptor (Tedla et al. J Leuk Bio 2008). Thus, one could speculate that LILRB5 may function to regulate inflammation in the skin.

LILRA4 (also termed ILT7) is selectively expressed on plasmacytoid dendritic cells (pDCs), has four extracellular Ig domains and associates with the FcεRIγ adaptor protein (Rissoan et al. Blood 2002). LILRA4 engagement would thus be expected to signal in an activatory fashion; however, TLR stimulation of primary pDCs in the presence of cross-linking antibodies to LILRA4 inhibits the production of type I IFNs (Cao et al. JEM 2006, Cho et al. Int Immun 2007). The ligand for LILRA4 was recently identified as being BST2 (Cao et al. JEM 2009), also known in the retroviral field as Tetherin and identified as being a host-encoded viral restriction element that prevents virus budding in certain cell lines (Neil et al. Nature 2008). As IFN-α upregulates BST2 expression, the LILRA4/BST2 interaction may

function during infection as a feedback inhibition loop to downregulate the antiviral responses of pDCs when type I IFN responses are sufficient (Blasius et al. JI 2006).

5.2 Attempted Crystallisation of Other Group II LILR D1 Domains

5.2.1 Cloning of Recombinant Group II LILR D1's

A construct for expression of the D1D2 domains of LILRA4 in *E. coli* was generated by cloning from the full-length LILRA4 gene in the plasmid pCMV-Flag (a kind gift from Dr. Rachel Allen). In brief, a PCR was conducted using primers to introduce a start codon and optimised codons for *E. coli* expression at the N-terminus and a premature stop codon at the C-terminal D2-D3 boundary, as estimated by primary amino acid sequence alignment with the other LILR family members (see **Figure 4.1a**). The nucleotide and amino acid sequence of LILRA4 D1D2 are shown in **Figure 5.1a**. These primers incorporated an NdeI restriction site (including an ATG codon for the initiating methionine) in the 5' primer and a HinDIII restriction site in the 3' primer (**Figure 5.1b**) in order to allow cloning into the MCS of pET23a.

After PCR generated a product of the expected mass (c. 600 bp, see **Figure 5.1c**), the PCR product was then digested with NdeI and HinDIII, gel purified and ligated into cut and gel purified pET23a vector. This ligation product was used to transform *E. coli* DH5α cells. Colonies were selected for plasmid miniprep and test digests with NdeI-HinDIII and agarose gel electrophoresis showed that a fragment of the expected size was generated (**Figure 5.1d**, arrowed). Subsequent DNA sequence analysis confirmed successful cloning of the LILRA4 D1D2 sequence into the pET23a vector. (Functional Genomics, Department of Biosciences, University of Birmingham).

(a)

```
   1 ctacgggcac cgtggccaca cctgcctgca cagccagggc caggaggagg agatgccatg
  61 accctcattc tcacaagcct gctcttcttt gggctgagcc tgggccccag gacccgggtg
 121 caggcagaaa acctacccaa acccatcctg tgggccgagc caggtcccgt gatcacctgg
 181 cataaccccg tgaccatctg gtgtcagggc accctggagg cccaggggta ccgtctggat
 241 aaagagggaa actcaatgtc gaggcacata ttaaaaacac tggagtctga aaacaaggtc
 301 aaactctcca tcccatccat gatgtgggaa catgcagggc gatatcactg ttactatcag
 361 agccctgcag gctggtcaga gcccagcgac cccctggagc tggtggtgac agcctacagc
 421 agacccaccc tgtccgcact gccaagccct gtggtgacct caggagtgaa cgtgaccctc
 481 cggtgtgcct cacggctggg actgggcagg ttcactctga ttgaggaagg agaccacagg
 541 ctctcctgga ccctgaactc acaccaacac aaccatggaa agttccaggc cctgttcccc
 601 atgggccccc tgaccttcag caacaggggt acattcagat gctacggcta tgaaaacaac
 661 accccatacg tgtggtcgga acccagtgac ccctgcagc tactggtgtc aggcgtgtct
```

*MTLILTSLLFFGLSLGPRTRVQA***ENLPKPILWAEP**GPVITWHNPVTIWCQGTLEAQG
YRLDKEGNSMSRHILKTLESENKVKLSIPSMMWEHAGRYHCYYQSPAGWSEPSDP
LELVVTAYSRPTLSALPSPVVTSGVNVTLRCASRLGLGRFTLIEEGDHRLSWTLNSH
QHNHGKFQALFPMGPLTFSNRGTFRCYGYENNTPYVWSEPSD**PLQLLVS**

(b)

5': **GGAATTC CATATG** GAAAACCTGCCGAAACCGATCCTGTGGGCTGAACCG

3' Primer: CCCCTGCAGCTACTGGTGTCA**TGA GGATCC GCG**

3' Reverse Complement: **CGC GGATCC TCA**TGACACCAGTAGCTGCAGGGG

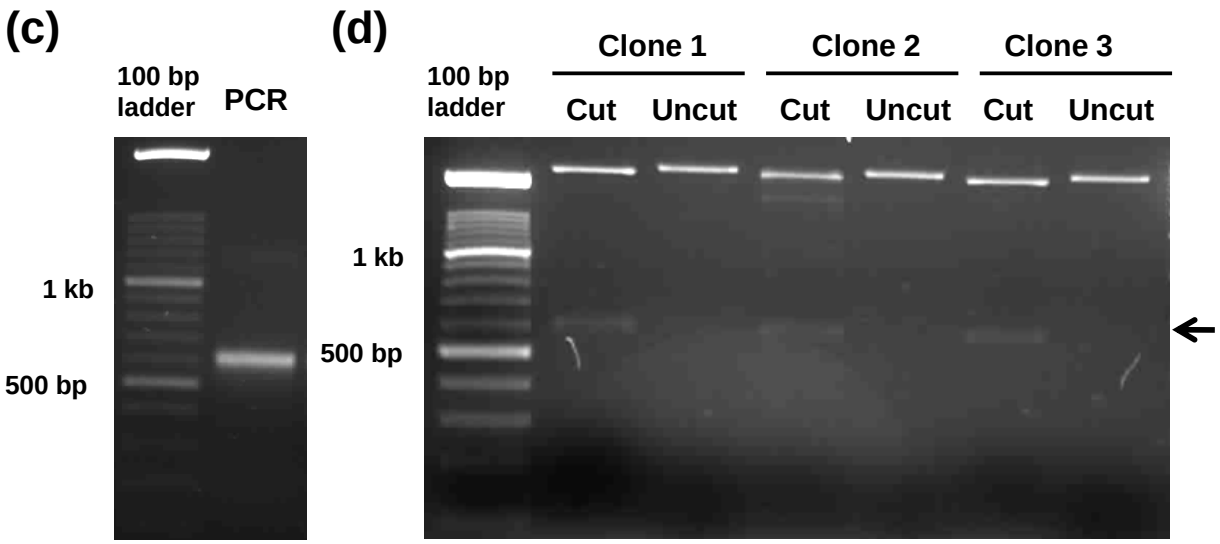

Figure 5.1. Cloning of LILRA4 D1D2 into pET23a vector. (a): Nucleotide sequence for LILRA4 D1D2. The boundaries of the coding sequence for the domain are underlined and in bold. The translation of the sequence is shown underneath with the signal peptide in italics and the D1D2 boundaries in bold. (b): Primer design for LILRA4 D1D2-pET23a construct showing insertion of the overhang and NdeI site into the 5' primer in bold (incorporating the ATG codon for the initiating methionine) and mutations to optimise codon usage underlined. The overhang, HinDIII site and stop codon are also highlighted in the 3' primer. (c): Agarose gel electrophoresis of the LILRA4 D1D2 PCR product and (d): test digests of three clones from minipreps of the LILRA4 D1D2 PCR product ligated into the pET23a vector.

Although expression of LILRA4 D1D2 as *E. coli* inclusion bodies was successful, attempts to chemically refold the protein were not, in common with previous attempts to generate correctly refolded LILRB3 and LILRB5 (data not shown). LILRB3 and LILRB5 two-domain constructs in pET23a vectors had previously been generated in the laboratory. Due to the success of the LILRB4 D1 strategy for generating high yields of correctly folded protein and data-quality grade crystals for X-ray diffraction studies, I decided to generate LILR D1-pET23a constructs for LILRA4, LILRB3 and LILRB5.

LILRB3 D1, LILRB5 D1 and LILRA4 D1 constructs were generated by SDM of the relevant two-domain pET23a plasmids. Primers were designed to introduce a premature stop codon at the D1-D2 boundary, at the residues corresponding to ...GAY of the LILRB4 D1 construct. After dpnI digestion to remove template plasmid, these new D1 plasmids were used to transform *E. coli* DH5α cells for plasmid miniprep and DNA sequencing to confirm the correct sequence. The cloning strategy and primer sequences are shown in **Figure 5.2**.

5.2.2 Protein Expression in *E. coli* and *in vitro* Refolding of Group II LILR D1 Domains

LILRB3 D1 pET23a, LILRB5 D1 pET23a and LILRA4 D1 pET23a plasmids were used to transform *E. coli* BL21(DE3) cells for test expression and subsequent analysis by SDS-PAGE (**Figure 5.3a**). Test expression was judged to be successful with significant upregulation of a single protein band of the expected apparent mass for each construct after IPTG induction. Bulk expression was then carried out for each construct, and after harvesting and washing of inclusion bodies, the protein was solubilised overnight at 4 ºC in Guanidine solubilisation buffer. Yields at this stage were high (typically 50 mg/L of solubilised denatured protein).

(a)

LILRA4

```
...
361 agccctgcag gctggtcaga gcccagcgac cccctg gagc tggtggtgac agcctacagc
421 agacccaccc tgtccgcact gcca agccct gtggtgacct caggagtgaa cgtgaccctc
...
```

LILRB3

```
...
421 gcaggctggt cagagcccag cgacccctg gag ctggtga tgacaggagc ctacagcaaa
481 cccaccctct cagccctgcc c agccctgtg gtggcctcag gggggaatat gaccctccga
...
```

LILRB5

```
...
361 tgctactatg agacccctgc aggctggtca gagcccagtg acccctgga g ctggtggcg
421 acaggattct atgcagaacc cactctttta gccctgccg a gtcctgtggt ggcctcagga
...
```

(b)

LILRA4 ...ELVV**TAY**SRPTLSALP...
LILRB3 ...LVMT**GAY**SKPTLSALP...
LILRB5 ... LVAT**GFY**AEPTLLALP...

(c)

LILRA4 GAGCTGGTGGTGACAGCCTACAGCAGACCCACCCTGTCCGCACTGCCA
LILRB3 CTGGTGATGACAGGAGCCTACAGCAAACCCACCCTCTCAGCCCTGCCC
LILRB5 CTGGTGGCGACAGGATTCTATGCAGAACCCACTCTTTTAGCCCTGCCG

(d)

LILRA4 5’ GAGCTGGTGGTGACAGCCTACTAATAACCCACCCTGTCCGCACTGCC
3’ GGCAGTGCGGACAGGGTGGGTTATTAGTAGGCTGTCACCACCAGCTC

LILRB3 5’ CTGGTGATGACAGGAGCCTACAGCAAACCCACCCTCTCAGCCCTGCC
3’ GGCAGGGCTGAGAGGGTGGGTTTGCTGTAGGCTCCTGTCATCACCAG

LILRB5 5’ CTGGTGGCGACAGGATTCTATGCAGAACCCACTCTTTTAGCCCTGCCG
3’ CGGCAGGGCTAAAAGAGTGGGTTCTGCATAGAATCCTGTCGCCACCAG

Figure 5.2. SDM primer design for LILRA4, LILRB3 and LILRB5 D1 constructs. (a): Nucleotide sequence corresponding to the D1D2 junction for each LILR. Nucleotide sequence selected for primer design is underlined and in bold. (b): Corresponding peptide translation of the underlined nucleotides. The terminal three D1 residues are in bold. (c): Target nucleotide sequences for each protein, with the codons to be mutated to stop residues underlined. (d): Final SDM primer designs for each construct.

In vitro refolding of inclusion bodies was conducted by the standard Garboczi method (PNAS 1992), and followed by purification by size exclusion chromatography into a buffer containing 50 mM NaCl 20 mM Tris pH 8.0. Single peaks corresponding to monomeric protein were detected at an elution volume of approximately 260 ml – in the expected range for a single Ig domain of 12 kDa – for each protein, with minimal aggregate peaks at earlier elution points (**Figure 5.3b**). Absorbance at 280 nm of these peaks was typically between 400-500 mAU indicating a high yield. Subsequent concentration of the peak fractions (using stirred cell (Amicon) and centrifugal filter devices (Microcon)) allowed protein concentrations of ~10 mg/ml to be achieved with an estimated final yield of 15 % per refold.

Protein samples were analysed by SDS-PAGE to ensure correct refolding and verify apparent molecular mass. As can be seen from **Figure 5.3c**, a single band corresponding to monomeric protein with an apparent mass of c. 12 kDa was visible for each protein after coomassie staining of the gel. In addition, a single band was detected under non-reducing conditions, suggestive of correct disulphide bond formation. The high yield and purity of the proteins was considered to be promising for successful crystallisation trials.

5.2.3 Crystallisation Screening of LILRB3 D1 and LILRB5 D1

Crystallisation screens were set up on a small scale using a Mosquito crystallisation robot, in a 100 nl plus 100 nl hanging drop format in 96-well plates, with 100 µl of reservoir solution in each well. Commercially available screens used were JCSG^{+}, Structure Screens I and II, and PACT (Molecular Dimensions Ltd.), PEG/Ion I and II, Index Screen (Hampton Research) and Wizard Screens I and II (Emerald Biosystems). Each of the six screens utilised one 96-well plate.

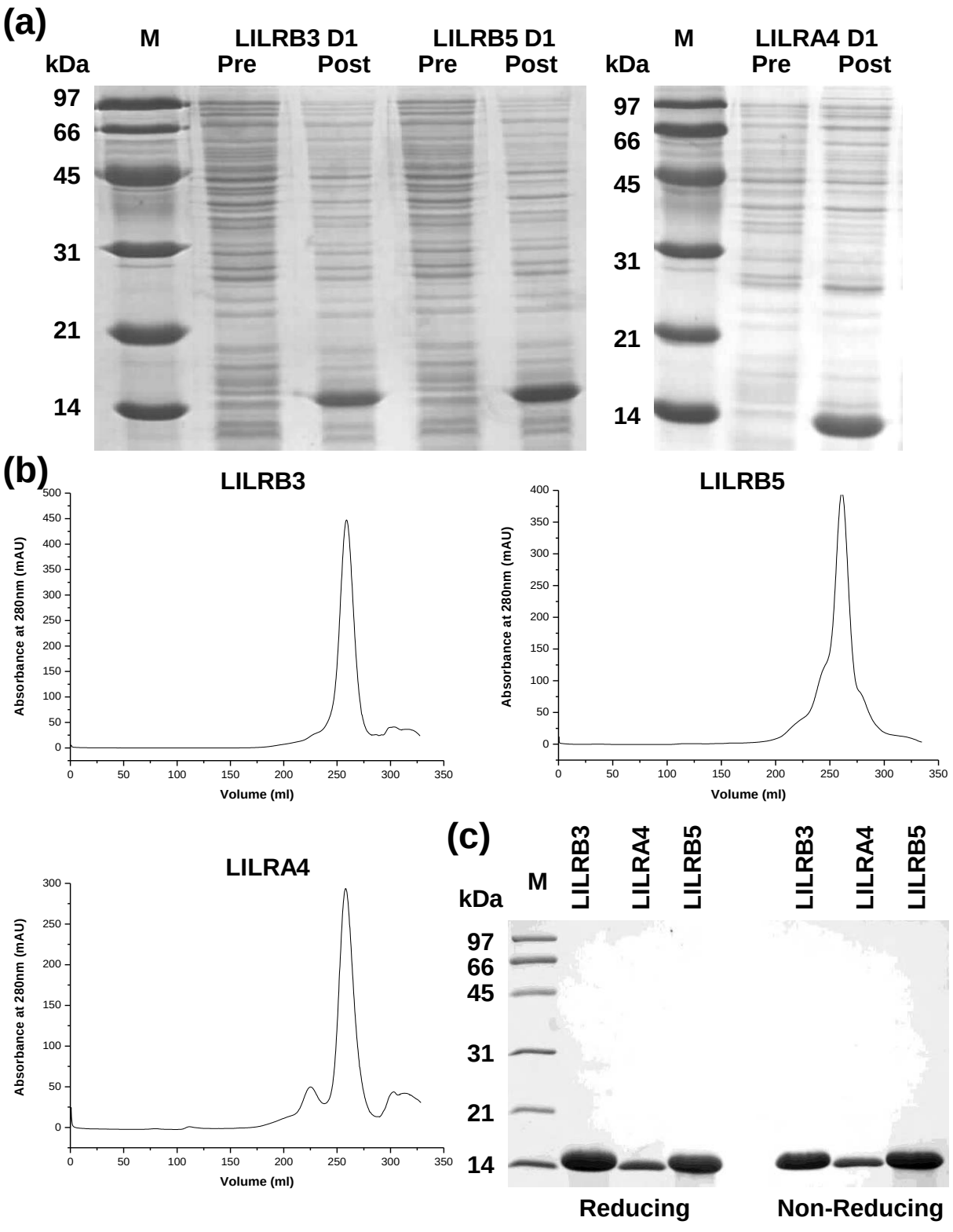

Figure 5.3. Purification and SDS-PAGE analysis of Group II LILR D1 proteins. (a): SDS-PAGE analysis of test expression samples of Group II LILR D1 domains. (b): size exclusion chromatography profiles for Group II LILR D1 proteins after FPLC using S200 column. (c): SDS-PAGE analysis of refolded, concentrated proteins under reducing and non-reducing conditions.

Initial attempts to crystallise LILRB3 D1 utilised protein primarily at 10 mg/ml, with some screens set up between 11-16 mg/ml (with one outlier at high concentration, 38 mg/ml). The protein buffer was varied between 50 mM Na Cl 20 mM Tris pH 8.0, and a buffer used for optimal stability with LILRB4, namely 50 mM Na citrate pH 5.5. Drops were inspected visually using a Leica light microscope at 3 days and at weekly intervals thereafter for a maximum of 2 months. Although a large number of the drops had visible precipitate (especially at the higher concentrations), no microcrystals were observed with the exception of JCSG^{+} condition number 22 (0.2 M magnesium chloride, 0.1 M Na cacodylate pH 6.5, 50 % v/v PEG 200) which yielded small poor quality crystals. However, attempts to repeat this hit both on the small and the large scale (1 µl plus 1 µl drops, 1 ml reservoir solution in a 24-well Limbro plate) were unsuccessful.

Due to the high levels of precipitation, a second round of crystallisation trials were screened at the lower concentration of 5 mg/ml and in 50 mM Na citrate pH 5.5 buffer. These drops were primarily clear and yielded no microcrystals. Further optimizations were attempted by varying the protein concentration, with screens set up at 20 mg/ml, but again no microcrystals were observed. As further strategies to promote crystallisation, sitting-drop crystal screens were attempted on the small scale utilising protein at 14 mg/ml, and each of the six screens were set up at 4 ºC also on the small scale but at lower protein concentration (5 mg/ml). None of these strategies produced any visible microcrystals.

In parallel, LILRB5 D1 screens were generated by the same methodology. An initial round of screening utilising all six commercial screens with LILRB5 D1 protein at a concentration of 10 mg/ml and in 50 mM Na citrate pH 5.5 buffer also produced no hits. A further round of screening was conducted at a concentration of 20 mg/ml and in 50 mM NaCl 20 mM Tris pH

8.0. This also failed to produce microcrystals.

In order to progress with crystallisation, thermal shift screening was conducted on LILRB3 D1 and LILRB5 D1 protein, to try to optimise protein solubility and stability, which might influence nucleation and subsequent formation of microcrystals (for review, see Macpherson et al. Methods 2004). This thermal stability screening process was conducted in collaboration with Dr. Timothy Knowles (Overduin Group, Cancer Sciences, University of Birmingham) and utilised Sypro Orange dye in combination with a thermal cycler and RT-PCR analysis software. Sypro Orange binds to exposed hydrophobic patches on denatured proteins and its fluorescence profile can thus be used as a measure of correct protein folding. A thermal cycler is used to analyse buffer conditions and protein in a 96-well format, with a stepwise 1 ºC increment in temperature from 25 ºC to 95 ºC. As the protein is exposed to increasing temperature, it undergoes unfolding and denaturation which leads to the exposure of hydrophobic core residues and an increase in Sypro Orange dye binding which can be detected spectroscopically. The melting temperature – T_m – of the protein is the point at which this binding is half maximal and is a measure of the protein stability and solubility in that specific buffer condition.

A plot of temperature versus fluorescence yielded the melting curve for that particular protein/buffer combination. A plot of temperature versus the first derivative of fluorescence (Rn (T)) generated a dissociation curve, the inflection point of which is the T_m for that protein in that buffer condition. Buffer optimisation is then a case of identifying which buffers increase the T_m. For LILRB3 D1, the buffer was optimised to 50 mM Bis-Tris propane pH 6.0. For LILRB5 D1, the optimal buffer was determined to be 150 mM NaCl, 50 mM Bis-Tris propane pH 6.0.

One final round of crystal screening was conducted using LILRB3 D1 and LILRB5 D1 at 20 mg/ml in optimised buffers. Hanging drops were set up on the small scale utilising all six commercial screens; however, no microcrystals were detectable at 3 days or weekly up to 2 months after setup. A list of screens and conditions for all three proteins (including LILRA4 D1, discussed below) is shown in **Table 5.1** (overleaf).

5.2.4 Crystallisation Screening and Optimisation for LILRA4 D1

Crystallisation screening for LILRA4 D1 was more successful. Although initial screens on the small scale (100 nl plus 100 nl hanging drops, 100 µl reservoir in 96-well plates) at 10 mg/ml in 50 mM Na Cl 20 mM Tris pH 8.0 buffer yielded no hits, further screens at 20 mg/ml in the same buffer yielded 23 hits across all six screens. The principle crystal morphology of these hits was long, thin needles. The screens and conditions which yielded microcrystals are shown in **Table 5.2** (overleaf).

To ensure crystals were protein and not crystallisation condition components, and to optimise crystal morphology, each of the 23 conditions was set up on the small scale with protein at a concentration of 0, 15, 20 or 25 mg/ml. After 3 days, all control drops were clear. Furthermore, although hanging drops set up at 15 mg/ml primarily contained precipitate only, all drops at 20 mg/ml and above contained microcrystals as before. Index Screen condition 35 was observed as generating the best morphology microcrystals for optimisation (1.0 M ammonium sulphate, 0.1 M HEPES pH 7.0, 0.5 % w/v PEG 8000), namely long thin needles but the thickest of those observed across all 23 conditions. Protein concentration was judged to be optimal at 20 mg/ml although the presence of multiple nucleation sites suggested that reducing protein concentration might lead to increased crystal size on the larger scale.

LILRB3		
Screen	**[Protein] mg/ml**	**Buffer**
JCSG+	5, 10, 20, 37.8	50 mM Na Citrate pH5.5
SS I&II	5, 10, 20	"
Wizard I & II	"	"
PACT	"	"
PEG-Ion I&II	"	"
Index	"	"
JCSG+	15.6	50 mM NaCl 20mM Tris pH8.0
SS I&II	14, 11	"
Wizard I & II	14, 10	"
PACT	"	"
PEG-Ion I&II	14, 11	"
Index	"	"
LILRB5		
Screen	**[Protein]**	**Buffer**
JCSG+	10	50 mM Na citrate pH 5.5
SS I&II	"	"
Wizard I & II	"	"
PACT	"	"
PEG-Ion I&II	"	"
Index	"	"
JCSG+	20	50 mM NaCl 20 mM Tris pH 8.0
SS I&II	"	"
Wizard I & II	"	"
PACT	"	"
PEG-Ion I&II	"	"
Index	"	"
JCSG+	20	150 mM NaCl 50mM Bis-Tris propane pH 6.0
SS I&II	"	"
Wizard I & II	"	"
PACT	"	"
PEG-Ion I&II	"	"
Index	"	"
LILRA4		
Screen	**[Protein]**	**Buffer**
Wizard I & II	10	50 mM NaC l 20 mM Tris pH 8.0
SS I&II	"	"
JCSG-plus	20	"
SS I&II	"	"
Wizard I & II	"	"
PACT	"	"
PEG-Ion I&II	"	"
Index	"	"

Table 5.1. Initial screens and conditions for Group II LILR D1 crystallisation trials.

PACT Premier

Well	Tube	Salt	Buffer	Precipitant	Morphology
F5	2-17	0.2 M sodium nitrate	0.1 M Bis-Tris propane pH 6.5	20 % w/v PEG 3350	long needles +ppt
F6	2-18	0.2 M sodium formate	0.1 M Bis-Tris propane pH 6.5	20 % w/v PEG 3350	long needles +ppt
F7	2-19	0.2 M sodium acetate	0.1 M Bis-Tris propane pH 6.5	20 % w/v PEG 3350	long needles +ppt
F10	2-22	0.2 M sodium sulphate	0.1 M Bis-Tris propane pH 6.5	20 % w/v PEG 3350	fine needles/rodballs +ppt

JCSG+

Well	Tube	Salt	Buffer	Precipitant	Morphology
A5	1-5	0.2 M magnesium formate	None	20 % w/v PEG 3350	multiple needles/rodballs +ppt
A8	1-8	0.2 M ammonium formate	None	20 % w/v PEG 3350	needles +ppt
D6	1-42	0.2 M magnesium chloride	0.1 M Tris pH 8.5	20 % w/v PEG 8000	long needles +ppt
H4	2-40	0.2 M calcium chloride	0.1 M BisTris pH 5.5	45 % v/v MPD	small rodballs at edge, clear

PEG/Ion I & II

Well	Tube	Salt	Buffer	Precipitant	Morphology
A6	1-6	0.2 M sodium chloride	None (pH 6.9)	20 % w/v PEG 3350	needles +ppt
B8	1-20	0.2 M magnesium formate dihydrate	None (pH 7.0)	20 % w/v PEG 3350	thick needles +ppt
C1	1-25	0.2 M magnesium acetate tetrahydrate	None (pH 7.9)	20 % w/v PEG 3350	needle clusters +ppt
C3	1-27	0.2 M sodium acetate trihydrate	None (pH 8.0)	20 % w/v PEG 3350	needles +ppt
F1	2-13	4 % v/v tacsimate pH 6.0	None	12 % w/v PEG 3350	needles +ppt
G6	2-30	0.2 M ammonium tartrate dibasic pH 7.0	None	20 % w/v PEG 3350	needles +ppt

Table 5.2. Screens and conditions yielding microcrystals of LILRA4 D1. (continued overleaf). ppt = precipitate.

Structure Screens I & II

Well	Tube	Salt	Buffer	Precipitant	Morphology
E6	2-6	0.01 M nickel chloride	0.1 M Tris pH 8.5	1 M lithium sulphate	needles/rodball +ppt

Index Screen

Well	Tube	Salt	Buffer	Precipitant	Morphology
C2	26	None	None	1.1 M NH_4 tartrate dibasic pH 7.0	microcrystals/needles
C11	35	1.0 M ammonium sulphate	0.1 M HEPES pH 7.0	0.5 % w/v PEG 8000	long thick needles +ppt
C12	36	15 % v/v tacsimate pH 7.0	0.1 M HEPES pH 7.0	2 % w/v PEG 3350	multiple needle clusters +ppt
E1	49	0.2 M CaCl2 dehydrate	0.1 M Bis-Tris pH 6.5	45 % v/v MPD	microcrystals

Wizard I & II

Well	Tube	Salt	Buffer	Precipitant	Morphology
B1	1-13	None	0.1 M cacodylate pH 6.5	1.26 M ammonium sulphate	needle clusters + ppt
D10	1-46	0.2 M calcium oxaloacetate	0.1 M imidazole pH 8.0	10 % w/v PEG 8000	needle cluster + ppt
E3	2-3	0.2 M magnesium chloride	0.1 M Tris pH 8.5	20 % w/v PEG 8000	needle cluster + ppt
H12	2-48	None	0.1 M MES pH 6.0	1 M Na / K tartrate	microcrystal dumbbells + ppt

Table 5.2. (continued).

Four conditions were selected as giving rise to the best morphologies and used as a base condition to screen for optimal buffer pH, which can affect crystal growth and morphology (McPherson J Appl Cryst 1995). These conditions were: PEG-Ion Screen I condition 6 (0.2 M Na Cl, pH 6.9, 20 % PEG 3350), PEG-Ion Screen I condition 25 (0.2 M magnesium acetate tetrahydrate, pH 7.9, 20 % PEG 3350), Index Screen condition 26 (1.1 M ammonium tartrate dibasic pH 7.0) and Index Screen condition 35 (1.0 M ammonium sulphate, 0.1 M HEPES pH 7.0, 0.5 % w/v PEG 8000). A small-scale hanging-drop screen was set up for each condition utilising the StockOptions pH Buffer Kit (Hampton Research), varying the pH of the added buffer from pH 2.2 to pH 11.0 in steps of 0.4 pH units. Protein concentration was kept fixed at 20 mg/ml. After 3 days incubation, the best morphology crystals were observed in the following conditions: 1.0 M ammonium sulphate, 0.1 M HEPES pH 6.8, 0.5 % w/v PEG 8000 and 1.0 M ammonium sulphate, 0.1 M Tris pH 9.0, 0.5 % w/v PEG 8000. These microcrystals were thicker, more oblate needles, but still of insufficient size for X-ray data collection.

The two optimised conditions were then repeated on the larger scale (1 µl + 1 µl hanging drops, 1 ml reservoir solution in a 24-well Limbro plate). Needle-shaped crystals were observed after 3 days incubation at 25 °C and were of the dimensions of approximately 500 x 25 x 25 µm. Unfortunately this was judged to be too small for X-ray data collection; attempts to loop these crystals were made by Dr. Mohammed but the crystals were too small and fragile for successful looping prior to flash-cooling.

Additional rounds of optimisation were conducted using the Mosquito robot. Varying concentrations, from 0.25 M to 1.5 M of NaCl, ammonium sulphate, ammonium chloride or ammonium acetate were used in combination with 0.1 M HEPES pH 7.0 and 0.5 % w/v PEG

8000. Protein concentration was varied at 5, 10, 15 or 20 mg/ml for each condition. No discernible improvement in crystal size or morphology was obtained. A commercially-available additive screen (Additive Screen, Hampton Research) was employed using the base condition (1 M ammonium sulphate, 0.1 M HEPES pH 7.8, 0.5 % PEG 8000), with protein concentration fixed at 20 mg/ml (protein buffer was 50 mM NaCl 20 mM Tris pH 8.0 as before). This screen includes a range of divalent cations, some of which have been noted to have favourable effects upon protein crystallization (Trakhanov and Quiocho Protein Science 1995). Numerous hits were obtained after 3 days and the conditions are tabulated in **Table 5.3** below.

Well	Additive
A6	**0.1 M Magnesium chloride hexahydrate**
A7	**0.1 M Manganese(II) chloride tetrahydrate**
A8	0.1 M Strontium chloride hexahydrate
B2	0.1 M Praseodymium(III) acetate hydrate
B3	**1.0 M Ammonium sulphate**
B4	**1.0 M Potassium chloride**
B5	**1.0 M Lithium chloride**
B7	0.5 M Sodium fluoride
C1	1.0 M Sodium malonate pH 7.0
C5	0.1 M Sodium bromide
C12	0.1 M Taurine
D1	0.1 M Betaine hydrochloride
D6	0.1 M Trimethylamine hydrochloride
D10	0.1 M Adenosine-5'-triphosphate disodium salt hydrate
D11	**0.1 M TCEP hydrochloride**

Table 5.3. LILRA4 D1 Hampton Research Additive Screen for crystallisation. Highlighted additives were used for scale-up screening.

From this screen, six additives were selected as giving rise to the most favourable morphologies, and were used in a larger scale screen (1 µl plus 1 µl hanging drops, 1 ml reservoir solution in a 24-well Limbro plate) utilising essentially the same conditions as the small-scale additive screen. These additives are highlighted in **Table 5.3**. A final condition

was selected (1 M ammonium sulphate, 0.1 M HEPES pH 7.8, 0.5 % PEG 8000, 10 mM manganese chloride tetrahydrate) and replica drops were set up on the larger scale at varying protein concentrations from 10 mg/ml to 20 mg/ml in 2 mg/ml steps. Crystals were visible in these drops after just 3 h incubation and were thick oblate/needle shaped crystals but with multiple nucleation sites in each drop. Reducing protein concentration only partly correlated with the number of crystals in each drop and the dimensions of the crystals were still not improved (i.e. the crystals were of sufficient length but insufficient depth and width to be viable for X-ray data collection).

Additional optimisations on the large scale were conducted. These included omitting the PEG 8000 (which appeared to have no effect), varying the well solution volume to attempt to change the rate of equilibration between the drop and the well solution, varying the drop size (using 2 µl plus 2 µl and 3 µl plus 3 µl size drops) and attempting sitting drops (1 µl plus 1 µl and 2 µl plus 2 µl in sitting-drop bridges). No improvements in terms of a reduction in the number of nucleations or an increase in the dimensions of the crystals were obtained. Using three-quarters and half-strength conditions (down to 0.5 M ammonium sulphate, 50 mM HEPES pH 7.8, 5 mM manganese chloride tetrahydrate) resulted in reduced numbers of nucleations but also slightly smaller, thinner needle crystals and thus offered no progress.

Streak seeding has previously been used to optimise crystal generation for LILRB2 (Willcox et al. 2002). In this process, whole microcrystals are touched with a fine hair or fibre and used to transfer nucleation sites to a sitting drop that has been pre-equilibrated overnight with half-strength condition and at a low protein concentration that is capable of supporting crystal growth but insufficient for *de novo* nucleation. Drops are streaked in a serial fashion to reduce the number of nucleation sites in each successive drop and thus encourage the growth

of single crystals of larger dimensions. For LILRA4 D1, large scale drops (1 µl plus 1 µl) were equilibrated against reservoir solution at half strength (0.5 M ammonium sulphate, 50 mM HEPES pH 7.8, 5 mM manganese chloride tetrahydrate) and protein concentration was varied between 1-4 mg/ml at 1 mg/ml steps with six repetitions. After overnight equilibration, previously grown microcrystals were touched with a clean cat whisker, and the streak-seeding drops were then opened and streaked serially with the whisker. Drops were then re-sealed and incubated at 25 ºC. Inspection was conducted using a light microscope after 3 days and weekly for five weeks but only small amounts of precipitate were visible; no crystals grew.

An alternative additive screen was then utilised on the larger scale (Molecular Dimensions Ltd., Additive Screen 1). 1 µl of protein solution at 16 mg/ml was mixed with 0.8 µl of condition at 1.25 x strength (i.e. 1.25 M ammonium sulphate, 125 mM HEPES pH 7.8, 12.5 mM manganese chloride tetrahydrate) and 0.2 µl of each of 24 additives, one for each well. After one week of incubation at 23 ºC, a heavy precipitate was visible in most drops. Those drops which gave microcrystals, the additive used and the morphologies are listed below in **Table 5.4** (overleaf).

Although seven of the additives yielded microcrystals, only slight improvements in crystal dimensions and morphologies were visible in two of the drops, one containing 5 mM DTT as an additive and the other containing 10 mM magnesium chloride. It was felt that this approach was not productive enough to pursue and that a more broad variation in condition was necessary.

Tube #	Compound	Type	Concentration	Observed Crystals
2	Glutamine	Amino acid	50 mM	Thick needles
3	Spermine tetra hydrochloride	Polyamine	10 mM	Bones/brush-forms
4	Spermidine	Polyamine	10 mM	Multiple needles
6	**Dithiothreitol**	**Reducing agent**	**5 mM**	**Thick bone-forms**
16	Ethylenediamine*	Amine*	5 mM	Multiple needles
19	**Magnesium chloride**	**Divalent cation**	**10 mM**	**Thick needles/bones**
23	2-propanol*	Organic*	3 %	Multiple needles/brushes

Table 5.4. LILRA4 D1 Molecular Dimensions Additive Screen for crystallisation. Highlighted additives produced marginally improved morphology microcrystals. Compounds marked with an asterisk are volatile and were added to the well solution at 1/10th volume as well as the drop, as per the screen instructions.

Three final rounds of optimisation were attempted on the small scale. A screen was produced which varied pH against percentage (w/v) of the precipitant, PEG 8000. The pH was varied between 6.8 and 9.0 units in 0.2 unit steps and the percentage of PEG 8000 was varied between 0.1 % and 0.8 % in steps of 0.1 %. LILRA4 D1 protein concentration remained fixed at 20 mg/ml in 50 mM Na Cl 20 mM Tris pH 8.0 buffer. In a separate screen, the protein concentration was varied from 20-8 mg/ml against a percentage of glycerol from 0 to 5.5 % in 0.5 % steps. Finally, the glycerol screen was repeated at 4 ºC. Despite this broad range of conditions, no improvement in crystal size was observed.

Figure 5.4 shows light microscope images of the LILRA4 crystals that were observed at various stages of the optimisation process.

(a)

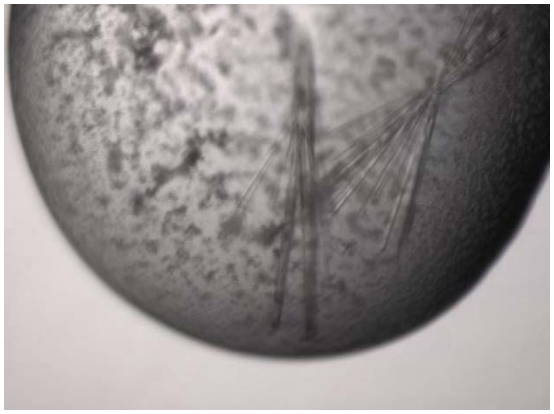

(b)

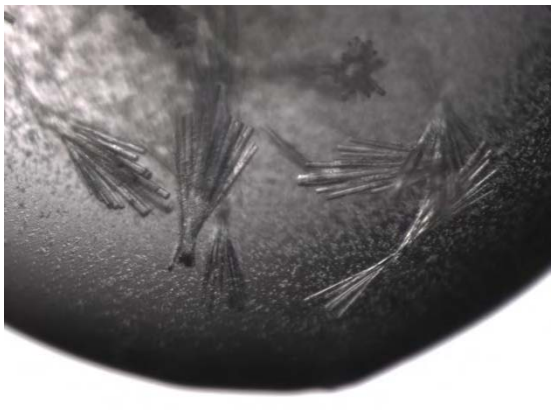

(c)

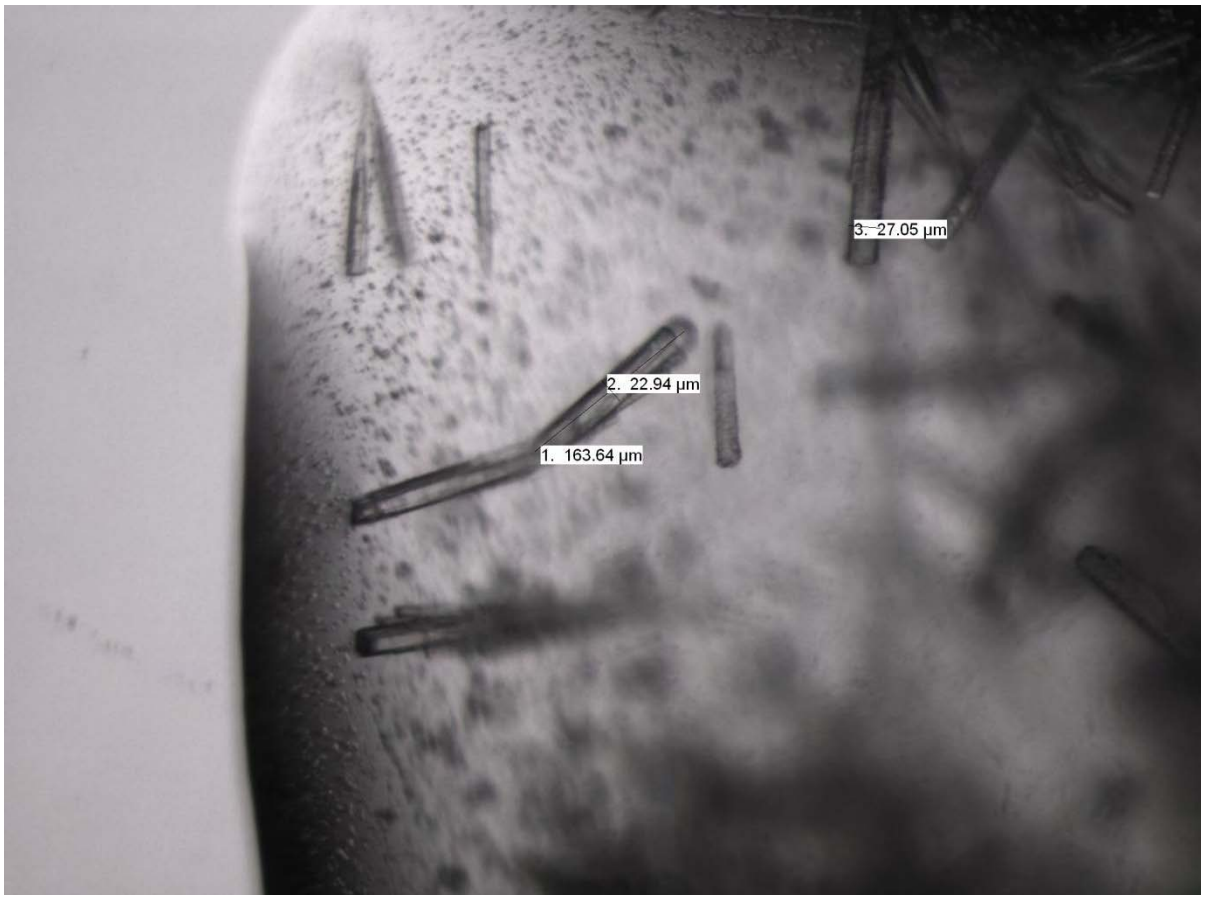

Figure 5.4. Light micrograph images of LILRA4 crystals. (a): Initial screen crystal hit at 20 mg/ml in Index condition #35 (1.0 M ammonium sulphate, 0.1 M HEPES pH 7, 0.5 % w/v PEG 8000). (b): scale-up of the condition described in (a), but at 25 mg/ml. (c): best morphology crystals of LILRA4 obtained. Protein is at 16 mg/ml in 1.0 M ammonium sulphate, 0.1 M HEPES pH 7.8, 0.5 % w/v PEG 8000, with 10 mM manganese chloride tetrahydrate as an additive. Dimensions (length, width) are marked in µm.

5.3 Nuclear Magnetic Resonance studies of LILRA4 D1

The unsuccessful attempts at crystallisation of LILRA4 D1 proved too problematic to overcome and an alternative structural strategy was adopted. NMR was an attractive alternative, since it provides detailed information about both the structures and dynamics of proteins but involves studying the target protein in solution, with no requirement for crystallisation. In addition, the D1 domains of the Group II LILRs that I generated refolded in high yields that were adequate for NMR methods. Furthermore, although NMR spectroscopy is limited by the size of the protein under study (typically under 50 kDa, although the technique is rapidly developing) and is not well suited to large macromolecular complexes, single Ig domains would theoretically be suitable for NMR analysis. An in-depth explanation of the underlying theory of NMR is beyond the scope of this thesis; however a brief outline of the principles involved has been presented in my Materials and Methods, Chapter 2. This work was conducted in collaboration with Dr. Timothy Knowles (Overduin NMR Group, Institute for Cancer Sciences, University of Birmingham).

5.3.1 NMR Analysis of Unlabelled LILRA4 D1

To determine the suitability of LILRA4 D1 for NMR analysis, an initial experiment was conducted with unlabelled LILRA4 D1 protein, produced as described in Section 5.2.2. A refolded protein sample was concentrated to approximately 1 mM in 50 mM Na Cl 20 mM Tris pH 8.0 buffer, [90 % H_2O / 10 % D_2O] and analysed using a Varian Inova 800 MHz NMR spectrometer equipped with an HCN 5 mm z-PFG cryogenic probe with enhanced ^{13}C and ^{1}H sensitivity (HWB-NMR, University of Birmingham). The resulting ^{1}H NMR spectrum is displayed in **Figure 5.5**. The presence of sharply-defined peaks is indicative that the protein is folded; sharp, dispersed peaks below 1.5 ppm to 0 and below indicate the presence of methyl groups, and those between 6-11 ppm represent amides and aromatics.

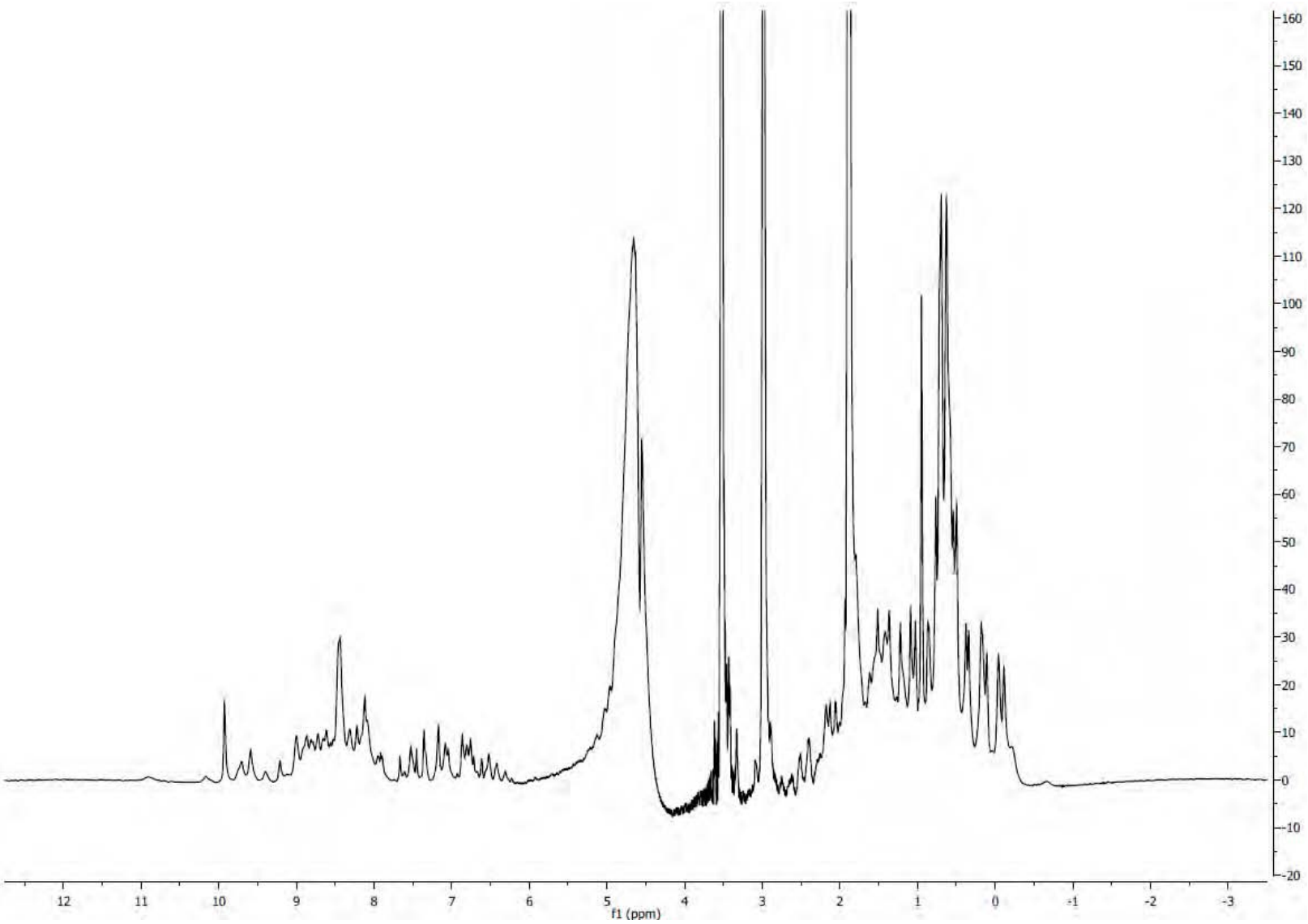

Figure 5.5. 1D Watergate NMR analysis of unlabelled LILRA4 D1.

The presence of sharp signals below 0 ppm is also indicative of a folded protein. The strong peak at 4.7 ppm is H2O, and other strong peaks at 3.5 ppm and 3.0 ppm are buffer components. These results were indicative that LILRA4 D1 was suitable for further analysis by NMR.

5.3.2 3D HSQC NMR Analysis of ^{13}C ^{15}N-labelled LILRA4 D1

The structural determination of a protein by NMR requires the assignment of all H/C/N residues within the protein. NMR assignment experiments tend to be lengthy and require a protein to be stable at RT for several days. Using thermal shift screening as discussed previously, 50 mM Na Cl 50 mM potassium phosphate pH 7.0 was chosen for its increased stability compared to the previously used Tris based buffer. A test aliquot of the refolded LILRA4 D1 protein was buffer exchanged with a PD-10 column, concentrated to 1 mM and left at room temperature for seven days to observe protein stability. No evidence for protein precipitation was visible and spectrophotometric analysis at 280 nm (following high-speed centrifugation at 13,000 g to pellet precipitates) showed no reduction in absorbance, suggesting that the protein was stable at room temperature in the new buffer for long periods of time.

For assignment to be performed isotope labelling of carbon and nitrogen residues by ^{13}C and ^{15}N is required. ^{12}C and ^{14}N are not NMR active and as such cannot be used for study. $^{13}C/^{15}N$ LILRA4 D1 was produced by expression in *E. coli* BL21(DE3) cells transfected with the LILRA4 D1-pET23a plasmid and grown in M9 minimal media supplemented with ^{13}C-labelled glucose and ^{15}N-labelled ammonium chloride. Induction, inclusion body purification and chemical refolding were as previously described. The final purification step by SEC utilised the new phosphate buffer. The protein was concentrated to 1 mM prior to analysis by

3D NMR spectroscopy. Backbone assignment spectra were recorded on LILRA4 using a Varian Inova 800 MHz spectrometer equipped with an HCN 5 mm z-PFG cryogenic probe with enhanced ^{13}C and ^{1}H sensitivity: HNCA, HNCACB, HNCO, HNCACO and CBCA(CO)NH (described more fully in Chapter 2 Section 2.6). Initial data processing was conducted using the NMRPipe program (Delaglio et al. J Biomol NMR 1995). Protein backbone assignments were conducted using the program SPARKY 3 (Goddard and Kneller, University of California, San Francisco). The backbone ^{1}H, ^{15}N, C_O, Cα and Cβ chemical shift values for each resonance – where assignable – are listed in **Table 5.5** (overleaf). A number of residues were un-assignable due to weak resonance signals from these residues, most likely due to dynamic/flexible regions within the protein. The final ^{1}H-^{15}N HSQC contour plot for LILRA4 D1 highlighting its backbone assignments is shown in **Figure 5.6**. **Figure 5.7a** shows which residues of LILRA4 D1 were successfully assigned or otherwise un-assignable.

5.3.3 TALOS Prediction of LILRA4 D1 Secondary Structure

The recorded assignments were submitted to the NMR structural web server, TALOS (Cornilescu et al. J Biomol NMR 1999). TALOS calculates the protein backbone dihedral angles, phi (φ) and psi (ψ), and can also be used to predict the secondary structure of the protein. The phi and psi angles for LILRA4 D1 are shown in **Table 5.6** and plotted in **Figure 5.7b**. The secondary structure prediction from TALOS is shown in graphical form in **Figure 5.7c.**

Residue	Chemical Shift Values (ppm)				
	H	N	CA	CB	CO
E1	-	-	56.611	30.285	175.799
N2	8.496	119.103	53.258	38.722	174.412
L3	8.193	123.629	52.866	41.694	174.842
P4	-	-	62.571	32.206	177.489
K5	8.542	124.883	55.012	32.732	175.022
I7	-	-	54.851	35.227	173.332
L8	9.029	125.906	53.349	45.604	174.531
W9	8.77	129.305	54.552	29.823	174.744
A10	8.525	119.965	52.877	48.6	-
P12	-	-	64.365	33.858	175.871
G13	7.169	110.082	45.16	-	-
P14	-	-	63.529	32.223	173.868
V15	7.159	119.054	61.381	31.688	175.576
I16	8.776	130.454	57.901	41.293	174.8
T17	8.217	123.872	62.903	68.978	173.791
R18	8.299	126.017	58.016	29.855	175.728
H19	9.608	116.961	57.324	27.384	174.935
N20	8.187	120.838	51.31	38.292	173.136
P21	-	-	62.355	33	176.147
V22	8.285	115.751	60.777	35.237	172.478
T23	8.456	122.48	61.566	70.447	172.13
I24	8.575	127.879	60.211	38.952	173.149
W25	8.574	126.601	54.924	30.375	174.057
C26	8.345	117.123	52.804	44.143	171.898
Q27	9.826	127.71	54.802	33.165	174.996
G28	8.526	119.359	45.662	-	-
T29	-	-	53.762	44.888	174.785
L30	8.547	121.919	57.713	63.027	173.516
E31	8.546	128.777	57.068	38.157	176.392
A32	7.207	122.262	53.041	18.942	177.58
Q33	8.983	119.729	55.674	-	-
G34	-	-	56.126	-	174.676
Y35	8.599	115.311	59.007	35.204	172.552
R36	7.652	115.508	52.43	34.649	174.244
L37	8.77	129.305	62.851	32.697	175.436
D38	8.581	120.414	60.751	40.433	173.48
K39	8.918	130.085	53.788	47.075	175.289
E40	9.338	127.655	57.566	32.132	0
G41	9.097	119.317	58.029	-	175.712
N42	9.608	116.969	57.324	27.384	174.935
S43	8.548	121.905	58.392	65.456	174.043
M44	8.071	117.776	55.396	29.298	174.043
S45	8.071	117.777	55.396	29.298	174.056
H47	-	-	62.851	32.697	175.437
I48	8.581	120.404	60.751	40.433	173.48
L49	8.918	130.085	53.788	47.075	175.289
K50	9.338	127.655	57.579	32.138	170.7

Table 5.5. Chemical shift values for LILRA4 D1 NMR data *(continued overleaf)*. For each residue in LILRA4, the ^{15}N, ^{1}H, and $^{13}C_{\alpha/\beta/o}$ chemical shifts are listed, where determined.

Residue	Chemical Shift Values (ppm)				
	H	N	CA	CB	CO
T51	8.796	120.706	49.579	22.911	176.036
L52	9.107	119.422	52.87	32.601	-
S54	-	-	62.173	30.604	177.901
E55	8.224	112.441	58.179	65.848	174.851
N56	8.91	121.037	52.917	43.13	174.694
K57	8.733	124.275	54.544	35.372	176.119
V58	7.994	124.702	64.525	33.546	173.777
K59	7.745	121.547	61.838	31.54	175.576
L60	8.796	120.706	53.762	44.888	174.785
S61	8.547	121.919	57.713	63.027	173.52
I62	8.547	128.776	58.404	55.532	174.241
P63	-	-	64.328	32.167	176.019
S64	6.76	109.193	55.786	62.802	173.731
M65	8.59	128.36	56.828	32.649	175.686
W67	-	-	60.722	-	179.611
E68	9.042	115.068	58.557	28.834	176.498
H69	7.658	117.186	58.368	33.368	177.09
A70	7.476	122.495	52.831	19.609	176.478
G71	8.557	108.764	44.258	-	170.859
R72	8.211	119.836	55.633	32.19	174.581
Y73	-	-	56.504	42.236	174.639
H74	8.671	114.106	56.593	34.256	173.305
C75	8.524	119.96	52.877	48.6	-
Y76	-	-	56.256	43.787	174.669
Y77	8.6	115.314	55.888	41.018	172.332
Q78	8.324	121.52	54.141	29.298	174.282
S79	8.492	126.121	56.77	65.085	173.052
P80	-	-	65.527	31.333	176.513
A81	7.658	116.837	52.102	19.6	176.861
G82	7.621	107.176	43.975	-	173.348
W83	8.558	121.489	57.866	30.515	176.938
S84	9.12	117.736	58.407	65.457	174.039
E85	8.071	117.777	55.396	29.298	-
P86	-	-	62.173	30.604	177.901
S87	8.224	112.441	58.179	65.848	174.858
D88	8.91	121.036	54.713	38.591	175.706
P89	-	-	62.402	31.759	176.168
L90	8.625	123.905	53.349	45.722	174.543
E91	-	-	54.61	-	174.751
L92	8.888	125.516	53.727	43.32	177.227
V93	9.122	127.335	61.437	35.607	173.459
V94	7.994	124.702	58.947	33.546	175.537
T95	8.262	118.658	59.64	70.095	173.72
A96	8.67	123.995	53.334	19.632	176.456
Y97	7.215	120.317	58.091	39.364	179.82

Table 5.5. Chemical shift values for LILRA4 D1 NMR data *(continued)*

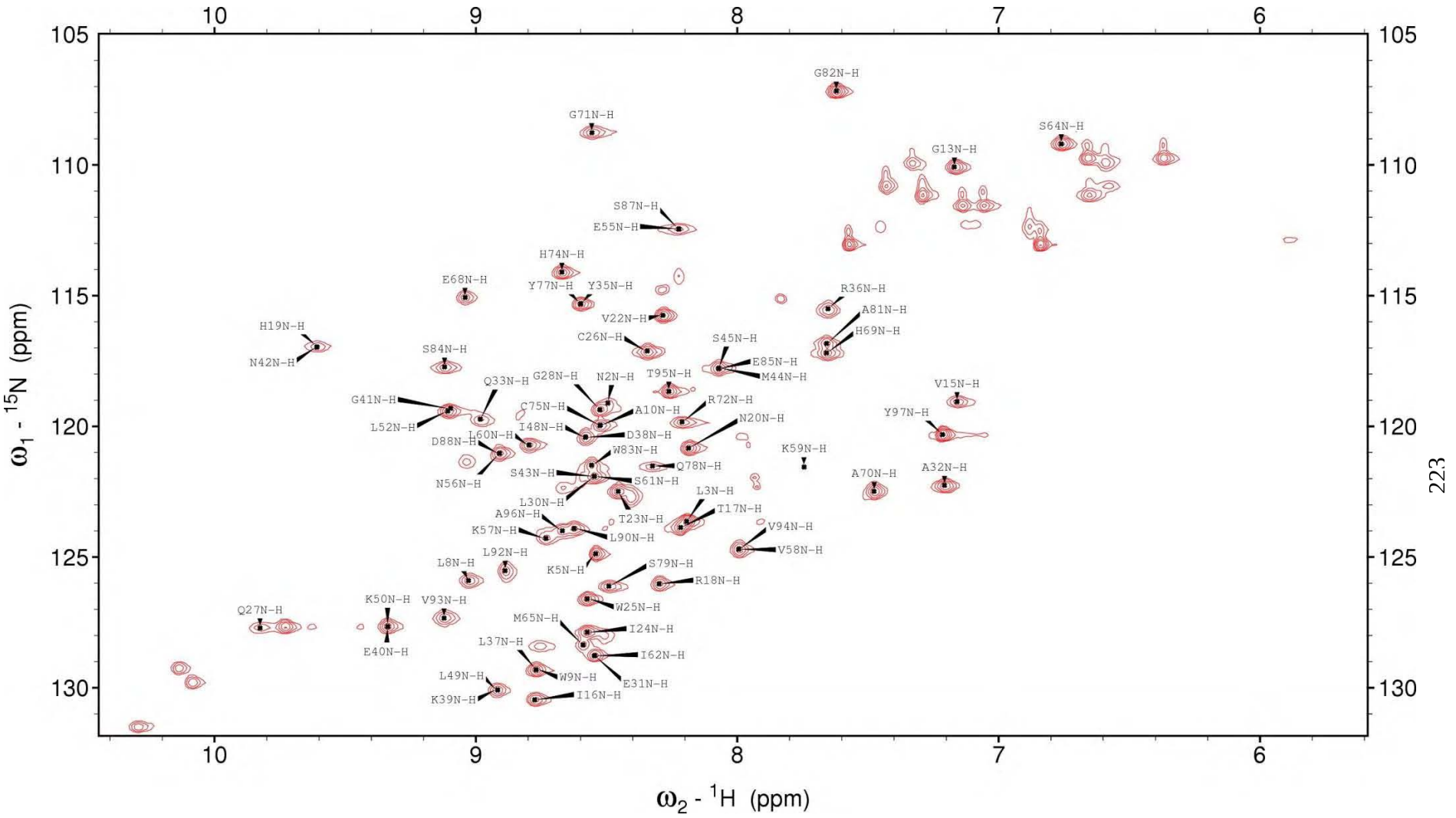

Figure 5.6. HSQC plot for $^{13}C^{15}N$-labelled LILRA4 D1. Peaks corresponding to assigned residues are marked.

Residue	Phi, ϕ	Psi, ψ
3	-94.7	126.1
4	-67.9	146.4
5	-88.8	131.4
6	-67.5	146.8
7	-111.9	144.9
8	-105	121.6
9	-120.5	138.5
10	-123.7	148
11	-95.1	118.7
12	-63.5	149.7
13	-119.9	147.6
15	-95.7	127.2
16	-122.6	138.5
17	-82.8	137.5
20	-80.1	136
21	-69.7	149.2
22	-132.8	140.3
23	-118.7	125.5
24	-115.1	130.4
25	-124.5	141.7
26	-125.8	140.1
27	-125.1	126.7
28	-130.4	137.8
29	-132.8	151.9
30	-87.2	125.5
32	-86.1	139.7
35	56.8	40.4
36	-122.1	141.9
38	-93.8	130.6
39	-111.5	125.7
40	-115.9	118.9
43	-104.8	-27.7
44	-146.7	172.2
45	-109	150.6
46	-76.7	143.1
47	-87.5	-34.4
48	-137	132.2

Residue	Phi, ϕ	Psi, ψ
49	-118	127.3
50	-101.1	122.6
51	-132.6	150.8
55	-93.7	0.8
56	-129.5	140.6
57	-126.1	142.8
60	-118.9	130.8
61	-100	122.8
62	-108.2	128.2
63	-58	-27
64	-121.6	124.8
68	-64.2	-27.4
69	-92.1	-16.9
70	-86.8	151.9
71	-162.5	162.4
72	-108.2	136.2
73	-118.9	154.9
74	-142.5	142.9
75	-117.5	139.6
76	-127.7	149.4
77	-147.2	154.6
78	-97.8	120.6
79	-100.9	141
80	-54.9	-33.3
81	-90.6	-1.8
82	-104.4	158.8
83	-89	123.5
85	-98	132.5
88	-66.9	147.4
89	-64.2	148.9
90	-121	139
91	-125.8	135.8
92	-109.3	125.9
93	-125.9	139.5
94	-114.2	123
95	-116	151.9

Table 5.6. TALOS output for LILRA4 D1 NMR data. Phi, Psi (ϕ,ψ) main-chain dihedral angles are tabulated for each residue with assigned resonance.

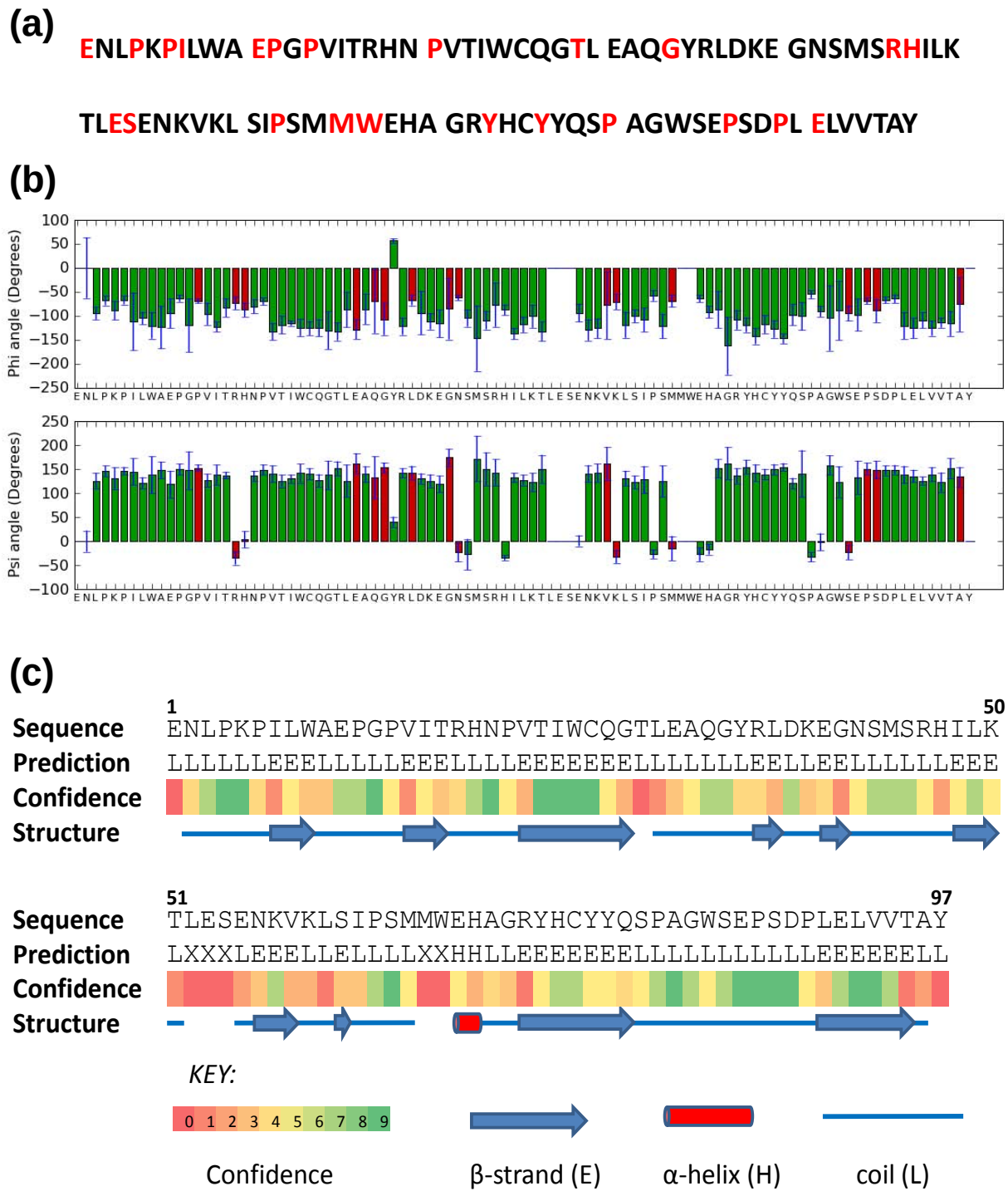

Figure 5.7. TALOS secondary structure prediction for LILRA4 D1. (a): Primary amino acid sequence of LILRA4 D1. Residues lacking ^{1}H, ^{15}N assignments are in red. (b): Output from TALOS showing Phi, Psi (ϕ,ψ) protein backbone dihedral angles for LILRA4 D1. (c): TALOS secondary structure prediction. The TALOS prediction is listed below the LILRA4 D1 primary sequence, showing β-strand (E), α-helix (H) and coil (L) regions. Confidence for each residue prediction is colour-coded red to green. The secondary structure prediction is also shown in diagrammatic form.

TALOS predicts the presence of ten β-strands and one α-helix in those regions of LILRA4 D1 for which we had assignable NMR resonances. By comparison with the known Group II LILR secondary structures, I would designate these strands AA'BCC'EFG as per standard C2-type Ig fold terminology (**Figure 5.8**). Disrupted strands are evident but may be a result of missing assignments and the resulting lower confidence of the predictions made by TALOS. Structural elucidation would be necessary for more precise analysis of the secondary structure of the LILRA4 D1 domain; however, the predictions are highly analogous to that of the other Group II LILRs that have structural solutions, i.e. LILRB4 and LILRA5. The single alpha-helical region in the D1 domain between the E and F strands is evident, and although TALOS is unable to predict the presence of the polyproline helix, the primary amino acid sequence is almost identical to LILRB4 and LILRA5 in this region.

The TALOS output file was submitted to the web server, CS-ROSETTA (Shen et al. J Biomol NMR 2009). CS-ROSETTA uses distributed computing power to predict the tertiary structure of proteins from backbone assignment (chemical shift) data. Unfortunately however, due to the missing assignments in the LILRA4 D1 NMR spectrum, CS-ROSETTA was unable to calculate a final structural solution. The absence of strong, assignable NMR resonances for many residues in the LILRA4 D1 protein could be attributable to flexibility within the molecule at these residues. This hypothesis fits with the observed intransigence of LILRA4 D1 to crystallisation, and is reflective of a common theme within the LILR receptors which may explain the refractoriness to chemical refolding and crystallisation exhibited by some members of the LILR family.

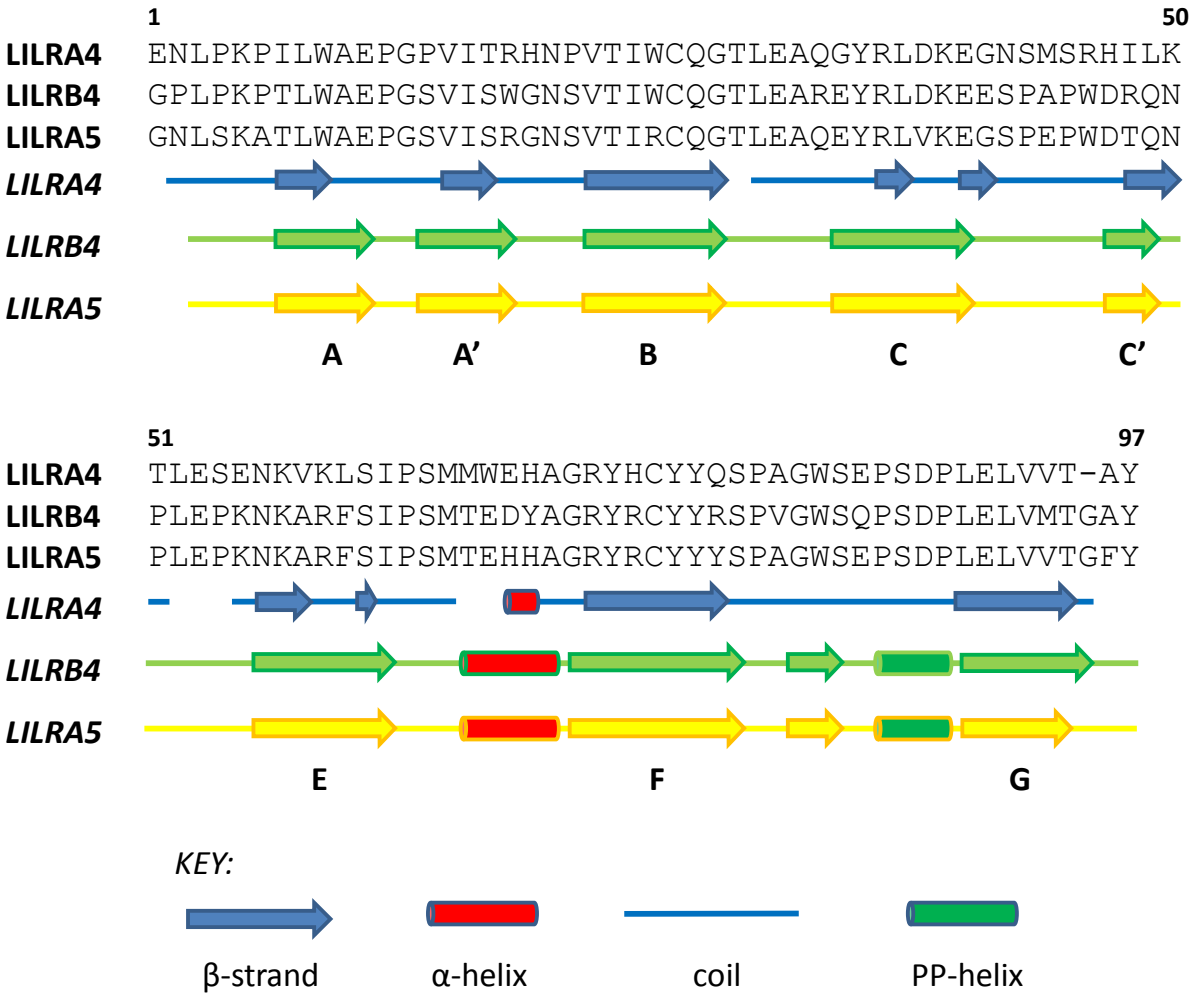

Figure 5.8. Comparison of secondary structures of Group II LILR D1 domains. TALOS secondary structure prediction for the LILRA4 D1 NMR data is shown alongside the PROCHECK secondary structure designation for the known Group II LILR D1 structures, LILRB4 D1 (from the LILRB4 ectodomain structure) and LILRA5 D1 (from Maenaka et al. 2006). Primary amino acid sequence for each molecule is listed with the secondary structures shown in diagrammatic form below. Strand designations are from LILRB4 and LILRA5, which have essentially identical secondary structures in the D1 domain.

5.4 Investigating LILRA4-Ligand Interactions

5.4.1 Introduction

While the molecular properties of Group I LILR/ligand interactions have been studied extensively, those of Group II LILRs have not, mainly due to a lack of ligands identified for this subset. Recently, the group of Professor Wei Cao (MD Anderson Cancer Centre, University of Texas) identified the ligand for LILRA4 as being BST2 (also known as Tetherin, CD317 or HM1.24), by an expression cloning approach (Cao et al, JEM 2009). BST2/Tetherin has also been the subject of a recent publication by Neil et al, who identified it as the host innate immune defence factor which inhibits the budding of enveloped viruses including HIV-1 from infected cells (Neil et al. Nature 2008 and see Introduction Section 1.2). While data described by Cao et al showed evidence for direct LILRA4/BST2 interaction, the approaches involved, namely a plate-bound ELISA and also SPR using LILRA4-Fc fusion protein injected over amine-immobilized BST2-Fc (Cao et al. JEM 2009), provided little information regarding the monomeric LILRA4/BST2 binding properties. We therefore established a collaboration with Professor Wei Cao to use SPR to investigate the molecular properties of the monomeric interaction by using monomeric LILRA4, either in 2-domain or full 4 ectodomain forms, in order to try to investigate the affinities and kinetics of LILRA4/BST2 recognition.

5.4.2 Production of Recombinant LILRA4 D1D2 in the *Drosophila* Expression System

Attempts to produce refolded LILRA4 – both two-domain and four-domain constructs – by chemical refolding from *E. coli* inclusion bodies were unsuccessful, as the protein proved to be refractory to standard Garboczi chemical refolding methods. Instead, I adopted a strategy utilising expression of the receptor in an insect cell expression system, using *Drosophila melanogaster* S2 cells. The coding region of the gene for the full-length LILRA4 ectodomain

was cloned into the pMT/BiP/V5-His expression vector, which includes a signal peptide for efficient export of soluble protein into the cell culture medium and an N-terminal His-tag (comprising six consecutive histidine residues) for purification by Ni-NTA column. Protein expression in this system is inducible by the addition of $CuSO_4$, under the control of the metallothionein promoter. The cloning process is outlined in **Figure 5.9**.

I designed primers to introduce a BglII restriction site into the 5' end of the LILRA4 gene and an AgeI restriction site into the 3' end of the coding region for the LILRA4 D2 domain, to allow cloning into pMT/BiP/V5-His. The 3' primer lacked a stop codon to allow read-through of this region and subsequent expression of the His tag encoded by the vector. The LILRA4-pCMV-FLAG construct provided by Dr. Allen was used as a template. Initial attempts at the PCR using pfu polymerase were unsuccessful, but PCR using expand enzyme was successful. The PCR product and the pMT/BiP/V5-His plasmid were digested with BglII and AgeI and gel purified then ligated overnight with T4 DNA ligase. The ligation product was used to transform *E. coli* DH5α cells and colonies were picked for plasmid miniprep and test digests. Successful test digests generated a fragment of the expected molecular weight (c. 600bp) as visualised by agarose gel electrophoresis. Correct LILRA4 D1D2-pMT/BiP/V5-His sequence was confirmed by DNA sequencing (Functional Genomics, University of Birmingham).

I decided to generate a full-length LILRA4-pMT/BiP/V5-His expression construct in order to try to express full-length LILRA4 (LILRA4 F). For LILRA4 F cloning, it was necessary to perform a SDM reaction to remove an internal BglII site within the LILRA4 gene. Confirmation of successful SDM was carried out by test digest of the LILRA4-pCMV-FLAG plasmid with BglII. I then designed a primer to the 3' end of the LILRA4 ectodomain coding

(a)

```
   1 ctacgggcac cgtggccaca cctgcctgca cagccagggc caggaggagg agatgccatg
  61 accctcattc tcacaagcct gctcttcttt gggctgagcc tgggccccag gacccgggtg
 121 caggcagaaa acctacccaa acccatcctg tgggccgagc caggtcccgt gatcacctgg
 181 cataaccccg tgaccatctg gtgtcagggc accctggagg cccaggggta ccgtctggat
 241 aaagagggaa actcaatgtc gaggcacata ttaaaaacac tggagtctga aaacaaggtc
 301 aaactctcca tcccatccat gatgtgggaa catgcagggc gatatcactg ttactatcag
 361 agccctgcag gctggtcaga gcccagcgac cccctggagc tggtggtgac agcctacagc
 421 agacccaccc tgtccgcact gccaagccct gtggtgacct caggagtgaa cgtgaccctc
 481 cggtgtgcct cacggctggg actgggcagg ttcactctga ttgaggaagg agaccacagg
 541 ctctcctgga ccctgaactc acaccaacac aaccatggaa agttccaggc cctgttcccc
 601 atgggccccc tgaccttcag caacaggggt acattcagat gctacggcta tgaaaacaac
 661 accccatacg tgtggtcgga acccagtgac ccctgcagc tactggtgtc aggcgtgtct
 721 aggaagccct ccctcctgac cctgcagggc cctgtcgtga cccccggaga gaatctgacc
 781 ctccagtgtg gctctgatgt cggctacatc agatacactc tgtacaagga gggggccgat
 841 ggcctccccc agcgccctgg ccggcagccc caggctgggc tctcccaggc caacttcacc
 901 ctgagccctg tgagccgctc ctacgggggc cagtacagat gctacggcgc acacaacgtc
 961 tcctccgagt ggtcggcccc cagtgacccc ctggacatcc tgatcgcagg acagatctct
1021 gacagaccct ccctctcagt gcagccgggc cccacggtga cctcaggaga gaaggtgacc
1081 ctgctgtgtc agtcatggga cccgatgttc actttccttc tgaccaagga gggggcagcc
1141 catcccccgt tgcgtctgag atcaatgtac ggagctcata agtaccaggc tgaattcccc
1201 atgagtcctg tgacctcagc ccacgcgggg acctacaggt gctacggctc acgcagctcc
1261 aacccctacc tgctgtctca ccccagtgag ccctggagc tcgtggtctc aggagcaact
```

*MTLILTSLLFFGLSLGPRTRVQA***ENLPKPI**LWAEPGPVITWHNPVTIWCQGTLEAQGY
RLDKEGNSMSRHILKTLESENKVKLSIPSMMWEHAGRYHCYYQSPAGWSEPSDPL
ELVVTAYSRPTLSALPSPVVTSGVNVTLRCASRLGLGRFTLIEEGDHRLSWTLNSHQ
HNHGKFQALFPMGPLTFSNRGTFRCYGYENNTPYVWSEPSD**PLQLLVS**GVSRKPS
LLTLQGPVVTPGENLTLQCGSDVGYIRYTLYKEGADGLPQRPGRQPQAGLSQANFT
LSPVSRSYGGQYRCYGAHNVSSEWSAPSDPLDILIAGQISDRPSLSVQPGPTVTSG
EKVTLLCQSWDPMFTFLLTKEGAAHPPLRLRSMYGAHKYQAEFPMSPVTSAHAGT
YRCYGSRSSNPYLLSHPSE**PLELVVS**

(b)

LILRA4 D1D2
5’ Primer: **GGAATTC AGATCT** GAAAACCTGCCGAAACCGATC
3’ Primer: CCCCTGCAGCTACTGGTGTCA **ACCGGT GGAATTC**
3’ Reverse Complement: **GAATTCC ACCGGT** TGACACCAGTAGCTGCAGGGG

LILRA4 F
3’ Primer: CCCCTGGAGCTCGTGGTCTCA **ACCGGT GGAATTC**
3’ Reverse Complement: **GAATTCC ACCGGT** TGAGACCACGAGCTCCAGGGG

Figure 5.9. Cloning of LILRA4 into pMT/BiP/V5-His for S2 cell expression (*continued overleaf*). (a): Gene sequence for LILRA4 up to the end of the fourth Ig domain. The amino acid translation is listed below the nucleotide sequence, with the leader peptide in italics and the N terminus of the D1 domain, the D2D3 boundary, and the C terminus of the D4 domain in bold. (b): Primer design for LILRA4 D1D2-pMT/BiP/V5-His and LILRA4 F-pMT/BiP/V5-His cloning.

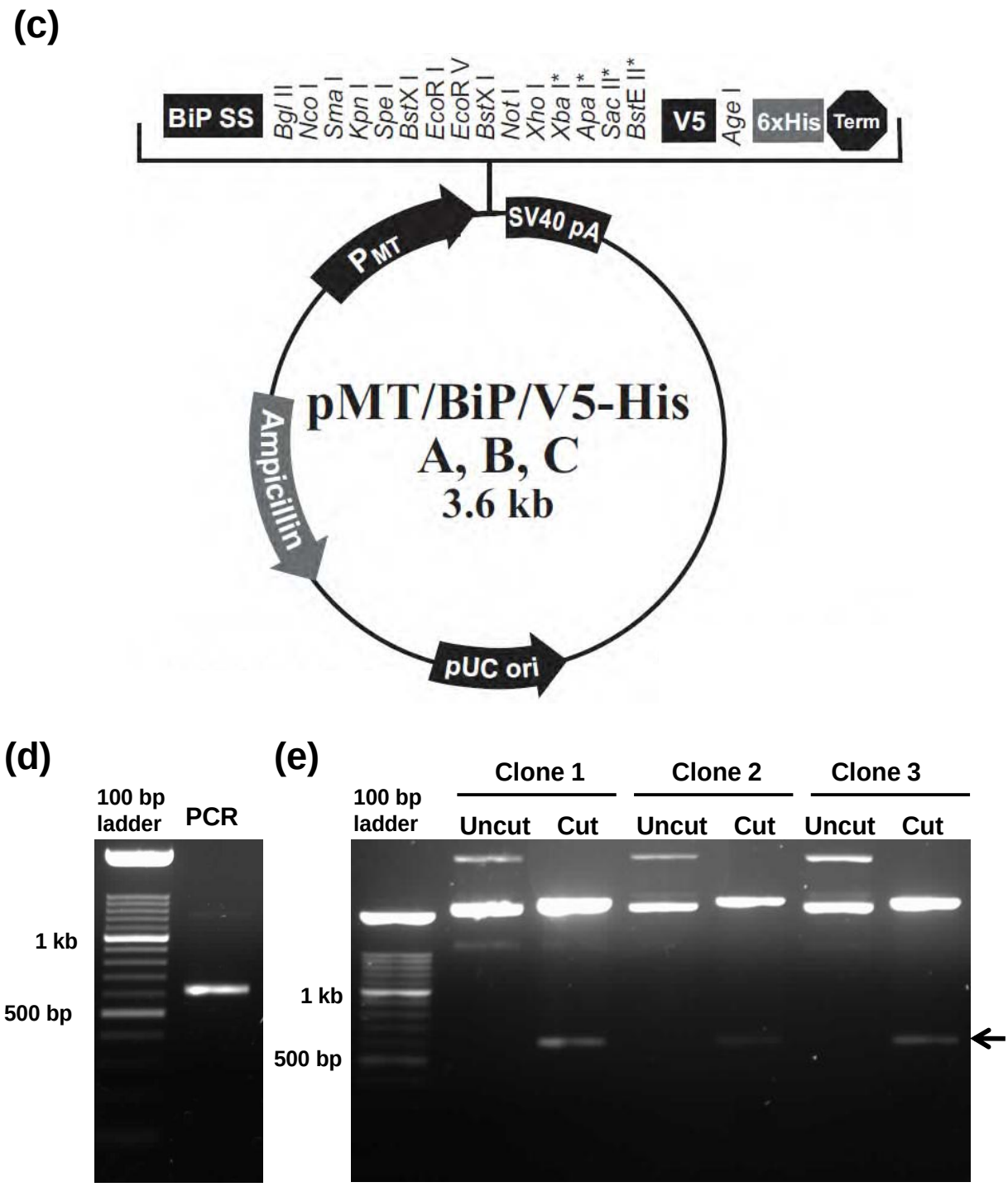

Figure 5.9. (*continued*). (c): Map of the pMT/BiP/V5-His vector, with the MCS expanded to show restriction sites and features such as the metallothionine promoter (P_{MT}), the *Drosophila* BiP signal sequence and the histidine tag (6xHis) highlighted. (from the Invitrogen pMT/BiP/V5-His manual). (d): Agarose gel electrophoresis of the LILRA4 D1D2 PCR product and (e): test digests of three clones from minipreps of the LILRA4 D1D2 PCR product ligated into the pMT/BiP/V5-His vector.

region, incorporating an AgeI restriction site, and used this primer in combination with the 5' primer described above to carry out PCR using the mutagenised LILRA4-pCMV-FLAG plasmid as a template. The PCR product was then digested with BglII and AgeI, gel purified and ligated into similarly digested pMT/BiP/V5-His expression vector. After transformation of *E. coli* DH5α, plasmid miniprep and successful test digests, the DNA sequence was verified (Functional Genomics, University of Birmingham).

The LILRA4 D1D2-pMT/Bip/V5-His and LILRA4 F-pMT/Bip/V5-His vectors were then plasmid maxiprepped and used to transfect *D. melanogaster* S2 cells by calcium phosphate transfection. Transient transfections and test expressions were conducted to show that the protein was correctly expressed; western blotting using an anti-His-tag antibody was performed to attempt to verify the presence of correctly-folded LILRA4 protein. As can be seen from **Figure 5.10a**, LILRA4 D1D2 is detectable under both reducing and non-reducing SDS-PAGE conditions at both 3 days and 4 days post-transfection, with a small shift in the apparent molecular mass between reducing and non-reducing conditions, indicative of correct disulphide bond formation. The apparent mass of the two-domain protein is much higher than the expected mass of 22 kDa, which is likely due to glycosylation. A previous publication had reported that LILRA4 is heavily glycosylated upon expression in 293T cells, as evidenced by a reduction in its apparent mass upon N-glycosidase treatment (Cho et al. Int Immun 2008), and that its apparent mass is heterogenous in this system. The SDS-PAGE analysis in **Figure 5.10a** also shows the presence of a doublet band, which is suggestive of differential glycosylation, in accordance with these published observations.

Unexpectedly, this analysis showed that LILRA4 F was undetectable under non-reducing conditions, which suggests the fully-folded full length protein may be masking the His tag.

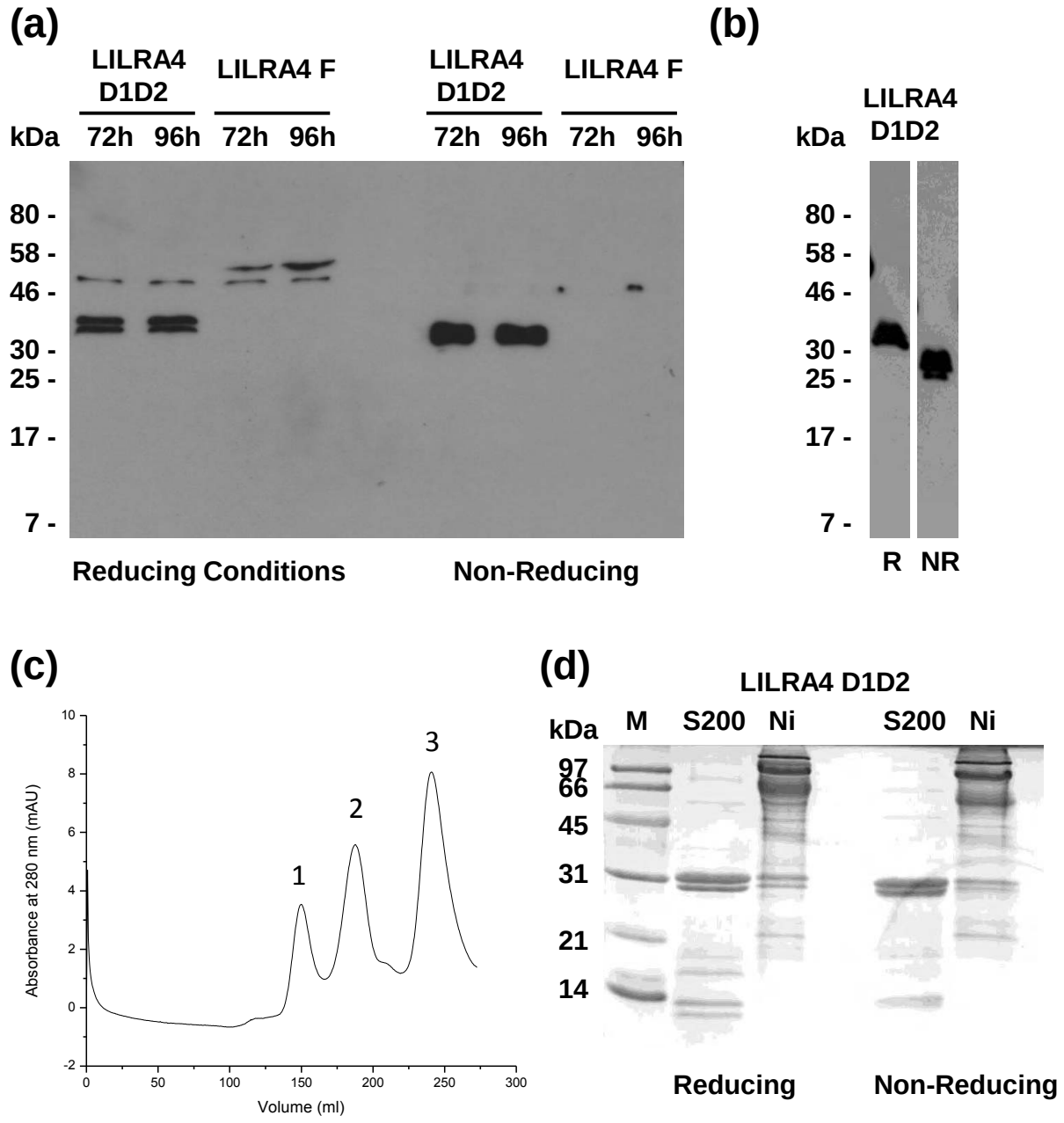

Figure 5.10. Test expression and WB detection of LILRA4 proteins from *Drosophila*. (a): Western blot detection of test expressions of LILRA4 D1D2 and LILRA4F, under reducing and non-reducing conditions, at 72 h and 96 h post-induction, using anti-His antibody. (b): Western blot of samples from bulk expression of the same constructs under reducing (R) and non-reducing (NR) conditions. (c): size exclusion chromatography elution profile for LILRA4 post-Ni-NTA purification using S200 column. Peak positions are indicated. (d): SDS-PAGE analysis of fractions constituting Peak 3 from the SEC elution profile, compared with a sample directly from Ni-NTA elution, under reducing and non-reducing conditions.

Since this would render purification of the full-length protein difficult, expression of LILRA4 F was abandoned in favour of LILRA4 D1D2.

Co-transfection with the pCoHygro plasmid, which includes the Hygromycin resistance gene, allowed the generation of a stable S2 cell line containing the LILRA4 D1D2-pMT/Bip/V5-His plasmid by selection with Hygromycin. Bulk expression of the protein was conducted by growing the cells in 1 L volumes of Schneider's medium and inducing expression when the cells reached log phase of growth (2-4 x 10^6 cells/ml) by the addition of 500 μM $CuSO_4$. The cells were then removed by low-speed centrifugation (to avoid lysis), and the supernatant retained. The supernatant was then analysed again by western blotting to verify expression of the LILRA4 protein (**Figure 5.10b**). The supernatant was then dialysed overnight into 150 mM NaCl 20 mM HEPES pH 7.0, a buffer suitable for purification by Ni-NTA column. 500 ml of dialysed supernatant was applied to the column overnight at 4 ºC, and then the column was washed with 10 mM Imidazole to remove unbound proteins. Elution was carried out with 250 mM Imidazole. To prevent precipitation of the eluted protein, which was of high concentration (approximately 250 μg/ml), the protein fractions were stored on ice.

Following Ni-NTA column purification, the protein sample was subjected to SEC using a Superdex S200 column, both to remove Imidazole and to increase purity. **Figure 5.10c** shows the SEC profile, and it can be seen from this figure that the yield was very low (only 10 mAU absorbance of the highest peak) and that multiple species exist as evidenced by the three peaks. SDS-PAGE analysis of fractions from the first two peaks showed high levels of contaminants but the third peak contained a protein species of the expected mass for two-domain LILRA4. Fractions from the third peak were pooled and concentrated by centrifugation filter device. **Figure 5.10d** shows the SDS-PAGE analysis of the purified and

concentrated protein, as well as a sample of the protein prior to SEC purification. As can be seen from **Figure 5.10d**, the resulting protein sample was not particularly pure, even after purification by SEC, however despite repeat attempts at bulk expression this was the best level of purity attained and so I therefore decided to conduct SPR experiments with this protein sample. I also retained a separate protein sample post Ni-NTA column elution but without purification by SEC. Instead this sample was buffer-exchanged by PD-10 column into 150 mM NaCl 20 mM HEPES pH 7.0.

5.4.3 SPR Analysis of LILRA4 D1D2/BST2 Interaction

Professor Cao kindly provided me with a construct for expression of the BST2-Fc fusion protein in 293T cells. BST2 expression was conducted by the Willcox group's technician, Sarah Nicholls. Purification was by Protein A column and SEC. Refolded soluble BST2-Fc was generated at high concentration and purity as assessed by SDS-PAGE (not shown).

BST2-Fc was immobilized on a CM5 sensor chip using the R10z8e9 anti-human Fc antibody, which was amine-coupled to the surface. As a negative control, a commercially available CTLA4-Fc fusion protein was immobilized to the surface of another flow cell by the same method. Two test injections were then conducted, each of 10 µl volume at a flow rate of 10 µl/min. The first test injection was with Ni-NTA and SEC-purified LILRA4 D1D2 at a concentration of 750 µg/ml; the second test injection was with non-SEC-purified LILRA4 D1D2 at a concentration of 357 µg/ml. Sensorgram traces for this experiment are shown in **Figure 5.11**, along with the immobilisation levels for the R10z8e9 antibody, the BST2-Fc fusion protein and the CTLA4-Fc control protein indicated.

(a)

FC	R10z8e9	Ligand	Level	Total
1	9390	CTLA4-Fc	2219	**11609**
2	9540	BST2-Fc	2062	**11602**

(b)

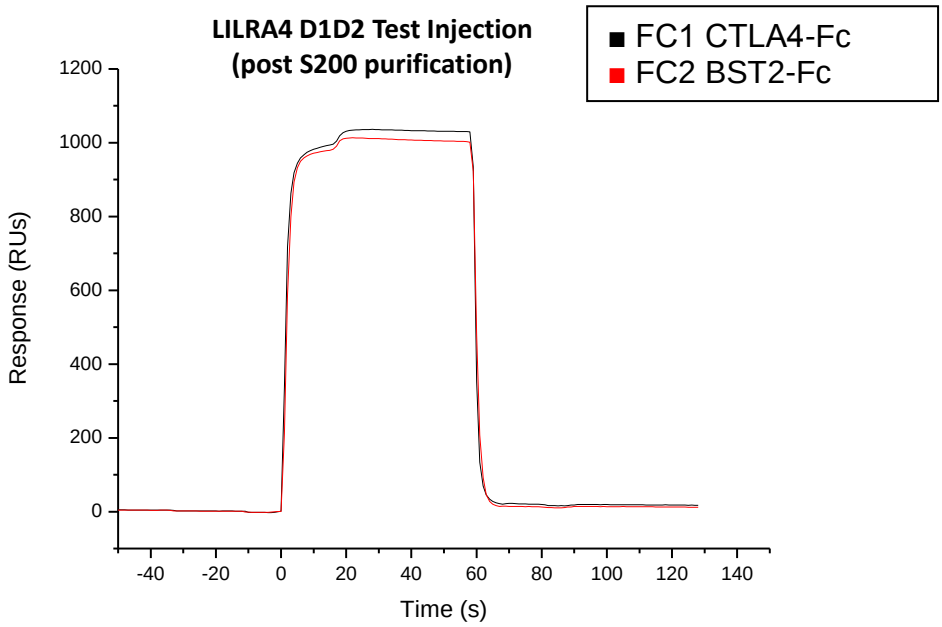

(c)

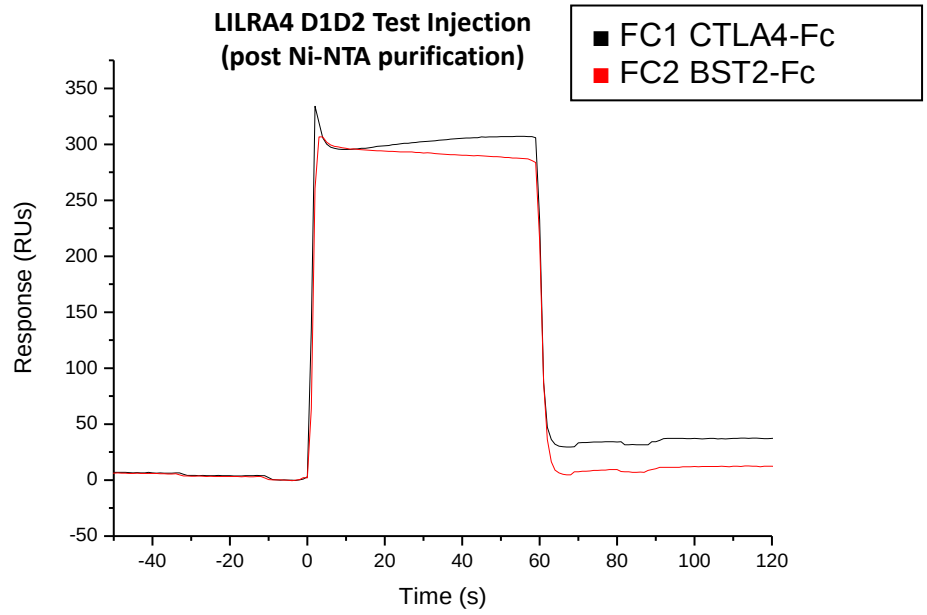

Figure 5.11. SPR analysis of LILRA4/BST2 interaction. (a): Immobilisation levels in resonance units (RUs) for R10z8e9 and proteins under test. (b): Test injection of LILRA4 D1D2 post S200 purification, at 750 µg/ml. (c): Test injection of LILRA4 D1D2 after Ni-NTA column elution, at 357 µg/ml. Flow cells were coated with CTLA4-Fc (FC1, black line) or BST2-Fc (FC2, red line).

From **Figure 5.11** it can be seen that there is no evidence for an interaction between the recombinant monomeric LILRA4 D1D2 protein that I produced, and R10z8e9-immobilised BST2-Fc. More specifically, injection of LILRA4 D1-D2 resulted in similar signals over BST2-Fc and control surfaces, thereby providing no evidence of specific interaction. In order to clarify this result I conducted a second SPR experiment using LILRA4 D1D2 after SEC purification, this time concentrated to 1.28 mg/ml. Immobilisation levels for this experiment are shown in **Figure 5.12a**, and the sensorgram is shown in **Figure 5.12b**. Although the total protein immobilisation levels are lower compared with the first experiment, (due to the reduced amine-coupling of R10z8e9 antibody in this experiment), the amount of potential ligand and control proteins immobilised are still at levels sufficient to see an interaction. In addition, the immobilisation levels were well controlled in these experiments; each flow cell had a roughly equivalent amount of total protein immobilised.

Nevertheless, there is no evidence from the sensorgram trace in **Figure 5.12b** of an interaction between soluble LILRA4 D1D2 and immobilised BST2-Fc. What is clear from these results is that binding of the recombinant soluble LILRA4 D1D2 to BST2-Fc is not detected in these experiments.

(a)

FC	R10z8e9	Ligand	Level	Total
1	4109	CTLA4-Fc	1231	**5340**
2	3958	BST2-Fc	1216	**5174**

(b)

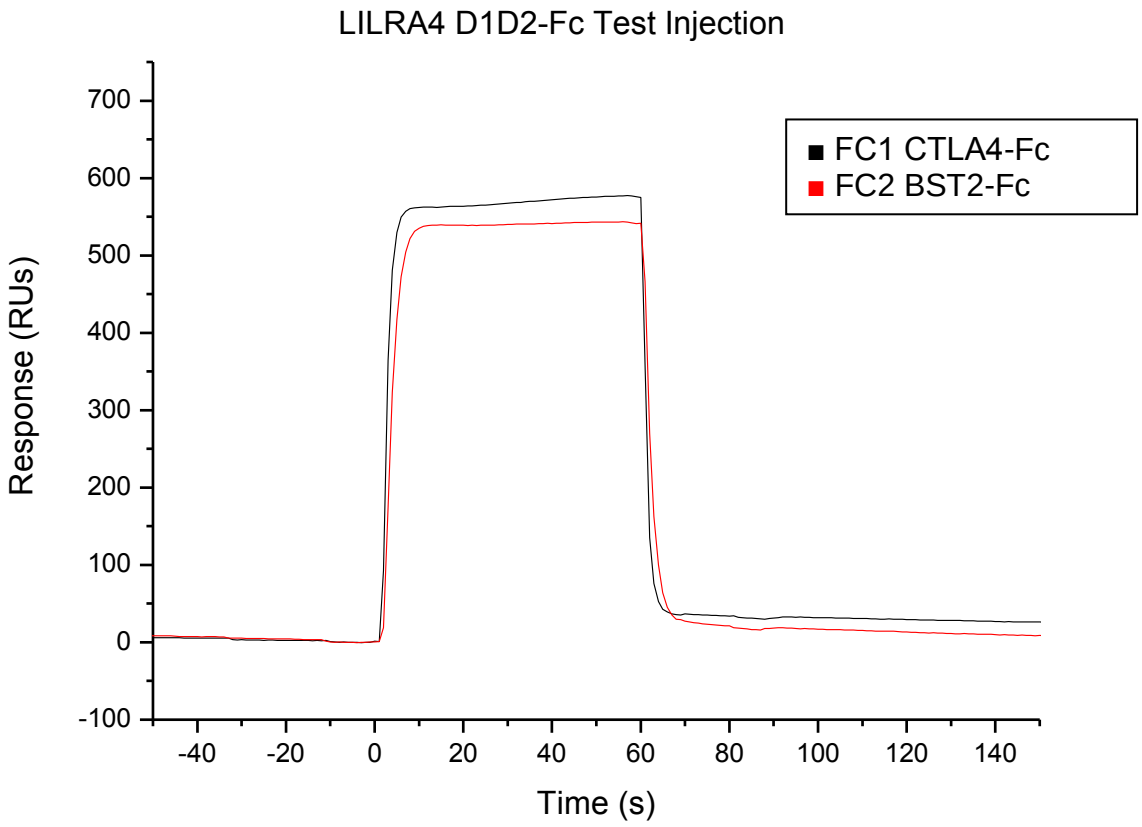

Figure 5.12. SPR analysis of LILRA4/BST2 interaction at higher concentration. (a): Immobilisation levels in resonance units (RUs) for R10z8e9 and proteins under test. (b): Test injection of LILRA4 D1D2 post S200 purification, at 1.28 mg/ml. Flow cells were coated with R10z8e9 alone as a blank (FC1, black line), or R10z8e9 plus CTLA4-Fc (FC2, red line) or BST2-Fc (FC3, blue line).

5.5 Chapter Summary and Discussion

In this chapter, I attempted a structural analysis of the Group II LILR family focussed on the membrane distal D1 domains of each receptor, in the hope of providing limited structural information across the whole Group II subfamily. However, crystallographic approaches proved very problematic, with LILRB3 and LILRB5 failing to crystallise in initial screens. LILRA4 was promising in that it yielded microcrystals in numerous conditions, but the morphology and size of these (i.e. thin needles) rendered them unsuitable for X-ray data collection and despite considerable attempts to overcome these problems data collection quality grade crystals were not generated.

In spite of problems with protein crystallisation, the high yields of the Group II D1 domains generated indicated that NMR methods were a feasible alternative to X-ray crystallographic approaches. LILRA4 was prioritised for these studies as recent studies have highlighted BST2 as a ligand (Cao et al. JEM 2009), the first such identification of a ligand for a Group II LILR. Using standard NMR-based approaches, I managed to produce labelled LILRA4 D1 in sufficient yields for partial assignment of the primary backbone of the protein by 3D NMR spectroscopy, and calculation of the chemical shifts allowed an NMR-based secondary structure prediction of the protein to be conducted using the program TALOS. This analysis, which represents the first structural information about this receptor, indicated the secondary structure of the LILRA4 D1 domain is likely to share many features with other Group II LILRs, and revealed areas of likely high flexibility that could explain the intransigence of this protein to formation of usable crystals.

A second aim was to study the molecular properties of the LILRA4/BST2 interaction, since previous studies have not provided information on the affinity or kinetics of this recognition

event. Such data would be of considerable interest since it would represent the first such analysis of a Group II LILR/ligand interaction. Although I was able to generate a recombinant form of the LILRA4 receptor comprising the membrane distal two domains (D1-D2), a second construct comprising the entire ectodomain (D1-D4) was not produced in a usable form, as a C-terminal His tag was obscured, precluding purification. SPR experiments involving the LILRA4 D1D2 protein failed to demonstrate binding of recombinant protein to immobilised BST2-Fc.

Several explanations for this could be envisaged. Firstly, since the LILRA4 protein utilised comprised only the membrane distal two domains, it is possible that the D3 and D4 domains, or the D2-D3 junction, are crucial for this interaction. If so, this would distinguish LILRA4 from the Group I LILRs, where the D1-D2 domains seem to dominate ligand interactions. A second possibility was that the affinity of the interaction was very low, such that monomeric interactions were undetectable. This remains an attractive possibility, since LILRA4 is, structurally at least, an "activatory" receptor on the basis of its short cytoplasmic tail and association with FcRγ, and both activatory Group I LILRs and activatory KIRs are thought to recognise MHC Class I with considerably lower affinities relative to their inhibitory counterparts. In addition, the Cao et al study on LILRA4/BST2 interaction found LILRA4-Fc protein bound GST-immobilised BST2 with an apparent affinity in the μM range, suggesting the monomeric interaction may indeed be extremely weak. A third possibility was that differences in *Drosophila*-expressed protein (e.g. in the glycosylation pattern) were responsible for lack of detectable binding in the SPR experiments. Heterogenous glycosylation is evident from the western blotting, SEC profile and SDS-PAGE analysis presented earlier. The post-translational modification of the expressed LILRA4 with large sugar moieties may mask the binding site for BST2 or otherwise disrupt the conformation of

the receptor such that it is unable to bind. If correct, this hypothesis would suggest that glycosylation plays a much more important role in LILRA4/BST2 interaction than in Group I LILR/ligand interactions analysed to date. Fourthly, the low purity of the protein that I generated may be responsible for inhibiting binding to immobilized BST2-Fc (see **Figure 5.9d**). Unfortunately, the low yield of expression of LILRA4 in the *Drosophila* system precluded extensive purification steps which might correct this. Finally, the BST2-Fc protein itself may be in a conformation unsuited to binding by LILRA4. There is some evidence from recent publications that BST2 may form a heterodimer at the cell surface (Ohtomo et al. BBRC 1999), and this dimerization may be necessary for its recognition by LILRA4.

CHAPTER 6 – CONCLUSION

The LILR receptor family is a relatively evolutionarily ancient family of immune receptors which most likely play diverse roles in immune regulation and tolerance. Although certain family members are expressed on lymphocytes such as T, B and NK cells, the predominant expression of most LILRs on monocytes, macrophages and dendritic cells suggests potentially important functions in the regulation of myeloid cell and antigen presenting cell function. Indeed, a growing body of evidence suggests engagement of LILRs on APC cells has major effects on maturation, functional efficacy in antigen presentation, and ability to initiate downstream tolerance mechanisms. Examples of effects on tolerance include implication of LILRs in the control of DC maturation, and differentiation of DCs to a tolerogenic phenotype capable of inducing T cell anergy and influencing generation of T regulatory cells. Such studies suggest that LILR expression or functions may be altered in pathogenic scenarios, and consistent with this, LILRs have been implicated in both autoimmune conditions such as rheumatoid arthritis, and also in cancer, where they may be involved in mediating suppressive effects of the tumour microenvironment via myeloid suppressor cells. Collectively, these studies highlight the potential clinical relevance of LILR immune function. Furthermore, they stress the importance of a comprehensive understanding of LILR immune biology, and raise the possibility that such an understanding would lead to novel LILR-focussed strategies to manipulate dendritic cell function to enhance suppressive effects in autoimmune conditions and decrease them in the context of cancer.

A more comprehensive understanding of LILR/ligand recognition events is likely to be key if we are to fully understand LILR function in the regulation of immune tolerance. Arguably the two LILRs most strongly implicated in the regulation of myeloid cell function are LILRB2 and LILRB4. Early work on the LILR family showed that the Group I receptor

LILRB2 (as well as the more broadly expressed LILRB1) bound to MHC molecules, and subsequent studies confirmed that LILRB2 interactions with MHC Class I molecules may underlie its tolerogenic effects on DC subsets. However, implication of the Group II receptor LILRB4 in such studies strongly suggests that ligands other than MHC Class I likely play important roles in LILR-mediated regulation of tolerogenic DC. The identity of such novel ligands is of considerable interest (particularly for LILRB4 as published data suggest an inhibitory signalling role for its ligand on T cells), and this issue was addressed in Chapter 3. Briefly, tetramers of the LILRB4 ectodomain were used to stain target cells to assess the pattern of ligand expression. While my T cell staining data were essentially analogous to those published by Saverino *et al* and similarly highlighted increases in staining on activated T cells, my dataset was novel in that it showed LILRB4 staining to B cells and monocytes. Based on this staining pattern, as well as the proposed inhibitory function for the LILRB4 ligand, and the finding that it was upregulated on T cell activation, I went on to test direct interaction between LILRB4 and various candidate ligands with roles in regulation of tolerance, predominantly belonging to the B7 family of costimulatory/inhibitory molecules. No interactions with LILRB4 were observed. Although key caveats should be mentioned with respect to my LILRB4 tetramer staining experiments – most notably the fact that such experiments are inherently difficult to control, and lack of staining to any *in vitro* cell lines tested – my staining dataset is potentially important since it implies LILRB4 may have immunosuppressive modulatory effects on multiple downstream effector populations rather than just T cells, and as such it further increases interest in the identity of its ligand(s).

These data raise the important question of how future studies could best determine the ligand or ligands of LILRB4. An important step forward would be if the ectodomain region of LILRB4 could be shown to confer binding or reactivity to specific target cells but not others.

While in principle this could be achieved using a staining reagent consisting of a multimeric form of the LILRB4 ectodomain to stain target cells, given my failure to stain *in vitro* cell lines with LILRB4 tetramers, an alternative approach would be to use a cell surface-expressed LILRB4 reporter construct such as an NFAT-GFP-linked construct. Irrespective of the strategy used, differential LILRB4-mediated binding or recognition of target cells would enable several downstream options to identify the ligand. One possibility would be a microarray comparison of the transcriptional profile in recognised *vs* non-recognised cells. While this has the potential to identify a relatively large number of differentially expressed genes, it is possible that the functional data on LILRB4 in immune tolerance, as well as the suggestion that its ligand has an inhibitory signalling function, would help prioritise attractive candidate ligands for further investigation. Alternatively, proteomics-based SILAC (stable isotope labelling by amino acids in cell culture) methods potentially provide a parallel methodology to identify in a comparable manner differentially expressed proteins enhanced in ligand-positive versus ligand-negative cell lines. A second strategy once ligand-positive and ligand-negative target cell lines are identified would be to adopt an expression cloning approach, involving transfection of cDNA derived from ligand-positive cells to ligand-negative cells in order to confer LILRB4 reactivity/binding. Finally, generation of antibodies against ligand-positive target cells that block LILRB4-dependent reactivity or binding remains a powerful approach, since such antibodies could potentially either be used to directly immunoprecipitate the LILRB4 ligand or conceivably as a tool to facilitate efficient selection of ligand-positive cells in expression cloning approaches. Recently, the group of Cao et al identified the ligand for LILRA4, an activatory receptor exclusively present on plasmacytoid dendritic cells, by combining several of these steps, using an ILT7-NFAT GFP reporter system to identify ligand-positive target cells, followed by generation of a blocking antibody that was used to select cDNA species that conferred reactivity to LILRA4-NFAT recognition.

While such ligand identification efforts remain speculative in nature, they are likely to prove seminal to our understanding of LILR receptor biology.

In Chapter 4, I addressed the related question of the structure of the LILRB4 receptor. After extensive attempts to crystallise the native D1D2 ectodomain failed, I chose to focus on the membrane distal D1 domain and successfully crystallised, solved, and analysed its structure using X-ray crystallography. In a collaboration with the group of Professor Gao, I also extensively analysed a structure of a D1D2 fragment of the LILRB4 ectodomain bearing a non-native disulphide bond to enhance protein stability. Collectively, these studies provide the first structural information on this important regulator of myeloid cell function. Arguably four key points emerged from these studies. Firstly, although broadly similar in structure to other LILRs, in comparison to other family members, LILRB4 has reduced hydrophobic contacts at the interdomain interface and an unusual obtuse interdomain angle, strongly suggestive of substantial flexibility between the LILRB4 D1 and D2 domains. Secondly, analysis of the LILRB4 structure in relation to structures of both LILRB1/B2 in complex with ligand confirms that LILRB4 is highly unsuited to binding MHC Class I, both in terms of conformation and the biophysical properties of its surface, confirming its status as a Group II LILR. Thirdly, the structure of the LILRB4 D1 domain is extremely similar to that of another Group II receptor, LILRA5, raising the question of whether they interact with structurally related ligands. Finally, analysis of the LILRB4 molecular surface for potential ligand binding sites identified several patches of interest. One, identified by manual inspection, was noted to bind to a sulphate ion in the crystal structure, whereas two others, identified by automated analysis, corresponded approximately to the D1 tip and D1-D2 hinge region sites on LILRB1 uses for binding MHC Class I. These data suggest there may be structural parallels between LILRB4 ligand recognition and that of LILRB1/B2, and they also highlight

putative binding sites on LILRB4 that can be analysed further once definitive ligands are identified. In addition, in principle the involvement of each site in LILRB4 ligand binding could be tested by carrying out tetramer staining studies using LILRB4 moieties bearing mutations in relevant residues from each site.

In Chapter 5, I first attempted to obtain comparable structural information on the D1 domains of other Group II LILRs, but ultimately adopted an NMR-based approach to analyse the structure of the Group II receptor LILRA4, which is expressed exclusively on plasmacytoid dendritic cells. LILRA4 was of particular interest for structural analyses because a recent potentially seminal study by Cao et al had identified its ligand. LILRA4, which negatively regulates pDC function, was found to recognise BST2, a type I IFN-induced cell surface protein with roles in antiviral defense. LILRA4 interactions with BST2 potentially function as a feedback inhibition loop to limit pDC cytokine production when IFN levels are sufficient. However, since BST2 was also found to be expressed on various tumour lines, this study raises the question of whether upregulation of BST2 on tumours could provide an axis of immunosuppression mediated through LILRA4 inhibition of pDC function.

In addition to these important immunological implications, the molecular and structural basis of LILRA4/BST2 interaction is of considerable interest, not least as a prototypic example of Group II LILR/ligand interaction. While my NMR-based experiments indicated the LILRA4 D1 domain has similar secondary structural features relative to other LILR D1 domains, and also highlighted regions of potentially high flexibility, clearly additional NMR analyses would be required for a full structure determination of the LILRA4 D1 domain. Analysis of the binding properties of LILRA4/BST2 interaction could also be highly informative about the mode of recognition, and to date the only data published on the interaction involved

binding of dimeric LILRA4-Fc protein to immobilised BST2. Unfortunately, I was unable to generate monomeric D1-D4 LILRA4 protein, and was unable to detect interaction using recombinant LILRA4 D1D2. One obvious explanation for this data is involvement of D3 and D4 in this interaction; however another possibility is that the LILRA4/BST2 interaction is extremely weak. This second possibility is consistent with the finding that LILRA4-Fc binds to BST2 with an apparent K_d in the μM range, and with the fact that MHC Class I interactions with other "activatory" (i.e. ITAM-associating) LILRs and KIRs are thought to involve extremely weak interactions. Clearly further analyses are required to address this issue, and to fully define the molecular and structural basis of LILRA4/BST2 interaction.

LIST OF REFERENCES

Achdout, H., Manaster, I., and Mandelboim, O. (2008). Influenza virus infection augments NK cell inhibition through reorganization of major histocompatibility complex class I proteins. J Virol *82*, 8030-8037.

Agata, Y., Kawasaki, A., Nishimura, H., Ishida, Y., Tsubata, T., Yagita, H., and Honjo, T. (1996). Expression of the PD-1 antigen on the surface of stimulated mouse T and B lymphocytes. Int Immunol *8*, 765-772.

Allan, D. S., Colonna, M., Lanier, L. L., Churakova, T. D., Abrams, J. S., Ellis, S. A., McMichael, A. J., and Braud, V. M. (1999). Tetrameric complexes of human histocompatibility leukocyte antigen (HLA)-G bind to peripheral blood myelomonocytic cells. J Exp Med *189*, 1149-1156.

Allen, R. C., Armitage, R. J., Conley, M. E., Rosenblatt, H., Jenkins, N. A., Copeland, N. G., Bedell, M. A., Edelhoff, S., Disteche, C. M., Simoneaux, D. K., and et al. (1993). CD40 ligand gene defects responsible for X-linked hyper-IgM syndrome. Science *259*, 990-993.

Allen, R. L., Raine, T., Haude, A., Trowsdale, J., and Wilson, M. J. (2001). Leukocyte receptor complex-encoded immunomodulatory receptors show differing specificity for alternative HLA-B27 structures. J Immunol *167*, 5543-5547.

Altman, J. D., Moss, P. A., Goulder, P. J., Barouch, D. H., McHeyzer-Williams, M. G., Bell, J. I., McMichael, A. J., and Davis, M. M. (1996). Phenotypic analysis of antigen-specific T lymphocytes. Science *274*, 94-96.

Anderson, K. J., and Allen, R. L. (2009). Regulation of T-cell immunity by leucocyte immunoglobulin-like receptors: innate immune receptors for self on antigen-presenting cells. Immunology *127*, 8-17.

Anderson, M. S., Venanzi, E. S., Chen, Z., Berzins, S. P., Benoist, C., and Mathis, D. (2005). The cellular mechanism of Aire control of T cell tolerance. Immunity *23*, 227-239.

Arase, H., Mocarski, E. S., Campbell, A. E., Hill, A. B., and Lanier, L. L. (2002). Direct recognition of cytomegalovirus by activating and inhibitory NK cell receptors. Science *296*, 1323-1326.

Arm, J. P., Nwankwo, C., and Austen, K. F. (1997). Molecular identification of a novel family of human Ig superfamily members that possess immunoreceptor tyrosine-based inhibition motifs and homology to the mouse gp49B1 inhibitory receptor. J Immunol *159*, 2342-2349.

Banchereau, J., Briere, F., Caux, C., Davoust, J., Lebecque, S., Liu, Y. J., Pulendran, B., and Palucka, K. (2000). Immunobiology of dendritic cells. Annu Rev Immunol *18*, 767-811.

Banchereau, J., and Steinman, R. M. (1998). Dendritic cells and the control of immunity. Nature *392*, 245-252.

Barclay, A. N., and Hatherley, D. (2008). The counterbalance theory for evolution and function of paired receptors. Immunity *29*, 675-678.

Barrow, A. D., and Trowsdale, J. (2006). You say ITAM and I say ITIM, let's call the whole thing off: the

ambiguity of immunoreceptor signalling. Eur J Immunol *36*, 1646-1653.

Beinhauer, B. G., McBride, J. M., Graf, P., Pursch, E., Bongers, M., Rogy, M., Korthauer, U., de Vries, J. E., Aversa, G., and Jung, T. (2004). Interleukin 10 regulates cell surface and soluble LIR-2 (CD85d) expression on dendritic cells resulting in T cell hyporesponsiveness in vitro. Eur J Immunol *34*, 74-80.

Belkaid, Y., and Oldenhove, G. (2008). Tuning microenvironments: induction of regulatory T cells by dendritic cells. Immunity *29*, 362-371.

Bellon, T., Kitzig, F., Sayos, J., and Lopez-Botet, M. (2002). Mutational analysis of immunoreceptor tyrosine-based inhibition motifs of the Ig-like transcript 2 (CD85j) leukocyte receptor. J Immunol *168*, 3351-3359.

Bender, A., Sapp, M., Schuler, G., Steinman, R. M., and Bhardwaj, N. (1996). Improved methods for the generation of dendritic cells from nonproliferating progenitors in human blood. J Immunol Methods *196*, 121-135.

Bennett, C. L., Christie, J., Ramsdell, F., Brunkow, M. E., Ferguson, P. J., Whitesell, L., Kelly, T. E., Saulsbury, F. T., Chance, P. F., and Ochs, H. D. (2001). The immune dysregulation, polyendocrinopathy, enteropathy, X-linked syndrome (IPEX) is caused by mutations of FOXP3. Nat Genet *27*, 20-21.

Blasius, A. L., Giurisato, E., Cella, M., Schreiber, R. D., Shaw, A. S., and Colonna, M. (2006). Bone marrow stromal cell antigen 2 is a specific marker of type I IFN-producing cells in the naive mouse, but a promiscuous cell surface antigen following IFN stimulation. J Immunol *177*, 3260-3265.

Bleharski, J. R., Li, H., Meinken, C., Graeber, T. G., Ochoa, M. T., Yamamura, M., Burdick, A., Sarno, E. N., Wagner, M., Rollinghoff, M., *et al.* (2003). Use of genetic profiling in leprosy to discriminate clinical forms of the disease. Science *301*, 1527-1530.

Borges, L., Hsu, M. L., Fanger, N., Kubin, M., and Cosman, D. (1997). A family of human lymphoid and myeloid Ig-like receptors, some of which bind to MHC class I molecules. J Immunol *159*, 5192-5196.

Borges, L., Kubin, M., and Kuhlman, T. (2003). LIR9, an immunoglobulin-superfamily-activating receptor, is expressed as a transmembrane and as a secreted molecule. Blood *101*, 1484-1486.

Borriello, F., Sethna, M. P., Boyd, S. D., Schweitzer, A. N., Tivol, E. A., Jacoby, D., Strom, T. B., Simpson, E. M., Freeman, G. J., and Sharpe, A. H. (1997). B7-1 and B7-2 have overlapping, critical roles in immunoglobulin class switching and germinal center formation. Immunity *6*, 303-313.

Braud, V. M., Allan, D. S., O'Callaghan, C. A., Soderstrom, K., D'Andrea, A., Ogg, G. S., Lazetic, S., Young, N. T., Bell, J. I., Phillips, J. H., *et al.* (1998). HLA-E binds to natural killer cell receptors CD94/NKG2A, B and C. Nature *391*, 795-799.

Brown, D. P., Jones, D. C., Anderson, K. J., Lapaque, N., Buerki, R. A., Trowsdale, J., and Allen, R. L. (2009). The inhibitory receptor LILRB4 (ILT3) modulates antigen presenting cell phenotype and, along with LILRB2 (ILT4), is upregulated in response to Salmonella infection. BMC Immunol *10*, 56.

Brunet, J. F., Denizot, F., Luciani, M. F., Roux-Dosseto, M., Suzan, M., Mattei, M. G., and Golstein, P. (1987). A new member of the immunoglobulin superfamily--CTLA-4. Nature *328*, 267-270.

Brunger, A. T. (1992). Free R value: a novel statistical quantity for assessing the accuracy of crystal

structures. Nature *355*, 472-475.

Brunger, A. T., Adams, P. D., Clore, G. M., DeLano, W. L., Gros, P., Grosse-Kunstleve, R. W., Jiang, J. S., Kuszewski, J., Nilges, M., Pannu, N. S., *et al.* (1998). Crystallography & NMR system: A new software suite for macromolecular structure determination. Acta Crystallogr D Biol Crystallogr *54*, 905-921.

Brunkow, M. E., Jeffery, E. W., Hjerrild, K. A., Paeper, B., Clark, L. B., Yasayko, S. A., Wilkinson, J. E., Galas, D., Ziegler, S. F., and Ramsdell, F. (2001). Disruption of a new forkhead/winged-helix protein, scurfin, results in the fatal lymphoproliferative disorder of the scurfy mouse. Nat Genet *27*, 68-73.

Butte, M. J., Keir, M. E., Phamduy, T. B., Sharpe, A. H., and Freeman, G. J. (2007). Programmed death-1 ligand 1 interacts specifically with the B7-1 costimulatory molecule to inhibit T cell responses. Immunity *27*, 111-122.

Canavez, F., Young, N. T., Guethlein, L. A., Rajalingam, R., Khakoo, S. I., Shum, B. P., and Parham, P. (2001). Comparison of chimpanzee and human leukocyte Ig-like receptor genes reveals framework and rapidly evolving genes. J Immunol *167*, 5786-5794.

Cao, W., Bover, L., Cho, M., Wen, X., Hanabuchi, S., Bao, M., Rosen, D. B., Wang, Y. H., Shaw, J. L., Du, Q., *et al.* (2009). Regulation of TLR7/9 responses in plasmacytoid dendritic cells by BST2 and ILT7 receptor interaction. J Exp Med *206*, 1603-1614.

Cao, W., Rosen, D. B., Ito, T., Bover, L., Bao, M., Watanabe, G., Yao, Z., Zhang, L., Lanier, L. L., and Liu, Y. J. (2006). Plasmacytoid dendritic cell-specific receptor ILT7-Fc epsilonRI gamma inhibits Toll-like receptor-induced interferon production. J Exp Med *203*, 1399-1405.

Caux, C., Massacrier, C., Vanbervliet, B., Dubois, B., Van Kooten, C., Durand, I., and Banchereau, J. (1994). Activation of human dendritic cells through CD40 cross-linking. J Exp Med *180*, 1263-1272.

Cella, M., Dohring, C., Samaridis, J., Dessing, M., Brockhaus, M., Lanzavecchia, A., and Colonna, M. (1997). A novel inhibitory receptor (ILT3) expressed on monocytes, macrophages, and dendritic cells involved in antigen processing. J Exp Med *185*, 1743-1751.

Cella, M., Scheidegger, D., Palmer-Lehmann, K., Lane, P., Lanzavecchia, A., and Alber, G. (1996). Ligation of CD40 on dendritic cells triggers production of high levels of interleukin-12 and enhances T cell stimulatory capacity: T-T help via APC activation. J Exp Med *184*, 747-752.

Chang, C. C., Ciubotariu, R., Manavalan, J. S., Yuan, J., Colovai, A. I., Piazza, F., Lederman, S., Colonna, M., Cortesini, R., Dalla-Favera, R., and Suciu-Foca, N. (2002). Tolerization of dendritic cells by T(S) cells: the crucial role of inhibitory receptors ILT3 and ILT4. Nat Immunol *3*, 237-243.

Chapman, T. L., Heikema, A. P., West, A. P., Jr., and Bjorkman, P. J. (2000). Crystal structure and ligand binding properties of the D1D2 region of the inhibitory receptor LIR-1 (ILT2). Immunity *13*, 727-736.

Chapman, T. L., Heikeman, A. P., and Bjorkman, P. J. (1999). The inhibitory receptor LIR-1 uses a common binding interaction to recognize class I MHC molecules and the viral homolog UL18. Immunity *11*, 603-613.

Chen, Y., Chu, F., Gao, F., Zhou, B., and Gao, G. F. (2007). Stability engineering, biophysical, and biological characterization of the myeloid activating receptor immunoglobulin-like transcript 1

(ILT1/LIR-7/LILRA2). Protein Expr Purif *56*, 253-260.

Chen, Y., Gao, F., Chu, F., Peng, H., Zong, L., Liu, Y., Tien, P., and Gao, G. F. (2009). Crystal structure of myeloid cell activating receptor leukocyte Ig-like receptor A2 (LILRA2/ILT1/LIR-7) domain swapped dimer: molecular basis for its non-binding to MHC complexes. J Mol Biol *386*, 841-853.

Chen, Y., Kuchroo, V. K., Inobe, J., Hafler, D. A., and Weiner, H. L. (1994). Regulatory T cell clones induced by oral tolerance: suppression of autoimmune encephalomyelitis. Science *265*, 1237-1240.

Cho, M., Ishida, K., Chen, J., Ohkawa, J., Chen, W., Namiki, S., Kotaki, A., Arai, N., Arai, K., and Kamogawa-Schifter, Y. (2008). SAGE library screening reveals ILT7 as a specific plasmacytoid dendritic cell marker that regulates type I IFN production. Int Immunol *20*, 155-164.

Collaborative Computational Project No. 4 (1994). The CCP4 suite: programs for protein crystallography. Acta Crystallogr D Biol Crystallogr *50*, 760-763.

Colonna, M., Navarro, F., Bellon, T., Llano, M., Garcia, P., Samaridis, J., Angman, L., Cella, M., and Lopez-Botet, M. (1997). A common inhibitory receptor for major histocompatibility complex class I molecules on human lymphoid and myelomonocytic cells. J Exp Med *186*, 1809-1818.

Colovai, A. I., Tsao, L., Wang, S., Lin, H., Wang, C., Seki, T., Fisher, J. G., Menes, M., Bhagat, G., Alobeid, B., and Suciu-Foca, N. (2007). Expression of inhibitory receptor ILT3 on neoplastic B cells is associated with lymphoid tissue involvement in chronic lymphocytic leukemia. Cytometry B Clin Cytom *72*, 354-362.

Conti, L., and Gessani, S. (2008). GM-CSF in the generation of dendritic cells from human blood monocyte precursors: recent advances. Immunobiology *213*, 859-870.

Cools, N., Ponsaerts, P., Van Tendeloo, V. F., and Berneman, Z. N. (2007). Balancing between immunity and tolerance: an interplay between dendritic cells, regulatory T cells, and effector T cells. J Leukoc Biol *82*, 1365-1374.

Coombes, J. L., Siddiqui, K. R., Arancibia-Carcamo, C. V., Hall, J., Sun, C. M., Belkaid, Y., and Powrie, F. (2007). A functionally specialized population of mucosal CD103+ DCs induces Foxp3+ regulatory T cells via a TGF-beta and retinoic acid-dependent mechanism. J Exp Med *204*, 1757-1764.

Coquerelle, C., and Moser, M. DC subsets in positive and negative regulation of immunity. Immunol Rev *234*, 317-334.

Cortesini, N. S., Colovai, A. I., Manavalan, J. S., Galluzzo, S., Naiyer, A. J., Liu, J., Vlad, G., Kim-Schulze, S., Scotto, L., Fan, J., and Cortesini, R. (2004). Role of regulatory and suppressor T-cells in the induction of ILT3+ ILT4+ tolerogenic endothelial cells in organ allografts. Transpl Immunol *13*, 73-82.

Cortesini, R. (2007). Pancreas cancer and the role of soluble immunoglobulin-like transcript 3 (ILT3). JOP *8*, 697-703.

Cosman, D., Fanger, N., Borges, L., Kubin, M., Chin, W., Peterson, L., and Hsu, M. L. (1997). A novel immunoglobulin superfamily receptor for cellular and viral MHC class I molecules. Immunity *7*, 273-282.

Coyle, A. J., Lehar, S., Lloyd, C., Tian, J., Delaney, T., Manning, S., Nguyen, T., Burwell, T., Schneider, H., Gonzalo, J. A., *et al.* (2000). The CD28-related molecule ICOS is required for effective T cell-

dependent immune responses. Immunity *13*, 95-105.

Croft, M., So, T., Duan, W., and Soroosh, P. (2009). The significance of OX40 and OX40L to T-cell biology and immune disease. Immunol Rev *229*, 173-191.

Davis, S. J., Ikemizu, S., Evans, E. J., Fugger, L., Bakker, T. R., and van der Merwe, P. A. (2003). The nature of molecular recognition by T cells. Nat Immunol *4*, 217-224.

Denning, T. L., Wang, Y. C., Patel, S. R., Williams, I. R., and Pulendran, B. (2007). Lamina propria macrophages and dendritic cells differentially induce regulatory and interleukin 17-producing T cell responses. Nat Immunol *8*, 1086-1094.

Diehn, M., Alizadeh, A. A., Rando, O. J., Liu, C. L., Stankunas, K., Botstein, D., Crabtree, G. R., and Brown, P. O. (2002). Genomic expression programs and the integration of the CD28 costimulatory signal in T cell activation. Proc Natl Acad Sci U S A *99*, 11796-11801.

Dietrich, J., Cella, M., and Colonna, M. (2001). Ig-like transcript 2 (ILT2)/leukocyte Ig-like receptor 1 (LIR1) inhibits TCR signaling and actin cytoskeleton reorganization. J Immunol *166*, 2514-2521.

Dong, H., Strome, S. E., Matteson, E. L., Moder, K. G., Flies, D. B., Zhu, G., Tamura, H., Driscoll, C. L., and Chen, L. (2003). Costimulating aberrant T cell responses by B7-H1 autoantibodies in rheumatoid arthritis. J Clin Invest *111*, 363-370.

Doucey, M. A., Scarpellino, L., Zimmer, J., Guillaume, P., Luescher, I. F., Bron, C., and Held, W. (2004). Cis association of Ly49A with MHC class I restricts natural killer cell inhibition. Nat Immunol *5*, 328-336.

Egen, J. G., and Allison, J. P. (2002). Cytotoxic T lymphocyte antigen-4 accumulation in the immunological synapse is regulated by TCR signal strength. Immunity *16*, 23-35.

Emsley, P., and Cowtan, K. (2004). Coot: model-building tools for molecular graphics. Acta Crystallogr D Biol Crystallogr *60*, 2126-2132.

Endharti, A. T., Rifa, I. M., Shi, Z., Fukuoka, Y., Nakahara, Y., Kawamoto, Y., Takeda, K., Isobe, K., and Suzuki, H. (2005). Cutting edge: CD8+CD122+ regulatory T cells produce IL-10 to suppress IFN-gamma production and proliferation of CD8+ T cells. J Immunol *175*, 7093-7097.

Fanger, N. A., Cosman, D., Peterson, L., Braddy, S. C., Maliszewski, C. R., and Borges, L. (1998). The MHC class I binding proteins LIR-1 and LIR-2 inhibit Fc receptor-mediated signaling in monocytes. Eur J Immunol *28*, 3423-3434.

Fathman, C. G., and Lineberry, N. B. (2007). Molecular mechanisms of CD4+ T-cell anergy. Nat Rev Immunol *7*, 599-609.

Feger, U., Tolosa, E., Huang, Y. H., Waschbisch, A., Biedermann, T., Melms, A., and Wiendl, H. (2007). HLA-G expression defines a novel regulatory T-cell subset present in human peripheral blood and sites of inflammation. Blood *110*, 568-577.

Fife, B. T., and Bluestone, J. A. (2008). Control of peripheral T-cell tolerance and autoimmunity via the CTLA-4 and PD-1 pathways. Immunol Rev *224*, 166-182.

Foster, C. E., Colonna, M., and Sun, P. D. (2003). Crystal structure of the human natural killer (NK) cell activating receptor NKp46 reveals structural relationship to other leukocyte receptor complex immunoreceptors. J Biol Chem *278*, 46081-46086.

Franchi, L., Warner, N., Viani, K., and Nunez, G. (2009). Function of Nod-like receptors in microbial recognition and host defense. Immunol Rev *227*, 106-128.

Frauwirth, K. A., Riley, J. L., Harris, M. H., Parry, R. V., Rathmell, J. C., Plas, D. R., Elstrom, R. L., June, C. H., and Thompson, C. B. (2002). The CD28 signaling pathway regulates glucose metabolism. Immunity *16*, 769-777.

Gallimore, A. M., and Simon, A. K. (2008). Positive and negative influences of regulatory T cells on tumour immunity. Oncogene *27*, 5886-5893.

Garboczi, D. N., Hung, D. T., and Wiley, D. C. (1992). HLA-A2-peptide complexes: refolding and crystallization of molecules expressed in Escherichia coli and complexed with single antigenic peptides. Proc Natl Acad Sci U S A *89*, 3429-3433.

Garner, L. I., Salim, M., Mohammed, F., and Willcox, B. E. (2006). Expression, purification, and refolding of the myeloid inhibitory receptor leukocyte immunoglobulin-like receptor-5 for structural and ligand identification studies. Protein Expr Purif *47*, 490-497.

Geijtenbeek, T. B., van Vliet, S. J., Engering, A., t Hart, B. A., and van Kooyk, Y. (2004). Self- and nonself-recognition by C-type lectins on dendritic cells. Annu Rev Immunol *22*, 33-54.

Geissmann, F., Manz, M. G., Jung, S., Sieweke, M. H., Merad, M., and Ley, K. Development of monocytes, macrophages, and dendritic cells. Science *327*, 656-661.

Gleissner, C. A., Zastrow, A., Klingenberg, R., Kluger, M. S., Konstandin, M., Celik, S., Haemmerling, S., Shankar, V., Giese, T., Katus, H. A., and Dengler, T. J. (2007). IL-10 inhibits endothelium-dependent T cell costimulation by up-regulation of ILT3/4 in human vascular endothelial cells. Eur J Immunol *37*, 177-192.

Greaves, D. R., and Gordon, S. (2009). The macrophage scavenger receptor at 30 years of age: current knowledge and future challenges. J Lipid Res *50 Suppl*, S282-286.

Greenwald, R. J., Freeman, G. J., and Sharpe, A. H. (2005). The B7 family revisited. Annu Rev Immunol *23*, 515-548.

Gregori, S., Magnani, C. F., and Roncarolo, M. G. (2009). Role of human leukocyte antigen-G in the induction of adaptive type 1 regulatory T cells. Hum Immunol *70*, 966-969.

Gregori, S., Tomasoni, D., Pacciani, V., Scirpoli, M., Battaglia, M., Magnani, C. F., Hauben, E., and Roncarolo, M. G. Differentiation of type 1 T regulatory cells (Tr1) by tolerogenic DC-10 requires the IL-10-dependent ILT4/HLA-G pathway. Blood *116*, 935-944.

Grimbacher, B., Hutloff, A., Schlesier, M., Glocker, E., Warnatz, K., Drager, R., Eibel, H., Fischer, B., Schaffer, A. A., Mages, H. W., *et al.* (2003). Homozygous loss of ICOS is associated with adult-onset common variable immunodeficiency. Nat Immunol *4*, 261-268.

Grossman, W. J., Verbsky, J. W., Barchet, W., Colonna, M., Atkinson, J. P., and Ley, T. J. (2004). Human

T regulatory cells can use the perforin pathway to cause autologous target cell death. Immunity *21*, 589-601.

Groux, H., Bigler, M., de Vries, J. E., and Roncarolo, M. G. (1996). Interleukin-10 induces a long-term antigen-specific anergic state in human CD4+ T cells. J Exp Med *184*, 19-29.

Groux, H., O'Garra, A., Bigler, M., Rouleau, M., Antonenko, S., de Vries, J. E., and Roncarolo, M. G. (1997). A CD4+ T-cell subset inhibits antigen-specific T-cell responses and prevents colitis. Nature *389*, 737-742.

Habicht, A., Dada, S., Jurewicz, M., Fife, B. T., Yagita, H., Azuma, M., Sayegh, M. H., and Guleria, I. (2007). A link between PDL1 and T regulatory cells in fetomaternal tolerance. J Immunol *179*, 5211-5219.

Hawiger, D., Inaba, K., Dorsett, Y., Guo, M., Mahnke, K., Rivera, M., Ravetch, J. V., Steinman, R. M., and Nussenzweig, M. C. (2001). Dendritic cells induce peripheral T cell unresponsiveness under steady state conditions in vivo. J Exp Med *194*, 769-779.

Hori, S., Nomura, T., and Sakaguchi, S. (2003). Control of regulatory T cell development by the transcription factor Foxp3. Science *299*, 1057-1061.

Horwitz, D. A., Zheng, S. G., and Gray, J. D. (2008). Natural and TGF-beta-induced Foxp3(+)CD4(+) CD25(+) regulatory T cells are not mirror images of each other. Trends Immunol *29*, 429-435.

Huang, J., Goedert, J. J., Sundberg, E. J., Cung, T. D., Burke, P. S., Martin, M. P., Preiss, L., Lifson, J., Lichterfeld, M., Carrington, M., and Yu, X. G. (2009). HLA-B*35-Px-mediated acceleration of HIV-1 infection by increased inhibitory immunoregulatory impulses. J Exp Med *206*, 2959-2966.

Hubert, P., Jacobs, N., Caberg, J. H., Boniver, J., and Delvenne, P. (2007). The cross-talk between dendritic and regulatory T cells: good or evil? J Leukoc Biol *82*, 781-794.

Hutloff, A., Dittrich, A. M., Beier, K. C., Eljaschewitsch, B., Kraft, R., Anagnostopoulos, I., and Kroczek, R. A. (1999). ICOS is an inducible T-cell co-stimulator structurally and functionally related to CD28. Nature *397*, 263-266.

Huynh, O. A., Hampartzoumian, T., Arm, J. P., Hunt, J., Borges, L., Ahern, M., Smith, M., Geczy, C. L., McNeil, H. P., and Tedla, N. (2007). Down-regulation of leucocyte immunoglobulin-like receptor expression in the synovium of rheumatoid arthritis patients after treatment with disease-modifying anti-rheumatic drugs. Rheumatology (Oxford) *46*, 742-751.

Ishii, K. J., Kawagoe, T., Koyama, S., Matsui, K., Kumar, H., Kawai, T., Uematsu, S., Takeuchi, O., Takeshita, F., Coban, C., and Akira, S. (2008). TANK-binding kinase-1 delineates innate and adaptive immune responses to DNA vaccines. Nature *451*, 725-729.

Janeway, C. A., Jr. (1989). Approaching the asymptote? Evolution and revolution in immunology. Cold Spring Harb Symp Quant Biol *54 Pt 1*, 1-13.

Jenmalm, M. C., Cherwinski, H., Bowman, E. P., Phillips, J. H., and Sedgwick, J. D. (2006). Regulation of myeloid cell function through the CD200 receptor. J Immunol *176*, 191-199.

Jiang, A., Bloom, O., Ono, S., Cui, W., Unternaehrer, J., Jiang, S., Whitney, J. A., Connolly, J.,

Banchereau, J., and Mellman, I. (2007). Disruption of E-cadherin-mediated adhesion induces a functionally distinct pathway of dendritic cell maturation. Immunity *27*, 610-624.

Jiang, L., and Barclay, A. N. (2009). New assay to detect low-affinity interactions and characterization of leukocyte receptors for collagen including leukocyte-associated Ig-like receptor-1 (LAIR-1). Eur J Immunol *39*, 1167-1175.

Joffre, O., Nolte, M. A., Sporri, R., and Reis e Sousa, C. (2009). Inflammatory signals in dendritic cell activation and the induction of adaptive immunity. Immunol Rev *227*, 234-247.

Jones, D. C., Roghanian, A., Brown, D. P., Chang, C., Allen, R. L., Trowsdale, J., and Young, N. T. (2009). Alternative mRNA splicing creates transcripts encoding soluble proteins from most LILR genes. Eur J Immunol *39*, 3195-3206.

Ju, X. S., Hacker, C., Scherer, B., Redecke, V., Berger, T., Schuler, G., Wagner, H., Lipford, G. B., and Zenke, M. (2004). Immunoglobulin-like transcripts ILT2, ILT3 and ILT7 are expressed by human dendritic cells and down-regulated following activation. Gene *331*, 159-164.

Jung, D., Giallourakis, C., Mostoslavsky, R., and Alt, F. W. (2006). Mechanism and control of V(D)J recombination at the immunoglobulin heavy chain locus. Annu Rev Immunol *24*, 541-570.

Kabalak, G., Koch, S., Dobberstein, B., The, Y. H., Matthias, T., Schnarr, S., Schmidt, R. E., and Witte, T. (2007). Immunoglobulin-like transcripts as risk genes for autoimmunity. Ann N Y Acad Sci *1110*, 10-14.

Kabsch, W. Xds. Acta Crystallogr D Biol Crystallogr *66*, 125-132.

Kamradt, T., and Mitchison, N. A. (2001). Tolerance and autoimmunity. N Engl J Med *344*, 655-664.

Karlsson, R., and Falt, A. (1997). Experimental design for kinetic analysis of protein-protein interactions with surface plasmon resonance biosensors. J Immunol Methods *200*, 121-133.

Katz, H. R. (2007). Inhibition of pathologic inflammation by leukocyte Ig-like receptor B4 and related inhibitory receptors. Immunol Rev *217*, 222-230.

Kawai, T., and Akira, S. The role of pattern-recognition receptors in innate immunity: update on Toll-like receptors. Nat Immunol *11*, 373-384.

Keir, M. E., Butte, M. J., Freeman, G. J., and Sharpe, A. H. (2008). PD-1 and its ligands in tolerance and immunity. Annu Rev Immunol *26*, 677-704.

Khakoo, S. I., and Carrington, M. (2006). KIR and disease: a model system or system of models? Immunol Rev *214*, 186-201.

Kiertscher, S. M., and Roth, M. D. (1996). Human CD14+ leukocytes acquire the phenotype and function of antigen-presenting dendritic cells when cultured in GM-CSF and IL-4. J Leukoc Biol *59*, 208-218.

Kim, J. S., Choi, S. E., Yun, I. H., Kim, J. Y., Ahn, C., Kim, S. J., Ha, J., Hwang, E. S., Cha, C. Y., Miyagawa, S., and Park, C. G. (2004). Human cytomegalovirus UL18 alleviated human NK-mediated swine endothelial cell lysis. Biochem Biophys Res Commun *315*, 144-150.

Kim-Schulze, S., Scotto, L., Vlad, G., Piazza, F., Lin, H., Liu, Z., Cortesini, R., and Suciu-Foca, N.

(2006). Recombinant Ig-like transcript 3-Fc modulates T cell responses via induction of Th anergy and differentiation of CD8+ T suppressor cells. J Immunol *176*, 2790-2798.

Kleywegt, G. J. (1996). Use of non-crystallographic symmetry in protein structure refinement. Acta Crystallogr D Biol Crystallogr *52*, 842-857.

Knoechel, B., Lohr, J., Zhu, S., Wong, L., Hu, D., Ausubel, L., and Abbas, A. K. (2006). Functional and molecular comparison of anergic and regulatory T lymphocytes. J Immunol *176*, 6473-6483.

Kobayashi, T., Walsh, M. C., and Choi, Y. (2004). The role of TRAF6 in signal transduction and the immune response. Microbes Infect *6*, 1333-1338.

Koch, S., Goedde, R., Nigmatova, V., Epplen, J. T., Muller, N., de Seze, J., Vermersch, P., Momot, T., Schmidt, R. E., and Witte, T. (2005). Association of multiple sclerosis with ILT6 deficiency. Genes Immun *6*, 445-447.

Kollnberger, S., Bird, L., Sun, M. Y., Retiere, C., Braud, V. M., McMichael, A., and Bowness, P. (2002). Cell-surface expression and immune receptor recognition of HLA-B27 homodimers. Arthritis Rheum *46*, 2972-2982.

Korthauer, U., Graf, D., Mages, H. W., Briere, F., Padayachee, M., Malcolm, S., Ugazio, A. G., Notarangelo, L. D., Levinsky, R. J., and Kroczek, R. A. (1993). Defective expression of T-cell CD40 ligand causes X-linked immunodeficiency with hyper-IgM. Nature *361*, 539-541.

Krangel, M. S., Hernandez-Munain, C., Lauzurica, P., McMurry, M., Roberts, J. L., and Zhong, X. P. (1998). Developmental regulation of V(D)J recombination at the TCR alpha/delta locus. Immunol Rev *165*, 131-147.

Kraulis, P. J. (1991). Journal of Applied Crystallography *24*, 946-950.

Kubagawa, H., Burrows, P. D., and Cooper, M. D. (1997). A novel pair of immunoglobulin-like receptors expressed by B cells and myeloid cells. Proc Natl Acad Sci U S A *94*, 5261-5266.

Kuipers, H., Muskens, F., Willart, M., Hijdra, D., van Assema, F. B., Coyle, A. J., Hoogsteden, H. C., and Lambrecht, B. N. (2006). Contribution of the PD-1 ligands/PD-1 signaling pathway to dendritic cell-mediated CD4+ T cell activation. Eur J Immunol *36*, 2472-2482.

Kupzig, S., Korolchuk, V., Rollason, R., Sugden, A., Wilde, A., and Banting, G. (2003). Bst-2/HM1.24 is a raft-associated apical membrane protein with an unusual topology. Traffic *4*, 694-709.

Kuroki, K., Tsuchiya, N., Shiroishi, M., Rasubala, L., Yamashita, Y., Matsuta, K., Fukazawa, T., Kusaoi, M., Murakami, Y., Takiguchi, M., *et al.* (2005). Extensive polymorphisms of LILRB1 (ILT2, LIR1) and their association with HLA-DRB1 shared epitope negative rheumatoid arthritis. Hum Mol Genet *14*, 2469-2480.

Kyewski, B., and Klein, L. (2006). A central role for central tolerance. Annu Rev Immunol *24*, 571-606.

Larkin, M. A., Blackshields, G., Brown, N. P., Chenna, R., McGettigan, P. A., McWilliam, H., Valentin, F., Wallace, I. M., Wilm, A., Lopez, R., *et al.* (2007). Clustal W and Clustal X version 2.0. Bioinformatics *23*, 2947-2948.

Laskowski, R. A., MacArthur, M. W., Moss, D. S., and Thornton, J. M. (1993). PROCHECK - a program to check the stereochemical quality of protein structures. J Appl Cryst *26*, 283-291.

Latchman, Y. E., Liang, S. C., Wu, Y., Chernova, T., Sobel, R. A., Klemm, M., Kuchroo, V. K., Freeman, G. J., and Sharpe, A. H. (2004). PD-L1-deficient mice show that PD-L1 on T cells, antigen-presenting cells, and host tissues negatively regulates T cells. Proc Natl Acad Sci U S A *101*, 10691-10696.

Lebbink, R. J., de Ruiter, T., Adelmeijer, J., Brenkman, A. B., van Helvoort, J. M., Koch, M., Farndale, R. W., Lisman, T., Sonnenberg, A., Lenting, P. J., and Meyaard, L. (2006). Collagens are functional, high affinity ligands for the inhibitory immune receptor LAIR-1. J Exp Med *203*, 1419-1425.

Lee, D. J., Sieling, P. A., Ochoa, M. T., Krutzik, S. R., Guo, B., Hernandez, M., Rea, T. H., Cheng, G., Colonna, M., and Modlin, R. L. (2007). LILRA2 activation inhibits dendritic cell differentiation and antigen presentation to T cells. J Immunol *179*, 8128-8136.

LeMaoult, J., Zafaranloo, K., Le Danff, C., and Carosella, E. D. (2005). HLA-G up-regulates ILT2, ILT3, ILT4, and KIR2DL4 in antigen presenting cells, NK cells, and T cells. FASEB J *19*, 662-664.

Leong, C. C., Chapman, T. L., Bjorkman, P. J., Formankova, D., Mocarski, E. S., Phillips, J. H., and Lanier, L. L. (1998). Modulation of natural killer cell cytotoxicity in human cytomegalovirus infection: the role of endogenous class I major histocompatibility complex and a viral class I homolog. J Exp Med *187*, 1681-1687.

Levings, M. K., Gregori, S., Tresoldi, E., Cazzaniga, S., Bonini, C., and Roncarolo, M. G. (2005). Differentiation of Tr1 cells by immature dendritic cells requires IL-10 but not CD25+CD4+ Tr cells. Blood *105*, 1162-1169.

Li, D., Wang, L., Yu, L., Freundt, E. C., Jin, B., Screaton, G. R., and Xu, X. N. (2009). Ig-like transcript 4 inhibits lipid antigen presentation through direct CD1d interaction. J Immunol *182*, 1033-1040.

Liang, S., Ristich, V., Arase, H., Dausset, J., Carosella, E. D., and Horuzsko, A. (2008). Modulation of dendritic cell differentiation by HLA-G and ILT4 requires the IL-6--STAT3 signaling pathway. Proc Natl Acad Sci U S A *105*, 8357-8362.

Lichterfeld, M., Kavanagh, D. G., Williams, K. L., Moza, B., Mui, S. K., Miura, T., Sivamurthy, R., Allgaier, R., Pereyra, F., Trocha, A., *et al.* (2007). A viral CTL escape mutation leading to immunoglobulin-like transcript 4-mediated functional inhibition of myelomonocytic cells. J Exp Med *204*, 2813-2824.

Liu, J., Liu, Z., Witkowski, P., Vlad, G., Manavalan, J. S., Scotto, L., Kim-Schulze, S., Cortesini, R., Hardy, M. A., and Suciu-Foca, N. (2004). Rat CD8+ FOXP3+ T suppressor cells mediate tolerance to allogeneic heart transplants, inducing PIR-B in APC and rendering the graft invulnerable to rejection. Transpl Immunol *13*, 239-247.

Liu, K., and Nussenzweig, M. C. Origin and development of dendritic cells. Immunol Rev *234*, 45-54.

Liu, Y. J. (2005). IPC: professional type 1 interferon-producing cells and plasmacytoid dendritic cell precursors. Annu Rev Immunol *23*, 275-306.

Liu, Z., Tugulea, S., Cortesini, R., and Suciu-Foca, N. (1998). Specific suppression of T helper alloreactivity by allo-MHC class I-restricted CD8+CD28- T cells. Int Immunol *10*, 775-783.

Lu, H. K., Rentero, C., Raftery, M. J., Borges, L., Bryant, K., and Tedla, N. (2009). Leukocyte Ig-like receptor B4 (LILRB4) is a potent inhibitor of FcgammaRI-mediated monocyte activation via dephosphorylation of multiple kinases. J Biol Chem *284*, 34839-34848.

Lutz, M. B., and Kurts, C. (2009). Induction of peripheral CD4+ T-cell tolerance and CD8+ T-cell cross-tolerance by dendritic cells. Eur J Immunol *39*, 2325-2330.

Ma, D. Y., and Clark, E. A. (2009). The role of CD40 and CD154/CD40L in dendritic cells. Semin Immunol *21*, 265-272.

Maasho, K., Masilamani, M., Valas, R., Basu, S., Coligan, J. E., and Borrego, F. (2005). The inhibitory leukocyte-associated Ig-like receptor-1 (LAIR-1) is expressed at high levels by human naive T cells and inhibits TCR mediated activation. Mol Immunol *42*, 1521-1530.

Mackey, M. F., Gunn, J. R., Maliszewsky, C., Kikutani, H., Noelle, R. J., and Barth, R. J., Jr. (1998). Dendritic cells require maturation via CD40 to generate protective antitumor immunity. J Immunol *161*, 2094-2098.

Maki, G., Hayes, G. M., Naji, A., Tyler, T., Carosella, E. D., Rouas-Freiss, N., and Gregory, S. A. (2008). NK resistance of tumor cells from multiple myeloma and chronic lymphocytic leukemia patients: implication of HLA-G. Leukemia *22*, 998-1006.

Mamegano, K., Kuroki, K., Miyashita, R., Kusaoi, M., Kobayashi, S., Matsuta, K., Maenaka, K., Colonna, M., Ozaki, S., Hashimoto, H., *et al.* (2008). Association of LILRA2 (ILT1, LIR7) splice site polymorphism with systemic lupus erythematosus and microscopic polyangiitis. Genes Immun *9*, 214-223.

Manavalan, J. S., Kim-Schulze, S., Scotto, L., Naiyer, A. J., Vlad, G., Colombo, P. C., Marboe, C., Mancini, D., Cortesini, R., and Suciu-Foca, N. (2004). Alloantigen specific CD8+CD28- FOXP3+ T suppressor cells induce ILT3+ ILT4+ tolerogenic endothelial cells, inhibiting alloreactivity. Int Immunol *16*, 1055-1068.

Manavalan, J. S., Rossi, P. C., Vlad, G., Piazza, F., Yarilina, A., Cortesini, R., Mancini, D., and Suciu-Foca, N. (2003). High expression of ILT3 and ILT4 is a general feature of tolerogenic dendritic cells. Transpl Immunol *11*, 245-258.

Manicassamy, S., Ravindran, R., Deng, J., Oluoch, H., Denning, T. L., Kasturi, S. P., Rosenthal, K. M., Evavold, B. D., and Pulendran, B. (2009). Toll-like receptor 2-dependent induction of vitamin A-metabolizing enzymes in dendritic cells promotes T regulatory responses and inhibits autoimmunity. Nat Med *15*, 401-409.

Martin, A. M., Kulski, J. K., Witt, C., Pontarotti, P., and Christiansen, F. T. (2002). Leukocyte Ig-like receptor complex (LRC) in mice and men. Trends Immunol *23*, 81-88.

Martin, M., Schneider, H., Azouz, A., and Rudd, C. E. (2001). Cytotoxic T lymphocyte antigen 4 and CD28 modulate cell surface raft expression in their regulation of T cell function. J Exp Med *194*, 1675-1681.

Masuda, A., Nakamura, A., Maeda, T., Sakamoto, Y., and Takai, T. (2007). Cis binding between inhibitory receptors and MHC class I can regulate mast cell activation. J Exp Med *204*, 907-920.

Matzinger, P. (1994). Tolerance, danger, and the extended family. Annu Rev Immunol *12*, 991-1045.

McAdam, A. J., Greenwald, R. J., Levin, M. A., Chernova, T., Malenkovich, N., Ling, V., Freeman, G. J., and Sharpe, A. H. (2001). ICOS is critical for CD40-mediated antibody class switching. Nature *409*, 102-105.

McCoy, A. J. (2007). Solving structures of protein complexes by molecular replacement with Phaser. Acta Crystallogr D Biol Crystallogr *63*, 32-41.

McGuirk, P., McCann, C., and Mills, K. H. (2002). Pathogen-specific T regulatory 1 cells induced in the respiratory tract by a bacterial molecule that stimulates interleukin 10 production by dendritic cells: a novel strategy for evasion of protective T helper type 1 responses by Bordetella pertussis. J Exp Med *195*, 221-231.

McPherson, A. (2004). Introduction to protein crystallization. Methods *34*, 254-265.

Medzhitov, R., and Janeway, C. A., Jr. (2002). Decoding the patterns of self and nonself by the innate immune system. Science *296*, 298-300.

Medzhitov, R., Preston-Hurlburt, P., and Janeway, C. A., Jr. (1997). A human homologue of the Drosophila Toll protein signals activation of adaptive immunity. Nature *388*, 394-397.

Melief, C. J. (2008). Cancer immunotherapy by dendritic cells. Immunity *29*, 372-383.

Mellor, A. L., and Munn, D. H. (2004). IDO expression by dendritic cells: tolerance and tryptophan catabolism. Nat Rev Immunol *4*, 762-774.

Merlo, A., Saverino, D., Tenca, C., Grossi, C. E., Bruno, S., and Ciccone, E. (2001). CD85/LIR-1/ILT2 and CD152 (cytotoxic T lymphocyte antigen 4) inhibitory molecules down-regulate the cytolytic activity of human CD4+ T-cell clones specific for Mycobacterium tuberculosis. Infect Immun *69*, 6022-6029.

Merwe, P. A. v. d. Chapter 6: Surface Plasmon Resonance. In Protein-ligand Interactions: Hydrodynamics and Calorimetry. Practical Approach Series. Oxford University Press, 2001.

Meyaard, L., Adema, G. J., Chang, C., Woollatt, E., Sutherland, G. R., Lanier, L. L., and Phillips, J. H. (1997). LAIR-1, a novel inhibitory receptor expressed on human mononuclear leukocytes. Immunity *7*, 283-290.

Meyaard, L., Hurenkamp, J., Clevers, H., Lanier, L. L., and Phillips, J. H. (1999). Leukocyte-associated Ig-like receptor-1 functions as an inhibitory receptor on cytotoxic T cells. J Immunol *162*, 5800-5804.

Miyara, M., Amoura, Z., Parizot, C., Badoual, C., Dorgham, K., Trad, S., Nochy, D., Debre, P., Piette, J. C., and Gorochov, G. (2005). Global natural regulatory T cell depletion in active systemic lupus erythematosus. J Immunol *175*, 8392-8400.

Monks, C. R., Freiberg, B. A., Kupfer, H., Sciaky, N., and Kupfer, A. (1998). Three-dimensional segregation of supramolecular activation clusters in T cells. Nature *395*, 82-86.

Monsivais-Urenda, A., Nino-Moreno, P., Abud-Mendoza, C., Baranda, L., Layseca-Espinosa, E., Lopez-Botet, M., and Gonzalez-Amaro, R. (2007). Analysis of expression and function of the inhibitory receptor

ILT2 (CD85j/LILRB1/LIR-1) in peripheral blood mononuclear cells from patients with systemic lupus erythematosus (SLE). J Autoimmun *29*, 97-105.

Moodie, S. J., Norman, P. J., King, A. L., Fraser, J. S., Curtis, D., Ellis, H. J., Vaughan, R. W., and Ciclitira, P. J. (2002). Analysis of candidate genes on chromosome 19 in coeliac disease: an association study of the KIR and LILR gene clusters. Eur J Immunogenet *29*, 287-291.

Morelli, A. E., and Thomson, A. W. (2007). Tolerogenic dendritic cells and the quest for transplant tolerance. Nat Rev Immunol *7*, 610-621.

Mori, Y., Tsuji, S., Inui, M., Sakamoto, Y., Endo, S., Ito, Y., Fujimura, S., Koga, T., Nakamura, A., Takayanagi, H., *et al*. (2008). Inhibitory immunoglobulin-like receptors LILRB and PIR-B negatively regulate osteoclast development. J Immunol *181*, 4742-4751.

Mueller, D. L. Mechanisms maintaining peripheral tolerance. Nat Immunol *11*, 21-27.

Munitz, A., McBride, M. L., Bernstein, J. S., and Rothenberg, M. E. (2008). A dual activation and inhibition role for the paired immunoglobulin-like receptor B in eosinophils. Blood *111*, 5694-5703.

Murshudov, G. N., Vagin, A. A., and Dodson, E. J. (1997). Refinement of macromolecular structures by the maximum-likelihood method. Acta Crystallogr D Biol Crystallogr *53*, 240-255.

Nakajima, H., Samaridis, J., Angman, L., and Colonna, M. (1999). Human myeloid cells express an activating ILT receptor (ILT1) that associates with Fc receptor gamma-chain. J Immunol *162*, 5-8.

Nakayama, M., Underhill, D. M., Petersen, T. W., Li, B., Kitamura, T., Takai, T., and Aderem, A. (2007). Paired Ig-like receptors bind to bacteria and shape TLR-mediated cytokine production. J Immunol *178*, 4250-4259.

Nakhaei, P., Genin, P., Civas, A., and Hiscott, J. (2009). RIG-I-like receptors: sensing and responding to RNA virus infection. Semin Immunol *21*, 215-222.

Navarro, F., Llano, M., Bellon, T., Colonna, M., Geraghty, D. E., and Lopez-Botet, M. (1999). The ILT2(LIR1) and CD94/NKG2A NK cell receptors respectively recognize HLA-G1 and HLA-E molecules co-expressed on target cells. Eur J Immunol *29*, 277-283.

Nemazee, D., Gavin, A., Hoebe, K., and Beutler, B. (2006). Immunology: Toll-like receptors and antibody responses. Nature *441*, E4; discussion E4.

Nguyen, L. T., Radhakrishnan, S., Ciric, B., Tamada, K., Shin, T., Pardoll, D. M., Chen, L., Rodriguez, M., and Pease, L. R. (2002). Cross-linking the B7 family molecule B7-DC directly activates immune functions of dendritic cells. J Exp Med *196*, 1393-1398.

Nicholls, A., Sharp, K., and Honig, B. (1991). GRASP. Proteins: Struc Funct Genet *11*.

Norman, P. J., Carey, B. S., Stephens, H. A., and Vaughan, R. W. (2003). DNA sequence variation and molecular genotyping of natural killer leukocyte immunoglobulin-like receptor, LILRA3. Immunogenetics *55*, 165-171.

Occhino, M., Ghiotto, F., Soro, S., Mortarino, M., Bosi, S., Maffei, M., Bruno, S., Nardini, M., Figini, M., Tramontano, A., and Ciccone, E. (2008). Dissecting the structural determinants of the interaction between

the human cytomegalovirus UL18 protein and the CD85j immune receptor. J Immunol *180*, 957-968.

Odeberg, J., Cerboni, C., Browne, H., Karre, K., Moller, E., Carbone, E., and Soderberg-Naucler, C. (2002). Human cytomegalovirus (HCMV)-infected endothelial cells and macrophages are less susceptible to natural killer lysis independent of the downregulation of classical HLA class I molecules or expression of the HCMV class I homologue, UL18. Scand J Immunol *55*, 149-161.

Ohtomo, T., Sugamata, Y., Ozaki, Y., Ono, K., Yoshimura, Y., Kawai, S., Koishihara, Y., Ozaki, S., Kosaka, M., Hirano, T., and Tsuchiya, M. (1999). Molecular cloning and characterization of a surface antigen preferentially overexpressed on multiple myeloma cells. Biochem Biophys Res Commun *258*, 583-591.

Ozinsky, A., Underhill, D. M., Fontenot, J. D., Hajjar, A. M., Smith, K. D., Wilson, C. B., Schroeder, L., and Aderem, A. (2000). The repertoire for pattern recognition of pathogens by the innate immune system is defined by cooperation between toll-like receptors. Proc Natl Acad Sci U S A *97*, 13766-13771.

Palm, N. W., and Medzhitov, R. (2009). Pattern recognition receptors and control of adaptive immunity. Immunol Rev *227*, 221-233.

Pandiyan, P., Zheng, L., Ishihara, S., Reed, J., and Lenardo, M. J. (2007). CD4+CD25+Foxp3+ regulatory T cells induce cytokine deprivation-mediated apoptosis of effector CD4+ T cells. Nat Immunol *8*, 1353-1362.

Parham, P. (2004). Killer cell immunoglobulin-like receptor diversity: balancing signals in the natural killer cell response. Immunol Lett *92*, 11-13.

Parish, I. A., Rao, S., Smyth, G. K., Juelich, T., Denyer, G. S., Davey, G. M., Strasser, A., and Heath, W. R. (2009). The molecular signature of CD8+ T cells undergoing deletional tolerance. Blood *113*, 4575-4585.

Pasquier, B., Launay, P., Kanamaru, Y., Moura, I. C., Pfirsch, S., Ruffie, C., Henin, D., Benhamou, M., Pretolani, M., Blank, U., and Monteiro, R. C. (2005). Identification of FcalphaRI as an inhibitory receptor that controls inflammation: dual role of FcRgamma ITAM. Immunity *22*, 31-42.

Paul, P., Rouas-Freiss, N., Khalil-Daher, I., Moreau, P., Riteau, B., Le Gal, F. A., Avril, M. F., Dausset, J., Guillet, J. G., and Carosella, E. D. (1998). HLA-G expression in melanoma: a way for tumor cells to escape from immunosurveillance. Proc Natl Acad Sci U S A *95*, 4510-4515.

Peggs, K. S., and Allison, J. P. (2005). Co-stimulatory pathways in lymphocyte regulation: the immunoglobulin superfamily. Br J Haematol *130*, 809-824.

Peggs, K. S., Quezada, S. A., and Allison, J. P. (2008). Cell intrinsic mechanisms of T-cell inhibition and application to cancer therapy. Immunol Rev *224*, 141-165.

Pereira, S., Zhang, H., Takai, T., and Lowell, C. A. (2004). The inhibitory receptor PIR-B negatively regulates neutrophil and macrophage integrin signaling. J Immunol *173*, 5757-5765.

Peterson, P., Org, T., and Rebane, A. (2008). Transcriptional regulation by AIRE: molecular mechanisms of central tolerance. Nat Rev Immunol *8*, 948-957.

Pfistershammer, K., Lawitschka, A., Klauser, C., Leitner, J., Weigl, R., Heemskerk, M. H., Pickl, W. F.,

Majdic, O., Bohmig, G. A., Fischer, G. F., *et al.* (2009). Allogeneic disparities in immunoglobulin-like transcript 5 induce potent antibody responses in hematopoietic stem cell transplant recipients. Blood *114*, 2323-2332.

Pinchuk, L. M., Polacino, P. S., Agy, M. B., Klaus, S. J., and Clark, E. A. (1994). The role of CD40 and CD80 accessory cell molecules in dendritic cell-dependent HIV-1 infection. Immunity *1*, 317-325.

Pomie, C., Menager-Marcq, I., and van Meerwijk, J. P. (2008). Murine CD8+ regulatory T lymphocytes: the new era. Hum Immunol *69*, 708-714.

Porollo, A., and Meller, J. (2007). Prediction-based fingerprints of protein-protein interactions. Proteins *66*, 630-645.

Pulendran, B., Tang, H., and Manicassamy, S. Programming dendritic cells to induce T(H)2 and tolerogenic responses. Nat Immunol *11*, 647-655.

Raab, M., Cai, Y. C., Bunnell, S. C., Heyeck, S. D., Berg, L. J., and Rudd, C. E. (1995). p56Lck and p59Fyn regulate CD28 binding to phosphatidylinositol 3-kinase, growth factor receptor-bound protein GRB-2, and T cell-specific protein-tyrosine kinase ITK: implications for T-cell costimulation. Proc Natl Acad Sci U S A *92*, 8891-8895.

Rajagopalan, S., and Long, E. O. (2005). Understanding how combinations of HLA and KIR genes influence disease. J Exp Med *201*, 1025-1029.

Randolph, G. J., Inaba, K., Robbiani, D. F., Steinman, R. M., and Muller, W. A. (1999). Differentiation of phagocytic monocytes into lymph node dendritic cells in vivo. Immunity *11*, 753-761.

Rescigno, M., Winzler, C., Delia, D., Mutini, C., Lutz, M., and Ricciardi-Castagnoli, P. (1997). Dendritic cell maturation is required for initiation of the immune response. J Leukoc Biol *61*, 415-421.

Reyburn, H. T., Mandelboim, O., Vales-Gomez, M., Davis, D. M., Pazmany, L., and Strominger, J. L. (1997). The class I MHC homologue of human cytomegalovirus inhibits attack by natural killer cells. Nature *386*, 514-517.

Riley, J. L., Mao, M., Kobayashi, S., Biery, M., Burchard, J., Cavet, G., Gregson, B. P., June, C. H., and Linsley, P. S. (2002). Modulation of TCR-induced transcriptional profiles by ligation of CD28, ICOS, and CTLA-4 receptors. Proc Natl Acad Sci U S A *99*, 11790-11795.

Rissoan, M. C., Duhen, T., Bridon, J. M., Bendriss-Vermare, N., Peronne, C., de Saint Vis, B., Briere, F., and Bates, E. E. (2002). Subtractive hybridization reveals the expression of immunoglobulin-like transcript 7, Eph-B1, granzyme B, and 3 novel transcripts in human plasmacytoid dendritic cells. Blood *100*, 3295-3303.

Rissoan, M. C., Soumelis, V., Kadowaki, N., Grouard, G., Briere, F., de Waal Malefyt, R., and Liu, Y. J. (1999). Reciprocal control of T helper cell and dendritic cell differentiation. Science *283*, 1183-1186.

Ristich, V., Zhang, W., Liang, S., and Horuzsko, A. (2007). Mechanisms of prolongation of allograft survival by HLA-G/ILT4-modified dendritic cells. Hum Immunol *68*, 264-271.

Romani, N., Koide, S., Crowley, M., Witmer-Pack, M., Livingstone, A. M., Fathman, C. G., Inaba, K., and Steinman, R. M. (1989). Presentation of exogenous protein antigens by dendritic cells to T cell clones.

Intact protein is presented best by immature, epidermal Langerhans cells. J Exp Med *169*, 1169-1178.

Sadegh-Nasseri, S., Dalai, S. K., Korb Ferris, L. C., and Mirshahidi, S. Suboptimal engagement of the T-cell receptor by a variety of peptide-MHC ligands triggers T-cell anergy. Immunology *129*, 1-7.

Saibil, S. D., Deenick, E. K., and Ohashi, P. S. (2007). The sound of silence: modulating anergy in T lymphocytes. Curr Opin Immunol *19*, 658-664.

Sakaguchi, S. (2005). Naturally arising Foxp3-expressing CD25+CD4+ regulatory T cells in immunological tolerance to self and non-self. Nat Immunol *6*, 345-352.

Sakaguchi, S., Sakaguchi, N., Asano, M., Itoh, M., and Toda, M. (1995). Immunologic self-tolerance maintained by activated T cells expressing IL-2 receptor alpha-chains (CD25). Breakdown of a single mechanism of self-tolerance causes various autoimmune diseases. J Immunol *155*, 1151-1164.

Sakaguchi, S., Takahashi, T., and Nishizuka, Y. (1982). Study on cellular events in post-thymectomy autoimmune oophoritis in mice. II. Requirement of Lyt-1 cells in normal female mice for the prevention of oophoritis. J Exp Med *156*, 1577-1586.

Sallusto, F., and Lanzavecchia, A. (1994). Efficient presentation of soluble antigen by cultured human dendritic cells is maintained by granulocyte/macrophage colony-stimulating factor plus interleukin 4 and downregulated by tumor necrosis factor alpha. J Exp Med *179*, 1109-1118.

Samaridis, J., and Colonna, M. (1997). Cloning of novel immunoglobulin superfamily receptors expressed on human myeloid and lymphoid cells: structural evidence for new stimulatory and inhibitory pathways. Eur J Immunol *27*, 660-665.

Sambrook, J. G., Bashirova, A., Andersen, H., Piatak, M., Vernikos, G. S., Coggill, P., Lifson, J. D., Carrington, M., and Beck, S. (2006). Identification of the ancestral killer immunoglobulin-like receptor gene in primates. BMC Genomics *7*, 209.

Sathish, J. G., Johnson, K. G., Fuller, K. J., LeRoy, F. G., Meyaard, L., Sims, M. J., and Matthews, R. J. (2001). Constitutive association of SHP-1 with leukocyte-associated Ig-like receptor-1 in human T cells. J Immunol *166*, 1763-1770.

Saulquin, X., Gastinel, L. N., and Vivier, E. (2003). Crystal structure of the human natural killer cell activating receptor KIR2DS2 (CD158j). J Exp Med *197*, 933-938.

Saverino, D., Fabbi, M., Ghiotto, F., Merlo, A., Bruno, S., Zarcone, D., Tenca, C., Tiso, M., Santoro, G., Anastasi, G., *et al.* (2000). The CD85/LIR-1/ILT2 inhibitory receptor is expressed by all human T lymphocytes and down-regulates their functions. J Immunol *165*, 3742-3755.

Saverino, D., Ghiotto, F., Merlo, A., Bruno, S., Battini, L., Occhino, M., Maffei, M., Tenca, C., Pileri, S., Baldi, L., *et al.* (2004). Specific recognition of the viral protein UL18 by CD85j/LIR-1/ILT2 on CD8+ T cells mediates the non-MHC-restricted lysis of human cytomegalovirus-infected cells. J Immunol *172*, 5629-5637.

Saverino, D., Merlo, A., Bruno, S., Pistoia, V., Grossi, C. E., and Ciccone, E. (2002). Dual effect of CD85/leukocyte Ig-like receptor-1/Ig-like transcript 2 and CD152 (CTLA-4) on cytokine production by antigen-stimulated human T cells. J Immunol *168*, 207-215.

Sayos, J., Martinez-Barriocanal, A., Kitzig, F., Bellon, T., and Lopez-Botet, M. (2004). Recruitment of C-terminal Src kinase by the leukocyte inhibitory receptor CD85j. Biochem Biophys Res Commun *324*, 640-647.

Scarpellino, L., Oeschger, F., Guillaume, P., Coudert, J. D., Levy, F., Leclercq, G., and Held, W. (2007). Interactions of Ly49 family receptors with MHC class I ligands in trans and cis. J Immunol *178*, 1277-1284.

Schmid, M. A., Kingston, D., Boddupalli, S., and Manz, M. G. Instructive cytokine signals in dendritic cell lineage commitment. Immunol Rev *234*, 32-44.

Schneider, H., Downey, J., Smith, A., Zinselmeyer, B. H., Rush, C., Brewer, J. M., Wei, B., Hogg, N., Garside, P., and Rudd, C. E. (2006). Reversal of the TCR stop signal by CTLA-4. Science *313*, 1972-1975.

Schneider, H., Smith, X., Liu, H., Bismuth, G., and Rudd, C. E. (2008). CTLA-4 disrupts ZAP70 microcluster formation with reduced T cell/APC dwell times and calcium mobilization. Eur J Immunol *38*, 40-47.

Schuler, G., and Steinman, R. M. (1985). Murine epidermal Langerhans cells mature into potent immunostimulatory dendritic cells in vitro. J Exp Med *161*, 526-546.

Schwartz, R. H. (2003). T cell anergy. Annu Rev Immunol *21*, 305-334.

Serbina, N. V., Salazar-Mather, T. P., Biron, C. A., Kuziel, W. A., and Pamer, E. G. (2003). TNF/iNOS-producing dendritic cells mediate innate immune defense against bacterial infection. Immunity *19*, 59-70.

Shen, Y., Vernon, R., Baker, D., and Bax, A. (2009). De novo protein structure generation from incomplete chemical shift assignments. J Biomol NMR *43*, 63-78.

Shiroishi, M., Kajikawa, M., Kuroki, K., Ose, T., Kohda, D., and Maenaka, K. (2006). Crystal structure of the human monocyte-activating receptor, "Group 2" leukocyte Ig-like receptor A5 (LILRA5/LIR9/ILT11). J Biol Chem *281*, 19536-19544.

Shiroishi, M., Kuroki, K., Ose, T., Rasubala, L., Shiratori, I., Arase, H., Tsumoto, K., Kumagai, I., Kohda, D., and Maenaka, K. (2006). Efficient leukocyte Ig-like receptor signaling and crystal structure of disulfide-linked HLA-G dimer. J Biol Chem *281*, 10439-10447.

Shiroishi, M., Kuroki, K., Rasubala, L., Tsumoto, K., Kumagai, I., Kurimoto, E., Kato, K., Kohda, D., and Maenaka, K. (2006). Structural basis for recognition of the nonclassical MHC molecule HLA-G by the leukocyte Ig-like receptor B2 (LILRB2/LIR2/ILT4/CD85d). Proc Natl Acad Sci U S A *103*, 16412-16417.

Shiroishi, M., Kuroki, K., Tsumoto, K., Yokota, A., Sasaki, T., Amano, K., Shimojima, T., Shirakihara, Y., Rasubala, L., van der Merwe, P. A., *et al.* (2006). Entropically driven MHC class I recognition by human inhibitory receptor leukocyte Ig-like receptor B1 (LILRB1/ILT2/CD85j). J Mol Biol *355*, 237-248.

Shiroishi, M., Tsumoto, K., Amano, K., Shirakihara, Y., Colonna, M., Braud, V. M., Allan, D. S., Makadzange, A., Rowland-Jones, S., Willcox, B., *et al.* (2003). Human inhibitory receptors Ig-like transcript 2 (ILT2) and ILT4 compete with CD8 for MHC class I binding and bind preferentially to HLA-G. Proc Natl Acad Sci U S A *100*, 8856-8861.

Siggs, O. M., Makaroff, L. E., and Liston, A. (2006). The why and how of thymocyte negative selection. Curr Opin Immunol *18*, 175-183.

Sloane, D. E., Tedla, N., Awoniyi, M., Macglashan, D. W., Jr., Borges, L., Austen, K. F., and Arm, J. P. (2004). Leukocyte immunoglobulin-like receptors: novel innate receptors for human basophil activation and inhibition. Blood *104*, 2832-2839.

Smith, C. M., Wilson, N. S., Waithman, J., Villadangos, J. A., Carbone, F. R., Heath, W. R., and Belz, G. T. (2004). Cognate CD4(+) T cell licensing of dendritic cells in CD8(+) T cell immunity. Nat Immunol *5*, 1143-1148.

Steinman, R. M. (2007). Dendritic cells: understanding immunogenicity. Eur J Immunol *37 Suppl 1*, S53-60.

Steinman, R. M., and Banchereau, J. (2007). Taking dendritic cells into medicine. Nature *449*, 419-426.

Steinman, R. M., and Cohn, Z. A. (1973). Identification of a novel cell type in peripheral lymphoid organs of mice. I. Morphology, quantitation, tissue distribution. J Exp Med *137*, 1142-1162.

Steinman, R. M., and Cohn, Z. A. (1974). Identification of a novel cell type in peripheral lymphoid organs of mice. II. Functional properties in vitro. J Exp Med *139*, 380-397.

Steinman, R. M., Kaplan, G., Witmer, M. D., and Cohn, Z. A. (1979). Identification of a novel cell type in peripheral lymphoid organs of mice. V. Purification of spleen dendritic cells, new surface markers, and maintenance in vitro. J Exp Med *149*, 1-16.

Steinman, R. M., and Nussenzweig, M. C. (2002). Avoiding horror autotoxicus: the importance of dendritic cells in peripheral T cell tolerance. Proc Natl Acad Sci U S A *99*, 351-358.

Steinman, R. M., Turley, S., Mellman, I., and Inaba, K. (2000). The induction of tolerance by dendritic cells that have captured apoptotic cells. J Exp Med *191*, 411-416.

Steinman, R. M., and Witmer, M. D. (1978). Lymphoid dendritic cells are potent stimulators of the primary mixed leukocyte reaction in mice. Proc Natl Acad Sci U S A *75*, 5132-5136.

Strasser, A., Puthalakath, H., O'Reilly, L. A., and Bouillet, P. (2008). What do we know about the mechanisms of elimination of autoreactive T and B cells and what challenges remain. Immunol Cell Biol *86*, 57-66.

Su, X. D., Gastinel, L. N., Vaughn, D. E., Faye, I., Poon, P., and Bjorkman, P. J. (1998). Crystal structure of hemolin: a horseshoe shape with implications for homophilic adhesion. Science *281*, 991-995.

Suciu-Foca, N., and Cortesini, R. (2007). Central role of ILT3 in the T suppressor cell cascade. Cell Immunol *248*, 59-67.

Suciu-Foca, N., Feirt, N., Zhang, Q. Y., Vlad, G., Liu, Z., Lin, H., Chang, C. C., Ho, E. K., Colovai, A. I., Kaufman, H., *et al.* (2007). Soluble Ig-like transcript 3 inhibits tumor allograft rejection in humanized SCID mice and T cell responses in cancer patients. J Immunol *178*, 7432-7441.

Sun, Y., Liu, J., Gao, P., Wang, Y., and Liu, C. (2008). Expression of Ig-like transcript 4 inhibitory receptor in human non-small cell lung cancer. Chest *134*, 783-788.

Tafuri, A., Shahinian, A., Bladt, F., Yoshinaga, S. K., Jordana, M., Wakeham, A., Boucher, L. M., Bouchard, D., Chan, V. S., Duncan, G., *et al.* (2001). ICOS is essential for effective T-helper-cell responses. Nature *409*, 105-109.

Takeda, K., Harada, Y., Watanabe, R., Inutake, Y., Ogawa, S., Onuki, K., Kagaya, S., Tanabe, K., Kishimoto, H., and Abe, R. (2008). CD28 stimulation triggers NF-kappaB activation through the CARMA1-PKCtheta-Grb2/Gads axis. Int Immunol *20*, 1507-1515.

Takeda, K., Kaisho, T., and Akira, S. (2003). Toll-like receptors. Annu Rev Immunol *21*, 335-376.

Tan, J. K., and O'Neill, H. C. (2005). Maturation requirements for dendritic cells in T cell stimulation leading to tolerance versus immunity. J Leukoc Biol *78*, 319-324.

Tang, Q., and Bluestone, J. A. (2008). The Foxp3+ regulatory T cell: a jack of all trades, master of regulation. Nat Immunol *9*, 239-244.

Taylor, A., Verhagen, J., Blaser, K., Akdis, M., and Akdis, C. A. (2006). Mechanisms of immune suppression by interleukin-10 and transforming growth factor-beta: the role of T regulatory cells. Immunology *117*, 433-442.

Tedla, N., Bandeira-Melo, C., Tassinari, P., Sloane, D. E., Samplaski, M., Cosman, D., Borges, L., Weller, P. F., and Arm, J. P. (2003). Activation of human eosinophils through leukocyte immunoglobulin-like receptor 7. Proc Natl Acad Sci U S A *100*, 1174-1179.

Tedla, N., Gibson, K., McNeil, H. P., Cosman, D., Borges, L., and Arm, J. P. (2002). The co-expression of activating and inhibitory leukocyte immunoglobulin-like receptors in rheumatoid synovium. Am J Pathol *160*, 425-431.

Tedla, N., Lee, C. W., Borges, L., Geczy, C. L., and Arm, J. P. (2008). Differential expression of leukocyte immunoglobulin-like receptors on cord-blood-derived human mast cell progenitors and mature mast cells. J Leukoc Biol *83*, 334-343.

Thomson, C. W., Lee, B. P., and Zhang, L. (2006). Double-negative regulatory T cells: non-conventional regulators. Immunol Res *35*, 163-178.

Torkar, M., Haude, A., Milne, S., Beck, S., Trowsdale, J., and Wilson, M. J. (2000). Arrangement of the ILT gene cluster: a common null allele of the ILT6 gene results from a 6.7-kbp deletion. Eur J Immunol *30*, 3655-3662.

Trakhanov, S., and Quiocho, F. A. (1995). Influence of divalent cations in protein crystallization. Protein Sci *4*, 1914-1919.

Trombetta, E. S., and Mellman, I. (2005). Cell biology of antigen processing in vitro and in vivo. Annu Rev Immunol *23*, 975-1028.

Tuettenberg, A., Huter, E., Hubo, M., Horn, J., Knop, J., Grimbacher, B., Kroczek, R. A., Stoll, S., and Jonuleit, H. (2009). The role of ICOS in directing T cell responses: ICOS-dependent induction of T cell anergy by tolerogenic dendritic cells. J Immunol *182*, 3349-3356.

Urosevic, M., Kamarashev, J., Burg, G., and Dummer, R. (2004). Primary cutaneous CD8+ and CD56+ T-

cell lymphomas express HLA-G and killer-cell inhibitory ligand, ILT2. Blood *103*, 1796-1798.

Vagin, A., and Teplyakov, A. Molecular replacement with MOLREP. Acta Crystallogr D Biol Crystallogr *66*, 22-25.

van der Kleij, D., Latz, E., Brouwers, J. F., Kruize, Y. C., Schmitz, M., Kurt-Jones, E. A., Espevik, T., de Jong, E. C., Kapsenberg, M. L., Golenbock, D. T., *et al.* (2002). A novel host-parasite lipid cross-talk. Schistosomal lyso-phosphatidylserine activates toll-like receptor 2 and affects immune polarization. J Biol Chem *277*, 48122-48129.

van der Merwe, P. A., and Barclay, A. N. (1996). Analysis of cell-adhesion molecule interactions using surface plasmon resonance. Curr Opin Immunol *8*, 257-261.

van der Merwe, P. A., Bodian, D. L., Daenke, S., Linsley, P., and Davis, S. J. (1997). CD80 (B7-1) binds both CD28 and CTLA-4 with a low affinity and very fast kinetics. J Exp Med *185*, 393-403.

van der Vuurst de Vries, A. R., Clevers, H., Logtenberg, T., and Meyaard, L. (1999). Leukocyte-associated immunoglobulin-like receptor-1 (LAIR-1) is differentially expressed during human B cell differentiation and inhibits B cell receptor-mediated signaling. Eur J Immunol *29*, 3160-3167.

Velten, F. W., Duperrier, K., Bohlender, J., Metharom, P., and Goerdt, S. (2004). A gene signature of inhibitory MHC receptors identifies a BDCA3(+) subset of IL-10-induced dendritic cells with reduced allostimulatory capacity in vitro. Eur J Immunol *34*, 2800-2811.

Vieira, P. L., de Jong, E. C., Wierenga, E. A., Kapsenberg, M. L., and Kalinski, P. (2000). Development of Th1-inducing capacity in myeloid dendritic cells requires environmental instruction. J Immunol *164*, 4507-4512.

Viola, A., and Lanzavecchia, A. (1996). T cell activation determined by T cell receptor number and tunable thresholds. Science *273*, 104-106.

Vitale, M., Castriconi, R., Parolini, S., Pende, D., Hsu, M. L., Moretta, L., Cosman, D., and Moretta, A. (1999). The leukocyte Ig-like receptor (LIR)-1 for the cytomegalovirus UL18 protein displays a broad specificity for different HLA class I alleles: analysis of LIR-1 + NK cell clones. Int Immunol *11*, 29-35.

Vlad, G., Chang, C. C., Colovai, A. I., Berloco, P., Cortesini, R., and Suciu-Foca, N. (2009). Immunoglobulin-like transcript 3: A crucial regulator of dendritic cell function. Hum Immunol *70*, 340-344.

Vlad, G., Cortesini, R., and Suciu-Foca, N. (2008). CD8+ T suppressor cells and the ILT3 master switch. Hum Immunol *69*, 681-686.

Vlad, G., Liu, Z., Zhang, Q. Y., Cortesini, R., and Suciu-Foca, N. (2006). Immunosuppressive activity of recombinant ILT3. Int Immunopharmacol *6*, 1889-1894.

Volz, A., Wende, H., Laun, K., and Ziegler, A. (2001). Genesis of the ILT/LIR/MIR clusters within the human leukocyte receptor complex. Immunol Rev *181*, 39-51.

von Boehmer, H., and Melchers, F. Checkpoints in lymphocyte development and autoimmune disease. Nat Immunol *11*, 14-20.

Voulgaraki, D., Mitnacht-Kraus, R., Letarte, M., Foster-Cuevas, M., Brown, M. H., and Barclay, A. N. (2005). Multivalent recombinant proteins for probing functions of leucocyte surface proteins such as the CD200 receptor. Immunology *115*, 337-346.

Wagner, C. S., Riise, G. C., Bergstrom, T., Karre, K., Carbone, E., and Berg, L. (2007). Increased expression of leukocyte Ig-like receptor-1 and activating role of UL18 in the response to cytomegalovirus infection. J Immunol *178*, 3536-3543.

Wagner, C. S., Rolle, A., Cosman, D., Ljunggren, H. G., Berndt, K. D., and Achour, A. (2007). Structural elements underlying the high binding affinity of human cytomegalovirus UL18 to leukocyte immunoglobulin-like receptor-1. J Mol Biol *373*, 695-705.

Wagner, C. S., Walther-Jallow, L., Buentke, E., Ljunggren, H. G., Achour, A., and Chambers, B. J. (2008). Human cytomegalovirus-derived protein UL18 alters the phenotype and function of monocyte-derived dendritic cells. J Leukoc Biol *83*, 56-63.

Wakkach, A., Cottrez, F., and Groux, H. (2001). Differentiation of regulatory T cells 1 is induced by CD2 costimulation. J Immunol *167*, 3107-3113.

Walker, L. S., and Abbas, A. K. (2002). The enemy within: keeping self-reactive T cells at bay in the periphery. Nat Rev Immunol *2*, 11-19.

Wang, C., Lin, G. H., McPherson, A. J., and Watts, T. H. (2009). Immune regulation by 4-1BB and 4-1BBL: complexities and challenges. Immunol Rev *229*, 192-215.

Wang, G., Khattar, M., Guo, Z., Miyahara, Y., Linkes, S. P., Sun, Z., He, X., Stepkowski, S. M., and Chen, W. IL-2-deprivation and TGF-beta are two non-redundant suppressor mechanisms of CD4+CD25+ regulatory T cell which jointly restrain CD4+CD25- cell activation. Immunol Lett *132*, 61-68.

Wang, H. Y., and Wang, R. F. (2007). Regulatory T cells and cancer. Curr Opin Immunol *19*, 217-223.

Wang, S., and Chen, L. (2004). T lymphocyte co-signaling pathways of the B7-CD28 family. Cell Mol Immunol *1*, 37-42.

Waterhouse, P., Penninger, J. M., Timms, E., Wakeham, A., Shahinian, A., Lee, K. P., Thompson, C. B., Griesser, H., and Mak, T. W. (1995). Lymphoproliferative disorders with early lethality in mice deficient in Ctla-4. Science *270*, 985-988.

Weaver, C. T., Harrington, L. E., Mangan, P. R., Gavrieli, M., and Murphy, K. M. (2006). Th17: an effector CD4 T cell lineage with regulatory T cell ties. Immunity *24*, 677-688.

Weiner, H. L. (2001). Induction and mechanism of action of transforming growth factor-beta-secreting Th3 regulatory cells. Immunol Rev *182*, 207-214.

Wells, A. D. (2009). New insights into the molecular basis of T cell anergy: anergy factors, avoidance sensors, and epigenetic imprinting. J Immunol *182*, 7331-7341.

Willcox, B. E., Thomas, L. M., and Bjorkman, P. J. (2003). Crystal structure of HLA-A2 bound to LIR-1, a host and viral major histocompatibility complex receptor. Nat Immunol *4*, 913-919.

Willcox, B. E., Thomas, L. M., Chapman, T. L., Heikema, A. P., West, A. P., Jr., and Bjorkman, P. J.

(2002). Crystal structure of LIR-2 (ILT4) at 1.8 A: differences from LIR-1 (ILT2) in regions implicated in the binding of the Human Cytomegalovirus class I MHC homolog UL18. BMC Struct Biol *2*, 6.

Wing, K., Onishi, Y., Prieto-Martin, P., Yamaguchi, T., Miyara, M., Fehervari, Z., Nomura, T., and Sakaguchi, S. (2008). CTLA-4 control over Foxp3+ regulatory T cell function. Science *322*, 271-275.

Wing, K., and Sakaguchi, S. Regulatory T cells exert checks and balances on self tolerance and autoimmunity. Nat Immunol *11*, 7-13.

Witsch, E. J., Peiser, M., Hutloff, A., Buchner, K., Dorner, B. G., Jonuleit, H., Mages, H. W., and Kroczek, R. A. (2002). ICOS and CD28 reversely regulate IL-10 on re-activation of human effector T cells with mature dendritic cells. Eur J Immunol *32*, 2680-2686.

Yang, Z., and Bjorkman, P. J. (2008). Structure of UL18, a peptide-binding viral MHC mimic, bound to a host inhibitory receptor. Proc Natl Acad Sci U S A *105*, 10095-10100.

Young, N. T., Canavez, F., Uhrberg, M., Shum, B. P., and Parham, P. (2001). Conserved organization of the ILT/LIR gene family within the polymorphic human leukocyte receptor complex. Immunogenetics *53*, 270-278.

Zhou, L. J., and Tedder, T. F. (1996). CD14+ blood monocytes can differentiate into functionally mature CD83+ dendritic cells. Proc Natl Acad Sci U S A *93*, 2588-2592.

Zou, G. M., and Tam, Y. K. (2002). Cytokines in the generation and maturation of dendritic cells: recent advances. Eur Cytokine Netw *13*, 186-199.